

ISSN 0233-7584

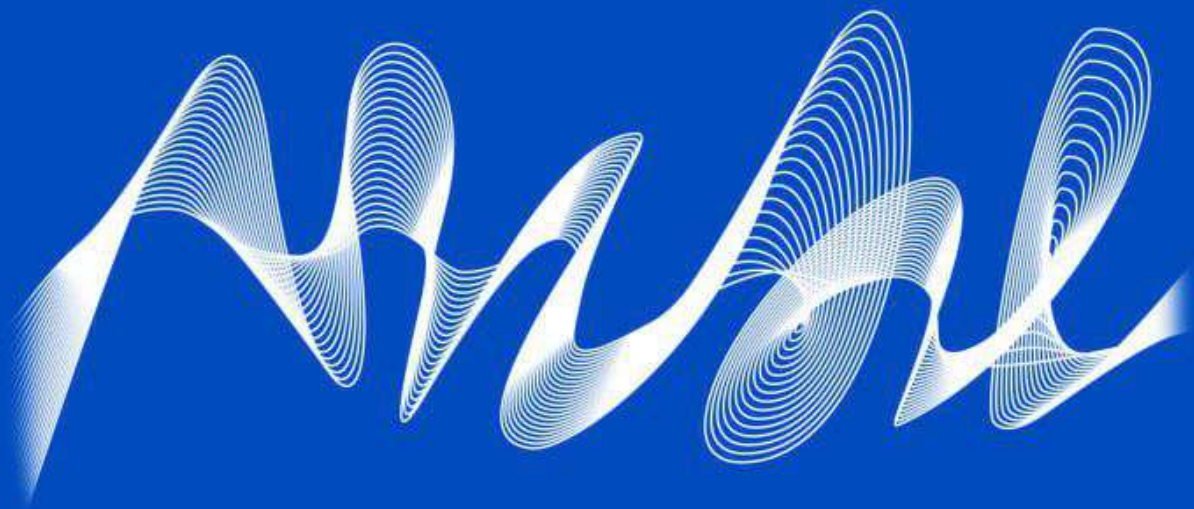
Vol. 31, Iss. 6 November – December 2024



Physical Oceanography

<http://physical-oceanography.ru/>

Topical Issue
“Formation of Carbon Fluxes In Marine Environment”



Edited by
Corresponding member of RAS S. K. Kononov

ISSN 1573-160X

Vol. 31, no. 6. 2024
November – December

Founded in January 1987

Publication frequency:

6 issues per year

Physical Oceanography

Scientific and theoretical journal

FOUNDER AND PUBLISHER:

Federal State Budget Scientific Institution

Federal Research Centre

“Marine Hydrophysical Institute of RAS”

Peer reviewed scientific journal.

The Journal publishes original research results, review articles (at the editorial board's request) and brief reports on the following sections of hydrophysics:

- thermohydrodynamics of the ocean and atmosphere;
- analysis of observational results and methods of calculation of ocean hydrophysical fields;
- experimental and expeditionary studies;
- satellite hydrophysics;
- mathematical modelling of marine systems;
- automation of scientific research of the seas and oceans.

Objectives

- familiarisation of the world and Russian scientific community with the results of theoretical, experimental and expeditionary studies of the World Ocean;
- exchange of scientific information, experience, research and observation data with specialists from different regions of the country and abroad;
- increase of publication activity of national authors, rating of scientific organisations of Russia and level of national publications in the world scientific community according to their citation data;
- theoretical and practical assistance to scientists in preparing articles for printing that meet modern requirements of publication and scientific ethics;
- strengthening the popularity and authority of the publication, increasing the number of regular subscribers

The Journal is indexed in:

Google Scholar
Web of Science (ESCI)
Scopus

journal@mhi-ras.ru

<http://physical-oceanography.ru/>

Founder, Publisher and Editorial Office address:

2, Kapitanskaya St., Sevastopol, 299011

Russia

Phone, fax: + 7 (8692) 54-02-23

EDITORIAL BOARD

- Sergey K. Kononov** – Editor-in-Chief, Director of FSBSI FRC MHI, corresponding member of RAS, Dr.Sci. (Geogr.), ORCID ID: 0000-0002-5200-8448, secretary@mhi-ras.ru (Sevastopol, Russia)
- Vladimir N. Belokopytov** – Deputy Editor-in-Chief, Head of Department of FSBSI FRC MHI, Dr.Sci. (Geogr.), ORCID ID: 0000-0003-4699-9588 (Sevastopol, Russia)
- Aleksandr I. Kubryakov** – Deputy Editor-in-Chief, Chief Scientist Researcher of FSBSI FRC MHI, Dr.Sci. (Phys.-Math.), ORCID ID: 0000-0003-1899-9230, ResearcherID: F-8959-2014, (Sevastopol, Russia)
- Anton A. Bukatov** – Executive Editor, Leading Research Associate of FSBSI FRC MHI, Ph.D. (Phys.-Math.), ORCID ID: 0000-0002-1165-8428, journal@mhi-ras.ru (Sevastopol, Russia)
- Yuri V. Artamonov** – Head Scientist Researcher of FSBSI FRC MHI, Dr.Sci. (Geogr.), ResearcherID: AAC-6651-2020 (Sevastopol, Russia)
- Sergey V. Berdnikov** – Director of FRC SSC of RAS, Dr.Sci. (Geogr.), ORCID ID: 0000-0002-3095-5532 (Rostov-on-Don, Russia)
- Valery G. Bondur** – Scientific Supervisor of ISR "AEROCOSMOS", academician of RAS, Dr.Sci. (Techn.), ORCID ID: 0000-0002-2049-6176 (Moscow, Russia)
- Demuri I. Demetrashvili** – Head of the sector of mathematical modeling of geophysical processes of sea and atmosphere, the Nodia Institute of Geophysics of the Javakhishvili Tbilisi State University, Dr.Sci. (Phys.-Math.), ORCID ID: 0000-0002-4789-4852 (Tbilisi, Georgia)
- Sergey A. Dobrolyubov** – Dean of Faculty of Geography of MSU, academician of RAS, Dr.Sci. (Geogr.), prof., ResearcherID: A-9688-2012 (Moscow, Russia)
- Grigory I. Dolgikh** – Director of POI FEB of RAS, Dr.Sci. (Phys.-Math.), academician of RAS, prof., ORCID ID: 0000-0002-2806-3834 (Vladivostok, Russia)
- Vladimir A. Dulov** – Head of Laboratory of FSBSI FRC MHI, Dr.Sci. (Phys.-Math.), prof., ORCID ID: 0000-0002-0038-7255, (Sevastopol, Russia)
- Vladimir V. Efimov** – Head of Department of FSBSI FRC MHI, Dr.Sci. (Phys.-Math.), prof., ResearcherID: P-2063-2017, (Sevastopol, Russia)
- Vladimir V. Fomin** – Head of Department of FSBSI FRC MHI, Dr.Sci. (Phys.-Math.), ORCID ID: 0000-0002-9070-4460, (Sevastopol, Russia)
- Isaac Gertman** – Head of the Physical Oceanography Department of Israel Oceanographic & Limnological Research, Head of IOLR data center ISRAMAR, Ph.D. (Geogr.), ORCID ID: 0000-0002-6953-6722 (Haifa, Israel)
- Dmitry G. Gryazin** – Head of Department, Chief Metrologist of SRC of the "Concern CSRI Elektropribor" JSC, Dr.Sci. (Techn.), prof. of Mechatronics of ITMO University, Scopus AuthorID: 25638150600, (Saint Petersburg, Russia)
- Rashit A. Ibraev** – Chief Scientist Researcher of INM of RAS, corresponding member of RAS, Dr.Sci. (Phys.-Math.), ORCID ID: 0000-0002-9099-4541 (Moscow, Russia)
- Igor K. Ivashchenko** – Senior Scientist of FSBSI FRC MHI, Ph.D. (Econ.) (Sevastopol, Russia)
- Vasily V. Knysh** – Head Scientist Researcher of FSBSI FRC MHI, Dr.Sci. (Phys.-Math.), prof., ResearcherID: B-3603-2018 (Sevastopol, Russia)
- Gennady K. Korotaev** – Scientific Supervisor of FSBSI FRC MHI, corresponding member of RAS, Dr.Sci. (Phys.-Math.), prof., ResearcherID: K-3408-2017 (Sevastopol, Russia)
- Vladimir N. Kudryavtsev** – Executive Director of Satellite Oceanography Laboratory of RSHU, Dr.Sci. (Phys.-Math.), prof., ResearcherID: G-1502-2014 (Saint Petersburg)
- Michael E. G. Lee** – Head of Department of FSBSI FRC MHI, Dr.Sci. (Phys.-Math.), prof., ORCID ID: 0000-0002-2292-1877 (Sevastopol, Russia)
- Gennady G. Matishov** – Deputy President of RAS, Deputy academician-Secretary of the Department of Earth Sciences of Supervisor of RAS – Head of the Oceanology, Atmospheric Physics and Geography Section, Scientific Supervisor of SSC of RAS, Supervisor of MMBI KSC of RAS, academician of RAS, Dr.Sci. (Geogr.), prof., ORCID ID: 0000-0003-4430-5220 (Rostov-on-Don, Russia)
- Nickolay A. Rimski-Korsakov** – Deputy Director (Marine Engineering) of FSBSI P.P. Shirshov IO of RAS, Dr.Sci. (Techn.), ResearcherID: K-8378-2017 (Moscow, Russia)
- Angelo Rubino** – Professor of Ca' Foscari University, Ph.D. (Phys. Oceanogr.), ORCID ID: 0000-0003-3857-4811 (Venice, Italy)
- Anatoly S. Samodurov** – Head of Department of FSBSI FRC MHI, Dr.Sci. (Phys.-Math.), ResearcherID: V-8642-2017 (Sevastopol, Russia)
- Georgy I. Shapiro** – Head of Plymouth Ocean Forecasting Centre of the University of Plymouth, Dr.Sci. (Phys.-Math.), prof. in Phys. Oceanogr., (Plymouth, Great Britain)
- Naum B. Shapiro** – Head Scientist Researcher of FSBSI FRC MHI, Dr.Sci. (Phys.-Math.), ResearcherID: A-8585-2017 (Sevastopol, Russia)
- Mikhail V. Shokurov** – Head Scientist Researcher of FSBSI FRC MHI, Dr.Sci. (Phys.-Math.), ORCID ID: 0000-0003-1595-8281 (Sevastopol, Russia)
- Elena F. Vasechkina** – Deputy Director of FSBSI FRC MHI, Chief Research Associate of FSBSI FRC MHI, Dr.Sci. (Geogr.), ORCID ID: 0000-0001-7007-9496 (Sevastopol, Russia)
- Elizaveta V. Zabolotskikh** – Head Scientist Researcher of RSHU, Dr.Sci. (Phys.-Math.), Scopus Author ID: 6506482460 (Saint Petersburg, Russian)
- Vladimir B. Zalesny** – Head Scientific Researcher of INM of RAS, Dr.Sci. (Phys.-Math.), prof., ORCID ID: 0000-0003-3829-3374 (Moscow, Russia)
- Andrey G. Zatsepin** – Chief of Laboratory of FSBSI P.P. Shirshov IO of RAS, Chief Research Associate of FSBSI P.P. Shirshov IO of RAS, Dr.Sci. (Phys.-Math.), ORCID ID: 0000-0002-5527-5234 (Moscow, Russia)
- George Zodiatis** – Senior Researcher of Laboratory of Coastal and Marine Research of the Institute of Applied and Computational Mathematics, for Research and Technology Foundation – Hellas, Ph.D. (Oceanol.), ResearcherID: J-3032-2013 (Heraklion, Crete, Greece)

CONTENTS

Vol. 31, no. 6. 2024

November – December, 2024

TOPICAL ISSUE

“Formation of carbon fluxes in marine environment”

Edited by Corresponding member of RAS **S. K. Konovalov**

ANALYSIS OF OBSERVATIONS AND METHODS OF CALCULATING HYDROPHYSICAL FIELDS IN THE OCEAN

- Sergeev D. A., Troitskaya Yu. I., Ermakova O. S., Orekhova N. A.** Investigation of the relationship between partial pressure of carbon dioxide and sea surface temperature in the cyclic seasonal variations in the Black Sea..... 757
- Sorokina V. V., Kulygin V. V.** Spatial and temporal dynamics of pH and total alkalinity of the Sea of Azov waters in 1950–2020..... 772
- Belokopytov V. N., Zhuk E. V.** Climatic variability of the Black Sea thermohaline characteristics (1950–2023)..... 788
- Churilova T. Ya., Suslin V. V., Krivenko O. V.** “Bloom” of coccolithophores in the Black Sea based on remote sensing data obtained in 1998–2023: Intensity and frequency 802

EXPERIMENTAL AND FIELD RESEARCH

- Alekseeva N. K., Nikulina A. L., Bloskina E. V., Shved Ya. V., Ryzhov I. V., Novikhin A. E., Makhotin M. S.** Biogeochemical characteristics of the surface layer and CO₂ fluxes in the ocean – atmosphere system in the fjords of Western Spitsbergen 826
- Mukoseev I. N., Orekhova N. A.** Suspended matter of the deep-water part of the Black Sea 838

MATHEMATICAL MODELING OF MARINE SYSTEMS

- Dorofeev V. L., Sukhikh L. I.** Distribution and vertical fluxes of particulate organic matter in the Black Sea based on the results of numerical modeling 851

AUTOMATION OF RESEARCH OF SEAS AND OCEANS

- Bovsun M. A., Dolgikh G. I., Dolgikh S. G., Ovcharenko V. V., Stepochkin I. E., Chupin V. A., Yatsuk A. V.** Results of monitoring of greenhouse gas concentrations and variations in the Earth’s crust deformations at Cape Schultz in winter period, 2023–2024..... 863



All the materials of the journal are available under Creative Commons Attribution-NonCommercial 4.0 International (CC BY-NC 4.0)

Original article

Investigation of the Relationship between Partial Pressure of Carbon Dioxide and Sea Surface Temperature in the Cyclic Seasonal Variations in the Black Sea

D. A. Sergeev^{1, 2, ✉}, Yu. I. Troitskaya¹, O. S. Ermakova¹,
N. A. Orekhova³

¹ Federal Research Center A. V. Gaponov-Grekhov Institute of Applied Physics of RAS,
Nizhny Novgorod, Russian Federation

² Lobachevsky State University of Nizhny Novgorod, Nizhny Novgorod, Russian Federation

³ Marine Hydrophysical Institute of RAS, Sevastopol, Russian Federation

✉ danil@ipfran.ru

Abstract

Purpose. The purpose of the study consists in describing the parameterization based on the field data, which take into account the relationship between the variability of $p\text{CO}_2$ sw and the state of the surface water layer, depending on the sea surface temperature and allowing for geographical location and seasonality at the example of the Black Sea.

Methods and Results. The main seasonal trends of changes in $p\text{CO}_2$ related to the variations in sea surface temperature are proposed based on special processing of direct measurement data on $p\text{CO}_2$ of the surface layer obtained in the cruises of R/V *Professor Vodyanitsky* in 2015–2023 and at the stationary observation point of the Black Sea Hydrophysical Subsatellite Polygon (BSHSP), Katsiveli, in 2012–2022. The basic approach consists in describing the variations in $p\text{CO}_2$ sw distribution over the sea surface using the linear approximations (trends) for three fixed seasons represented by four months (January – April, May – August and September – December) in each of the grid cells. It is shown that both in the coastal zone and in the open sea, the hysteresis dependences of $p\text{CO}_2$ upon the sea surface temperature are manifested: the ratios of partial pressure and temperature during the periods of spring warming and autumn cooling are different. The reason for the observed hysteresis is related to a shift of the $p\text{CO}_2$ sw fluctuation phase and a temperature change of about 1.5–2 months.

Conclusions. The dependence of $p\text{CO}_2$ upon the sea surface temperature in an autumn-winter period turns out to be close to the dependences typical for the oceanic conditions in mid latitudes of the Northern Hemisphere (the Atlantic and Pacific oceans). This can indicate the universal mechanisms of influence of the sea surface temperature (SST) upon $p\text{CO}_2$ sw both for the local conditions in the Black Sea and for the open ocean during a certain seasonal period. Besides, such a similarity of dependences can mean that, most likely, SST directly conditions a value of $p\text{CO}_2$ sw, whereas biological activity is not a determining factor. The obtained results can be used for describing and studying the variations of the CO_2 sea – air fluxes in the Black Sea.

Keywords: $p\text{CO}_2$, sea surface temperature, Black Sea

Acknowledgements: The study was carried out with financial support from grant No. 169-15-2023-002 (dated 01.03.2023) provided by the Federal Service for Hydrometeorology and Environmental Monitoring and within the framework of state assignment of FSBSI FRC MHI FNNN-2022-0002 on the theme “Monitoring of the carbonate system, CO_2 content and fluxes in the marine environment of the Black and Azov seas”. The data were analyzed and compared to the open ocean data with the support of the RSF project No. 24-17-00299.

For citation: Sergeev, D.A., Troitskaya, Yu.I., Ermakova, O.S. and Orekhova, N.A., 2024. Investigation of the Relationship between Partial Pressure of Carbon Dioxide and Sea Surface Temperature in the Cyclic Seasonal Variations in the Black Sea. *Physical Oceanography*, 31(6), pp. 757-771.

© 2024, D. A. Sergeev, Yu. I. Troitskaya, O. S. Ermakova, N. A. Orekhova

© 2024, Physical Oceanography



Introduction

The development of methods and approaches for estimating the global carbon dioxide (CO₂) flux between the atmosphere and the hydrosphere of our planet, with a particular focus on the World Ocean, is a vital aspect of comprehensive studies of the Earth's carbon cycle.

A comparison of the estimated annual CO₂ emissions associated with anthropogenic activity, the estimated net CO₂ absorption by the land and the hydrosphere of our planet and the observed rate of CO₂ content increase reveals an imbalance in the atmosphere [1–3]. The magnitude of this imbalance, according to estimates by different authors, also varies and can be 10–50% [2, 3]. According to the authors of [3], the estimated imbalance for each year since 1960 fluctuates between +3 and –2 PgC/year (where 1 PgC = 10¹⁵ g of pure carbon). Such values are comparable with the approximate average estimates of the volume of annual CO₂ absorption by the ocean, which is approximately 2 PgC/year (for the period 1990–2020, according to the 5th and 6th reports of the Intergovernmental Panel on Climate Change^{1, 2}). The high error, estimated at ± 0.5 PgC/year (90% confidence interval), demonstrates the challenges in correct assessment of this very important component of the carbon cycle. At the same time, the results of studies [2] indicate that the discrepancy in CO₂ calculated for 2013–2022 decreased to –0.4 PgC/year by 2023, representing 10% of the total carbon budget. However, different approaches are applied to estimate the global CO₂ flux between the atmosphere and the ocean, which can result in discrepancies in the magnitude of the imbalance:

- calculations using 3D models of global biogeochemical ocean circulation, taking into account interactions with the atmosphere (Global Circulation Model – GCM) [4–9];

- 3D models of atmospheric CO₂ inversion based on indirect analysis of long-term observation data from ground-based sensor networks [10–13] and remote sensing methods [14];

- methods for calculating CO₂ flux [15, 16] based on the data on spatio-temporal dynamics of CO₂ partial pressure in the surface layer of the ocean ($p\text{CO}_2_{sw}$) and in the atmospheric surface layer ($p\text{CO}_2_{air}$) applied in the model of the gas exchange rate k across the water – atmosphere interface. This approach takes into account the dependence on hydrometeorological factors and the solubility coefficient α :

$$F = k\alpha\Delta p\text{CO}_2 = k\alpha(p\text{CO}_2_{sw} - p\text{CO}_2_{air}). \quad (1)$$

¹ Canadell, J.G. and Monteiro, P.M.S., 2023. Global Carbon and Other Biogeochemical Cycles and Feedbacks. In: V. P. Masson-Delmotte and P. Zhai, eds., 2023. *Climate Change 2021: The Physical Science Basis. Working Group I Contribution to the Sixth Assessment Report of the Intergovernmental Panel on Climate Change*. New York, NY, USA; Cambridge, United Kingdom: Cambridge University Press, pp. 673-816. <https://doi.org/10.1017/9781009157896.007>

² Ciais, P. and Sabine, C., 2013. Carbon and Other Biogeochemical Cycles. In: T. F. Stoker, G.-K. Plattner, M. Tignor, S.K. Allen, J. Boschung, A. Nauels, Y. Xia, V. Bex and P.M. Midgley, eds., 2013. *Climate Change 2013: The Physical Science Basis. Working Group I Contribution to the Fifth Assessment Report of the Intergovernmental Panel on Climate Change*. New York, NY, USA; Cambridge, United Kingdom: Cambridge University Press, pp. 465-570. <https://doi.org/10.1017/CBO9781107415324.015>

The latter approach has the potential to yield the most accurate results; however, the results obtained using this method are highly dependent on the field data quality and the gas exchange rate model.

The selection of gas exchange rate model is important for correct assessment of CO₂ fluxes. Gas exchange rate k depends on the physicochemical properties (solubility and diffusion capacity D) of the gas and conditions of the atmosphere and ocean. Studies have revealed that the rate of gas exchange is also determined by turbulence in the boundary microlayers of air and water, which occurs as a result of wind stress [17, 18]. Consequently, the parameter k is typically parameterized through the wind velocity at a height of 10 m (U_{10}), in addition to wave parameters. Since measuring waves in natural conditions is usually challenging, the simplest models do not include wave parameters. Instead, they implicitly take into account their relationship with wind velocity. Such models include, for example, the widely used empirical formula for the gas exchange rate proposed in [19]:

$$k = [2.5 (0.5246 + 1.6256 \cdot 10^{-2} t + 4.9946 \cdot 10^{-4} t^2) + 0.3U_{10}^2] \left(\frac{Sc}{660}\right)^{1/2},$$

where Sc is the Schmidt number equal to the ratio of water kinematic viscosity to the diffusion capacity of the gas; t is the water temperature in °C. This approach to estimating CO₂ fluxes is widely used for the Black Sea.

The homogeneity of $p\text{CO}_2$ distribution in the near-surface layer of the ocean in time and space (across the entire World Ocean) is of particular importance for the accurate assessment of gas fluxes. Despite a notable increase in the number of shipboard measurements over the past decade, the installation of new measuring systems on large stationary platforms and the centralized replenishment of the SOCAT atlas database of partial pressure distribution in the World Ocean upper layer (accessible via <https://socat.info/>), these data remain assessed as scarce^{1,2}. This is primarily due to the significant spatio-temporal heterogeneity of population.

To populate the database with data of given spatial and temporal resolution based on available measurement results with no “gaps”, various approaches, including both classical 2D transport models in the near-surface layer [1] and new methods based on the use of neural networks and machine learning methods, are applied [20–28]. However, due to the limited amount of initial data, the final resolution, primarily spatial one, remains insufficient to determine the balance of carbon sources and sinks in the earth system.

The development of satellite methods makes it possible to obtain CO₂ flux estimates for the entire World Ocean. Nevertheless, these methods are indirect, and direct observations for the purpose of validating satellite measurements, the availability of which is limited, are still required [29, 30]. In any case, in order to determine the gas flux from satellite data, it is necessary to know the CO₂ concentrations both at the ocean surface and in the atmospheric surface layer. Furthermore, the gas transfer coefficient is also required [30]. Unfortunately, none of these parameters are determined directly from satellite data. In this case, the parameterization of the relationship between $p\text{CO}_2$ and sea surface temperature (SST) may assist in addressing the issue of data availability.

The uncertainty of CO₂ fluxes is particularly pronounced in coastal zones and inland seas, which are more dynamic systems on the scale of the World Ocean.

In such ecosystems, the impact of water dynamics, temperature fluctuations and the intensity of production and destruction processes on the carbon balance is considerably more significant and rapid than in the open ocean [31, 32].

The most promising approaches for correct balance assessment are those that construct models based on field data, taking into account the relationship between the variability of $p\text{CO}_2_{\text{sw}}$ value and the state of the near-surface water layer in a wide range of changing conditions, including SST, with regard to geographic location, seasonality, etc. The model was initially proposed in [33], wherein a database of monthly average values of $p\text{CO}_2_{\text{sw}}$ distribution on a uniform grid covering the entire World Ocean surface (free of ice) [15] was employed to develop algorithms for constructing $p\text{CO}_2_{\text{sw}}$ empirical dependencies on T_{sw} (the ocean surface temperature). The main objective of this study was to describe fluctuations in the $p\text{CO}_2_{\text{sw}}$ distribution across the surface using linear approximations (trends) for three fixed seasons of four months each (January – April, May – August, September – December) within each grid cell.

In [34] this method was significantly modified: the authors abandoned the fixed number of seasons (it can vary within 1–4) and used a minimum season duration of three months. For this period, linear approximations of $p\text{CO}_2_{\text{sw}}$ dependence on T_{sw} were selected once more. In this case, the number of linear approximations applied and the duration of seasons were selected based on the criterion of obtaining the maximum correlation coefficient when approximating the data ($p\text{CO}_2_{\text{sw}}$ and T_{sw}). The modified method was then applied to the updated database containing information on $p\text{CO}_2_{\text{sw}}$ [16]. As demonstrated by [34], this relatively straightforward approach made it possible to describe up to 70% of the variations in the CO_2 flux between the atmosphere and the ocean, obtained from the results of GCM modeling [7] and long-term data collected from several marine platforms.

The objective of this study is to apply a similar approach to describe the seasonal variations of $p\text{CO}_2_{\text{sw}}$ in the Black Sea and to perform parameterization based on field data that accounts for the relationship between $p\text{CO}_2_{\text{sw}}$ variability and the state of near-surface water layer depending on the water surface temperature, taking into account the geographical location and seasonality.

Research materials and methods

This study used the data from two different types of field measurements. Firstly, the data were obtained from shipboard measurements of $p\text{CO}_2$ in the surface water layer, conducted on board the R/V *Professor Vodyanitsky* (cruises No. 81, 87, 89, 91, 94, 95, 98, 101, 102, 108, 114, 117, 119, 125, 126) between November 2015 and March 2023. These measurements covered all hydrological seasons, with the exception of the winter period (January, February). Secondly, the measurement data were obtained at a stationary point for the carbon dioxide flux observations located on the oceanographic platform of the Black Sea Hydrophysical Subsatellite Polygon (BSHSP, Katsiveli) from May 2012 to October 2022. Taking into account the fundamentally different conditions of measurements (including their frequencies on a spatio-temporal scale and the distance from the shore), the shipboard data and

the data obtained at the platform were processed separately. The area under study and the scheme of sampling points are illustrated in Fig. 1.

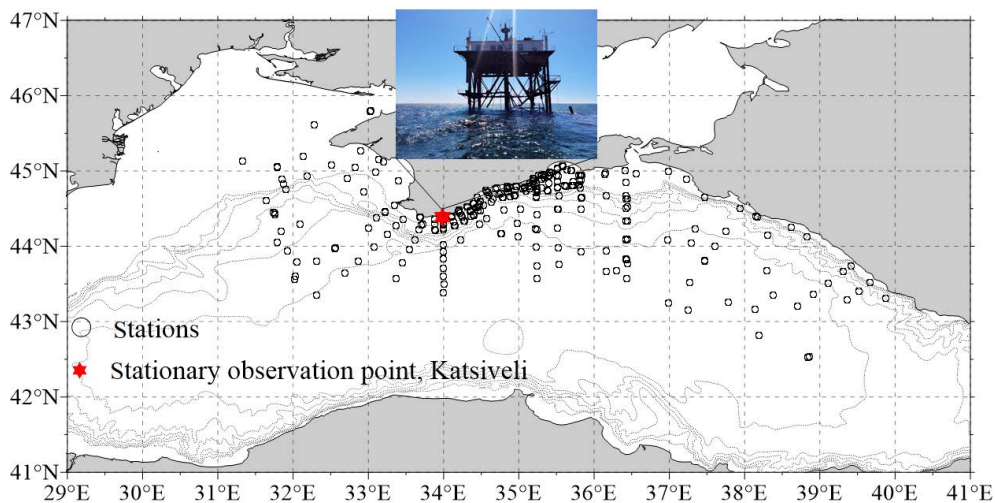


Fig. 1. Study area and sampling points for determining $p\text{CO}_2$ $_{\text{sw}}$ and the associated hydrometeorological conditions obtained at the R/V *Professor Vodyanitsky* and BSHSP stationary observation point

The hydrological characteristics (temperature and salinity of the surface water layer) were determined from the R/V *Professor Vodyanitsky* using the Sea-Bird 911 plus CTD or IDRONAUT OCEAN SEVEN 320PlusM probing systems. At stations with a depth of less than 50 m, a GAP AK-16 hydrological CTD probe was applied. The same characteristics at the BSHSP stationary observation point were obtained using a CTD48M hydrological probe (Sea & Sun Technology). In all cases, samples of the surface water layer (1.5–3.0 m) were collected using a submersible pump.

The volume concentration and $p\text{CO}_2$ were determined using LI-7000 infrared analyzer. The range of measured CO_2 concentrations is 0–3000 $\mu\text{mol/mol}$ with an error of 1% of the measured value [35]. The instrument was calibrated on a daily basis at two points: pure argon ($\text{CO}_2 = 0 \mu\text{mol/mol}$) and a certified calibration mixture with a volume fraction of CO_2 equal to 440 $\mu\text{mol/mol}$. Premium argon was used as the carrier gas. The conversion of CO_2 concentration ($\mu\text{mol/mol}$) to partial pressure of carbon dioxide (μatm) is performed using the following formula:

$$p\text{CO}_2 = x(\text{CO}_2) p_{\text{atm}}, \quad (2)$$

where $x(\text{CO}_2)$ is carbon dioxide concentration; p_{atm} is atmospheric pressure. A full description of the calculation is given in ³.

³ Dickson, A.G. and Goyet, C., 1994. *Handbook of Methods for the Analysis of the Various Parameters of the Carbon Dioxide System in Sea Water. Version 2*. Oak Ridge, TN: Oak Ridge National Laboratory (ORNL), 198 p. <https://doi.org/10.2172/10107773>

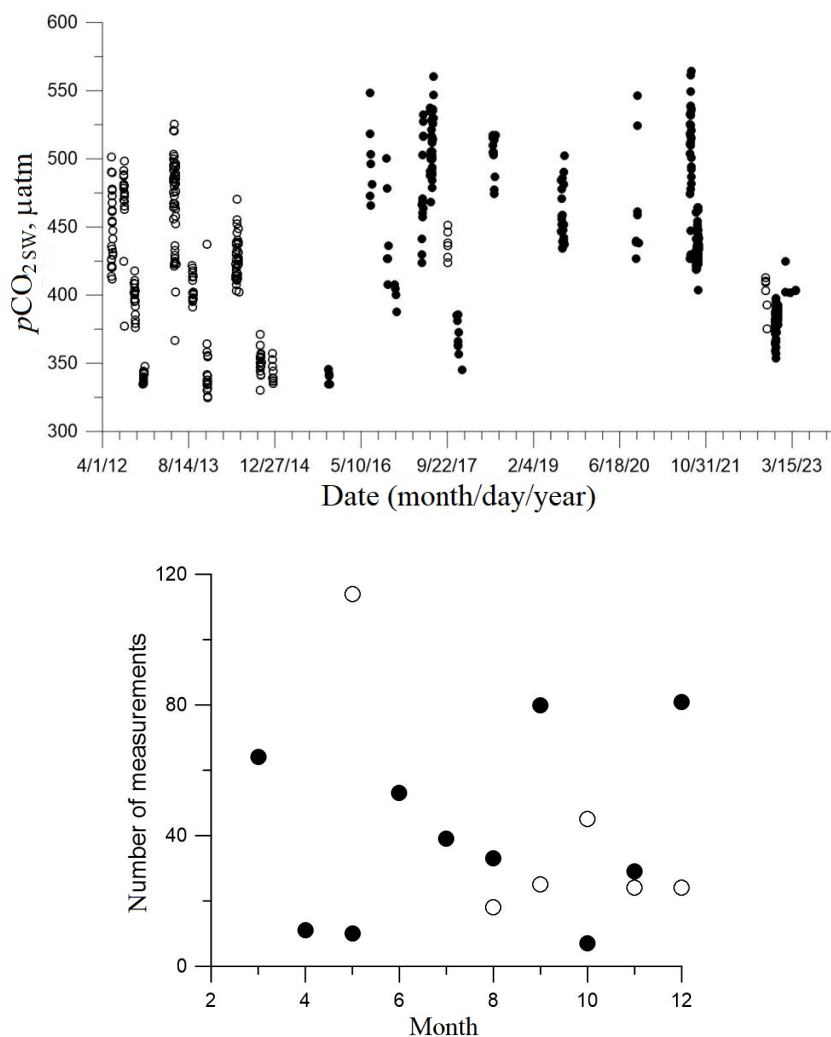


Fig. 2. Results of $p\text{CO}_{2\text{sw}}$ measurements: for the whole observation period (a) and a number of measurements by months (b). Dark circles denote the ship measurements, light ones – the measurements taken at the BSHSP stationary observation point

In conjunction with $p\text{CO}_{2\text{sw}}$, the accompanying meteorological parameters, namely wind velocity, atmospheric pressure and air temperature, were measured in the atmospheric surface layer using the recording equipment of the hydrometeorological data collection complex [36]. The data underwent quality control, with unreliable fragments being rejected, and were reduced to the standard observation height (10 m). According to the guidelines set forth by the World Meteorological Organization, the recorded data were averaged over a 10-minute period and further analysis was conducted on the averaged values [36].

Data were obtained on 395 measurements carried out from the vessel and 250 from the stationary observation point of the BSHSP. Figure 2 presents

a comprehensive overview of $p\text{CO}_2_{\text{sw}}$ measurements. These dependencies indicate that the data are distributed very unevenly with regard to both years and seasons.

The data for January and February are unavailable, which is due to the difficulties of performing expeditionary research. Furthermore, the quantity of data in spring is limited. The largest quantity of data was obtained in summer and early autumn, which is due to favorable conditions for carrying out expeditionary work. Taking into account such strong heterogeneity in time due to the small amount of data, it was decided not to separate the shipboard measurements by space and to combine the data from different points in the Black Sea. In addition, as shown in [37], the $p\text{CO}_2$ data for the water surface layer, shelf and deep-water areas of the Black Sea do not differ statistically.

Results and discussion

Due to the insufficient amount of data, it is not possible to identify correlations between seasonal changes in $p\text{CO}_2_{\text{sw}}$ and T_{sw} based on the results of studies conducted in any particular year for the specified periods. In this regard, a parallel can be drawn with [16], whereby all data are recalculated for one of the selected (central) years. When processing data for both types of measurements, 2019 was selected as the central reference point. The data for this year were used without adjustments, whereas the data obtained in previous years were adjusted in consideration of the interannual trend in atmospheric CO_2 concentration. Correct assessment of the interannual trend in $p\text{CO}_2_{\text{sw}}$ is an important point. Small amount of data and their uneven distribution by seasons do not allow to obtain an accurate estimate. In the study [16], which analyzed the data for almost 50 years of observations, it was noted that when the data from the entire ocean area were averaged within confidence intervals ($\sim 30\%$), the global trends in the $p\text{CO}_2$ increase in the ocean and atmosphere coincided. On this basis, the authors of the study [34] proposed that the observed changes in $p\text{CO}_2$ can be described as a superposition of the global atmospheric trend and variations associated with changes in water temperature T_{sw} . Taking this into account, we applied a trend of $2.4 \mu\text{atm}/\text{year}$ for $p\text{CO}_2$ in the atmosphere obtained from the measurement data of the Mauna Loa Observatory (Hawaii) for the period 2012–2022. This estimate is also close to the one determined by NCEP reanalysis data for the Black Sea over the period 2015–2022.

Once all the data had been reduced to 2019, the mean values and standard deviations for the measured parameters ($p\text{CO}_2$ and surface water temperature) for each month were calculated.

A preliminary analysis identified three characteristic seasonal trends in the dependence of $p\text{CO}_2_{\text{sw}}$ on temperature, which form a cycle of seasonal changes in partial pressure (Fig. 3, *a*).

In Fig. 3, the following notations are used: black circles – according to measurements from the vessel, red ones – from the stationary observation point of the BSHSP; lines are results of linear approximation for the selected seasonal periods: green line for the end of winter – end of spring, red one – for the end of

spring – end of summer, blue – for the end of summer – autumn – beginning of winter; solid lines are for data from vessel measurements, dashed lines are for data from the platform; light circles are data for the Atlantic Ocean, triangles are for the Pacific Ocean (data for the oceans are taken from the study [34]) with the corresponding linear approximations.

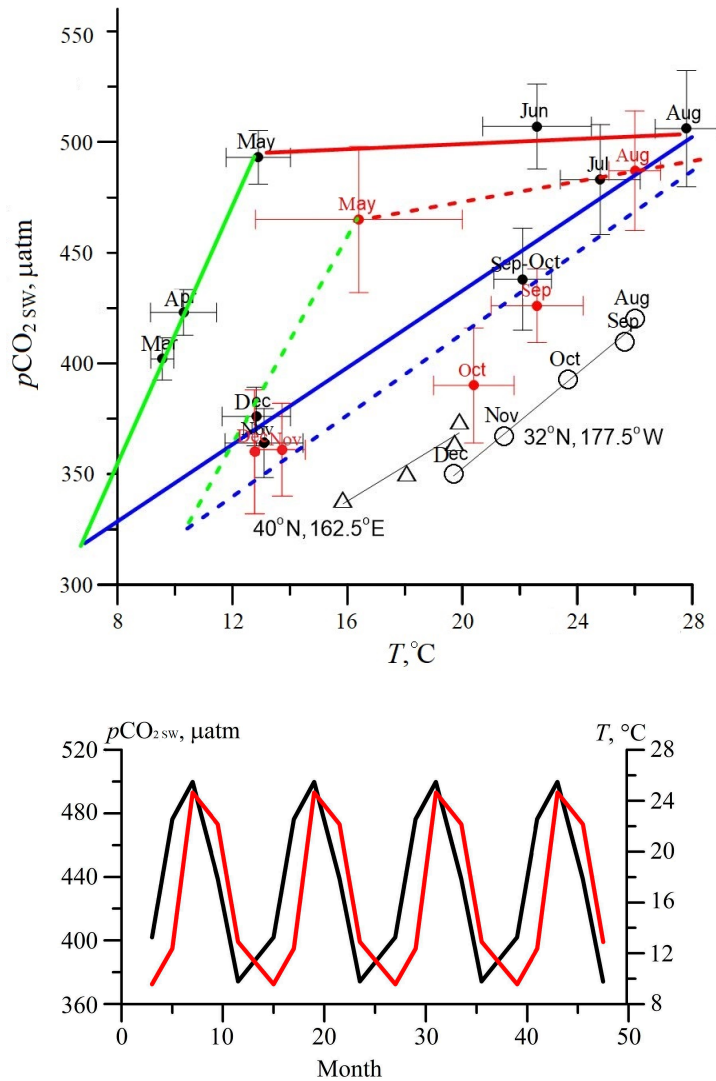


Fig. 3. Dependences of the monthly average $p\text{CO}_2 \text{ sw}$ on SST (all the data are reduced to 2019) (a), and periodically continued dependences of $p\text{CO}_2 \text{ sw}$ (black line) and SST (red line) upon time (b)

The first trend is a sharp increase in $p\text{CO}_2_{\text{sw}}$ levels with a temperature rise in the latter half of the spring season (late March – April – mid-May). Unfortunately, there is little data available for this time of year; however, the upward trend is evident. Subsequently, during the summer months (June – August), there is a gradual increase in $p\text{CO}_2_{\text{sw}}$ with a significant temperature rise. Furthermore, from September to December, there is a gradual decline (compared to spring) in CO_2 concentration with a temperature drop. Thus, the $p\text{CO}_2_{\text{sw}}$ dependence on water temperature is of hysteresis nature: the same value of water temperature corresponds to different $p\text{CO}_2_{\text{sw}}$ values during the spring and autumn periods. By plotting the $p\text{CO}_2$ and T_{sw} dependences on time and continuing the resulting periodic dependence with a 12-month period (Fig. 3, *b*), it becomes evident that the observed hysteresis is associated with a phase shift in $p\text{CO}_2_{\text{sw}}$ oscillations and a temperature variation by approximately 1.5–2 months.

Extremely uneven data distribution across different seasons is also worth noting. For example, in April, little data was received and they correspond either to the beginning or the end of the month, i.e., they most likely refer to March or May, respectively. A similar situation is observed with the data for October, which can be combined with those obtained in September. The average SST recorded in August was found to be almost two degrees higher than the average SST for 2019. This discrepancy can be attributed to the limited number of measurements conducted at the beginning of the month, with the majority of data obtained in the daytime.

The linear approximations were determined for each of the three seasonal sections in accordance with the processing results. It should be noted that the spring (green line) and winter (blue) periods intersect at a point with a temperature of $7.6\text{ }^\circ\text{C}$, which is only $0.2\text{ }^\circ\text{C}$ less than the average SST for February 2019. This provides evidence that the constructed approximations are accurate. In other words, the corner points in Fig. 3 correspond to the “triangular” cycle of seasonal changes, and they can be attributed to February, late May – early June and August.

A comparable methodology was used in the analysis of the data obtained from the BSHSP stationary observation point. It is noteworthy that a limited amount of data was recorded during the summer months (specifically, in August) and the spring season (in May). At the same time, there was a significant amount of data in autumn and early winter. For comparison with the shipboard measurements, the data from the BSHSP observation point were adjusted for 2019 with the same coefficient of $p\text{CO}_2$ variation in the atmosphere and averaged for each month. The greatest difference by month between the measurements from R/V *Professor Vodyanitsky* during the expeditions and at the stationary observation point in Katsiveli was observed in the data for May, although a considerable variability in the data set should also be noted.

Based on the foregoing, we can assume that the most significant changes in the nature of the dependence occur during May – June. Since there are no available data for January – April for the stationary observation point, the spring approximation (green dashed line) was taken as a straight line connecting the point corresponding to May and the point on the blue dashed line where the water temperature is approximately equal to the average temperature for February 2019 for the area of the stationary observation point ($7.6\text{ }^\circ\text{C}$). The comparison demonstrated

that, despite the absence of data during the spring and summer periods and a considerable scatter in May, the general nature of the cyclical seasonal dependence of $p\text{CO}_2_{\text{sw}}$ on SST was preserved (Fig. 3, *a*).

Taking into account the obtained data, the “triangle” of seasonal changes for the data from the stationary observation point has shifted slightly downwards and sideways (almost parallel transport), which is associated, among other things, with a higher average water temperature in the coastal zone.

The revealed similarity in the behavior of $p\text{CO}_2_{\text{sw}}$ dependence on temperature for the measurements from the stationary observation point and numerous shipboard ones carried out over the past 10 years indicates that this dependence is universal for the entire Black Sea.

Furthermore, the constructed dependencies of monthly average $p\text{CO}_2_{\text{sw}}$ on surface water temperature were compared with similar dependencies obtained earlier for the open ocean using the data from [34]. The comparison demonstrated that, in the absence of similarities between the late winter to spring to mid-summer period and the late summer – autumn – early winter period in the subtropical and temperate zones of the Atlantic and Pacific Oceans of the Northern Hemisphere, the change trends were very close to each other (Fig. 3, *a*). In the Black Sea the trend was $\sim 8.8 \mu\text{atm/degree}$, in the Atlantic Ocean $10.1 \mu\text{atm/degree}$, in the Pacific Ocean $7.9 \mu\text{atm/degree}$. This may indicate universal mechanisms of the SST effect on $p\text{CO}_2_{\text{sw}}$ both for local conditions of the Black Sea and for the open ocean during this seasonal period.

Trends in the dependence of $p\text{CO}_2_{\text{sw}}$ on temperature determined based on monthly average data regarding to 2019

Month	Based on expedition data obtained at <i>Professor Vodyanitsky</i>	Based on data obtained at BSHSP stationary point
January	$p\text{CO}_2_{\text{sw}} = 8.85 \cdot T + 253.30$ (no data for January, it is an assumption)	$p\text{CO}_2_{\text{sw}} = 8.75 \cdot T + 237.76$ (no data for January, it is an assumption)
February	$p\text{CO}_2_{\text{sw}} = 8.85 \cdot T + 253.30$ (no data for February, it is an assumption)	?? (dependence is not defined)
March	$p\text{CO}_2_{\text{sw}} = 27.16 \cdot T + 142.73$?? (dependence is not defined)
April	$p\text{CO}_2_{\text{sw}} = 27.16 \cdot T + 142.73$?? (dependence is not defined)
May	$p\text{CO}_2_{\text{sw}} = 27.16 \cdot T + 142.73$ $p\text{CO}_2_{\text{sw}} = 0.44 \cdot T + 487.47$?? (dependence is not defined) $p\text{CO}_2_{\text{sw}} = 2.29 \cdot T + 427.42$
June	$p\text{CO}_2_{\text{sw}} = 0.44 \cdot T + 487.47$	$p\text{CO}_2_{\text{sw}} = 2.29 \cdot T + 427.42$
July	$p\text{CO}_2_{\text{sw}} = 0.44 \cdot T + 487.47$	$p\text{CO}_2_{\text{sw}} = 2.29 \cdot T + 427.42$
August	$p\text{CO}_2_{\text{sw}} = 0.44 \cdot T + 487.47$ $p\text{CO}_2_{\text{sw}} = 8.85 \cdot T + 253.30$	$p\text{CO}_2_{\text{sw}} = 2.29 \cdot T + 427.42$ $p\text{CO}_2_{\text{sw}} = 8.75 \cdot T + 237.76$
September	$p\text{CO}_2_{\text{sw}} = 8.85 \cdot T + 253.30$	$p\text{CO}_2_{\text{sw}} = 8.75 \cdot T + 237.76$
October	$p\text{CO}_2_{\text{sw}} = 8.85 \cdot T + 253.30$	$p\text{CO}_2_{\text{sw}} = 8.75 \cdot T + 237.76$
November	$p\text{CO}_2_{\text{sw}} = 8.85 \cdot T + 253.30$	$p\text{CO}_2_{\text{sw}} = 8.75 \cdot T + 237.76$
December	$p\text{CO}_2_{\text{sw}} = 8.85 \cdot T + 253.30$	$p\text{CO}_2_{\text{sw}} = 8.75 \cdot T + 237.76$

Note: The table cells corresponding to May and August are highlighted in gray since two approximations converge in them.

The formulas for all linear approximations obtained during the data processing stage are presented in the Table. The basic formula represents the linear approximation of the dependence of partial pressure on water temperature with reference to the global trend of CO₂ concentration in the atmosphere. Using the obtained dependencies, it is possible to estimate the average monthly difference in $p\text{CO}_2$ at the interface between the water surface layer and the atmosphere for any given month of any given year as follows:

$$\Delta p\text{CO}_{2\ y,m} = \left[p\text{CO}_{2\ sw,2019\ m} + \left(\frac{\partial p\text{CO}_{2\ sw}}{\partial T^\circ} \right)_{2019\ m} \cdot \Delta T^\circ_{y,m-2019} \right] - p\text{CO}_{2\ air,2019\ m}, \quad (3)$$

in this case, the data on $p\text{CO}_2$ for the atmosphere can be obtained from reanalysis (similar to that presented in [38]) or by direct measurement.

In order to calculate the average monthly CO₂ flux through the sea surface, the $p\text{CO}_2$ gradient between the water surface layer and the atmospheric surface layer must be multiplied by the gas exchange rate and solubility, according to the equation (1) presented previously.

Conclusion

In this study, we proposed a model to describe the dependencies linking seasonal variations in $p\text{CO}_{2\ sw}$ with SST seasonal changes. These dependences are based on a special processing of direct $p\text{CO}_{2\ sw}$ measurements data carried out in expeditionary conditions from the R/V *Professor Vodyanitsky* (2015–2023) and at BSHSP stationary observation point (2012–2022). As a result, a cycle characterised by a rapid increase in $p\text{CO}_{2\ sw}$ in spring, an insignificant increase in summer and a smooth decrease in autumn–winter was obtained. The $p\text{CO}_{2\ sw}$ dependence upon water temperature is hysteresis in nature, whereby the same value of water temperature corresponds to different $p\text{CO}_{2\ sw}$ values in spring and autumn. This dependence is associated with a phase shift in $p\text{CO}_{2\ sw}$ oscillations and a temperature change of about 1.5–2 months.

A similar type of this cycle was independently demonstrated by processing measurements derived from both the vessel and the platform. It is noteworthy that the downward trend observed during the autumn-winter and winter periods was comparable to the trend observed in the open ocean conditions at Northern Hemisphere temperate and subtropical latitudes. It seems probable that the SST is the primary factor determining $p\text{CO}_{2\ sw}$, with biological activity having a lesser influence.

The sharp $p\text{CO}_{2\ sw}$ increase observed in spring requires further research to determine its underlying causes, primarily due to the limited amount of field data currently available. However, it can also be argued that at least biological processes associated with photosynthesis do not play a decisive role in this case. Otherwise, a negative trend would be expected rather than a positive one. Thus far, no negative trends have been identified when $p\text{CO}_{2\ sw}$ decreases with an increase in temperature, or vice versa, based on the available data set. In the future, it is necessary to continue research using accompanying data on ongoing biogeochemical processes.

The obtained result enables us to estimate interannual variations in the global CO₂ flux associated with corresponding temperature changes. It should be emphasized once again that the result was obtained on the basis of the assumption that the interannual trend in $p\text{CO}_2_{\text{sw}}$ is equivalent to that observed in the atmosphere of our planet. This assumption also requires further study, primarily to obtain more data, given that regional differences in $p\text{CO}_2_{\text{sw}}$ interannual trends can still be observed, particularly in coastal areas.

The $p\text{CO}_2_{\text{sw}}$ measurements were conducted at the Shared Use Center of the R/V *Professor Vodyanitsky* of FSBSI FRC “A.O. Kovalevsky Institute of Biology of Southern Seas” of RAS.

REFERENCES

1. Sarmiento, J.L. and Gruber, N., 2002. Sinks for Anthropogenic Carbon. *Physics Today*, 55(8), pp. 30-36. <https://doi.org/10.1063/1.1510279>
2. Friedlingstein, P., O’Sullivan, M., Jones, M.W., Andrew, R.M., Bakker, D.C.E., Hauck, J., Landschützer, P., Le Quéré, C., Luijckx, I.T. [et al.], 2023. Global Carbon Budget 2023. *Earth System Science Data*, 15(12), pp. 5301-5369. <https://doi.org/10.5194/essd-15-5301-2023>
3. Le Quéré, C., Raupach, M.R., Canadell, J.G., Marland, G., Bopp, L., Ciais, P., Conway, T.J., Doney, S.C., Feely, R.A. [et al.], 2009. Trends in the Sources and Sinks of Carbon Dioxide. *Nature Geoscience*, 2(12), pp. 831-836. <https://doi.org/10.1038/ngeo689>
4. Le Quéré, C., Aumont, O., Bopp, L., Bousquet, P., Ciais, P., Francey, R., Heimann, M., Keeling, C.D., Keeling, R.F. [et al.], 2003. Two Decades of Ocean CO₂ Sink and Variability. *Tellus B: Chemical and Physical Meteorology*, 55(2), pp. 649-656. <https://doi.org/10.3402/tellusb.v55i2.16719>
5. Obata, A. and Kitamura, Y., 2003. Interannual Variability of the Sea-Air Exchange of CO₂ from 1961 to 1998 Simulated with a Global Ocean Circulation-Biogeochemistry Model. *Journal of Geophysical Research: Oceans*, 108(C11), 3337. <https://doi.org/10.1029/2001JC001088>
6. McKinley, G.A., Rödenbeck, C., Gloor, M., Houweling, S. and Heimann, M., 2004. Pacific Dominance to Global Air-Sea CO₂ Flux Variability: A Novel Atmospheric Inversion Agrees with Ocean Models. *Geophysical Research Letters*, 31(22), L22308. <https://doi.org/10.1029/2004GL021069>
7. Doney, S.C., Lima, I., Feely, R.A., Glover, D.M., Lindsay, K., Mahowald, N., Moore, J.K. and Wanninkhof, R., 2009. Mechanisms Governing Interannual Variability in Upper-Ocean Inorganic Carbon System and Air-Sea CO₂ Fluxes: Physical Climate and Atmospheric Dust. *Deep Sea Research II*, 56(8-10), pp. 640-655. <https://doi.org/10.1016/j.dsr2.2008.12.006>
8. Law, R.M., Ziehn, T., Matear, R.J., Lenton, A., Chamberlain, M.A., Stevens, L.E., Wang, Y.-P., Sribinovsky, J., Bi, D. [et al.], 2017. The Carbon Cycle in the Australian Community Climate and Earth System Simulator (ACCESS-ESM1) – Part 1: Model Description and Pre-Industrial Simulation. *Geoscientific Model Development*, 10(7), pp. 2567-2590. <https://doi.org/10.5194/gmd-10-2567-2017>
9. Hauck, J., Köhler, P., Wolf-Gladrow, D. and Völker, C., 2016. Iron Fertilisation and Century-Scale Effects of Open Ocean Dissolution of Olivine in a Simulated CO₂ Removal Experiment. *Environmental Research Letters*, 11(2), 024007. <https://doi.org/10.1088/1748-9326/11/2/024007>
10. Bousquet, P., Peylin, P., Ciais, P., Le Quéré, C., Friedlingstein, P. and Tans, P.P., 2000. Regional Changes in Carbon Dioxide Fluxes of Land and Oceans since 1980. *Science*, 290(5495), pp. 1342-1346. <https://doi.org/10.1126/science.290.5495.1342>
11. Rödenbeck, C., Houweling, S., Gloor, M. and Heimann, M., 2003. CO₂ Flux History 1982–2001 Inferred from Atmospheric Data Using a Global Inversion of Atmospheric Transport. *Atmospheric Chemistry and Physics*, 3(6), pp. 1919-1964. <https://doi.org/10.5194/acp-3-1919-2003>

12. Saeki, T. and Patra, P.K., 2017. Implications of Overestimated Anthropogenic CO₂ Emissions on East Asian and Global Land CO₂ Flux Inversion. *Geoscience Letters*, 4(1), 9. <https://doi.org/10.1186/s40562-017-0074-7>
13. Van der Laan-Luijkx, I.T., Van der Velde, I.R., Van der Veen, E., Tsuruta, A., Stanislawski, K., Babenhauserheide, A., Zhang, H.F., Liu, Y., He, W. [et al.], 2017. The Carbon Tracker Data Assimilation Shell (CTDAS) v1.0: Implementation and Global Carbon Balance 2001–2015. *Geoscientific Model Development*, 10(7), pp. 2785-2800. <https://doi.org/10.5194/gmd-10-2785-2017>
14. Chevallier, F., Fisher, M., Peylin, P., Serrar, S., Bousquet, P., Bréon, F.-M., Chédin, A. and Ciais, P., 2005. Inferring CO₂ Sources and Sinks from Satellite Observations: Method and Application to TOVS Data. *Journal of Geophysical Research: Atmospheres*, 110(D24), D24309. <https://doi.org/10.1029/2005jd006390>
15. Takahashi, T., Feely, R.A., Weiss, R.F., Wanninkhof, R.H., Chipman, D.W., Sutherland, S.C. and Takahashi, T.T., 1997. Global Air-Sea Flux of CO₂: An Estimate Based on Measurements of Sea-Air pCO₂ Difference. *Proceedings of the National Academy of Sciences of the USA*, 94(16), pp. 8292-8299. <https://doi.org/10.1073/pnas.94.16.8292>
16. Takahashi, T., Sutherland, S.C., Wanninkhof, R., Sweeney, C., Feely, R.A., Chipman, D.W., Hales, B., Friederich, G., Chavez, F. [et al.], 2009. Climatological Mean and Decadal Change in Surface Ocean pCO₂, and Net Sea-Air CO₂ Flux over the Global Oceans. *Deep Sea Research Part II: Topical Studies in Oceanography*, 56(8–10), pp. 554-577. <https://doi.org/10.1016/j.dsr2.2008.12.009>
17. Jähne, B., Münnich, K.O., Börsinger, R., Dutzi, A., Huber, W.A. and Libner, P., 1987. On the Parameters Influencing Air-Water Gas Exchange. *Journal of Geophysical Research: Oceans*, 92(C2), pp. 1937-1949. <https://doi.org/10.1029/JC092iC02p01937>
18. Komori, S., Nagaosa, R. and Murakami, Y., 1993. Turbulence Structure and Mass Transfer across a Sheared Air-Water Interface in Wind-Driven Turbulence. *Journal of Fluid Mechanics*, 249, pp.161-183. <https://doi.org/10.1017/S0022112093001120>
19. Wanninkhof, R., 1992. Relationship between Wind Speed and Gas Exchange over the Ocean. *Journal of Geophysical Research*, 97(C5), pp. 7373-7382. <https://doi.org/10.1029/92JC00188>
20. Zeng, J., Nojiri, Y., Landschützer, P., Telszewski, M. and Nakaoka, S., 2014. A Global Surface Ocean fCO₂ Climatology Based on a Feed-Forward Neural Network. *Journal of Atmospheric and Oceanic Technology*, 31(8), pp. 1838-1849. <https://doi.org/10.1175/jtech-d-13-00137.1>
21. Rödenbeck, C., Bakker, D.C.E., Gruber, N., Iida, Y., Jacobson, A.R., Jones, S., Landschützer, P., Metz, N., Nakaoka, S. [et al.], 2015. Data-Based Estimates of the Ocean Carbon Sink Variability – First Results of the Surface Ocean pCO₂ Mapping Intercomparison (SOCOM). *Biogeosciences*, 12(23), pp. 7251-7278. <https://doi.org/10.5194/bg-12-7251-2015>
22. Bakker, D.C.E., Pfeil, B., Landa, C.S., Metz, N., O'Brien, K.M., Olsen, A., Smith, K., Cosca, C., Harasawa, S. [et al.], 2016. A Multi-Decade Record of High-Quality fCO₂ Data in Version 3 of the Surface Ocean CO₂ Atlas (SOCAT). *Earth System Science Data Discussions*, 8(2), pp. 383-413. <https://doi.org/10.5194/essd-2016-15>
23. Landschützer, P., Gruber, N. and Bakker, D.C.E., 2016. Decadal Variations and Trends of the Global Ocean Carbon Sink. *Global Biogeochemical Cycles*, 30(10), pp. 1396-1417. <https://doi.org/10.1002/2015gb005359>
24. McKinley, G.A., Fay, A.R., Lovenduski, N.S. and Pilcher, D.J., 2017. Natural Variability and Anthropogenic Trends in the Ocean Carbon Sink. *Annual Review of Marine Science*, 9(1), pp. 125-150. <https://doi.org/10.1146/annurevmarine-010816-060529>
25. Gregor, L., Lebehot, A.D., Kok, S. and Scheel Monteiro, P.M., 2019. A Comparative Assessment of the Uncertainties of Global Surface Ocean CO₂ Estimates Using a Machine-Learning Ensemble (CSIR-ML6 Version 2019a) – Have we Hit the Wall? *Geoscientific Model Development*, 12(12), pp. 5113-5136. <https://doi.org/10.5194/gmd-12-5113-2019>
26. Gruber, N., Clement, D., Carter, B.R., Feely, R.A., van Heuven, S., Hoppema, M., Ishii, M., Key, R.M., Kozyr, A. [et al.], 2019. The Oceanic Sink for Anthropogenic CO₂ from 1994 to 2007. *Science*, 363(6432), pp. 1193-1199. <https://doi.org/10.1126/science.aau5153>

27. Denvil-Sommer, A., Gehlen, M., Vrac, M. and Mejia, C., 2019. LSCE-FFNN-v1: A Two-Step Neural Network Model for the Reconstruction of Surface Ocean pCO₂ over the Global Ocean. *Geoscientific Model Development*, 12(5), pp. 2091-2105. <https://doi.org/10.5194/gmd-12-2091-2019>
28. Iida, Y., Takatani, Y., Kojima, A. and Ishii, M., 2020. Global Trends of Ocean CO₂ Sink and Ocean Acidification: An Observation-Based Reconstruction of Surface Ocean Inorganic Carbon Variables. *Journal of Oceanography*, 77(2), pp. 323-358. <https://doi.org/10.1007/s10872-020-00571-5>
29. Gulev, S.K., 2023. Global Climate Change and the Oceans. *Studies on Russian Economic Development*, 34(6), pp. 738-745. <https://doi.org/10.1134/S1075700723060060>
30. Pipko, I.I., Pugach, S.P., Repina, I.A., Dudarev, O.V., Charkin, A.N. and Semiletov, I.P., 2015. Distribution and Air-Sea Fluxes of Carbon Dioxide on the Chukchi Sea Shelf. *Izvestiya, Atmospheric and Oceanic Physics*, 51, pp. 1088-1102. <https://doi.org/10.1134/S0001433815090133>
31. Bates, N.R., 2018. Seawater Carbonate Chemistry Distributions across the Eastern South Pacific Ocean Sampled as Part of the GEOTRACES Project and Changes in Marine Carbonate Chemistry over the Past 20 Years. *Frontiers in Marine Science*, 5, 398. <https://doi.org/10.3389/fmars.2018.00398>
32. Bauer, J.E., Cai, W.-J., Raymond, P.A., Bianchi, T.S., Hopkinson, C.S. and Régnier, P.A.G., 2013. The Changing Carbon Cycle of the Coastal Ocean. *Nature*, 504, pp. 61-70. <https://doi.org/10.1038/nature12857>
33. Lee, K., Wanninkhof, R., Takahashi, T., Doney, S.C. and Feely, R.A., 1998. Low Interannual Variability in Recent Oceanic Uptake of Atmospheric Carbon Dioxide. *Nature*, 396, pp. 155-159. <https://doi.org/10.1038/24139>
34. Park, G.-H., Wanninkhof, R., Doney, S.C., Takahashi, T., Lee, K., Feely, R.A., Sabine, C.L., Triñanes, J. and Lima, I.D., 2010. Variability of Global Net Sea-Air CO₂ Fluxes over the Last Three Decades Using Empirical Relationships. *Tellus B: Chemical and Physical Meteorology*, 62(5), pp. 352-368. <https://doi.org/10.1111/j.1600-0889.2010.00498.x>
35. Khoruzhiy, D.S., 2010. Usage of Device Complex AS-C3 for Detection of Carbon Dioxide Partial Pressure and Inorganic Carbon Concentration in Sea Environment. MHI, 2010. *Ekologicheskaya Bezopasnost' Pribrezhnoy i Shel'fovoy Zon i Kompleksnoe Ispol'zovanie Resursov Shel'fa* [Ecological Safety of Coastal and Shelf Zones and Comprehensive Use of Shelf Resources]. Sevastopol: MHI. Iss. 23, pp. 260-272 (in Russian).
36. Garmashov, A., 2020. Hydrometeorological Monitoring on the Stationary Oceanographic Platform in the Black Sea. In: SGEM, 2020. *20th International Multidisciplinary Scientific GeoConference SGEM 2020: Proceedings*. Sofia, Bulgaria. Vol. 20, Book 3.1, pp. 171-176. <https://doi.org/10.5593/sgem2020/3.1/s12.023>
37. Konovalov, S.K. and Orekhova, N.A., 2024. New View of the CO₂ Content in Surface Waters of the Black Sea Based on Direct Measurements. *Doklady Earth Science*, 518, pp. 1737-1742. <https://doi.org/10.1134/S1028334X24602943>
38. Watson, A.J., Schuster, U., Bakker, D.C.E., Bates, N.R., Corbière, A., González-Dávila, M., Friedrich, T., Hauck, J., Heinze, C. [et al.], 2009. Tracking the Variable North Atlantic Sink for Atmospheric CO₂. *Science*, 326, pp. 1391-1393. <https://doi.org/10.1126/science.1177394>

Submitted 14.06.2024; approved after review 09.07.2024;

accepted for publication 12.09.2024.

About the authors:

Daniil A. Sergeev, Head of Laboratory of Experimental Methods in Geophysical and Technical Hydrodynamics, Federal Research Center A.V. Gaponov-Grekhov Institute of Applied Physics of RAS (46 Ulyanova Str., Nizhny Novgorod, 603950, Russian Federation), CSc (Phys.-Math.), **ORCID ID: 0000-0003-4910-3935**, **ResearcherID: L-4569-2016**, **Scopus Author ID: 660388734**, daniil@ipfran.ru

Yulia I. Troitskaya, Head of the Department of Nonlinear Geophysical Processes, Federal Research Center A.V. Gaponov-Grekhov Institute of Applied Physics of RAS (46 Ulyanova Str., Nizhny Novgorod, 603950, Russian Federation), DSc (Phys.-Math.), **ORCID ID: 0000-0002-1387-970X**, **ResearcherID: F-1352-2015**, **Scopus Author ID: 35784884700**, yuliya@ipfran.ru

Olga S. Ermakova, Senior Researcher, Laboratory of Nonlinear Physics of Natural Processes, Federal Research Center A.V. Gaponov-Grekhov Institute of Applied Physics of RAS (46 Ulyanova Str., Nizhny Novgorod, 603950, Russian Federation), CSc (Phys.-Math.), **ORCID ID: 0000-0003-0687-4000**, **ResearcherID: D-3643-2015**, **Scopus Author ID: 16051997000**, o.s.ermakova@mail.ru

Natalia A. Orekhova, Head of Laboratory for Monitoring and Research of Greenhouse Gases and Oxygen in the Marine Environment, Marine Hydrophysical Institute of RAS (2 Kapitanskaya Str., Sevastopol, 299011, Russian Federation), CSc (Geogr.), **ORCID ID: 0000-0002-1387-970X**, **ResearcherID: I-1755-2017**, **Scopus Author ID: 35784884700**, natalia.orekhova@mhi-ras.ru

Contribution of the co-authors:

Daniil A. Sergeev – literary review, selection of data processing method

Yulia I. Troitskaya – data processing, preparation of illustrations

Olga S. Ermakova – data analysis

Natalia A. Orekhova – literary review, data analysis of $p\text{CO}_2$

The authors have read and approved the final manuscript.

The authors declare that they have no conflict of interest.

Original article

Spatial and Temporal Dynamics of pH and Total Alkalinity of the Sea of Azov Waters in 1950–2020

V. V. Sorokina , V. V. Kulygin*Federal Research Centre the Southern Scientific Centre of RAS, Rostov-on-Don, Russian Federation*
 v.sorok@mail.ru

Abstract

Purpose. The purpose of the study consists in analyzing the spatial-temporal dynamics of pH and total alkalinity of the Sea of Azov waters in 1950–2020.

Methods and Results. Statistical analysis of the data on the Sea of Azov for 1950–2020 derived from the oceanographic database of the Southern Scientific Center of RAS made it possible to determine the average long-term values of the parameters under consideration in the Taganrog Bay, the open part of the Sea of Azov and the Kerch Strait by seasons. For the first time, the long-term changes in pH and total alkalinity of the Sea of Azov waters, as well as the distribution features of these parameters in the regions affected by the river runoffs are shown.

Conclusions. Two zones of low *Alk* values of seawater with the salinity ranges of 2–4 and 11–13‰ were identified in the Taganrog Bay. In these regions, under significant supersaturation of water with calcium carbonate the processes of chemogenic calcite formation are potentially possible. One zone of the increased pH values with the salinity range 4–6‰ coincides with the area of maximum phytoplankton productivity. In the Taganrog Bay, a pH increase in summer and autumn was noted, which can be explained by the growing production of organic matter against the background of salinity decrease starting from the second half of the 1970s and by a rise of water temperature in the first decade of the 2000s. The open part of the sea and the Kerch Strait are characterized by a general trend towards a decrease in pH values, except for the period of an intensive river runoff. The general pattern of *Alk* distribution in the Sea of Azov consists in its relatively elevated values in the Taganrog Bay (especially in the regions with salinity range of 5–8‰) which decrease towards the open sea and then increase towards the Kerch Strait. The average *Alk* value in the Taganrog Bay tended to decrease during the low-water periods (1972–1978 and 2011–2020) against the background of its general increase over the past seventy years. A noticeable growth of the average *Alk* values was noted during the period of increasing average water temperature in the Sea of Azov at the beginning of the 21st century.

Keywords: pH, total alkalinity, spatial-temporal dynamics, Sea of Azov, Taganrog Bay, Kerch Strait

Acknowledgments: The publication was prepared within the framework of the state assignment of SSC, RAS (project state registration No. 123071900007-8), Agreement No. 169-15-2023-002 (dated 01.03.2023) of the Federal Service for Hydrometeorology and Environmental Monitoring according to Agreement No. 72-223/VIPGZ-23 (dated 03.04.2023) between the IO, RAS and SSC, RAS within the framework of Consortium-2. The authors are grateful to the reviewers for their useful comments.

For citation: Sorokina, V.V. and Kulygin, V.V., 2024. Spatial and Temporal Dynamics of pH and Total Alkalinity of the Sea of Azov Waters in 1950–2020. *Physical Oceanography*, 31(6), pp. 772-787.

© 2024, V. V. Sorokina, V. V. Kulygin

© 2024, Physical Oceanography

Introduction

Total alkalinity (*Alk*) and pH are the parameters of the chemical equilibrium system of water bodies. They are applied in calculations of the content of the water carbonate system components, the direction of CO₂ exchange between the sea and the atmosphere, and serve as origin indicators of water masses and photosynthetic



processes ¹ [1–6]. The studies of long-term changes in these characteristics in relation to climate change and increased anthropogenic pressure on marine ecosystems and the ocean are of particular interest [7, 8].

The first systematic expeditionary observations of pH and *Alk* were carried out in the middle of the 20th century (1953–1959). A comprehensive review of these observations can be found in [9]. The materials of the studies performed by Azov-Black Sea Scientific Fisheries Station in 1953 and 1955, Hydrometeorological Observatory of the Black Sea and the Sea of Azov (HMO BSA) and State Oceanographic Institute (SOI) in 1958 and 1959 were summarized in the Hydrometeorological Handbook of the Sea of Azov ² and the fundamental work Hydrochemistry of the Sea of Azov ³ (1964), which, among other things, revealed the main patterns of pH and *Alk* distribution.

In the subsequent period (from 1960 to the present), the measurement of *Alk* and pH was incorporated into the standard observation program for the spatio-temporal variability of hydrochemical parameters. These observations are conducted by organizations under the supervision of the Hydrometeorological Service (State Hydrometeorological Committee, now Roshydromet) and Fisheries (Ministry of Fisheries, now Rosrybolovstvo), as part of the state scientific and technical program for national development [9]. Hydrological and hydrochemical studies are carried out under the supervision of SOI and Azov Research Institute of Fisheries (Azov-Black Sea branch of VNIRO AzNIIRKH) on a single methodological basis. The program of AzNIIRKH marine measurements includes identification of hydrogen index but not the total alkalinity.

In 1991, SOI generalized the materials of expeditionary observations of the seasonal and spatial distribution of pH (a total of 6,320 observations) for the 1960–1985 period and *Alk* (a total of 5,000 observations) for the 1960–1981 period. The results are presented in the project “Seas of the USSR” (Volume 5. The Sea of Azov) ⁴. During the 1990s, there was a decline in the number of pH and *Alk* observations, with these measurements being discontinued in certain sea areas.

In the 2000s and to the present day, observations of the considered parameters of the Sea of Azov waters have been carried out by the divisions of Roshydromet (Donskaya and Kubanskaya estuarine hydrometeorological stations; the Sevastopol branch of SOI, SB FSBI “SOI”); and the Southern Scientific Center of the Russian Academy of Sciences, SSC RAS, from 2002 to the present). Furthermore, from 1997 to 2008, research was conducted by the Azov branch of the Murmansk Marine Biological Institute (AzMMBI).

¹ Dickson, A.G. and Goyet, C., 1994. *Handbook of Methods for the Analysis of the Various Parameters of the Carbon Dioxide System in Sea Water. Version 2*. US, 198 p. <https://doi.org/10.2172/10107773>

² Aksenov, A.A., ed., 1962. *Hydrometeorological Reference Book of the Sea of Azov*. Leningrad: Gidrometeoizdat, 853 p. (in Russian).

³ Tsurikova, A.P. and Shulgina, E.F., 1964. *Hydrochemistry of the Sea of Azov*. Leningrad: Gidrometeoizdat, 258 p. (in Russian).

⁴ Goptarev, N.P., Simonov, A.I., Zatuchnaya, B.M. and Gershanovich, D.E., eds., 1991. *[Hydrometeorology and Hydrochemistry of the Seas of the USSR. Vol. 5. The Sea of Azov]*. Saint Petersburg: Gidrometeoizdat, 237 p. (in Russian).

All organizations involved in the study of the hydrochemical regime of the Sea of Azov used the widely accepted method of hydrochemical determinations²⁻⁵, which is described in detail in the relevant practical guidelines⁶⁻⁹.

Until 1960, the determination of pH colorimetric value using Palich boric-borate solutions with thymol blue and cresol red indicators was conducted immediately after the elevation of the bathometer on board the vessel². The colorimetric method for determining pH involves the introduction of temperature and salt corrections. The pH determination method⁷ has been shown to have an operator-specific accuracy range of $\pm 0.01-0.02$, and in the case of different operators, up to 0.05 pH units. The method for determining pH using different types of pH meters (with a set of measuring electrodes) was later applied^{7, 8}. The absolute average systematic error in determining pH by this method⁷ is 0.01–0.04 pH units. The majority of serial pH meters permit measurements with an accuracy of 0.02 pH units⁹.

As stated in reference publications^{2, 5}, which provide a summary of the data for the period 1953–1980, the determination of total alkalinity was achieved through direct titration with hydrochloric acid. The application of a mixed indicator and the use of a blowing technique with a stream of air devoid of carbon dioxide were also reported^{6, 7}. Since the 2000s, the use of alkalinity titrators based on the potentiometric method of determination has become prevalent in research. The titration process is conducted automatically, thereby eliminating the need for operator intervention and resulting in enhanced efficiency and precision. The total error of this method, as defined in RD 52.10.243-92⁸, is 4.7%.

Consequently, over the past seventy years, a large volume of information on the pH and *Alk* of the Sea of Azov waters was obtained. This information has been accumulated within the framework of the standard program of expeditionary observations of Roshydromet and the Russian Academy of Sciences organizations. Moreover, the latest generalization of long-term data on pH and *Alk* (for 1960–1985) was carried out in the work entitled “Hydrometeorology and hydrochemistry of the seas of the USSR. Vol. 5. The Sea of Azov”⁴ (1991). A considerable amount of time has passed since that study was conducted, and significant changes in the hydrological, hydrochemical, hydrobiological and sedimentation processes in the Sea of Azov have been observed as a result of climatic fluctuations and anthropogenic activity [10–13].

The objective of the present study is to analyze the spatio-temporal dynamics of pH and *Alk* in the Sea of Azov waters (from the Don mouth to the Kerch Strait inclusively) for the period 1950–2020. The analysis is based on a database of hydrological and hydrochemical indicators collected at the SSC of RAS.

⁵ Glukhovskiy, B.Kh., ed., 1986. [*Hydrometeorological Conditions of the Shelf Zone of the Seas of the USSR. Vol. 3. The Sea of Azov*]. Leningrad: Gidrometeoizdat, 218 p. (in Russian).

⁶ Blinov, L.K., ed., 1959. [*Guide on Marine Hydrochemical Research for Hydrometeorological Observatories and Marine Hydrometeorological Stations*]. Moscow: Gidrometeoizdat, 255 p. (in Russian).

⁷ Oradovskiy, S.G., ed., 1977. [*Guide to Methods of Chemical Analysis of Sea Waters*]. Leningrad: Gidrometeoizdat, 206 p. (in Russian).

⁸ Oradovskiy, S.G., ed., 1993. [*RD 52.10.243-92 Guide to Chemical Analysis of Sea Waters*]. Saint Petersburg: Gidrometeoizdat, 264 p. (in Russian).

⁹ Alekin, O.A., Semenov, A.D. and Skopintsev, B.A., 1973. [*Guide on Chemical Analysis of Land Waters*]. Leningrad: Gidrometeoizdat, 272 p. (in Russian).

Materials and methods

The present study is based on the Sea of Azov oceanographic database for the period 1924–2020 [14, 15]. Coastal stations (up to 1 m depth) performed by the SSC of RAS were excluded from the analysis.

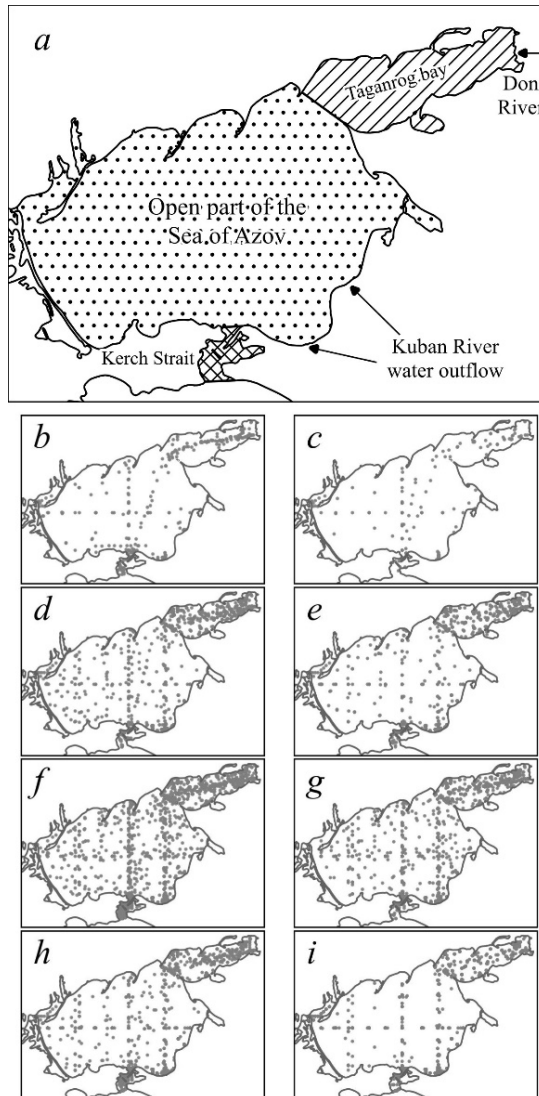


Fig. 1. Study area (a) and seasonal distribution of a number of hydrological stations for measuring pH (b, d, f, h) and Alk (c, e, g, i) in winter (b, c), spring (d, e), summer (f, g) and autumn (h, i)

The total number of oceanographic stations at which pH or Alk were determined between 1950 and 2020 exceeds 14,000, and the number of stations that carried out synchronous measurements of both indicators is more than 8,000. The studies covered the entire water area of the Sea of Azov, with the most detailed investigations focused on the Taganrog Bay and the Kerch Strait (Fig. 1).

With regard to the number of stations, the 1970s represented the period with the most data, while the 1950s and 1990s had the least (Fig. 2). In general, for the sea, the 1960s and 1970s were the decades in which the majority of stations with *Alk* measurements were located. Other decades are characterised by a higher prevalence of stations equipped with pH measurements.

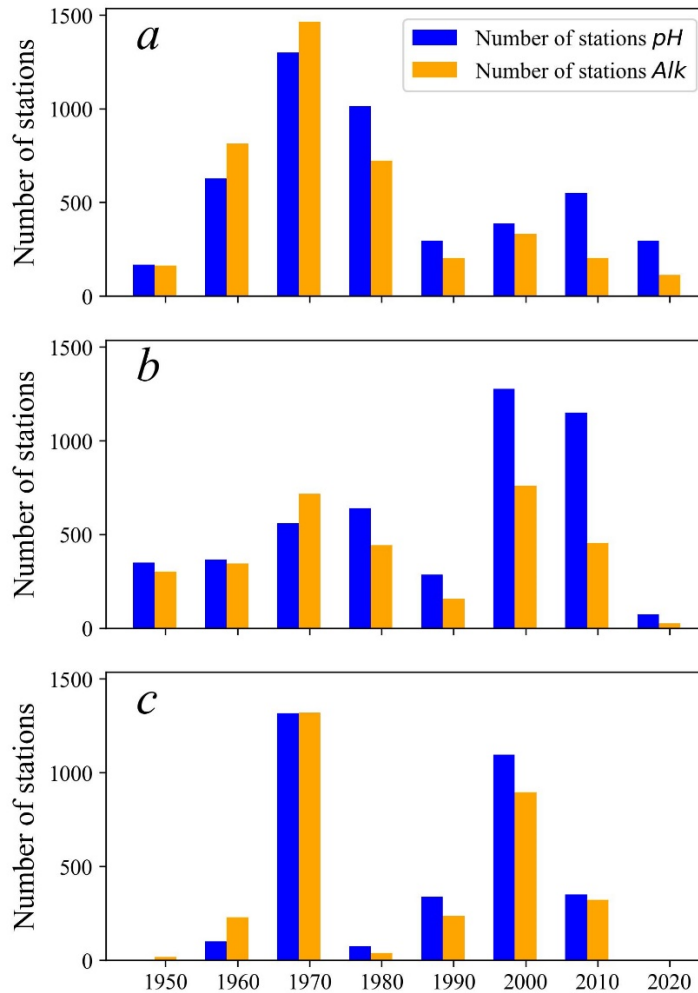


Fig. 2. Number of stations for measuring pH and *Alk* in the Taganrog Bay (*a*), the Sea of Azov (*b*) and the Kerch Strait (*c*) by decades

An analysis of the intra-annual distribution of the number of hydrological stations with pH and *Alk* measurements is presented in [9]. It is noted that not all stations possess a vertical distribution of the parameters under study, consequently, this paper examined data on the surface layer.

Until now, it has been problematic to track long-term changes in pH and *Alk* in the Sea of Azov. However, the database of hydrochemical indicators prepared at the SSC of RAS facilitates the analysis of these changes based on numerous sources, including a published analysis of long-term changes in the temperature and salinity

of the Sea of Azov waters [10]. The data underwent differentiation, leading to the identification of trends and patterns in both the spatial (associated with the heterogeneity of the Sea of Azov waters) and temporal (long-term and seasonal changes) distribution of instrumental observation data for the period 1950–2020. The average pH and *Alk* values were calculated for the characteristic periods of change in temperature and salinity of the of the Sea of Azov waters identified in [10].

Results and discussion

The following areas are distinguished according to the degree of impact of river and the Black Sea waters: the Taganrog Bay, the Sea of Azov open part and the Kerch Strait (Fig. 1, *a*). The average long-term values of the studied quantities are calculated for these areas.

In the Taganrog Bay region, there is a notable increase in both pH and *Alk* values across all seasons, with the widest variations observed in the pH range (see Table). No statistically significant differences in pH values by season are observed. Previous studies have indicated that the spring season is characterized by the highest pH values in the Taganrog Bay, with a decrease towards the sea⁵. In winter, a decrease in pH values in the Taganrog Bay and in the open part of the sea is observed³. The increased pH levels observed in the Taganrog Bay during winter months attract attention in this study. This phenomenon has been previously documented in the literature³, where the authors associated it with the processes of intensive life development at the ice edge.

Characteristics of pH and *Alk* in different regions of the Azov Sea by seasons

Region	Winter	Spring	Summer	Autumn	Average annual value
<i>pH</i>					
Taganrog Bay	8.55 ± 0.33*	8.55 ± 0.24	8.54 ± 0.24	8.53 ± 0.27	8.54 ± 0.25
Open part of the sea	8.29 ± 0.17	8.33 ± 0.20	8.34 ± 0.22	8.31 ± 0.20	8.33 ± 0.20
Kerch Strait	8.24 ± 0.15	8.30 ± 0.16	8.33 ± 0.17	8.38 ± 0.15	8.33 ± 0.16
<i>Alk, mmol/l</i>					
Taganrog Bay	3.77 ± 0.84	2.91 ± 0.49	2.88 ± 0.45	2.89 ± 0.46	2.90 ± 0.48
Open part of the sea	2.70 ± 0.50	2.82 ± 0.39	2.69 ± 0.39	2.69 ± 0.35	2.72 ± 0.39
Kerch Strait	2.66 ± 0.32	2.84 ± 0.25	2.83 ± 0.28	2.95 ± 0.29	2.87 ± 0.29

* Average value ± standard deviation.

The increased mean *Alk* value in the specified region during winter can be attributed to the fact that most of the determinations applied in the averaging process refer to the period 2000–2010. This period is characterized by relatively higher *Alk* values in all areas of the Sea of Azov, although in winter, the *Alk* values typically decrease, a phenomenon determined by the relatively small river runoff^{3,5}.

The general pattern of pH distribution in the Sea of Azov is characterized by elevated pH values in the Taganrog Bay (averaging 8.54), particularly in areas exhibiting water salinity levels of 4–6‰. However, a decline in pH values (averaging 8.33) is observed towards the open part of the sea and the Kerch Strait (Table, Fig. 3).

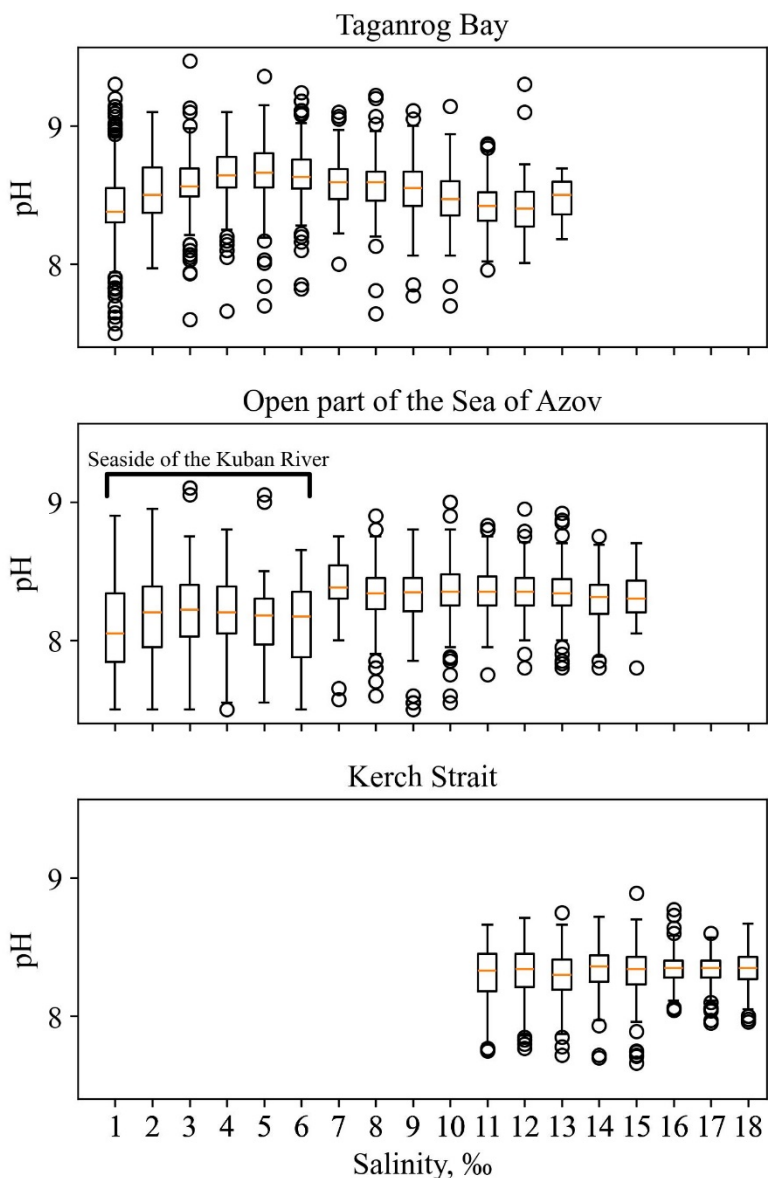


Fig. 3. Diagram of the range of pH values in the Sea of Azov and the Kerch Strait depending on water salinity

The greatest range of pH and *Alk* variation is observed in the zones affected by the Don and Kuban runoff, which reflects the peculiarities of the hydrochemical and hydrobiological regimes of these areas. The disturbance of carbonate equilibrium, resulting from the mixing of river and sea waters with different ionic compositions, leads to alterations in pH and *Alk* values. The pH value is found to be dependent on the $[\text{HCO}_3^-]/[\text{CO}_2]$ ratio, with higher values resulting in higher hydrogen indices. Photosynthesis, which consumes carbon dioxide, contributes to an increase in pH and a decrease in *Alk*. The elevated pH values observed in the Taganrog Bay (with the exception of the estuary section up to the 2‰ isohaline) are predominantly

associated with photosynthesis, which is most active in this area compared to other areas of the sea [16]. Furthermore, the river runoff typically exhibits a lower pH value compared to the waters of the bays³, resulting in comparatively lower pH levels in the vicinity of the Don and Kuban mouths.

In the open sea, the mean long-term pH values are distributed relatively evenly both seasonally and geographically, with a slight decrease near the Kuban mouth (by 0.15 relative to the mean pH (8.33) over the entire salinity range of this part of the sea) (Fig. 3, Table).

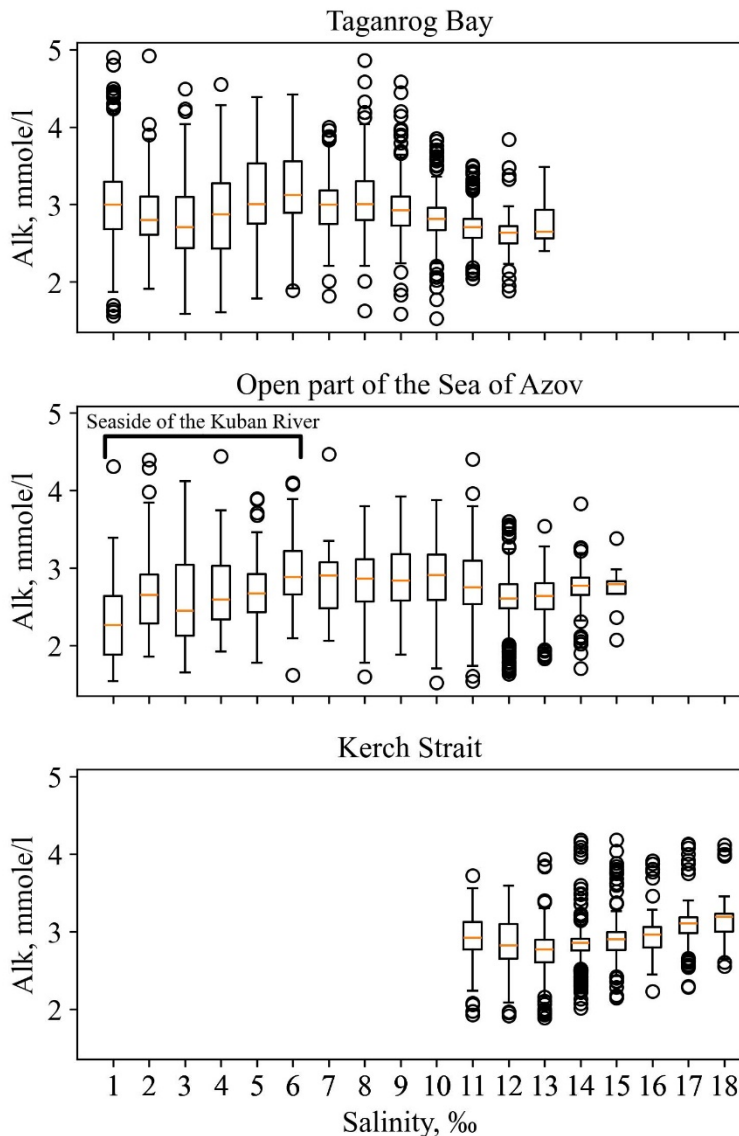


Fig. 4. Diagram of the range of *Alk* values in the Sea of Azov and the Kerch Strait depending on water salinity

In the southern part of the sea, pH values may be lower than in its northern part due to the possible propagation of the Black Sea waters and less intensive

development of phytoplankton. However, when the waters of the Sea of Azov exit through the Kerch Strait into the Black Sea, elevated pH values may be observed due to intensive photosynthesis during the warm season (see Table).

The general pattern of *Alk* distribution in the Sea of Azov and the Kerch Strait consists of relatively high values in the Taganrog Bay area (see Table), especially in the areas where the water salinity is within the range of 5–8‰, with a decrease towards the open sea and then an increase in the Kerch Strait area (Fig. 4).

The alkaline-saline coefficient is indicative of the mixing of water masses of different genesis. It has been observed that the Don seaside exhibits the highest values of the coefficient, a phenomenon attributable to the presence of desalinated river waters. A decline in the coefficient's value is evident towards the Kerch Strait and the Black Sea, regions distinguished by elevated levels of salinity (Fig. 5). The widest distribution of values for this quantity is observed in the sea areas with water salinity within the range of 1–4‰.

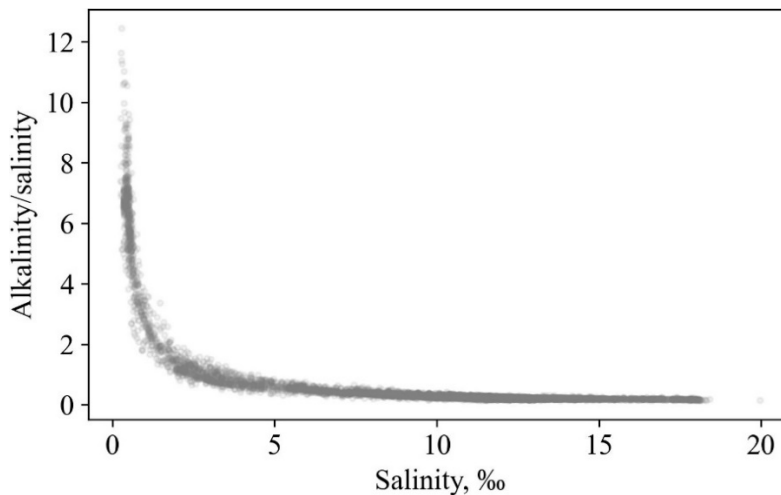


Fig. 5. Dependence of the alkaline-saline coefficient on salinity in the Sea of Azov and the Kerch Strait

The increase in alkalinity may be related to different processes in different parts of the sea. For example, increased *Alk* values along the Don seaside may be due to the influx of highly alkaline river waters (3.5–4 mmole/l)⁵; near the coast in the winter-spring period – due to the runoff of carbonate-enriched meltwater caused by the erosion of limestone; in the southern part of the open sea and the Kerch Strait – due to the influx of the Black Sea waters with the highest salinity.

In the eastern part of the Taganrog Bay, which is affected by the Don runoff, the alkalinity values can vary widely due to a combination of physical, chemical and biological processes that are directed in different ways and occur at different times. The observed variations in alkalinity depend mainly on the inflow of Don water and the influx of carbonates into the river, the saturation of water with calcium and hydrocarbonate ions (supersaturation of water with these ions), and factors that disrupt carbonate equilibrium (changes in temperature and biota activity).

In water with salinity levels ranging from 1.5 to 5‰, the processes of coagulation of the suspension pelitic component and the formation of chemogenic

calcite¹⁰ are observed to be most intense. A significant range of sorption phenomena and two oppositely directed processes of adsorption and desorption are observed in the pre-estuary areas [17]. This indicates primarily the presence of an unbalanced physical and chemical system in the transition zone.

An analysis of alkalinity values in the Don estuary and the Taganrog Bay revealed different types of dependence between Alk and salinity S in this area. The first type, which is the most common, is characterized by the curve $Alk = f(S)$ turning convex downwards at low salinity values. In contrast, the second type is characterized by a curve $Alk = f(S)$ that is convex upwards across the entire salinity range of the Taganrog Bay.

In the first case, from the mouth of the Don River towards the Taganrog Bay, the Alk values (3 mmole/l and above) initially decrease, reaching a minimum in waters with 2–4‰ salinity. Thereafter, they increase again in the Taganrog Bay waters with salinity varying from 5 to 7‰, before decreasing again towards the open part of the Sea of Azov. This phenomenon is illustrated in Fig. 4, which is a generalization of long-term data. In the second case (rarely), relatively low Alk values (less than 3 mmole/l) can increase, reaching an average of ~ 3 mmole/l and more in waters with 2.5–7‰ salinity, then decrease again towards the central part of the sea (waters of ~ 11–13‰ salinity). In addition to these two types, cases of a monotonous decrease in alkalinity depending on the salinity throughout the Taganrog Bay can be noted.

The most typical situation of decreasing Alk values in the estuary region in the Taganrog Bay eastern part in the waters of 2–4‰ salinity is associated with a carbonate equilibrium shift, the transition of carbonates into a solid phase (suspended chemogenic calcite) from the waters supersaturated with calcium and hydrocarbonate ions^{3, 10} [17]. Aside from the cause mentioned above, such a decrease in Alk values in the specified salinity range may be associated with CO₂ removal during photosynthesis (as a result of this process, the concentration of hydrocarbonates decreases and the pH increases). The extraction of carbonates from water by plankton, with a partial transition of carbonate-containing detritus into bottom sediments (in this case, the alkaline-saline coefficient decreases), and a temperature increase at which the carbonate equilibrium shifts towards an increase in the concentration of carbonates and a decrease in the concentration of hydrocarbonates and CO₂. All these factors should be given full consideration when analyzing the behavior of the carbonate system in the Taganrog Bay, a subject which requires further research (for example, analysis of oxygen dynamics and production processes, water saturation with calcium ions and hydrocarbonates, etc.).

In publication¹⁰, the authors demonstrated similar types of dependence in the Taganrog Bay region between the concentrations of calcium and chlorine ions. The occurrence of dissolution of solid phases of calcium carbonates is indicated by a convex upward turn in the curve $Ca^{2+} = f(Cl)$. In a subsequent study [17], Yu. P. Khrustalev reports that such a phenomenon is rarely observed in the Taganrog Bay and mainly in its central part. In another typical case, when the curve $Ca^{2+} = f(Cl)$ turns convex downward, usually at low concentrations of chlorine ions, chemogenic

¹⁰ Tsurikova, A.P. and Tsurikov, P.L., 1966. [On the Sedimentation of Calcium and Changes in Salinity during the Mixing of Waters]. In: S. V. Bruevich, ed., 1966. *Chemical Processes in the Seas and Oceans*. Moscow: Nauka, pp. 12-18 (in Russian).

CaCO₃ sedimentation is possible. The authors of the work¹⁰ noted that such a dependence is clearly manifested at the bay head when river and sea waters mix and confirmed by the presence of needle-shaped calcite of chemogenic origin. In the western, seaward part of the Taganrog Bay, the authors of the abovementioned work identified a second zone of calcium carbonate sedimentation where the Taganrog Bay and the Sea of Azov waters mix. It should be borne in mind that carbonate sedimentation can lead to a decrease in the alkalinity transported to the open part of the sea during the spring phase of production processes development.

The dynamics of pH (and other parameters of the carbonate system) in the shallow Sea of Azov are challenging to predict due to the influence of numerous factors, including changes in the catchment area (the amount of precipitation, weathering, liming, the input volume of biogenic and organic substances), as well as the timing and scale of the processes of organic matter production/oxidation. Nevertheless, based on a large amount of instrumental observation data over an extended period, it becomes possible to trace the main trends and patterns of hydrogen index variations.

The pH levels in the Taganrog Bay have exhibited a marked increase during the summer and autumn months, as evidenced by the data collected from 1950 to 2020. Conversely, the highest recorded values in spring were observed during the period of 1972–1978 (average for the period – 8.60), which was characterized by a low-water regime and an increase in water salinity (from an average of 11.5‰ for 1950–1971 to 12.9‰ for 1972–1978 [10]). This increase in salinity was also evident in the subsequent period of 2011–2020 (average for the period – 8.57), which was characterized by a prolonged low-water level period, accompanied by relatively higher water temperatures (Fig. 6). Despite the low-water regime of the two indicated periods, photosynthesis processes were most likely of great importance in the Taganrog Bay and served as the cause of a relative pH increase. On the contrary, during periods of low water and increasing sea salinity, the production of organic matter decreased and the average pH values decreased. This is clearly seen in the spring and autumn of 1972–1978, as well as in the spring of 2011–2020. The lack of pH increase in summer for both low-water periods and in autumn for the second period may be associated with a recent shift of the maximum peak of primary production in the sea to the summer-autumn period [16], which requires further research.

The importance of salinity as a factor leading to a decrease in the value of organic matter primary production in the Sea of Azov was initially noted in the 1970s¹¹ and later confirmed by modern studies [18, 19]. During salinization periods, the average level of organic matter primary production of organic matter by phytoplankton was low, and the highest primary production was observed during freshening periods. The main explanation for the observed dependence is the change in phytoplankton taxonomic groups when primary production decreases in the open part of the sea with a decrease in the blue-green algae biomass [18].

¹¹ Bronfman, A.M., Dubinina, V.G. and Makarova, G.D., 1979. [*Hydrological and Hydrochemical Foundations of the Productivity of the Sea of Azov*]. Moscow: Pishchevaya Promyshlennost, 288 p. (in Russian).

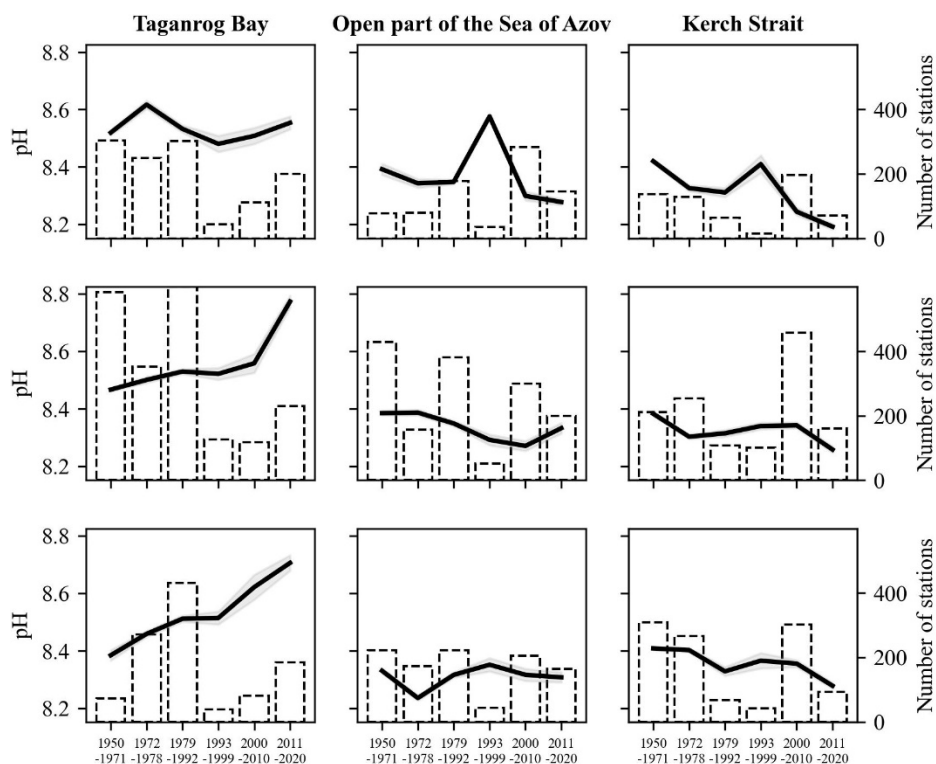


Fig. 6. Spatial-temporal changes in pH in the Sea of Azov and the Kerch Strait by seasons: *a* – spring, *b* – summer and *c* – autumn

The period 1993–1999 was characterized by the highest average river runoff, relatively lower salinity and water temperature [10]. During this period, a slight increase in the average pH value in the sea was noted in spring (maximum) and autumn (Fig. 6). Of particular interest is the observation that in the Taganrog Bay during the spring period, the average pH value remained unchanged in comparison to adjacent periods, suggesting that the processes of organic matter production were not strongly developed. At the same time, in the open sea, the pH values were the highest compared to other periods, a phenomenon that can be explained by the inflow of a greater volume of the Taganrog Bay waters with a higher pH, as well as, potentially, active photosynthesis. During summer, the intensity of production processes somewhat decreased.

The Kerch Strait and the sea itself are characterized by similar trends in the average pH value variation in spring and summer over the entire observation period. However, in autumn, the observed changes differ, particularly during the last low-water period (2007–2020), which may be associated with relatively less active production processes in this area due to salinization.

The mean values of total alkalinity demonstrate a predominantly unidirectional change across seasons within the specified areas (Fig. 7). In the Taganrog Bay area, a decrease in the average *Alk* values was observed during the low-water period of 1972–1978 compared to previous years, followed by a steady increase until the last period of 2011–2020, which is also characterized by a significant reduction in river runoff (Fig. 7). In the open part of the Sea of Azov, as well as in the Kerch Strait,

there was an increase in average alkalinity values during the salinization period of 1972–1978, with the highest increases observed in the autumn and summer months, compared to spring. This phenomenon can be attributed to the possible penetration of more saline Black Sea waters with increased alkalinity (averaging 3.3 mmole/l in the surface (100 m) layer [20, 21]).

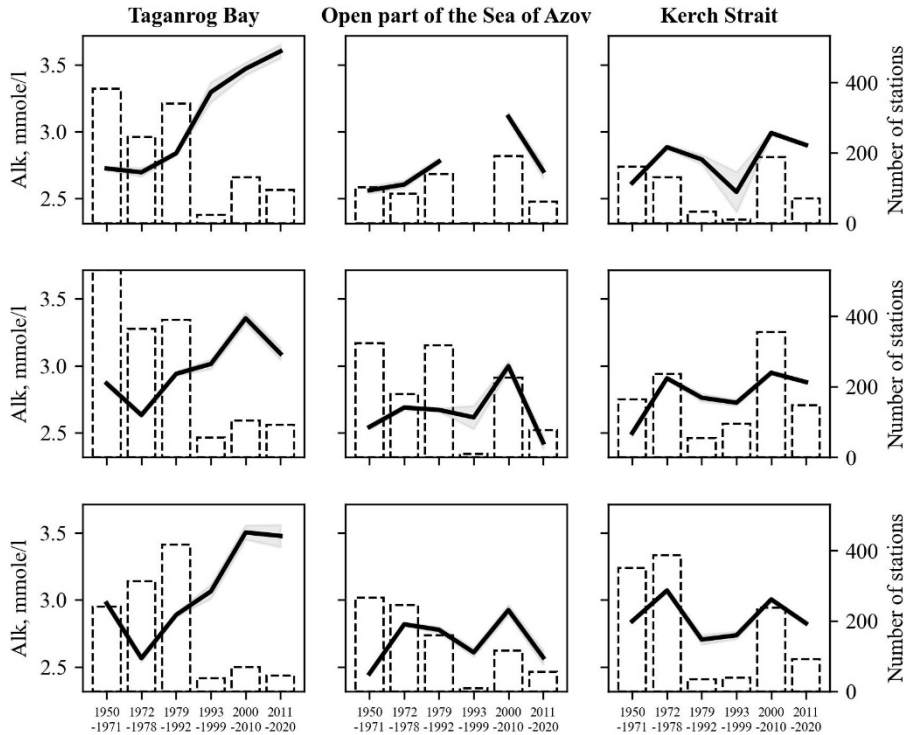


Fig. 7. Spatial-temporal changes in *Alk* in the Sea of Azov and the Kerch Strait by seasons: *a* – spring, *b* – summer and *c* – autumn

A significant increase in *Alk* has been observed in all areas of the sea since the early 2000s, with the sea salinity remaining relatively low during this time (the average value for the sea is 10.2‰) and the water temperature has increased significantly (on average by more than 1 °C) compared to previous periods. During the 2011–2020 low-water period, characterized by elevated salinity levels and relatively high water temperatures, no further increase in alkalinity was observed; on the contrary, a decrease in its average values was noted in all areas. There is probably a limit to the increase in this parameter under the new conditions. During the period of reduced river runoff into the Sea of Azov, the influx of Black Sea waters no longer significantly affected the average *Alk* value.

It can thus be stated that at the end of the 20th – beginning of the 21st centuries, not only the hydrological regime documented in the work [10], but also the hydrochemical state of the Sea of Azov changed. The underlying causes of these observed trends in total alkalinity variation still need to be clarified by identifying relationships with such factors as river runoff, water temperature and salinity, organic matter production and destruction, as well as by comprehensively examining the behavioral features of the Azov Sea carbonate system.

Conclusion

An analysis of spatio-temporal changes in the pH and *Alk* of the Sea of Azov and the Kerch Strait waters was performed for the period 1950–2020. The analysis was based on a database of hydrological and hydrochemical indicators collected at the Southern Scientific Center of RAS. The calculation of average values for the parameters under study was conducted on a seasonal basis for three distinct areas: the Taganrog Bay, the open part of the Sea of Azov and the Kerch Strait.

The following observations can be made about the general patterns of distribution of the parameters under study in the Sea of Azov, depending on salinity. In the Taganrog Bay area, two zones of low total alkalinity values were identified in waters with salinity levels ranging from 2–4 and 11–13‰. These zones exhibited significant water supersaturation with calcium carbonate, thereby creating conditions conducive to chemogenic calcite formation. Furthermore, an elevated pH level was identified in waters with a salinity of 4–6‰, which corresponds to the region of maximum phytoplankton productivity.

This paper presents an analysis of long-term seasonal changes in pH and *Alk* of the Sea of Azov waters (from the Don mouth to the Kerch Strait inclusively). The analysis is based on previously determined periods of temperature and salinity variation of the Sea of Azov waters, which made it possible to explain the observed trends.

In the Taganrog Bay, an increase in pH was observed in the surface layer during summer and autumn months. This phenomenon can be attributed to the rise in organic matter production, coinciding with a decline in salinity from the mid-1970s onwards, and an increase in water temperature in the first decade of the 21st century.

The open part of the sea (with the exception of the autumn period) and the Kerch Strait are distinguished by a general tendency towards a decrease in pH. The 1993–1999 period is notable for its desalination of the Sea of Azov, attributable to comparatively elevated river runoff, which resulted in elevated pH values in spring, as compared to previous and subsequent periods. No pronounced trend in the variation of average pH values in the open sea during autumn has been identified.

The general pattern of *Alk* distribution in the Sea of Azov and the Kerch Strait consists of relatively increased values in the Taganrog Bay, especially in the waters with 5–8‰ salinity, with a decrease towards the open sea and then an increase towards the Kerch Strait.

The average value of total alkalinity in the Taganrog Bay exhibited a tendency to decrease during the low-water periods of 1972–1978 and 2011–2020, despite the overall positive growth observed. At the same time, the *Alk* values increased in the open sea and the Kerch Strait during the initial period compared to the previous and subsequent periods, which is most likely due to the influx of more alkaline Black Sea waters. A positive trend was not observed in the latter period, as total alkalinity values were already elevated compared to those recorded prior to the 2000s. A significant increase in the average *Alk* values occurred during the period of rising average water temperature in the Sea of Azov in the early 20th century. During the last period of low river water levels and increased salinity of the Sea of Azov (2011–2020), a total alkalinity rise, as well as pH, was not observed in the majority of the cases examined.

It is evident that the standard deviation and scatter of the values of the parameters under study have increased since the 1990s. A notable observation is the contrasting behavior exhibited by the parameters during the low-water periods of 1972–1978 and 2011–2020. This phenomenon is most likely explained by differences in the average temperature of the water mass and shifts in the seasonal temperature variation.

At the end of the 20th – beginning of the 21st centuries, changes in the Sea of Azov hydrochemical regime occurred, which have yet to be studied in detail. The present study is the basis for a comprehensive analysis of the carbonate system and the production-destruction processes within the Sea of Azov.

REFERENCES

1. Millero, F.J., 2007. The Marine Inorganic Carbon Cycle. *Chemical Reviews*, 107(2), pp. 308-341. <https://doi.org/10.1021/cr0503557>
2. Cai, W.-J. and Wang, Y., 1998. The Chemistry, Fluxes, and Sources of Carbon Dioxide in the Estuarine Waters of the Satilla and Altamaha Rivers, Georgia. *Limnology and Oceanography*, 43(4), pp. 657-668. <http://doi.org/10.4319/lo.1998.43.4.0657>
3. Álvarez, M., Sanleón-Bartolomé, H., Tanhua, T., Mintrop, L., Luchetta, A., Cantoni, C., Schroeder, K. and Civitarese, G., 2014. The CO₂ System in the Mediterranean Sea: A Basin Wide Perspective. *Ocean Science*, 10(1), pp. 69-92. <http://doi.org/10.5194/os-10-69-2014>
4. Copin-Montégut, C., 1993. Alkalinity and Carbon Budgets in the Mediterranean Sea. *Global Biogeochemical Cycles*, 7(4), pp. 915-925. <http://doi.org/10.1029/93gb01826>
5. Orekhova, N.A., Medvedev, E.V. and Konovalov, S.K., 2016. Carbonate System Characteristics of the Sevastopol Bay Waters in 2009–2015. *Physical Oceanography*, (3), pp. 36-46. <http://doi.org/10.22449/1573-160X-2016-3-36-46>
6. Makkaveev, P.N., Polukhin, A.A., Kostyleva, A.V., Protsenko, E.A., Stepanova, S.V. and Yakubov, S.K., 2017. Hydrochemical Features of the Kara Sea Aquatic Area in Summer 2015. *Oceanology*, 57(1), pp. 48-57. <http://doi.org/10.1134/S0001437017010088>
7. St-Laurent, P., Friedrichs, M.A.M., Najjar, R.G., Shadwick, E.H., Tian, H. and Yao, Y., 2020. Relative Impacts of Global Changes and Regional Watershed Changes on the Inorganic Carbon Balance of the Chesapeake Bay. *Biogeosciences*, 17(14), pp. 3779-3796. <https://doi.org/10.5194/bg-17-3779-2020>
8. Moiseenko, O.G., Konovalov, S.K. and Kozlovskaya, O.N., 2010. Intraannual and Long-Term Variations of the Carbonate System of the Aerobic Zone in the Black Sea. *Physical Oceanography*, 20(6), pp. 435-450. <https://doi.org/10.1007/s11110-011-9097-3>
9. Sorokina, V.V. and Kulygin, V.V., 2023. Database of Hydrochemical Indicators of the Sea of Azov: Ph and Total Alkalinity. *Ecology. Economy. Informatics. System Analysis and Mathematical Modeling of Ecological and Economic Systems*, 1(8), pp. 110-115. <https://doi.org/10.23885/2500-395X-2023-1-8-110-115> (in Russian).
10. Berdnikov, S.V., Dashkevich, L.V. and Kulygin, V.V., 2022. A New State in the Hydrological Regime of the Sea of Azov in the 21st Century. *Doklady Earth Sciences*, 503(1), pp. 123-128. <https://doi.org/10.1134/S1028334X22030059>
11. Sorokina, V.V., 2020. Current Challenges of the Carbon Cycle Research in the Sea of Azov. *Ecology. Economy. Informatics. System Analysis and Mathematical Modeling of Ecological and Economic Systems*, 1(5), pp. 185-191. <https://doi.org/10.23885/2500-395X-2020-1-5-185-191> (in Russian).
12. Sorokina, V.V. and Berdnikov, S.V., 2008. Mathematical Modeling of the Terrigenous Sedimentation in the Sea of Azov. *Oceanology*, 48(3), pp. 418-427. <https://doi.org/10.1134/S0001437008030144>

13. Matishov, G.G., ed., 2020. *The Sea of Azov: Oceanography, Physical Geography, and Hydrobiology (in Scientific Works of Academician RAS G.G. Matishov)*. Rostov-on-Don: SSC RAS Publishing. Vol. II (2018–2020), 448 p. (in Russian).
14. Matishov, G.G., Sherman, K. and Levitus, S., eds., 2014. *Atlas of Climatic Changes in Nine Large Marine Ecosystems of the Northern Hemisphere (1827–2013)*. NOAA Atlas NESDIS 78. Washington, D.C.: U.S. Government Printing Office, 131 p. <http://doi.org/10.7289/V5Q52MK5>
15. Matishov, G.G. and Stepanyan, O.V., 2018. Research Vessel Deneb: 10 Years of Marine Scientific Research. *Physical Oceanography*, 25(6), pp. 501-508. <https://doi.org/10.22449/1573-160X-2018-6-501-508>
16. Saprygin, V.V., Berdnikov, S.V., Kulygin, V.V., Dashkevich, L.V. and Mestetskiy, L.M., 2018. Spatial Distribution and Seasonal Dynamics of the Chlorophyll a Concentration in the Sea of Azov Based on Meris Images. *Oceanology*, 58(5), pp. 689-699. <https://doi.org/10.1134/S0001437018050132>
17. Khrustalev, Yu.P., 1999. *The Fundamental Problems of the Sedimentogenesis Geochemistry in the Azov Sea*. Apatity: MMBI KSC RAS, 247 p. (in Russian).
18. Kosenko, Ju.V., Barabashin, T.O. and Baskakova, T.E., 2017. Dynamics of Hydrochemical Characteristics of the Sea of Azov in Modern Period of Salinization. *Bulletin of Higher Educational Institutions. North Caucasus Region. Natural Sciences*, (3-1), pp. 76-82. <https://doi.org/10.23683/0321-3005-2017-3-1-76-82> (in Russian).
19. Kosenko, Yu.V., Baskakova, T.E., Zhukova, S.V., Barabashin, T.O. and Piatinskii, M.M., 2023. The Influence of Water Salinity on Generation of Near-Bottom Hypoxic Phenomena and the Level of Primary Production of Organic Matter in the Taganrog Bay. *Aquatic Bioresources & Environment*, 6(1), pp. 34-47. https://doi.org/10.47921/2619-1024_2023_6_1_34 (in Russian).
20. Kondratev, S.I., Medvedev, E.V. and Konovalov, S.K., 2017. Total Alkalinity and Ph in the Black Sea Waters in 2010–2011. *Physical Oceanography*, (4), pp. 35-45. <https://doi.org/10.22449/1573-160X-2017-4-35-45>
21. Goyet, C., Bradshaw, A.L. and Brewer, P.G., 1991. *The Carbonate System in the Black Sea. Deep Sea Research Part A. Oceanographic Research Papers*, 38(2), pp. S1049-S1068. [https://doi.org/10.1016/S0198-0149\(10\)80023-8](https://doi.org/10.1016/S0198-0149(10)80023-8)

About the authors:

Vera V. Sorokina, Senior Research Associate, Federal Research Centre the Southern Scientific Centre of Russian Academy of Sciences (41 Chekhova Str., Rostov-on-Don, 344006, Russian Federation), CSc (Geogr.), **ORCID ID: 0000-0002-3742-892X**, **Scopus Author ID: 36795587800**, **ResearcherID: E-4729-2014**, v.sorok@mail.ru

Valeriy V. Kulygin, Leading Research Associate, Federal Research Centre the Southern Scientific Centre of Russian Academy of Sciences (41 Chekhova Str., Rostov-on-Don, 344006, Russian Federation), CSc (Tech.), **ORCID ID: 0000-0001-9748-6497**, **Scopus Author ID: 24399335100**, **ResearcherID: I-3194-2013**, kulygin@ssc-ras.ru

Contribution of the co-authors:

Vera V. Sorokina – research development, data analysis, article writing

Valeriy V. Kulygin – statistical analysis of data, preparation of graphic materials, discussion of results

The authors have read and approved the final manuscript.

The authors declare that they have no conflict of interest.

Original article

Climatic Variability of the Black Sea Thermohaline Characteristics (1950–2023)

V. N. Belokopytov , E. V. Zhuk*Marine Hydrophysical Institute of RAS, Sevastopol, Russian Federation*
 v.belokopytov@gmail.com

Abstract

Purpose. The purposes of the study are to create a new climatic array of thermohaline fields in the Black Sea, to estimate (on its basis) climate changes during the last decades and to compare them with the global climatic tendencies in the World Ocean.

Methods and Results. A new climatic array of thermohaline fields in the Black Sea (MHI-2024) with a spatial grid of $1/6^\circ \times 1/4^\circ$ has been created in Marine Hydrophysical Institute of RAS based on statistical processing of more than 123 thousand hydrological stations for 1950–2023 using optimal interpolation methods. The climate atlas and the digital array are the open access products and can be used in climate studies, mathematical modeling, as well as in solving various applied problems. The deviations of initial data and averaged values from the climatic fields in the MHI-2024 array have constituted a basis for calculating the parameters of temporal variability at different scales and forming the time series of average monthly/annual anomalies. It is revealed that after 2015, sea warming in the 0–100 m layer steadily exceeded the natural background of interannual variability, at that its maximum increase fell on the summer-autumn seasons. Since about 2010–2012, a sharp salinity growth has been observed which does not yet surpass the standard deviation (SD) of interannual variability. The highest salinity increase in the course of a seasonal cycle occurs in spring and autumn when the water balance in the basin is at its maximum.

Conclusions. The Black Sea is related to the areas with the increased rates of climate changes, such as tropical parts of the World Ocean. The high temperature rise in the Black Sea over the past 40 years is the second in intensity as compared to that of the Arctic seas. Salinity growth in the Black Sea over a 70-year period is close to that in the areas of subtropical anticyclonic gyres where sharp salinification, atypical for the ocean, has been observed for the past 20 years. The current warm and saline stage of the Black Sea hydrologic state is similar to the conditions in 1960–1970, but with greater oscillation amplitude. The obtained results have a wide range of applications including formation of general ideas about the carbon cycle mechanisms in the Azov-Black Sea basin.

Keywords: Black Sea, thermohaline structure, climatic array, climate change, global warming, salinity, water temperature

Acknowledgments: The study was carried out within the framework of state assignments of FSBSI FRC MHI on themes FNNN-2024-0014 and FNNN-2023-0001.

For citation: Belokopytov, V.N. and Zhuk, E.V., 2024. Climatic Variability of the Black Sea Thermohaline Characteristics (1950–2023). *Physical Oceanography*, 31(6), pp. 788-801.

© 2024, V. N. Belokopytov, E. V. Zhuk

© 2024, Physical Oceanography

Introduction

The calculation of deviations of current values of hydrometeorological elements from climatic values remains the traditional, fundamental approach in the vast set of climate research methods. In the case of oceanographic characteristics that are unevenly distributed in time and space, the process of obtaining statistically reliable



climate values is a more uncertain task than it is for long-term observation series at stationary meteorological stations or for remote sensing data on a regular basis.

When absolute or normalized anomalies relative to the long-term seasonal course are used as general indicators of climatic variability, the estimate of the intensity of ongoing large-scale variations is influenced by the values of previously calculated climatic values. A number of climatic arrays of thermohaline fields have been created for the Black Sea over the last 40 years: SB SOI [1], WOA-2018 [2, 3], MEDATLAS¹, SeaDataNet Climatology², MHI-2004^{3, 4, 5} [4]. These arrays cover different historical periods, so their average characteristics reflect differently the influence of long-term trends and variability in the decadal and multidecadal range.

Works on climatic variability in the Black Sea described mainly the changes in the characteristics of the thermohaline structure of waters themselves and paid less attention to their relationship to climate averages and general level of interannual-multidecadal variability. In [5–7], general long-term trends also covering the modern period of sharp warming of the upper sea layer in the late 20th – early 21st centuries were considered. Many studies were devoted to the processes in the cold intermediate layer (CIL) [8–12]. They showed that in recent years, following the surface layer warming, this characteristic element of the thermohaline structure of the Black Sea waters (in its classical definition as a subsurface layer with a temperature of $\leq 8^{\circ}\text{C}$) had begun to disappear by the early 2010s. A slow, constant temperature and salinity increase in the permanent pycnocline layer has also been repeatedly noted in [1, 5].

The subject of long-term fluctuations in the Black Sea salinity has been addressed to a lesser extent in the literature. The results of ship observations suggest that the decrease in the salinity of the surface layer, which began in the 1980s and was first documented in [1], had been generally completed by 2005–2010. The subsequent general increase in the sea salt content was discussed by specialists mostly within the framework of scientific conferences. Signs of the beginning of basin salinization can be found only in individual works, e. g., in the plots of salinity time series in [11, Fig. 5, p. 4812].

¹ MEDAR Group, 2002. *MEDATLAS/2002 Database. Mediterranean and Black Sea Database of Temperature Salinity and Bio-Chemical Parameters. Climatological Atlas*. Institut Français de Recherche pour L'Exploitation de la Mer (IFREMER) and Instituto Nazionale di Oceanografia e di Geofisica Sperimentale (OGS), 4 CD-ROMs.

² Myroshnychenko, V. and Simoncelli, S., 2020. *SeaDataCloud Temperature and Salinity Climatology for the Black Sea (Version 2)*. Product Information Document. SeaDataCloud, 37 p. <https://doi.org/10.13155/77420>

³ Belokopytov, V.N., 2004. *Thermohaline and Hydrologic-Acoustical Structure of the Black Sea Waters. Abstract of PhD Thesis*. Sevastopol: ECOSI-Gidrofizika, 24 p. (in Russian).

⁴ Simonenko, S.V., ed., 2009. *Oceanographic Atlas of the Black Sea and The Sea of Azov*. Kyiv: Derzhgidrografiya, 356 p.

⁵ Mokievsky, V.O., Tsetlin, A.B., Ignatov, E.I., Belokopytov, V.N., Zatsepin, A.G., Zernov, A.S., Litvinskaya, S.A., Repina, I.A., Isachenko, A.I. [et al.], 2019. *Ecological Atlas. Black and Azov Seas*. Moscow: NIR Foundation, 464 p. (in Russian).

The urgent need to carry out more accurate and substantiated estimates of modern regional climate changes and compare them with global trends stimulates work on determining the characteristics of the full range of temporal variability and creating new versions of climate fields. The increase in the number of observations in the Black Sea over the last decade has facilitated an enhancement in the spatial resolution of climatic arrays which have a diverse range of applications. In particular, the estimates of climate anomalies derived on their basis are important not only as traditional climatological characteristics but also to solve new urgent problems, such as the formation of general ideas about the carbon cycle mechanisms in the Azov-Black Sea basin.

The present paper aims at estimating climate changes in the thermohaline characteristics of the Black Sea in recent decades based on deviations from the new climatic array and comparing them with global climate trends in the World Ocean.

Data and research methods

The existing climatic arrays of the Black Sea were calculated based on the data for different historical periods: SB SOI – up to 1977, MEDATLAS – up to 1997, MHI-2004 – for 1923–2004, SeaDataNet – for 1955–1994, 1995–2019 and 1955–2019, with the 1981–2010 and 2005–2017 periods from the WOA-2018 array list most temporally proximate to the present day.

The new climatic array (MHI-2024) covers the 1950–2023 period with two climate periods of the World Meteorological Organization (WMO): 1961–1990 and 1991–2020. Also, it is close to the periods of quantitative estimates of long-term changes in the World Ocean from the report of the Intergovernmental Panel on Climate Change (IPCC) ⁶.

The existing Black Sea climatic arrays also have various spatial resolutions in addition to different averaging periods: SB SOI – $2/3^\circ \times 1^\circ$ ($40' \times 60'$, 74×78 km), MHI-2004 – a combined grid of $2/3^\circ \times 1^\circ$ ($40' \times 60'$, 74×78 km) and $1/3^\circ \times 1/5^\circ$ ($20' \times 30'$, 37×39 km – for more areas with sufficient amount of data available), WOA-2018 – $1^\circ \times 1^\circ$ (111×78 km) and $1/4^\circ \times 1/4^\circ$ ($15' \times 15'$, 28×19 km), SeaDataNet – $1/8^\circ \times 1/8^\circ$ ($7.5' \times 7.5'$, 14×10 km), MEDATLAS – 958 unevenly spaced nodes. To create the MHI-2024 array, a grid of $1/6^\circ \times 1/4^\circ$ ($10' \times 15'$, 19×19 km) was chosen as a compromise between the desire for a higher, uniform spatial resolution and the need to take into account the significant difference for data between the northern and southern parts of the sea (Fig. 1).

The MHI-2024 array is based on 123,533 vertical temperature and salinity profiles collected for the 1950–2023 period from the oceanographic database of Marine Hydrophysical Institute of RAS (MHI ODB) ⁷, SeaDataNet ⁸ information

⁶ IPCC, 2021. *Climate Change 2021 – The Physical Science Basis. Working Group I Contribution to the Sixth Assessment Report of the Intergovernmental Panel on Climate Change*. Cambridge, United Kingdom and New York, NY, USA: Cambridge University Press, 2391 p. <https://doi.org/10.1017/9781009157896>

⁷ Godin, E.A., Belokopytov, V.N., Ingerov, A.V., Plastun, T.V., Galkovskaya, L.K., Kasyanenko, T.E., Zhuk, E.V. and Isaeva, E.A., 2019. *Black Sea: Hydrology – 2018. Database*. RU Patent 2019621008, Russian Patent Office.

⁸ SeaDataNet. *Pan-European Infrastructure for Ocean & Marine Data Management*. [online] Available at: <https://cdi.seadatanet.org/search> [Accessed: 16 March 2023].

resources, and Argo⁹ floats databases. All temperature and salinity profiles were quality-controlled using standard oceanographic tests and statistical criteria (3σ). To calculate the climate fields in the deep layers, we used data from CTD probes (starting from the 1990s) and Argo floats after 2010 (when the stability of salinity measuring sensors during long-term drift improved significantly), a total of 28,885 stations for the period under consideration.

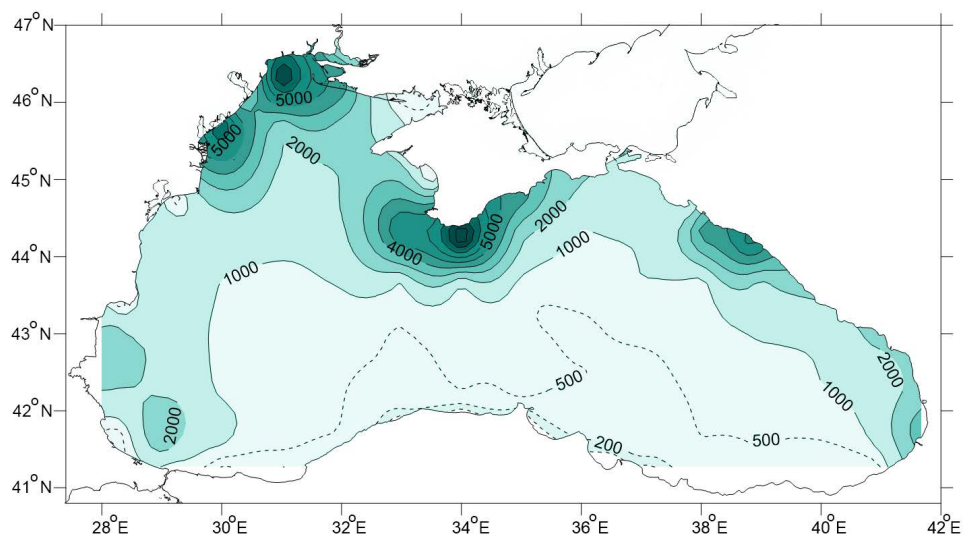


Fig. 1. Amount of oceanographic stations in the Black Sea in the $2/3^\circ \times 1^\circ$ ($40' \times 60'$) quadrants over 1950–2023

The methodological basis for calculating the existing climatic arrays is also different: in the SO SOI array, spline functions and standard statistical methods were used, in WOD-18 and MHI-2004 – the method of successive approximations [13, 14], in MEDATLAS [15] and SeaDataNet [16] (DIVAnd ver. 2.6.4) – variation inverse methods.

The calculation method of the MHI-2024 climatic array consisted of the sequential implementation of three stages.

At the first stage, the longest one, an initial array of average 10-day values for the entire observation period on a $10' \times 15'$ grid was formed for regularizing the spatiotemporal heterogeneity of the initial data and filtering out mesoscale variability [17]. The optimal interpolation method¹⁰ [18] was used with the assumption of isotropy of the spatial correlation of thermohaline fields in the Black Sea [19, 20] and the autocorrelation function from [19]. Compared to the original data (Fig. 2, *a*), the interpolated data have a more uniform distribution; however, the periods before 1957 and covering 1997–2013 remain the least covered

⁹ Coriolis Operational Oceanography. *Data Selection*. [online] Available at: <https://www.coriolis.eu.org/Data-Products/Data-selection> [Accessed: 29 December 2023].

¹⁰ Gandin, L.S., 1963. *Objective Analysis of Meteorological Fields*. Leningrad: Gidrometeoizdat, 287 p. (in Russian).

by observation data. The relative proportion of the Black Sea area covered by data in $10' \times 15'$ grid nodes does not exceed 10–15% per month in these years (Fig. 3).

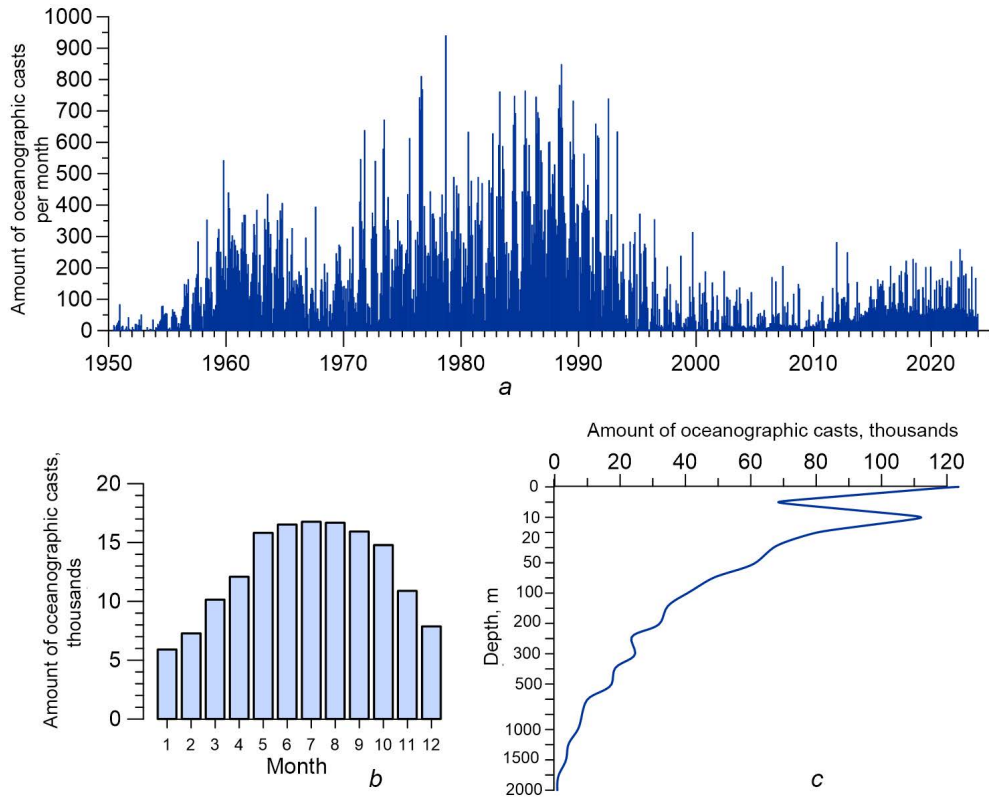


Fig. 2. Amount of oceanographic casts in the Black Sea over 1950–2023: distribution by years and months (a), months (b) and depth (c)

At the second stage, the average monthly values for each year were calculated based on the average 10-day values at the grid nodes, then the climate average monthly values were calculated as the arithmetic means of those available for 1950–2023.

At the third stage, the obtained average fields were smoothed by a Gaussian filter with a radius of 3–5 grid nodes with 2–6 iterations depending on the data availability and intraseasonal variability degree.

The resulting climatic array contains monthly average temperature and salinity fields (up to 350 m) and annual average fields (starting from 400 m) at 67 horizons: every 5 m in the 0–100 m layer with a sequential increase in the vertical step from 10 to 200 m. The climate atlas and digital array are available at the MHI ODB website ¹¹ (available for free access from 01.01.2025).

¹¹ Bank of Oceanographic Data of Marine Hydrophysical Institute of RAS. *Climatic Atlas of the Black Sea (MHI-2024): Dataset*. 2024. [online] Available at: http://bod-mhi.ru/ru/climaticAtlas_2024.shtml [Accessed: 01 January 2025].

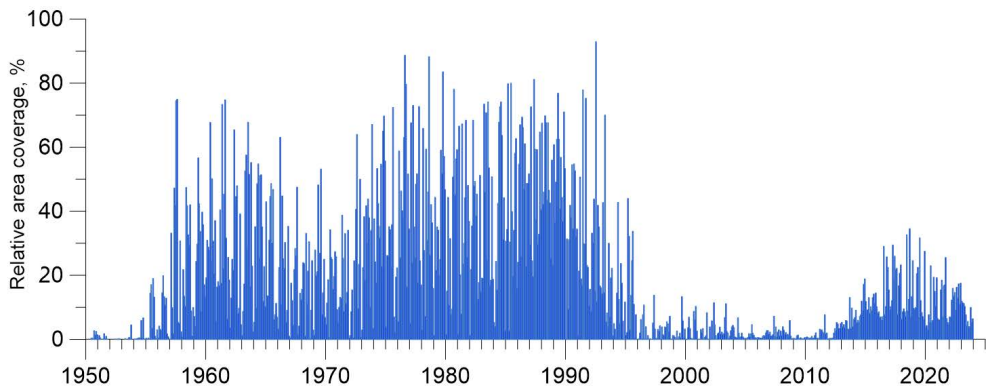


Fig. 3. Relative monthly coverage of the Black Sea water area by temperature and salinity observation data reduced to a $10' \times 15'$ grid by the optimal interpolation method

Table 1

Qualitative assessments of distinctions in spatial structure of water temperature fields for February and August in the MHI-2004, WOD-18 and SeaDataNet arrays as compared to the MHI-2024 array

Depth, m	Month	MHI-2004 (1923–2004)	WOD-18 (1981–2010)	SeaDataNet (1955–2019)
0	2	–	+	–
50	2	–	+	–
100	2	+	+	×
0	8	+	+	–
50	8	+	–	–
100	8	+	+	–
500	8	–	–	–
1000	8	–	–	+

Note: here and in Table 2, + means qualitative correspondence between field spatial structures and close quantitative values; × – qualitative correspondence between field spatial structures and significant difference of quantitative values; – – discrepancy between field spatial structures and quantitative values.

Comparison of the MHI-2024 array with the available analogues shows that their differences in the spatial structure of hydrological fields (location of minima and maxima, seasonal configuration of cyclonic gyres) are not clearly expressed systematically as they vary by seasons and depths. Tables 1 and 2 show qualitative estimates of the differences between the arrays, using February and August as the central months of the hydrological seasons. Despite the almost identical averaging period with SeaDataNet, the MHI-2024 array is generally more similar to WOD-18 and MHI-2004, although the historical periods in them coincide only partially. Most likely, it is stipulated by the more traditional nature of the approaches used to create these arrays than SeaDataNet. Considering the fact that the set of available initial oceanographic data is almost identical due to the international

exchange of hydrometeorological information, the choice of calculation methods is a determining factor for modeling the features of the spatial structure of the fields.

Table 2

Qualitative assessments of distinctions in spatial structure of salinity fields for February and August in the MHI-2004, WOD-18 and SeaDataNet arrays as compared to the MHI-2024 array

Depth, m	Month	MHI-2004 (1923–2004)	WOD-18 (1981–2010)	SeaDataNet (1955–2019)
0	2	+	+	+
100	2	+	–	–
200	2	×	–	–
0	8	+	+	×
100	8	+	–	×
200	8	+	–	×
500	8	+	+	×
1000	8	–	–	–

It is also important to consider the reliability of quantitative estimates in the deep layers of the Black Sea, where the spatiotemporal variability of thermohaline characteristics decreases sharply. The standard deviations of temperature and salinity series for the entire observation period, starting from the lower part of the main pycnocline, do not exceed 10^{-1} °C and salinity units, and they are within 10^{-3} – 10^{-2} °C and salinity units for individual ship surveys or periods of operation of specific profiling buoys. With such homogeneity of thermohaline fields, instrumental and systematic measurement errors are comparable to natural variability, while the influence of emissions or untimely calibration of instruments increases sharply. The choice of reliable deep-sea measurement data according to metrological standards is very subjective, and strict filtering of values reduces their number necessary for reliable estimates of average values. In this regard, the spatial structure of average thermohaline fields at depths > 1000 m can be considered only as approximate one in all the arrays under consideration including MHI-2024. This also applies to average annual fields, not to mention the average monthly values presented in WOD-18 and SeaDataNet. Only vertical profiles averaged over the entire deep-water area from carefully filtered data obtained by modern measuring instruments have the greatest reliability.

It is also pertinent to highlight a further issue that frequently emerges when calculating climatic arrays. This is the formation of artificial vertical inversions, which can occur as a consequence of inconsistent spatial smoothing of fields at different horizons. When creating the MHI-2024 array, an iterative procedure for monitoring the presence of density inversions was used at the third stage of calculations, followed by an increase/decrease in the radius and the number of smoothing iterations at different horizons.

Based on the deviations of the initial data and average decadal values from the climate fields, estimates of the temporal variability intensity were calculated for different scales:

- seasonal variability $D[X_{mc}]$,
- interannual-multidecadal variability $D[X'_m]$,
- mesoscale variability $D[X'_s]$,
- submesoscale variability $D[X'] - (D[X'_m] + D[X'_s])$,
- intraseasonal variability $D[X']$, which means the total variability minus the seasonal cycle, i.e. the sum of submesoscale, mesoscale and lower-frequency (from interannual to multidecadal) variability. Here,

D – variance operator;

X – initial observation data;

X_{mc} – climate average monthly seasonal course;

$X'_m = M[X'_d]$ – monthly average anomalies,

M – mean value operator,

$X'_d = X_d - X_{mc365}$ – average 10-day anomalies (from the climate seasonal cycle and linear trend (at depths >100 m)),

X_d – average 10-day values (for 10 days),

X_{mc365} – climate average monthly seasonal course, approximated for each day of the year by two harmonics;

$X'_s = X'_d - X'_m$ – mesoscale anomalies,

$X'_d = X_d - X_{mc365}$ – average 10-day anomalies (from the climate seasonal cycle and linear trend (at depths >100 m)).

Estimates of the intensity of interannual-multidecadal variability are necessary to determine the significance of long-term climate anomalies, estimates of the total intraseasonal variability help to filter measured and calculated values and estimates of mesoscale and submesoscale variability can be taken into account when studying processes of the corresponding scales.

Discussion of results

As described earlier in [21], the average vertical distribution of the estimates of the water temperature temporal variability for the Black Sea (Fig. 4, *a*) is characterized by one maximum: at the sea surface for the seasonal course, in the seasonal thermocline layer for the other ranges of variability. As for salinity (Fig. 4, *b*), all types of temporal variability have two maxima: first, at the sea surface and second, in the main halocline. Compared to [21], the estimate of the amplitude of the salinity seasonal course in the surface layer has increased as well as the estimate of the contribution of temperature and salinity submesoscale variability, which is most likely due to the fact that it was previously determined based on a fairly small number of multi-day stations. The spatial distribution of seasonal variability in the Black Sea corresponds to traditional concepts [1, 21], new estimates cover the southern part of the sea in more detail (Fig. 5).

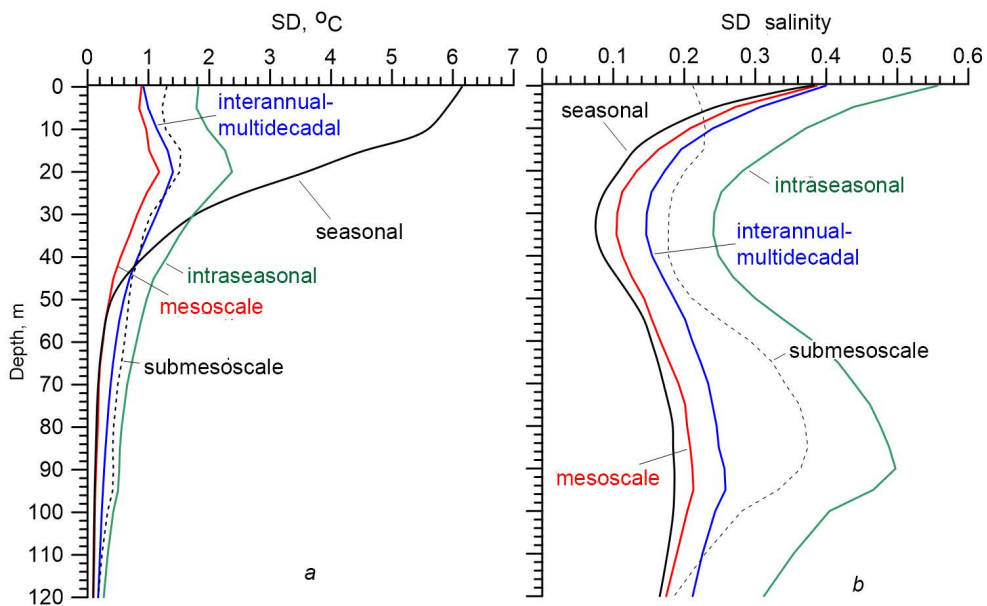


Fig. 4. Vertical distribution of the Black Sea average estimates of temporal variability of different scales for water temperature (a) and salinity (b)

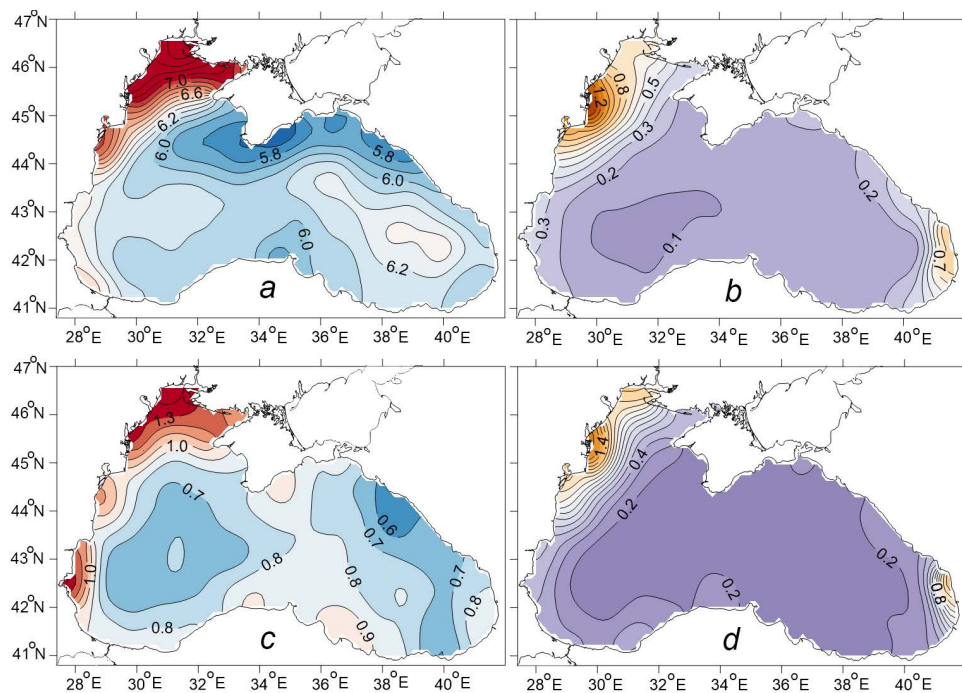


Fig. 5. Spatial distribution of temporal variability estimates on the sea surface: seasonal (a) and intraseasonal (c) water temperature SD; seasonal (b) and intraseasonal (d) salinity SD

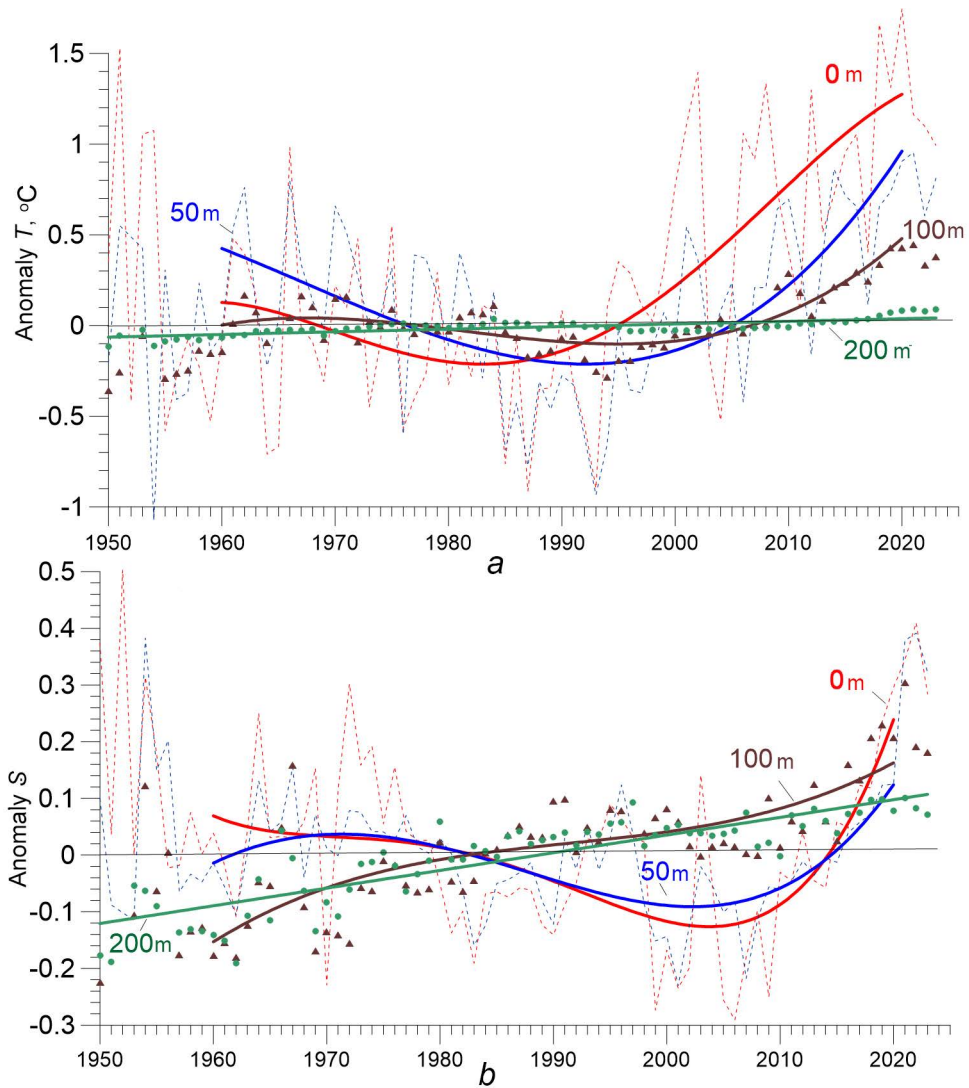


Fig. 6. Time-series of the Black Sea average annual anomalies relative to climatic seasonal values at different depths for 1950–2023: water temperature (*a*) and salinity (*b*). Thin dashed lines and symbols show anomaly values, thick lines – polynomial approximation; individual depths are highlighted in different colors

To estimate the scale of regional climate changes, average monthly and average annual temperature and salinity anomalies were calculated relative to the seasonal climate cycle at the regular grid nodes of the MHI-2024 array (Figs. 6, 7). The ratio of current anomalies to the interannual-multidecadal variability SD characterizes the relative intensity of climate changes.

After the 1980–1990s relative cooling, positive annual average anomalies prevail in the temperature field of the Black Sea waters (Fig. 6, *a*). In the surface layer, the excess of the interannual SD (1.0 °C) has been observed in some years since 2000. After 2015, the warming has been steadily exceeding the average background of interannual variability. At the 50 m horizon (CIL), the excess of the interannual

SD ($0.6\text{ }^{\circ}\text{C}$) by temperature anomalies has been appearing in some years since 2010, steadily – since 2015, which is often noted in the literature as the CIL going beyond the $8\text{ }^{\circ}\text{C}$ isotherm. It should be noted that the excess of the CIL core temperature by $8\text{ }^{\circ}\text{C}$ is not an extremely rare phenomenon as it occurred earlier at times (in the late 1930s and in 1962–1972).

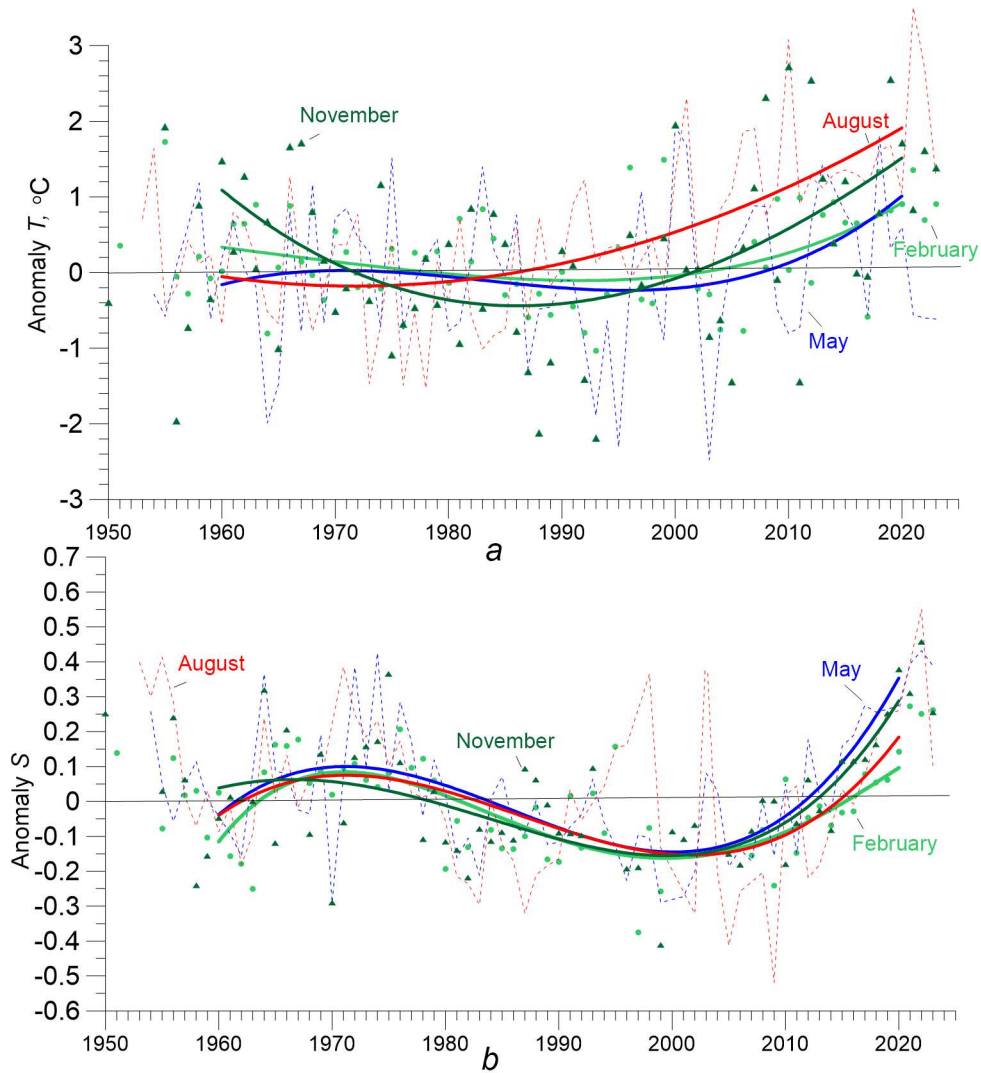


Fig. 7. Time-series of the Black Sea average monthly anomalies relative to climatic values on the sea surface in the central months of hydrological seasons for 1950–2023: water temperature (*a*) and salinity (*b*). Thin dashed lines and symbols show anomaly values, thick lines –polynomial approximation; individual months are highlighted in different colors

Also, since 2015, a stable excess of the interannual SD ($0.2\text{ }^{\circ}\text{C}$) has been observed at the 100 m horizon. Below the 150 m depth, a stable long-term water temperature rise has been observed from the very beginning of oceanographic observations in the Black Sea. The highest seasonal increase in temperature in

the surface layers occurs in summer-autumn period when the warming rate is 1.5–2 times higher than in winter-spring one (Fig. 7, *a*).

After the period of surface layer freshening in the Black Sea in 1980–2010, a sharp increase in salinity has been observed approximately from 2010–2012 (Fig. 6, *b*). However, the average annual anomalies do not yet exceed the interannual salinity SD (0.4) and are comparable in magnitude with the positive anomalies of 1950–1970. The quality of salinity measurements in hydrological surveys of the 1950s can be questionable; however, measurements at coastal hydrometeorological stations also indicate high salinity values during that period.

The CIL (50 m depth) and surface layer interannual-multidecadal trends are similar, with a constant long-term increase in salinity continuing in the main halocline (≥ 75 m). The greatest seasonal increase in salinity in the surface layers takes place in spring and autumn, during the months of the positive phase of the basin water balance, indicating its general decrease and transition of the region to more arid conditions (Fig. 7, *b*).

Conclusion

Compared with global estimates of the 1950–2020 climate warming rate, the linear trend of surface temperature increase in the Black Sea (0.2 °C/10 years) is generally higher than the World Ocean average trend. According to this indicator, the Black Sea belongs to areas with an increased warming rate, such as the tropical parts of the Atlantic and the Indian Ocean and the western half of the Pacific Ocean. At the same time, the Black Sea trend over a 70-year period does not reach such high values as in the Arctic seas, in the Gulf Stream-Labrador Current interaction zone or in the Falkland Current. In 1980–2020, there was a notable rise in the surface temperature of the Black Sea amounted to 0.5 °C/10 years, second only to the trends in the Arctic regions.

Compared to global climate trends in salinity changes over 1950–2020, the Black Sea trend in the surface layer of $0.03/10$ years corresponds to positive trends in high salinity areas, in particular in large-scale subtropical gyres. Such a rate of sharp salinization as in the Black Sea in 2000–2020 ($0.18/10$ years) is generally not typical for the ocean. Such rapid processes are typical of inland seas with limited external water exchange, strongly dependent on the regional freshwater balance.

In the sequence of multidecadal fluctuations in the Black Sea general hydrological state, the current warm and salty phase is similar to the 1960–1970s, but with a greater amplitude of fluctuations. Both current state and the period of 1960–1970s, in turn, follow the colder and less salty phases preceded.

REFERENCES

1. Gertman, I.F., 1991. [Thermohaline Structure of the Black Sea]. In: A. I. Simonov and E. N. Altman, eds., 1991. *Hydrometeorology and Hydrochemistry of Seas in the USSR. Vol. 4. Black Sea. Issue 1. Hydrometeorological Conditions*. St. Petersburg: Gidrometeoizdat, pp. 146–195 (in Russian).
2. Locarnini, R.A., Mishonov, A.V., Baranova, O.K., Boyer, T.P., Zweng, M.M., Garcia, H.E., Reagan, J.R., Seidov, D., Weathers, K.W. [et al.], 2019. *World Ocean Atlas 2018. Volume 1: Temperature*. Silver Spring, MD, USA: NOAA Atlas NESDIS, 52 p.

3. Zweng, M.M., Reagan, J.R., Seidov, D., Boyer, T.P., Locarnini, R.A., Garcia, H.E., Mishonov, A.V., Baranova, O.K., Weathers, K.W. [et al.], 2019. *World Ocean Atlas 2018. Volume 2: Salinity*. Silver Spring, MD, USA: NOAA Atlas NESDIS, 50 p.
4. Suvorov, A.M., Palmer, D.R., Khaliulin, A.K., Godin, E.A. and Belokopytov, V.N., 2003. Digital Atlas and Evaluation of the Influence of Inter-Annual Variability on Climate Analyses. In: *Oceans 2003. Celebrating the Past... Teaming Toward the Future*. San Diego, CA, USA: IEEE. Vol. 2, pp. 990-995. <https://doi.org/10.1109/OCEANS.2003.178468>
5. Polonsky, A.B., Shokurova, I.G. and Belokopytov, V.N., 2013. Decadal Variability of Temperature and Salinity in the Black Sea. *Morskoy Gidrofizicheskiy Zhurnal*, (6), pp. 27-41 (in Russian).
6. Miladinova, S., Stips, A., Garcia-Gorriiz, E. and Macias Moy, D., 2017. Black Sea Thermohaline Properties: Long-Term Trends and Variations. *Journal of Geophysical Research: Oceans*, 122(7), pp. 5624-5644. <https://doi.org/10.1002/2016JC012644>
7. Polonsky, A.B. and Serebrennikov, A.N., 2023. Changes in the Nature of Temperature Anomalies of the Black Sea Surface during the Warming Period of the Late 20th – Early 21st Centuries. *Issledovanie Zemli iz Kosmosa*, (6), pp. 118-132. <https://doi.org/10.31857/S0205961423060064> (in Russian).
8. Belokopytov, V.N., 2011. Interannual Variations of the Renewal of Waters of the Cold Intermediate Layer in the Black Sea for the Last Decades. *Physical Oceanography*, 20(5), pp. 347-355. <https://doi.org/10.1007/s11110-011-9090-x>
9. Capet, A., Troupin, C., Carstensen, J., Grégoire, M. and Beckers, J.-M., 2014. Untangling Spatial and Temporal Trends in the Variability of the Black Sea Cold Intermediate Layer and Mixed Layer Depth Using the DIVA Detrending Procedure. *Ocean Dynamics*, 64(3), pp. 315-324. <https://doi.org/10.1007/s10236-013-0683-4>
10. Miladinova-Marinova, S., Stips, A., Garcia Gorris, E. and Macias Moy, D., 2018. Formation and Changes of the Black Sea Cold Intermediate Layer. *Progress in Oceanography*, 167, pp. 11-23. <https://doi.org/10.1016/j.pocean.2018.07.002>
11. Stanev, E.V., Peneva, E. and Chtirkova, B., 2019. Climate Change and Regional Ocean Water Mass Disappearance: Case of the Black Sea. *Journal of Geophysical Research: Oceans*, 124(7), pp. 4803-4819. <https://doi.org/10.1029/2019JC015076>
12. Polonskii, A.B. and Novikova, A.M., 2020. Interdecadal Variability of the Black Sea Cold Intermediate Layer and Its Causes. *Russian Meteorology and Hydrology*, 45(10), pp. 694-700. <https://doi.org/10.3103/S1068373920100039>
13. Cressman, G.P., 1959. An Operational Objective Analysis System. *Monthly Weather Review*, 87(10), pp. 367-374. [https://doi.org/10.1175/1520-0493\(1959\)087<0367:AOOAS>2.0.CO;2](https://doi.org/10.1175/1520-0493(1959)087<0367:AOOAS>2.0.CO;2)
14. Barnes, S.L., 1964. A Technique for Maximizing Details in Numerical Weather Map Analysis. *Journal of Applied Meteorology and Climatology*, 3(4), pp. 396-409. [https://doi.org/10.1175/1520-0450\(1964\)003<0396:ATFMDI>2.0.CO;2](https://doi.org/10.1175/1520-0450(1964)003<0396:ATFMDI>2.0.CO;2)
15. Rixen, M., Beckers, J.-M., Brankart, J.-M. and Brasseur, P., 2000. A Numerically Efficient Data Analysis Method with Error Map Generation. *Ocean Modelling*, 2(1-2), pp. 45-60. [https://doi.org/10.1016/S1463-5003\(00\)00009-316](https://doi.org/10.1016/S1463-5003(00)00009-316)
16. Barth, A., Beckers, J.-M., Troupin, C., Alvera-Azcàrate, A. and Vandenbulcke, L., 2014. DIVAnd-1.0: n-Dimensional Variational Data Analysis for Ocean Observations. *Geoscientific Model Development*, 7(1), pp. 225-241. <https://doi.org/10.5194/gmd-7-225-2014>
17. Belokopytov, V.N., 2018. Retrospective Analysis of the Black Sea Thermohaline Fields on the Basis of Empirical Orthogonal Functions. *Physical Oceanography*, 25(5), pp. 380-389. <https://doi.org/10.22449/1573-160X-2018-5-380-389>
18. Bretherton, F.P., Davis, R.E. and Fandry, C.B., 1976. A Technique for Objective Analysis and Design of Oceanographic Experiments Applied to MODE-73. *Deep Sea Research and Oceanographic Abstracts*, 23(7), pp. 559-582. [https://doi.org/10.1016/0011-7471\(76\)90001-2](https://doi.org/10.1016/0011-7471(76)90001-2)
19. Grigor'ev, A.V., Ivanov, V.A. and Kapustina, N.A., 1996. Correlation Structure of the Black Sea Thermohaline Fields in the Summer Season. *Oceanology*, 36(3), pp. 334-339.

20. Polonskii, A.B. and Shokurova, I.G., 2008. Statistical Structure of the Large-Scale Fields of Temperature and Salinity in the Black Sea. *Physical Oceanography*, 18(1), pp. 38-51. <https://doi.org/10.1007/s11110-008-9008-4>
21. Ivanov, V.A. and Belokopytov, V.N., 2013. *Oceanography of the Black Sea*. Sevastopol: ECOSI-Gidrofizika, 212 p.

Submitted 03.07.2024; approved after review 28.08.2024;
accepted for publication 12.09.2024.

About the authors:

Vladimir N. Belokopytov, Leading Researcher, Head of the Oceanography Department, Marine Hydrophysical Institute of RAS (2 Kapitanskaya Str., Sevastopol, 299011, Russian Federation), DSc (Geogr.), **WoS ResearcherID: ABA-1230-2020**, **ORCID ID: 0000-0003-4699-9588**, **Scopus Author ID: 6602381894**, v.belokopytov@gmail.com

Elena V. Zhuk, Junior Researcher, Marine Hydrophysical Institute of RAS (2 Kapitanskaya Str., Sevastopol, 299011, Russian Federation), **ORCID ID: 0000-0002-4263-7734**, **WoS ResearcherID: JCD-8660-2023**, **Scopus Author ID: 57191412660**, alenixx@gmail.com

Contribution of the co-authors:

Vladimir N. Belokopytov – methods development; data processing; qualitative and quantitative analysis of research results, discussion and conclusions

Elena V. Zhuk – data processing; preparation and carrying out calculations; visualization and analysis of the results

The authors have read and approved the final manuscript.

The authors declare that they have no conflict of interest.

Original article

“Bloom” of Coccolithophores in the Black Sea Based on Remote Sensing Data Obtained in 1998–2023: Intensity and Frequency

T. Ya. Churilova^{1,✉}, V. V. Suslin², O. V. Krivenko¹¹ A. O. Kovalevsky Institute of Biology of the Southern Seas of RAS, Sevastopol, Russian Federation² Marine Hydrophysical Institute of RAS, Sevastopol, Russian Federation

✉ tanya.churilova@gmail.com

Abstract

Purpose. Monitoring of coccolithophore “bloom” is becoming increasingly important due to their influence on the biogeochemical cycles. The purpose of the study is to analyze the frequency, intensity and area of *Gephyrocapsa huxleyi* “bloom” in different sub-regions of the Black Sea, as well as to assess the effect of environmental conditions on the intensity and interannual variability of “bloom”.

Methods and Results. Based on the satellite data and using the regional algorithms, the values of chlorophyll a concentration, the particulate backscattering coefficient and the coefficient of light absorption by colored detrital matter were retrieved with a two-week averaging for different Black Sea sub-regions for the period 1998–2023. Application of the normalized anomalies made it possible to reveal the annual cycles of variability of these parameters, as well as to identify their common patterns and variability features in particular sub-regions of the sea.

Conclusions. It has been established that in early June in all the regions of the sea, the “bloom” of *Gephyrocapsa huxleyi* was regularly observed; at that it was characterized by a year-to-year variability in its intensity and area. High light intensity in the sea upper mixed layer is a key factor for a shift in the phytoplankton species structure and for the transition to *Gephyrocapsa huxleyi* dominance and “bloom” due to the physiologically determined ability of these algae to grow at an extremely high light intensity with no inhibition, whereas at similar light conditions the growth of other plankton microalgae is suppressed. In most sub-regions of the Black Sea, the “bloom” of *Gephyrocapsa huxleyi* is not followed by an increase in the phytoplankton biomass, only the structure of phytoplankton species changes. The exception is the coastal waters affected by the river runoffs: the “bloom” there is observed when the phytoplankton biomass grows. In the coastal waters during a cold period (December, February), the *Gephyrocapsa huxleyi* abundance sometimes increases due to a decrease of nutrient supply that results from weakening of the river runoffs and/or increasing stability of the water column. Decrease in phytoplankton supply with nutrients contributes to the competitive growth of coccolithophores as compared to other types of phytoplankton. The development of *Gephyrocapsa huxleyi* “bloom” in different seasons can reflect its genetic and physiological plasticity.

Keywords: coccolithophores, *Gephyrocapsa huxleyi*, *Emiliania huxleyi*, coccolithophore “bloom”, water bloom, chlorophyll concentration, light scattering, light absorption, colored detrital matter, remote sensing, Black Sea

Acknowledgments: The frequency, intensity and area of *Gephyrocapsa huxleyi* “bloom” in different sub-regions of the Black Sea were studied within the framework of a state assignment of FSBSI FRC MHI on theme No. FNNN-2023-0001, annual and interannual variability of bio-optical water features – within the framework of a state assignment of FRC IBSS on theme No. 124030100106-2, the long-term data series were obtained based on satellite data and using the regional algorithms within the framework of a state assignment of FSBSI FRC MHI on theme No. FNNN-2024-0012.

For citation: Churilova, T.Ya., Suslin, V.V. and Krivenko, O.V., 2024. “Bloom” of Coccolithophores in the Black Sea Based on Remote Sensing Data Obtained in 1998–2023: Intensity and Frequency. *Physical Oceanography*, 31(6), pp. 802-825.

© 2024, T. Ya. Churilova, V. V. Suslin, O. V. Krivenko

© 2024, Physical Oceanography



Introduction

Coccolithophores (*Coccolothophyceae*) are planktonic haptophyte algae that are ubiquitous throughout the World Ocean [1]. Their distinctive feature is calcareous (CaCO_3) plates – coccoliths – covering the entire cell surface. The most extensively studied species of this group is *Gephyrocapsa huxleyi* (Lohmann) P. Reinhardt, 1972 syn. *Emiliana huxleyi* (Lohmann) W.W. Hay & H. Mohler 1967¹. The massive development of this species is periodically recorded in different areas of the ocean, that leads to a powerful sea blooming, covering an area of hundreds of thousands of square kilometers [1, 2].

Coccolithophores are important producers of organic matter in the ocean, with an estimated contribution to primary production of 1–10%. They also play a crucial role in the downward transport of CaCO_3 and the formation of calcareous bottom sediments [3, 4]. The optical characteristics of the sea are subject to significant change as a result of the accumulation of coccospheres and coccoliths in the water [2, 3]. It is predicted that current climate changes may significantly affect the growth of coccolithophores and calcification processes, in different ways at low and high latitudes [5, 6]. Over the past two decades, a significant increase in the number of coccolithophores has been noted in the Atlantic Ocean [7, 8]. Due to the essential impact of these microalgae on the global carbon cycle [5, 6, 9], the study of *G. huxleyi* “blooms” remains a priority [2].

In the most general terms, a “bloom” can be defined as the accumulation of phytoplankton biomass within a certain water area as a result of the microalgae growth rate exceeding the cell loss rate. The cell loss is determined by the natural mortality of algae and the consumption by zooplankton. Following an increase in biomass, values return to levels close to the baseline [10]. Commonly, there is an outbreak of one (monospecific “bloom”) or 2–3 species of microalgae, accompanied by an increase in phytoplankton biomass, lasting between a week and a month [11, 12]. A high degree of dominance by a single taxon is an important sign of “bloom”, and it is determined by the capacity of certain species to grow faster than other algae species under given environmental conditions [11, 13, 14].

Spring phytoplankton “bloom”, which are regularly observed in mid- and high-latitude regions, are associated with the rapid growth of diatoms against the background of favorable light conditions, abundant nutrient availability, and weak grazing pressure typical of that season [15–17]. The growth rate of diatoms reaches a maximum under conditions of intense vertical mixing of waters at high dissolved inorganic nutrient concentrations in the environment [13, 18]. The accumulation of algal biomass persists until the number of zooplankton feeding on them enhance in response to an increase in food availability and/or when nutrient supply becomes depleted [19]. The identification of the “bloom” and its subsequent dynamics analysis are based on the phytoplankton biomass, which is often recorded using the concentration of the main photosynthetically active pigment, chlorophyll *a*, as a marker [11].

¹ AlgaeBase. *Listing the World's Algae*. [online] Available at: <https://www.algaebase.org> [Accessed: 17 July 2024].

In contrast to the spring “bloom” of diatoms, massive development of coccolithophores is typically not accompanied by a meaningful increase in phytoplankton biomass [20, 21]. Accordingly, the criterion for identifying the “bloom” of *G. huxleyi* is based on its abundance, with a threshold value of 1 million cells per liter. The *G. huxleyi* “bloom” typically occurs in the context of elevated solar radiation and limited availability of nutrients [1–3].

Regular studies carried out in the Black Sea over a two-years period revealed a change in the species composition of phytoplankton in late spring – early summer, with a constant chlorophyll a concentration [20]. In May, dinoflagellates formed the majority of phytoplankton, while coccolithophores contributed up to 80% of the phytoplankton biomass in June [20]. Furthermore, high abundances of *G. huxleyi*, exceeding a million cells per liter, have been recorded in coastal and shelf waters, as well as during the cold season [22].

Remote sensing methods offer a broad range of opportunities for the study of water quality and productivity at different temporal and spatial scales. The remote diagnostic of coccolithophore “blooms” is based on the unique optical characteristics of their cells, which exhibit an order of magnitude higher backscattering index (b_{bp}) compared to other microalgae due to a high refractive index of coccoliths and coccosphere [23]. Satellite data have demonstrated that coccolithophore “blooms” in the Black Sea are observed annually at the beginning of summer [24–28]. However, the intra-annual dynamics of *G. huxleyi* concentrations in different regions of the Black Sea have not been sufficiently studied yet, as well as their relationship with chlorophyll a concentration (a marker of phytoplankton biomass) and the effect of environmental factors on these dynamics.

The following regional satellite algorithms have been developed for the Black Sea: 1) retrieval of primary hydrooptical properties of the sea surface layer [29], including b_{bp} ; 2) assessment of the chlorophyll a (C_a) concentration [30]. These allow analysis of the seasonal and interannual dynamics of these parameters in different areas of the sea, their relationship with environmental characteristics, such as sea surface temperature (SST), depth of the upper mixed layer (Z_{UML}) and photosynthetically available radiation incident on the sea surface (PAR_0).

The aim of this study is to investigate the frequency, intensity, and area of the *Gephyrocapsa huxleyi* “bloom” in different parts of the Black Sea, as well as to evaluate the impact of environmental factors on the strength and interannual variation of blooming events.

Methods

The b_{bp} value at 555 nm ($b_{bp}(555)$) was estimated from satellite data using a regional model [29]. The *G. huxleyi* cell concentration (NEh) was determined from the NEh versus $b_{bp}(555)$ dependence established from in situ NEh data [31].

The values of C_a and light absorption coefficient by colored detrital matter at 490 nm ($a_{CDM}(490)$) were estimated based on satellite data using regional algorithm [30]. The Z_{UML} values were determined according to [32].

For the Black Sea sub-regions (Fig. 1), as identified according to hydrophysical features [33], the mean values of the studied parameters were calculated with two-week averaging for the period 1998–2023. A 2-km zone along the entire Black Sea coast was excluded from the analysis. To assess the seasonal dynamics of $b_{bp}(555)$,

NEh , SST , C_a , $a_{CDM}(490)$ and Z_{UML} , the monthly mean anomalies normalized by the standard deviation (X_{ij}^σ), were used:

$$X_{ij}^\sigma = (\bar{X}_{ij} - \bar{\bar{X}}_j) / \sigma \bar{\bar{X}}_j, \quad (1)$$

where X is the parameter under consideration; \bar{X}_{ij} is its monthly mean for the i month and j region; $\bar{\bar{X}}_j$ and $\sigma \bar{\bar{X}}_j$ are the long-term mean and its standard deviation (SD) for the j region.

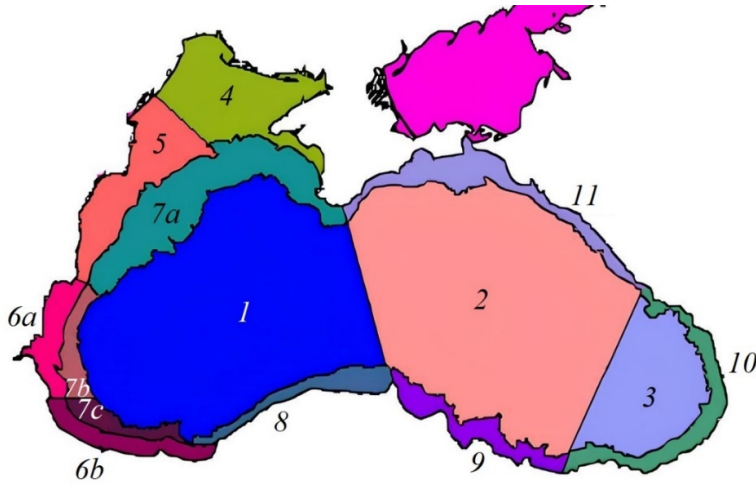


Fig. 1. Map of Black Sea sub-regions defined by hydrodynamic features [33]

The interannual variability of the X parameter was estimated using annual averages of monthly mean anomalies normalized by $SD(X_{ijy}^\sigma)$, which was calculated as follows:

$$X_{ijy}^\sigma = (\bar{X}_{ijy} - \bar{\bar{X}}_{ij}) / \sigma \bar{\bar{X}}_{ij},$$

where \bar{X}_{ijy} is its monthly mean for the i month, y year and j region; $\bar{\bar{X}}_{ij}$ and $\sigma \bar{\bar{X}}_{ij}$ is the long-term mean and SD for the i month and j region.

Radiance within the upper mixed layer was determined from PAR_0 (*SeaWiFS* and *MODIS* spectroradiometer data) using the relationship between the depth of the photosynthetic zone ($Z_{1\%}$) and Z_{UML} . $Z_{1\%}$ values were estimated from the diffuse attenuation index of light at 490 nm wavelength, reconstructed from *SeaWiFS* and *MODIS* satellite data, according to [34].

Results

Data series ($b_{bp}(555)$, NEh , SST , C_a , $a_{CDM}(490)$ and Z_{UML}), calculated with two-week averaging for each sea sub-region (Fig. 1) from 1998 to 2023, were obtained. Fig. 2 shows the dynamics of $b_{bp}(555)$ in each sub-region over the specified period. Seasonal and interannual variability in this parameter are evident in all sub-regions (Fig. 2).

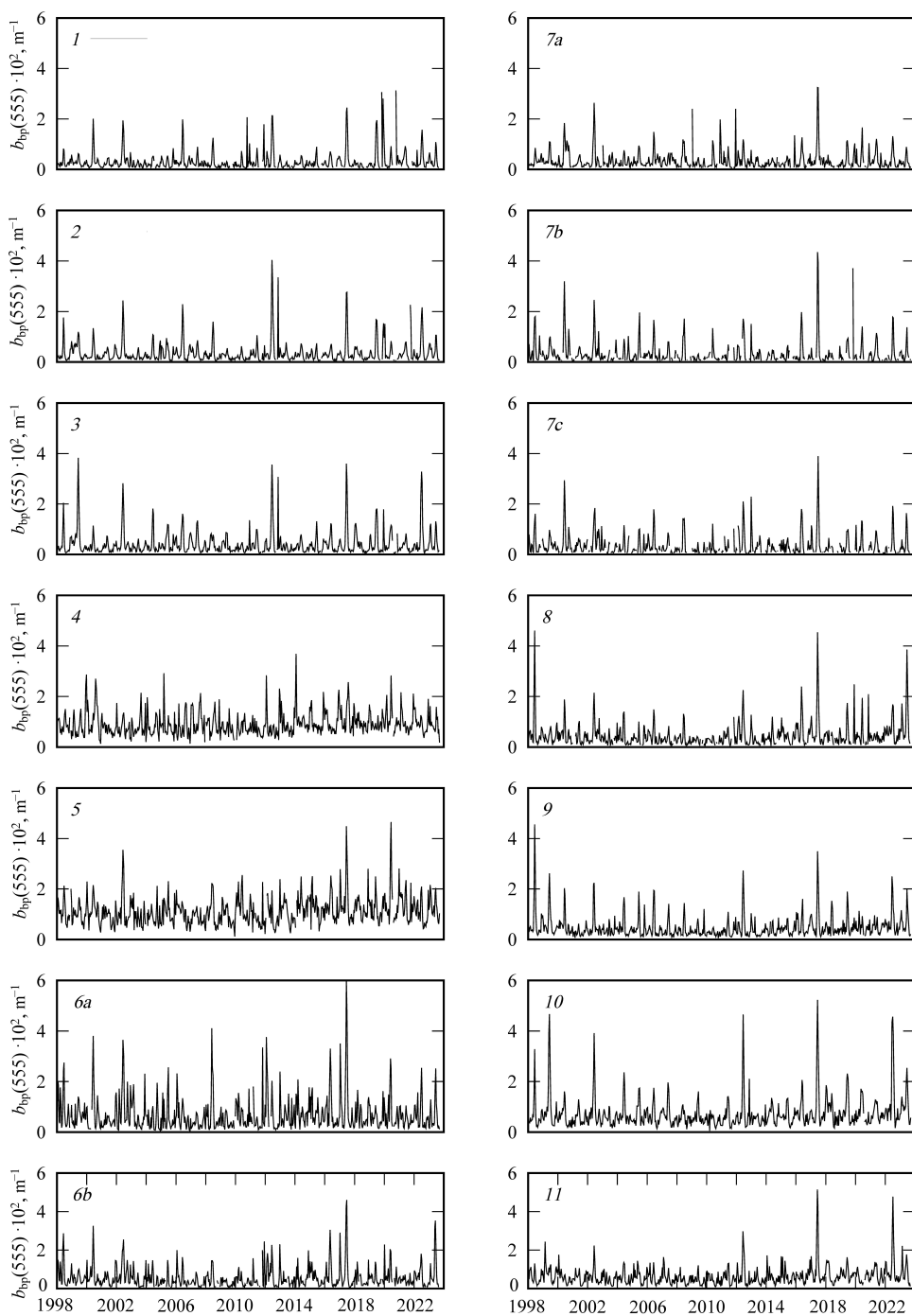


Fig. 2. Dynamics of two-week averages of particulate back scattering coefficient at wavelength 555 nm ($b_{bp}(555) \cdot 10^2$) calculated for the sub-regions of the Black Sea (in this and the following figures, the region number is in the upper left corner of each fragment)

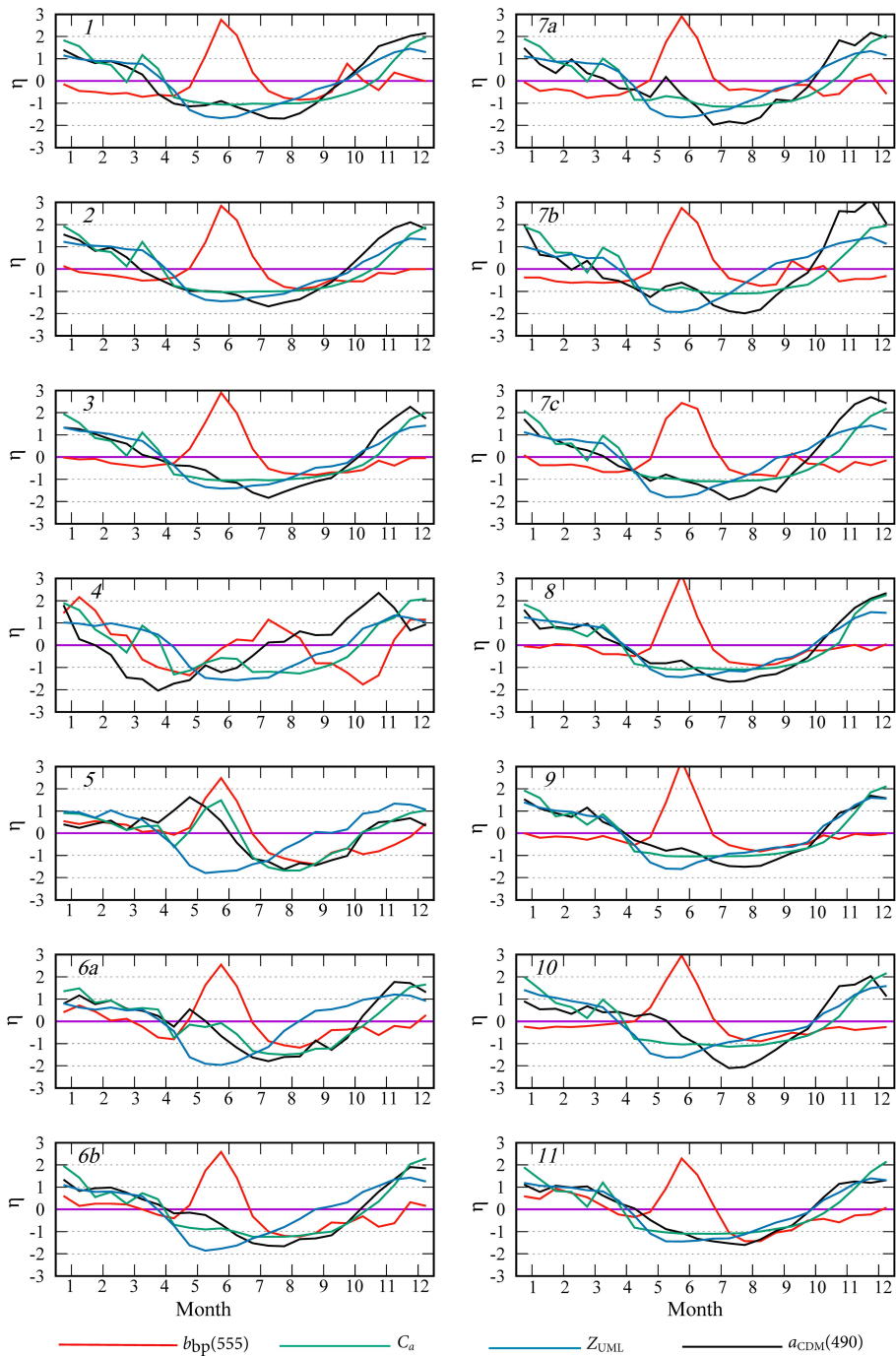


Fig. 3. Normalized monthly mean anomalies (η) of the particulate backscattering coefficient at wavelength 555 nm ($b_{bp}(555)$), concentration of chlorophyll a (C_a), thickness of the upper mixed layer (Z_{UML}), coefficient of light absorption by colored detrital matter at wavelength 490 nm ($a_{CDM}(490)$) in particular sub-regions of the Black Sea

Normalized anomalies allow the identification of intra-annual cycles in all parameters (Fig. 3). The peak value of $b_{bp}(555)$ is recorded in June with a high probability (normalized anomaly exceeding 2) in almost all sub-regions. On the northwestern shelf (region 4), the $b_{bp}(555)$ maximum is observed in different months throughout summer, which reduces the statistical probability of its occurrence (normalized anomaly about 1) (Fig. 3). In the Black Sea, C_a concentrations are lowest in summer, except for areas affected by the Danube, Dnieper and Dniester runoff (sub-regions 4, 5 and 6, *a*). In these sub-regions an increase in C_a levels is observed during summer months (Fig. 3). The long-term means of the (\bar{X}_j) and SD ($\sigma\bar{X}_j$) (see Table) together with the annual dynamics of the normalized anomalies (see Fig. 2) allow us to calculate the monthly averages of each parameters in a specific sub-region of the sea using equation (1). In the deep-water sub-regions (sub-regions 1–3), the monthly long-term mean of C_a in June was between 0.15 and 0.25 $mg \cdot m^{-3}$.

A comparison of the annual cycles of $b_{bp}(555)$ and C_a revealed no relationship between these parameters (Fig. 3). The regularly observed maximum of $b_{bp}(555)$ in June is not accompanied by an increase in C_a values in all the sea sub-regions, with the exception of coastal waters subject to the Danube, Dnieper and Dniester runoff (sub-regions 4, 5, 6, *a*), where the summer maximum of $b_{bp}(555)$ is observed against a spring-summer C_a increase (Fig. 3). In these sub-regions (4, 5 and 6, *a*), the $b_{bp}(555)$ values demonstrate an inverse proportionality to the C_a values (Fig. 4).

Long-term average values of chlorophyll a concentration (C_a), $mg \cdot m^{-3}$, light absorption coefficient by colored detrital matter at wavelength 490 nm ($a_{CDM}(490)$), m^{-1} , and concentration of *G. huxleyi* cells (NEh), $mln \cdot cell \cdot l^{-1}$ calculated for the water upper layer in different regions of the Black Sea

Region	$a_{CDM}(490) \pm SD$	$C_a \pm SD$	$NEh \pm SD$
1	0.050 ± 0.045	0.69 ± 0.50	0.32 ± 0.30
2	0.051 ± 0.046	0.69 ± 0.50	0.36 ± 0.38
3	0.056 ± 0.051	0.67 ± 0.49	0.42 ± 0.45
4	0.112 ± 0.107	0.91 ± 0.79	0.91 ± 0.93
5	0.134 ± 0.133	1.43 ± 1.36	1.12 ± 1.17
6a	0.109 ± 0.104	0.96 ± 0.86	0.69 ± 0.71
6b	0.090 ± 0.083	0.75 ± 0.63	0.57 ± 0.59
7a	0.058 ± 0.055	0.68 ± 0.58	0.35 ± 0.37
7b	0.062 ± 0.056	0.66 ± 0.56	0.35 ± 0.35
7c	0.064 ± 0.057	0.64 ± 0.53	0.37 ± 0.38
8	0.077 ± 0.070	0.69 ± 0.56	0.47 ± 0.47
9	0.074 ± 0.069	0.65 ± 0.55	0.48 ± 0.50
10	0.084 ± 0.077	0.68 ± 0.57	0.73 ± 0.79
11	0.068 ± 0.064	0.60 ± 0.50	0.64 ± 0.67

Note: SD is standard deviation.

An increase in C_a and $a_{CDM}(490)$ is observed in the northwestern shelf (sub-region 4) in May – June (Fig. 3). In the area of the Danube mouth (sub-region 5), this increase is more pronounced, and the normalized values of the anomalies of these parameters exceed 1 (Fig. 3).

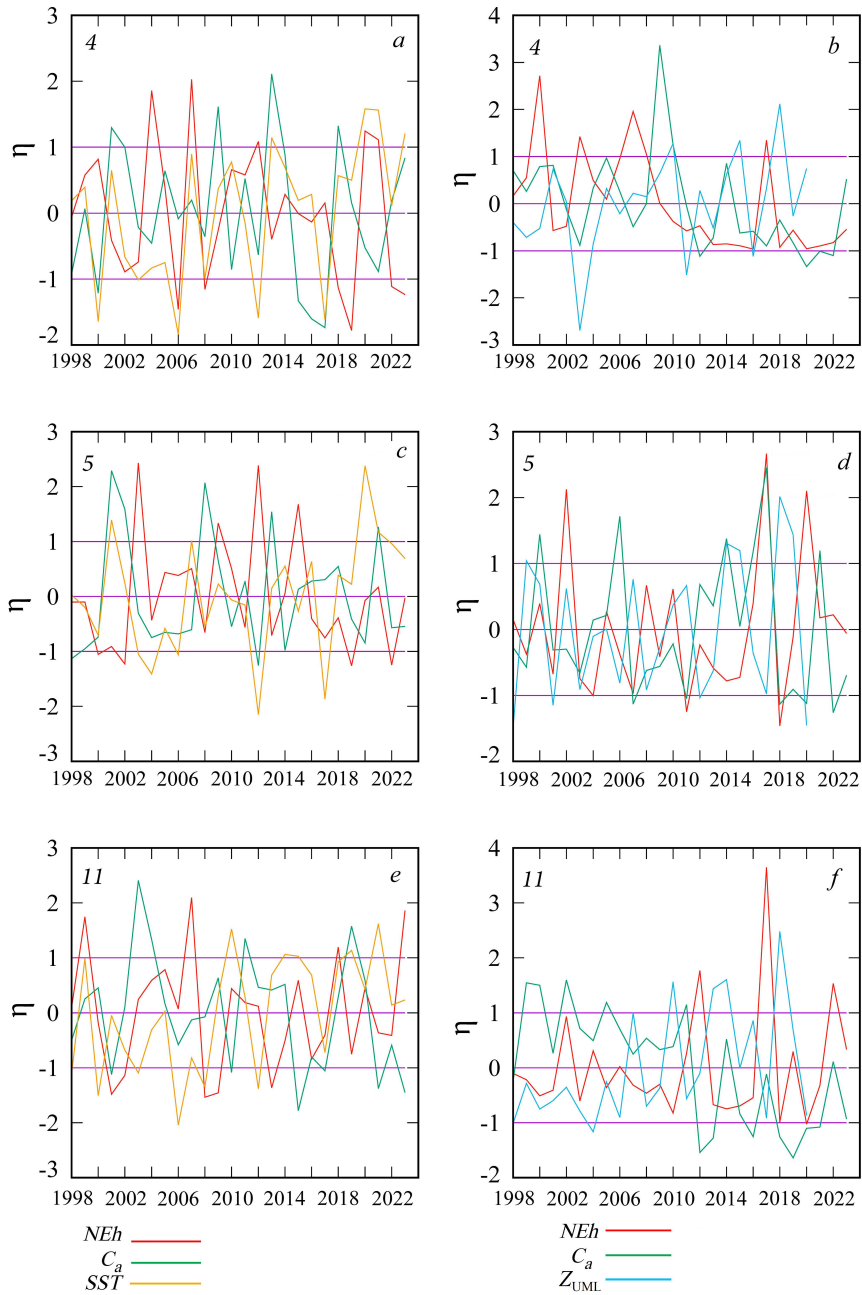


Fig. 4. Interannual variability of normalized monthly mean anomalies (η) of *G. huxleyi* cell abundance (NEh), chlorophyll a concentration (C_a), sea surface temperature (SST), and thickness of the upper mixed layer (Z_{UML}) in February (*a, c, e*), June (*d, f*) and August (*b*) in sub-regions 4, 5 and 11

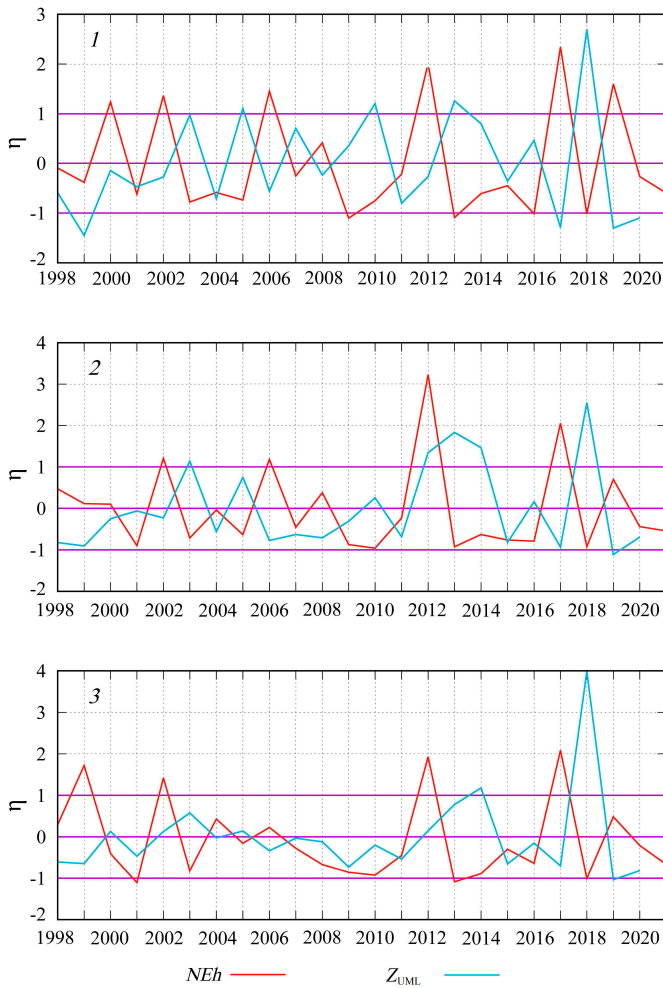


Fig. 5. Interannual variability of normalized monthly mean anomalies (η) of *G. huxleyi* cell abundance (NEh) and thickness of the upper mixed layer (Z_{UML}) in June in sub-regions 1, 2 and 3 in the Black Sea

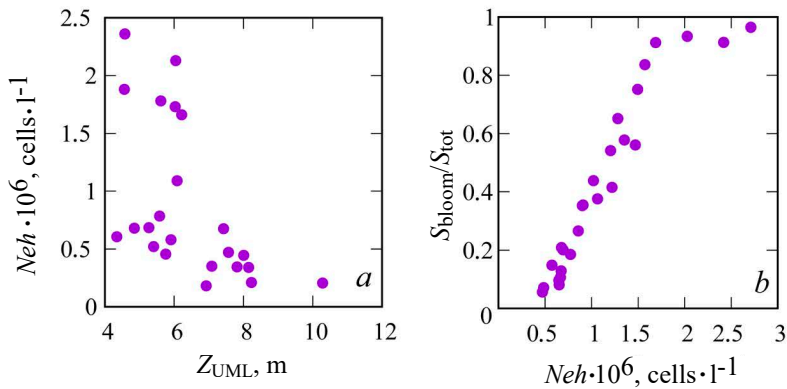


Fig. 6. Relationship between the upper mixed layer thickness (Z_{UML}) in June and the *G. huxleyi* cell abundance (NEh) in the western deep part (sub-region 1) (a), and between (NEh) in the deep part of the sea (sub-region 1 and 2) and “bloom” area to the total sea area ratio (S_{bloom}/S_{tot}) (b)

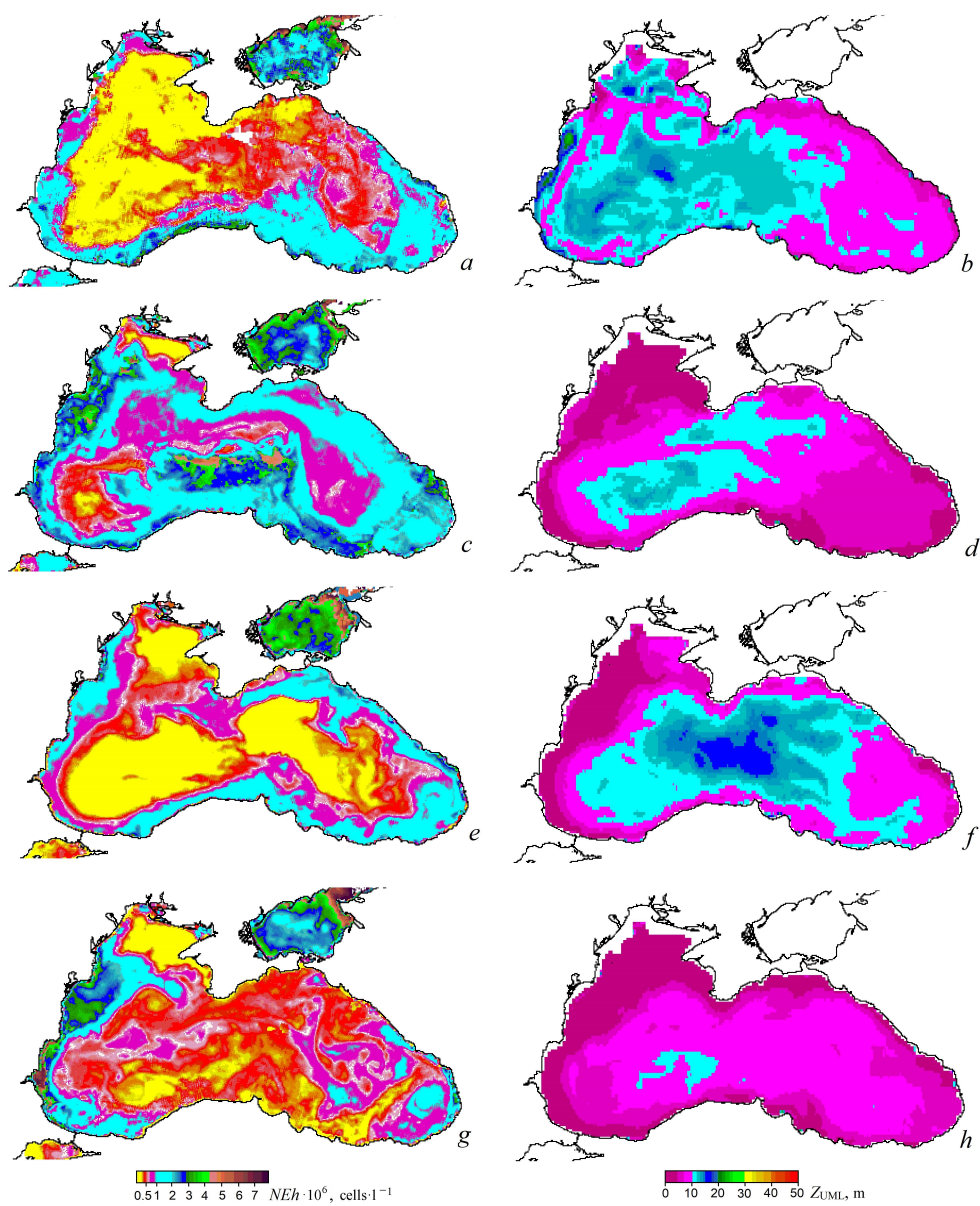


Fig. 7. Maps of *G. huxleyi* cell abundance (NEh) (a, c, e, g) and upper mixed layer thickness (Z_{UML}) (b, d, f, h) at the onset of “bloom” in the second half of May, 1998 (a, b), 2002 (c, d), 2004 (e, f), 2008 (g, h) (data on Z_{UML} are from [32])

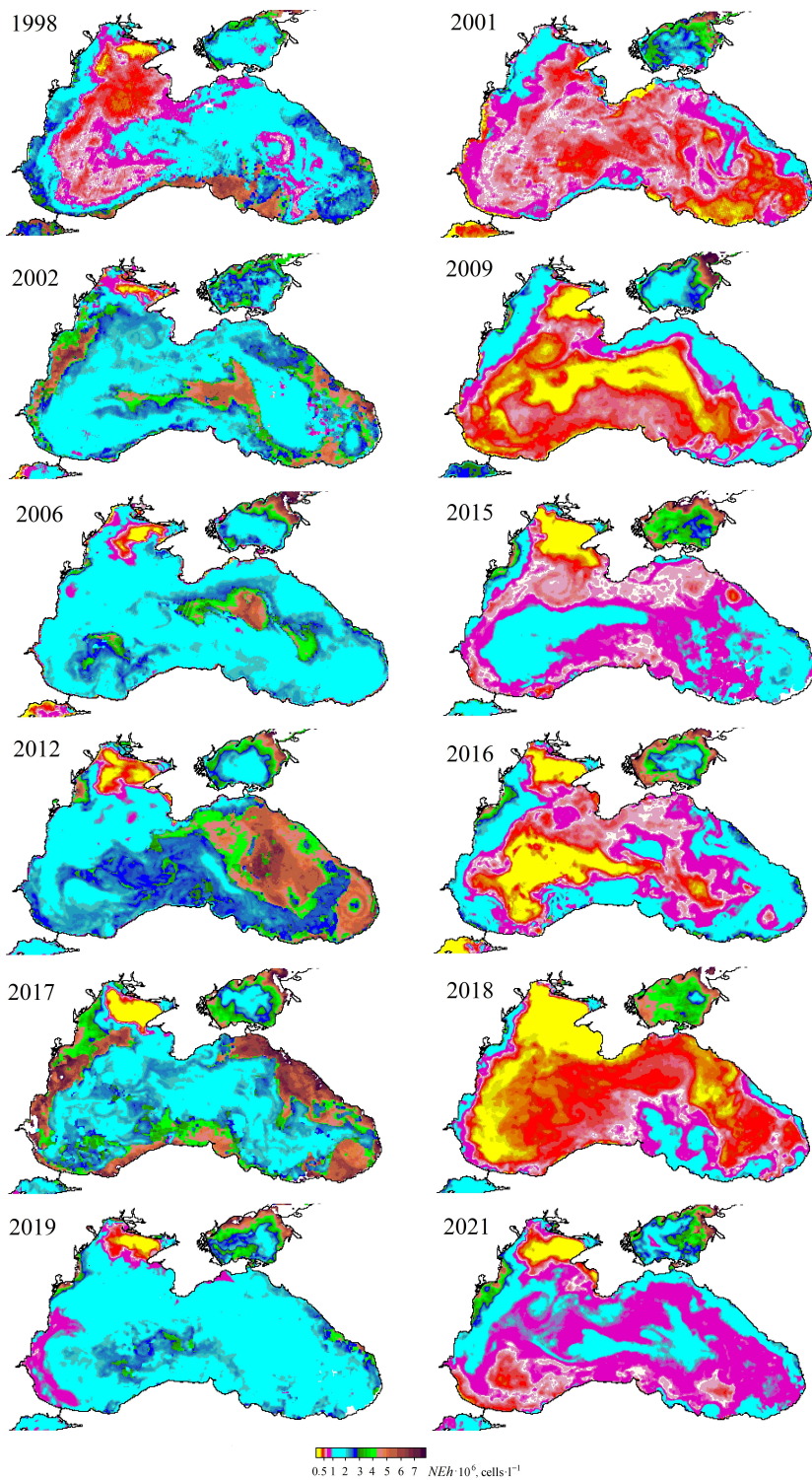


Fig. 8. Maps of spatial distribution of *G. huxleyi* cell concentration (NEh) in the Black Sea surface layer: in the first half of June in 1998, 2002, 2005, 2006, 2012, 2017 (*left*), 2001, 2009, 2011, 2015, 2016, 2018, 2021 (*right*)

The $b_{bp}(555)$ maximum, which is regularly observed in all the sea regions at the beginning of summer, is associated with the *G. huxleyi* “bloom”, as confirmed by field observations. The *G. huxleyi* cell abundance (N , million cells·l⁻¹) can be estimated with a high accuracy based on the relationship between the $b_{bp}(555)$ values, m⁻¹, retrieved based on satellite data, and the number of coccolithophore cells determined directly in seawater samples [31]:

$$N = 160 \cdot b_{bp}(555) - 0.32, n = 36, r^2 = 0.82.$$

A thorough analysis of the interannual variability of NEh and Z_{UML} , calculated based on normalized anomaly values, reveals that the extremes of these two curves are in antiphase in the majority of cases (Fig. 5). A comparison of the mean of NEh and Z_{UML} for June, obtained in different years, indicates an inverse relationship between these parameters, which is most pronounced at NEh values less than 1 (Fig. 6).

The maps of NEh distribution at the end of May, when the “bloom” begins, demonstrate a concurrence between areas of higher coccolithophore abundance and those of a thinner upper mixed layer (Fig. 7). This feature of NEh distribution may indicate the Z_{UML} effect on the *G. huxleyi* “bloom” start. In 1998, 2002, 2006, 2012, 2017 and 2019, when a relatively narrow upper mixed layer was observed in June, a more intense *G. huxleyi* “bloom” was documented: NEh values exceeded 2 million cells·l⁻¹, reaching 6 million cells·l⁻¹ in some years. On the contrary, in 2001, 2009, 2015, 2016, 2018 and 2021, when the upper mixed layer was more profound, the abundance of coccolithophores was lower (NEh less than 1.2 million cells·l⁻¹) (Fig. 8). Furthermore, an assessment of the interannual variability of the *G. huxleyi* “bloom” area from 1998 to 2022 demonstrated that the largest areas, accounting for over 80% of the sea surface, were recorded in 2002, 2006, 2012, 2017 and 2019 (Fig. 9). Moreover, the “bloom” area in particular years was directly proportional to the mean of NEh in the deep-water part of the sea (Fig. 6, b).

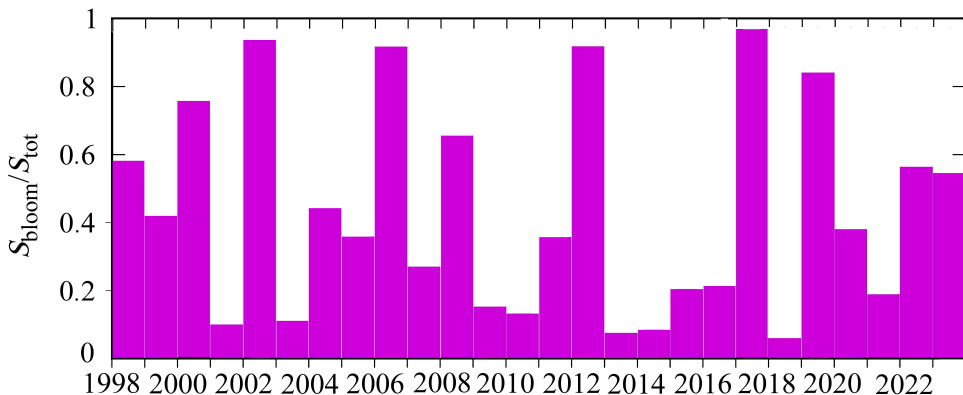


Fig. 9. Interannual variability of *G. huxleyi* “bloom” area (S_{bloom}/S_{tot}) in June

On the northwestern shelf (sub-region 4), besides the $b_{bp}(555)$ maximum at the beginning of summer, a marked increase in $b_{bp}(555)$ is evident in December and February. Along the eastern coast (sub-region 11), an increase in $b_{bp}(555)$

(normalized monthly mean anomaly greater than 1) is observed in February (Fig. 3). In these areas, the winter and summer $b_{bp}(555)$ maxima are statistically significant, since the normalized monthly mean anomaly is equal to 1 or greater. In contrast to the summer $b_{bp}(555)$ maximum, which coincides with the annual the annual minimum chlorophyll a concentration, the winter $b_{bp}(555)$ maximum is observed during a period of elevated C_a values.

Discussion

Analysis of time series of normalized monthly mean anomalies in the abundance of *G. huxleyi* cells revealed that in all the Black Sea sub-regions, the “bloom” occurs regularly in early June (Fig. 3). Across the sea, with the exception of specific areas of the northwestern shelf (4, 5, and 6, a), the *G. huxleyi* “bloom” is observed when the concentration of chlorophyll a is minimal in the annual cycle (Fig. 3) and the species structure of phytoplankton changes significantly [20, 21]. Such changes in phytoplankton are caused by a pronounced increase in the abundance of a particular species compared to others [11]. The increase in abundance is determined by the excess of the algae growth rate over the rate of cell loss, associated with mortality and consumption by zooplankton [14, 16, 35, 36]. Therefore, the increase in the *G. huxleyi* contribution to the phytoplankton biomass may be resulted from relatively high (in comparison with other species) growth rate and/or less intensive grazing.

The growth rate of planktonic algae is regulated by a complex of factors, including light, temperature, and the nutrient availability [37, 38]. Of these factors, light has the greatest effect on changes in the phytoplankton growth [39]. The strategy of microalgae adaptation to light is aimed at maintaining a constant growth rate within a wide range of light intensities in the environment [40]. The light intensity saturating the growth rate of diatoms and dinoflagellates is 50–80 $\mu\text{E}\cdot\text{m}^{-2}\cdot\text{s}^{-1}$ [40]. In earlier studies, it was observed that the *G. huxleyi* growth rate reached a state of saturation at a light intensity of 100–200 $\mu\text{E}\cdot\text{m}^{-2}\cdot\text{s}^{-1}$ [41, 42]. In subsequent studies [43], light saturation of the growth rate was observed at 65 $\mu\text{E}\cdot\text{m}^{-2}\cdot\text{s}^{-1}$, which corresponds to the values characteristic of dinoflagellates and diatoms [40]. A constant growth rate (the so-called plateau of light curve) is observed up to $\sim 800 \mu\text{E}\cdot\text{m}^{-2}\cdot\text{s}^{-1}$. Light of higher intensity inhibits the growth of microalgae of different taxonomic groups [44]. However, for *G. huxleyi* this “plateau” extends up to 1200 $\mu\text{E}\cdot\text{m}^{-2}\cdot\text{s}^{-1}$ [43, 45].

The inhibition of cell growth rate is caused by destruction of photosystem reaction centers in cells, namely, D1 protein damage in the photosystem II reaction center [46]. A detailed study of the pigment complex structure and the functional characteristics of *G. huxleyi* demonstrated that high light intensity does not inhibit growth due to the active photoprotective function of the pigment-protein complex. Photoprotective pigments protect cells from extremely high light intensity by minimizing the accumulation of reactive oxygen species and preventing oxidative damage [9], which increases the resistance of photosystem II reaction centers to high-intensity light [43]. Furthermore, coccoliths covering the *G. huxleyi* cell provide more efficient light scattering compared to other types of microalgae

(b_{bp} differs by almost an order of magnitude) [23], which additionally protects the photosynthetic apparatus of coccolithophores [2].

The June *G. huxleyi* “bloom” period in the Black Sea is characterized by the highest levels of the sea surface insolation ($50 \pm 4.3 \text{ E}\cdot\text{m}^{-2}\cdot\text{day}^{-1}$) of during the annual cycle [47, 48] and the thinnest upper mixed layer (Fig. 3), associated with the beginning of a seasonal water stratification [21, 33, 49]. The temperature stratification of surface waters was observed at the beginning of summer during the *G. huxleyi* “bloom” in various sub-regions of the World Ocean [50–53], while the light intensity within the upper mixed layer was extremely high levels of within the annual cycle (approximately $1000 \mu\text{E}\cdot\text{m}^{-2}\cdot\text{s}^{-1}$) [1, 21, 53–57].

In such conditions, the morphological features and stability of the photosynthetic apparatus of coccolithophores provide them with an advantage in terms of growth rate over other planktonic algae. As a result, an increase in the number of coccolithophores leads to the development of a “bloom”. At its peak, the phytoplankton biomass in the Black Sea can be represented mainly (up to $\sim 80\%$) by one species – *G. huxleyi* [20, 21].

The maximum growth rate of algae (the plateau on the light curve) was shown to decrease under nutrient limitation [37, 58–60]. The seasonal water stratification results in limited nutrient supply to the upper mixed layer from the nutrient-rich lower layers of water. This results in reduced nutrient availability to phytoplankton in surface waters [5]. Numerous studies demonstrate that at low concentrations of inorganic nitrogen and phosphorus compounds, *G. huxleyi* grows at higher rate compared to other microalgae taxa. Furthermore, the competitive advantages of *G. huxleyi* growth under phosphorus deficiency are manifested to a greater extent than under nitrogen deficiency [44, 61–63]. This may provide additional advantages for the *G. huxleyi* growth in the Black Sea at the beginning of summer. During the formation of seasonal stratification of surface waters due to depletion of nutrients in the cold intermediate layer as a result of winter convection, their upward flow into the euphotic zone is sharply reduced [64]. The plankton community undergoes a transition from external sources of nutrients to internal ones [65]. Here, an imbalance between the influx and consumption of inorganic phosphorus in the euphotic zone is more pronounced than that for nitrogen compounds [66]. As a result, *G. huxleyi* has additional advantages for growth compared to algae of other taxonomic groups.

It is assumed that certain coccolithophores may adopt a mixotrophic or phagocytic lifestyle, as evidenced by their occurrence below the euphotic zone [67]. Experimental studies on algae cultures have demonstrated that mixotrophy is a survival strategy for coccolithophore at light intensities below the compensation point (light intensity where the photosynthesis rate is equal to the respiration rate) due to the use of organic compounds as energy and/or carbon sources [68]. At the same time, in the surface layer with high light intensity, *G. huxleyi* coccolithophores are evidently typical autotrophs.

The calcareous shell weakly protects coccolithophores from grazing by both micro- and mesozooplankton. [69]. However, the level of phytoplankton grazing is likely to decrease with an increase in the proportion of coccolithophores in the community. Studies in the Black Sea have shown that the proportion of coccolithophores in the copepod diet is negligible. However, *G. huxleyi* may form the basis for the nutrition of filter feeders *Oikopleura dioica* and the heterotrophic dinoflagellate *Noctiluca* [70]. Consequently, an increase in the proportion of

coccolithophores in phytoplankton may result in a decrease of its grazing by mesozooplankton, particularly if the latter is dominated by crustacean.

As a consequence, the increase in *G. huxleyi* biomass may lead to an increase in the abundance of filter feeder species. At the same time, in most part of the Black Sea, there is a decrease in mesozooplankton biomass from May to June, which is observed simultaneously with changes in community structure. Cold-water crustaceans dominate in March – April, while warm-water species begin their intensive growth in June [71, 72]. Therefore, a decline in the grazing pressure exerted by forage zooplankton at the beginning of summer can stimulate an increase in the phytoplankton biomass at that time.

Microzooplankton can also affect the abundance of *G. huxleyi* cells [73]. A number of studies indicate that dinoflagellates are a higher priority food source for protozoa compared to coccolithophores [74–76]. Therefore, it is possible to allow some reduction in grazing pressure from the side of microzooplankton, too, under the dominance of *G. huxleyi*. The combined effect of these factors can result in a consistent increase in the *G. huxleyi* abundance during the early summer in the majority of sub-regions of the Black Sea.

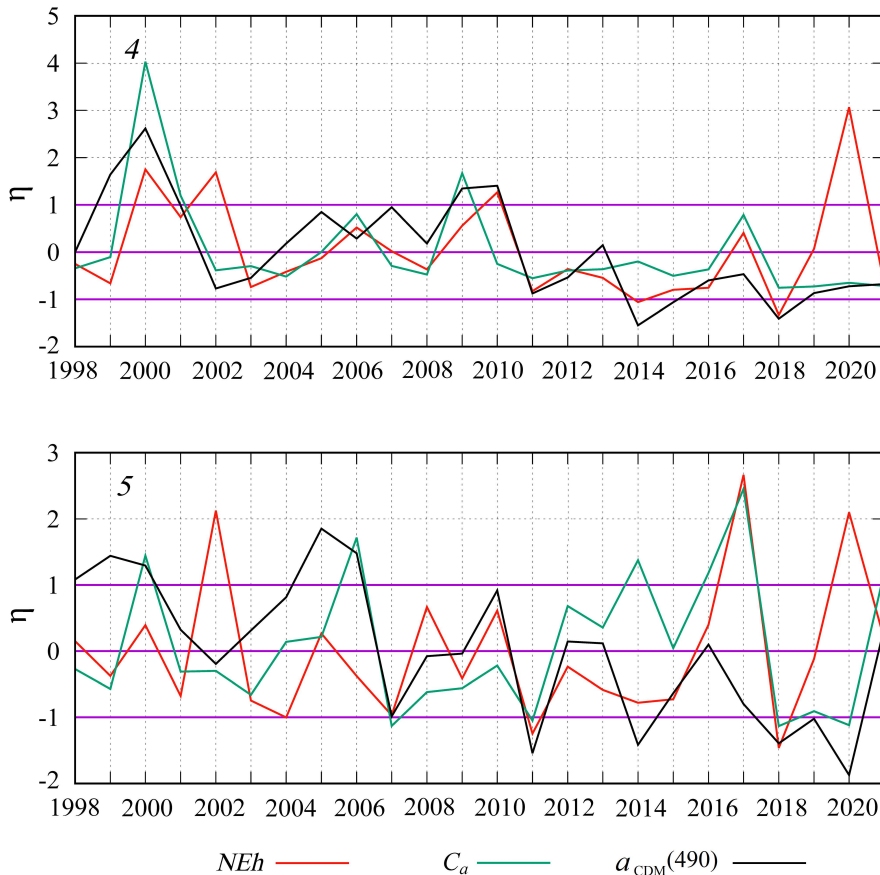


Fig. 10. Interannual variability of normalized monthly mean anomalies of *G. huxleyi* "bloom" intensity (NEh), chlorophyll a concentration (C_a) and light absorption coefficient by colored detrital matter ($a_{CDM(490)}$) in June in sub-regions 4 and 5 in the Black Sea

In coastal waters influenced by the Danube, Dnieper and Dniester runoff (sub-region 4, 5, 6a), the summer $b_{bp}(555)$ maximum is observed in conjunction with an increase in phytoplankton biomass (Fig. 3). The interannual variability of C_a , which is considered a marker of phytoplankton biomass in these waters, shows a close correlation with $a_{CDM}(490)$ (Fig. 10).

It should be noted that the $a_{CDM}(490)$ value in estuarine areas is mainly determined by the amount of suspended and dissolved substances entering with river runoff [77]. In addition, river waters carry nutrients required for phytoplankton growth [78], therefore, variability of the river runoff intensity during the flood period determines the interannual variability of C_a (phytoplankton biomass) at the beginning of summer (Fig. 10).

The observed increase in $b_{bp}(555)$ during this time is primarily associated with an increase in the content of coccolithophores and coccoliths. This is because organic suspended matter, including other types of phytoplankton, has an order of magnitude lower $b_{bp}(555)$ values [23]. The influence of non-algal particles on the $b_{bp}(555)$ was minimized by excluding from the analysis a 2-kilometer zone of coastal waters, where most mineral particles brought in with river runoff are deposited.

It should be noted that interannual variability in the normalized anomalies of $b_{bp}(555)$ in these sub-regions was inverse to variability of the C_a and $a_{CDM}(490)$ anomalies (Fig. 10). Based on such dynamics, it can be assumed that, the relatively low level of river runoff and, accordingly, a lower input of nutrients create favorable conditions for the competitive growth of coccolithophores, which are able to maintain higher growth rates under conditions of low nutrient supply compared to other species, especially diatoms [1, 13].

In the shallow northwestern shelf (sub-region 4), high anomalies in the seasonal variation of $b_{bp}(555)$ are observed not only in June, but also in the winter months (Fig. 3). A comparison of the interannual variability of February values of the $b_{bp}(555)$ and C_a anomalies (Fig. 4) demonstrates that in most cases the extremes of these two curves are in antiphase. This suggests that the increase in the abundance of coccolithophore on the northwestern shelf occurs concurrently with a decline in the total phytoplankton biomass, which is associated with the decreasing of the growth of a typical winter phytoplankton complex dominated by the diatoms.

Regular monitoring in 1998–2000 allowed for the comparison of the intra-annual dynamics of the phytoplankton structure in the western deep-sea in years with cold and warm winters [20]. In the cold winter of 1998, phytoplankton was represented by a complex of diatom species, and a sharp increase of phytoplankton biomass was observed in early March caused by an intense "bloom" of *Proboscia alata*.

During the relatively warm winter of 1999, a significant number of the *G. huxleyi* coccolithophores were observed. Its contribution to the total phytoplankton biomass in the central western deep-water part and in the continental slope area reached 40–70% [20]. No spring "bloom" of diatoms was observed after the warm winter [20]. The elevated abundance of *G. huxleyi* in the phytoplankton during this period can be explained by the higher stability of the water column, leads to a decrease in upward inorganic nutrient fluxes, which are the main source for phytoplankton growth in the euphotic zone during the cold period [64, 65].

The decrease in the availability of dissolved inorganic nitrogen and phosphorus gives *G. huxleyi* an advantage, allowing it to achieve higher growth rates compared to diatoms in low nutrient environments [1, 79–81]. In combination with favorable light conditions due to weak vertical mixing of waters, this leads to an increase in *G. huxleyi* abundance in warm winters. Conversely, during cold winters, active mixing of waters significantly worsens light conditions in the photosynthesis zone. However, mixing intensifies the upward nutrient fluxes into the euphotic zone, thereby creating favorable conditions for the diatoms growth. This is due to the fact that the level of light saturation of growth for diatoms is significantly lower compared to coccolithophores [3, 22, 82].

The development of *G. huxleyi* in different seasons reflects its genetic and physiological plasticity [1]. Molecular genetic studies have revealed the presence of at least two distinct groups within *G. huxleyi*, distinguished by variations in the mitochondrial genome sequences. These groups exhibit different temperature preferences, with the cold-water group inhabiting the subarctic waters of the North Atlantic and Pacific Oceans, and the warm-water group occupying the subtropical waters of the Atlantic and Pacific Oceans, as well as the Mediterranean Sea [81]. The relationship between specific genetic strains of *G. huxleyi* and the physical and chemical conditions of their habitats is illustrated through the analysis of data from various sub-regions of the World Ocean [83]. Intraspecific genetic variability can be traced observed not only between strains of *G. huxleyi* from different sub-regions, but also within the boundaries of a single “bloom”. This variability is associated with key physiological processes in cells, such as rates of calcification, photosynthesis, sulfur and lipids biochemical transformation, nitrogen and phosphorus assimilation, which ultimately affect the entire ecosystem [84]. Therefore, targeted genetic studies of the Black Sea population of *G. huxleyi* are essential to identify patterns in the dynamics of “bloom” of this species or a complex of related species.

Conclusions

Based on satellite data and regional algorithms, the values of chlorophyll a concentration, the particulate backscattering coefficient and the absorption coefficient of light by colored detrital matter, were retrieved with two-week averaging for various sub-regions of the Black Sea from 1998 to 2023.

The analysis of the normalized monthly mean anomalies’ variability allows us to reveal annual cycles of these parameters, to determine the general patterns and features of their dynamics in particular sea sub-regions. It was demonstrated that in early June, coccolithophores “bloom” with interannual variations in its intensity and area is regularly observed in all sub-regions. The *G. huxleyi* “bloom” is observed annually at the beginning of summer in many regions of the World Ocean under at least one general condition – the highest light intensity within the upper mixed layer (about $1000 \mu\text{Em}^{-2}\cdot\text{s}^{-1}$). This is evidently a key factor in the changing the phytoplankton species structure, leading to the dominance of coccolithophores (particularly *G. huxleyi*). The *G. huxleyi* dominates due to its physiologically determined capacity to grow without inhibition under extremely high light intensities, which inhibit the growth of most other algae.

It has been demonstrated that in the majority of sub-regions in the Black Sea, during the *G. huxleyi* “bloom” in early summer, the algae species are replaced by

G. huxleyi, which is not accompanied by an increase in phytoplankton biomass (using the concentration of photosynthetically active pigment as a biomass marker).

In coastal waters influenced by river runoff, *G. huxleyi* abundance and phytoplankton biomass increase. Level of river runoff was shown to influence the increase in phytoplankton biomass in spring in these Black Sea sub-regions. Higher abundance of coccolithophores was observed while the chlorophyll a concentration decreased. In addition, increase in the number of coccolithophores in the Black Sea has been observed in the cold period; however, the intensity and time scale of such processes vary significantly across the water area in different years. Consequently, no significant increase in normalized anomalies of particle backscattering coefficients in the cold period is observed in most sub-regions.

However, a notable and relatively consistent increase in this indicator is observed during the cold period (December – February) on the northwestern shelf. Significant increase in the number of *G. huxleyi* is evident, despite a decline in the total phytoplankton biomass. Significant increase in the number of *G. huxleyi* is observed, while the phytoplankton biomass decreases.

It is evident that the primary factor contributing to abundance of *G. huxleyi* in the Black Sea throughout the year is the capacity of coccolithophores to maintain elevated growth rates in low-nutrient environments. Consequently, the proportion of *G. huxleyi* in the phytoplankton exhibits a periodic increase in different sub-regions, coinciding with nutrients depletion. This is particularly evident in instances of decreased nutrient flow, resulting from increased water column stability and/or reduced coastal runoff levels. However, at the beginning of summer, the key factor determining the regular “bloom” of *G. huxleyi* throughout the Black Sea and other World Ocean sub-regions is the capacity of coccolithophores to maintain maximum growth at a wide range of light intensity, extending to extremely high intensity, inhibiting the growth of all other groups of microalgae.

REFERENCES

1. Iglesias-Rodríguez, M.D., Brown, C.W., Doney, S.C., Kleypas, J., Kolber, D., Kolber, Z., Hayes, P.K. and Falkowski, P.G., 2002. Representing Key Phytoplankton Functional Groups in Ocean Carbon Cycle Models: Coccolithophorids. *Global Biogeochemical Cycles*, 16(4), 1100. <https://doi.org/10.1029/2001GB001454>
2. Balch, W.M., 2018. The Ecology, Biogeochemistry, and Optical Properties of Coccolithophores. *Annual Review of Marine Science*, 3(10), pp. 71-98. <https://doi.org/10.1146/annurev-marine-121916-063319>
3. Balch, W.M., Holligan, P.M. and Kilpatrick, K.A., 1992. Calcification, Photosynthesis and Growth of the Bloom-Forming Coccolithophore, *Emiliana Huxleyi*. *Continental Shelf Research*, 12(12), pp. 1353-1374. [https://doi.org/10.1016/0278-4343\(92\)90059-s](https://doi.org/10.1016/0278-4343(92)90059-s)
4. Poulton, A.J., Adey, T.R., Balch, W.M. and Holligan, P.M., 2007. Relating Coccolithophore Calcification Rates to Phytoplankton Community Dynamics: Regional Differences and Implications for Carbon Export. *Deep Sea Research Part II: Topical Studies in Oceanography*, 54(5-7), pp. 538-557. <https://doi.org/10.1016/j.dsr2.2006.12.003>
5. Krumhardt, K.M., Lovenduski, N.S., Iglesias-Rodríguez, M.D. and Kleypas, J.A., 2017. Coccolithophore Growth and Calcification in a Changing Ocean. *Progress in Oceanography*, 159(23), pp. 276-295. <https://doi.org/10.1016/j.pocean.2017.10.007>
6. Krumhardt, K.M., Lovenduski, N.S., Long, M.C., Levy, M., Lindsay, K., Moore, J.K. and Nissen, C., 2019. Coccolithophore Growth and Calcification in an Acidified Ocean: Insights from

- Community Earth System Model Simulations Ocean. *Journal of Advances in Modeling Earth Systems*, 11(5), pp. 1418-1437. <https://doi.org/10.1029/2018MS001483>
7. Krumhardt, K.M., Lovenduski, N.S., Freeman, N.M. and Bates, N.R., 2016. Apparent Increase in Coccolithophore Abundance in the Subtropical North Atlantic from 1990 to 2014. *Biogeosciences*, 13(4), pp. 1163-1177. <https://doi.org/10.5194/bg-13-1163-2016>
 8. Winter, A., Henderiks, J., Beaufort, L., Rickaby, R.E.M. and Brown, C.W., 2014. Poleward Expansion of the Coccolithophore *Emiliana Huxleyi*. *Journal of Plankton Research*, 36(2), pp. 316-325. <https://doi.org/10.1093/plankt/ftt110>
 9. Read, B.A., Kegel, J., Klute, M.J., Kuo, A., Lefebvre, S.C., Maumus, F., Mayer, C., Miller, J., Monier, A. [et al.], 2013. Pan Genome of the Phytoplankton *Emiliana* Underpins Its Global Distribution. *Nature*, 499, pp. 209-213. <https://doi.org/10.1038/nature12221>
 10. Kjørboe, T., Hansen, J.L.S., Alldredge, A.L., Jackson, G.A., Passow, U., Dam, H.G., Drapeau, D.T., Waite, A. and Garcia, C.M., 1996. Sedimentation of Phytoplankton during a Diatom Bloom: Rates and Mechanisms. *Journal of Marine Research*, 54(6), pp. 1123-1148. <https://doi.org/10.1357/0022240963213754>
 11. Smayda, T.J., 1997. What is a Bloom? A Commentary. *Limnology and Oceanography*, 42(5), pp. 1132-1136. https://doi.org/10.4319/lo.1997.42.5_part_2.1132
 12. Lassus, P., 2016. *Toxic and Harmful Microalgae of the World Ocean*. Nantes: International Society for the Study of Harmful Algae/Intergovernmental Oceanographic Commission of UNESCO, 523 p.
 13. Makareviciute-Fichtner, K., Matthiessen, B., Lotze, H.K. and Sommer, U., 2024. Nutrient Enrichment Alters Phytoplankton Biomass and Composition via Silicon Limitation. *Frontiers in Marine Science*, 11, 1289768. <https://doi.org/10.3389/fmars.2024.1289768>
 14. Richardson, K., 1997. Harmful or Exceptional Phytoplankton Blooms in the Marine Ecosystem. *Advances in Marine Biology*, 31, pp. 301-385. [https://doi.org/10.1016/S0065-2881\(08\)60225-4](https://doi.org/10.1016/S0065-2881(08)60225-4)
 15. Kahru, M. and Nommann, S., 1990. The Phytoplankton Spring Bloom in the Baltic Sea in 1985, 1986: Multitude of Spatiotemporal Scales. *Continental Shelf Research*, 10(4), pp. 329-354. [https://doi.org/10.1016/0278-4343\(90\)90055-Q](https://doi.org/10.1016/0278-4343(90)90055-Q)
 16. Carstensen, J., Henriksen, P. and Heiskanen, A.-S., 2007. Summer Algal Blooms in Shallow Estuaries: Definition, Mechanisms, and Link to Eutrophication. *Limnology and Oceanography*, 52(1), pp. 370-384. <https://doi.org/10.4319/lo.2007.52.1.0370>
 17. Paerl, H.W., 1988. Nuisance Phytoplankton Blooms in Coastal, Estuarine and Inland Waters. *Limnology and Oceanography*, 33(4), part 2, pp. 823-843. <https://doi.org/10.4319/lo.1988.33.4part2.0823>
 18. Margalef, R., 1978. Life-Forms of Phytoplankton as Survival Alternatives in an Unstable Environment. *Oceanologica Acta*, 1(4), pp. 493-509.
 19. Isles, P.D. and Pomati, F., 2021. An Operational Framework for Defining and Forecasting Phytoplankton Blooms. *Frontiers in Ecology and the Environment*, 19(8), pp. 443-450. <https://doi.org/10.1002/fee.2376>
 20. Berseneva, G., Churilova, T. and Georgieva, L., 2004. Seasonal Variability in Pigment Concentration, Taxonomic Structure of Phytoplankton Community in Western Part of the Black Sea. *Oceanology*, 44(3), pp. 362-371. <https://doi.org/10.1594/PANGAEA.762833>
 21. Pautova, L.A., Mikaelyan, A.S. and Silkin, V.A., 2007. Structure of Plankton Phytocoenoses in the Shelf Waters of the Northeastern Black Sea during the *Emiliana Huxleyi* Bloom in 2002-2005. *Oceanology*, 47(3), pp. 408-417. <https://doi.org/10.1134/S0001437007030101>
 22. Moncheva, S., Gotsis-Skretas, O., Pagou, K. and Krastev, A., 2001. Phytoplankton Blooms in Black Sea and Mediterranean Coastal Ecosystems Subjected to Anthropogenic Eutrophication: Similarities and Differences. *Estuarine Coastal and Shelf Science*, 53(3), pp. 281-295. <https://doi.org/10.1006/ecss.2001.0767>

23. Stramski, D. and Kiefer, D.A., 1991. Light Scattering by Microorganisms in the Open Ocean. *Progress in Oceanography*, 28(4), pp. 343-383. [https://doi.org/10.1016/0079-6611\(91\)90032-h](https://doi.org/10.1016/0079-6611(91)90032-h)
24. Cokacar, T., Oguz, T. and Kubilay, N., 2004. Satellite-Detected Early Summer Coccolithophore Blooms and Their Interannual Variability in the Black Sea. *Deep Sea Research Part I: Oceanographic Research Papers*, 51(8), pp. 1017-1031. <https://doi.org/10.1016/j.dsr.2004.03.007>
25. Kopelevich, O., Burenkov, V., Sheberstov, S., Vazyulya, S., Kravchishina, M., Pautova, L., Silkin, V., Artemiev, V. and Grigoriev, A., 2014. Satellite Monitoring of Coccolithophore Blooms in the Black Sea from Ocean Color Data. *Remote Sensing of Environment*, 146, pp. 113-123. <https://doi.org/10.1016/j.rse.2013.09.009>
26. Kubryakov, A.A., Mikaelyan, A.S. and Stanichny, S.V., 2019. Summer and Winter Coccolithophore Blooms in the Black Sea and Their Impact on Production of Dissolved Organic Matter from Bio-Argo Data. *Journal of Marine Systems*, 199, 103220. <https://doi.org/10.1016/j.jmarsys.2019.103220>
27. Vazyulya, S., Deryagin, D., Glukhovets, D., Silkin, V. and Pautova, L., 2023. Regional Algorithm for Estimating High Coccolithophore Concentration in the Northeastern Part of the Black Sea. *Remote Sensing*, 15(9), 2219. <https://doi.org/10.3390/rs15092219>
28. Cazzaniga, I., Zibordi, G. and Mélin, F., 2021. Spectral Variations of the Remote Sensing Reflectance during Coccolithophore Blooms in the Western Black Sea. *Remote Sensing of Environment*, 264, 112607. <https://doi.org/10.1016/j.rse.2021.112607>
29. Suslin, V., Pryahina, S., Churilova, T. and Slabakova, V., 2016. The Black Sea IOPs Based on SeaWiFS Data. In: G. G. Matvienko and O. A. Romanovskii, eds., 2016. *Proceedings of SPIE – the International Society for Optical Engineering. XXII International Symposium on Atmospheric and Ocean Optics: Atmospheric Physics*. Tomsk: SPIE. Vol. 10035, 1003531. <https://doi.org/10.1117/12.2248332>
30. Suslin, V. and Churilova, T., 2016. A Regional Algorithm for Separating Light Absorption by Chlorophyll-*a* and Coloured Detrital Matter in the Black Sea, Using 480–560 nm Bands from Ocean Colour Scanners. *International Journal of Remote Sensing*, 37(18), pp. 4380-4400. <https://doi.org/10.1080/01431161.216.1211350>
31. Churilova, T.Ya. and Suslin, V.V., 2012. On Causes of *Emiliana Huxleyi* Domination in Phytoplankton of Deep Waters Part of the Black Sea in Early Summer. In: MHI, 2012. *Ecological Safety of Coastal and Shelf Zones and Comprehensive Use of Shelf Resources*. Sevastopol: ECOSI-Gidrofizika. Iss. 26, vol. 2, pp. 195-203 (in Russian).
32. Dorofeev, V.L., 2009. Modeling of Decadal Variations in the Black-Sea Ecosystem. *Physical Oceanography*, 19(6), pp. 400-409. <https://doi.org/10.1007/s11110-010-9062-6>
33. Ivanov, V.A. and Belokopytov, V.N., 2013. *Oceanography of the Black Sea*. Sevastopol: MHI, 210 p.
34. Suslin, V.V. and Churilova, T.Ya., 2010. Simplified Method of Calculation of Spectral Diffuse Beam Attenuation Coefficient in the Black Sea Upper Layer on the Basis of Satellite Data. In: MHI, 2010. *Ecological Safety of Coastal and Shelf Zones and Comprehensive Use of Shelf Resources*. Sevastopol: ECOSI-Gidrofizika. Iss. 22, pp. 47-60 (in Russian).
35. Behrenfeld, M.J., 2010. Abandoning Sverdrup's Critical Depth Hypothesis on Phytoplankton Blooms. *Ecology*, 91(4), pp. 977-989. <https://doi.org/10.1890/09-1207.1>
36. González-Gil, R., Banas, N.S., Bresnan, E. and Heath, M.R., 2022. The Onset of the Spring Phytoplankton Bloom in the Coastal North Sea Supports the Disturbance Recovery Hypothesis. *Biogeosciences*, 19(9), pp. 2417-2426. <https://doi.org/10.5194/bg-19-2417-2022>
37. MacIntyre, H.L., Kana, T.M., Anning, T. and Geider, R.J., 2002. Photoacclimation of Photosynthesis Irradiance Response Curves and Photosynthetic Pigments in Microalgae and Cyanobacteria. *Journal of Phycology*, 38(1), pp. 17-38. <https://doi.org/10.1046/j.1529-8817.2002.00094.x>

38. Falkowski, P.G., Woodhead, A.D. and Vivirito, K., eds., 1992. *Primary Productivity and Biogeochemical Cycles in the Sea*. New York: Springer, 550 p. <https://doi.org/10.1007/978-1-4899-0762-2>
39. Falkowski, P.G. and Raven, J.A., 2007. *Aquatic Photosynthesis*. New Jersey: Princeton University Press, 488 p. <https://doi.org/10.1515/9781400849727>
40. Richardson, K., Beardall, J. and Raven, J.A., 1983. Adaptation of Unicellular Algae to Irradiance: An Analysis of Strategies. *New Phytologist*, 93, pp. 157-191. <https://doi.org/10.1111/J.1469-8137.1983.TB03422.X>
41. Van Bleijswijk, J.D.L., Kempers, R.S., Veldhuis, M.J. and Westbroek, P., 1994. Cell and Growth Characteristics of Types A and B of *Emiliana Huxleyi* (Prymnesiophyceae) as Determined by Flow Cytometry and Chemical Analyses. *Journal of Phycology*, 30(2), pp. 230-241. <https://doi.org/10.1111/j.0022-3646.1994.00230.x>
42. Nielsen, M.V., 1997. Growth, Dark Respiration and Photosynthetic Parameters of the Coccolithophorid *Emiliana Huxleyi* (Prymnesiophyceae) Acclimated to Different Day Length-Irradiance Combinations. *Journal of Phycology*, 33(5), pp. 818-822. <https://doi.org/10.1111/j.0022-3646.1997.00818.x>
43. McKew, B.A., Davey, P., Finch, S.J., Hopkins, J., Lefebvre, S.C., Metodiev, M.V., Oxborough, K., Raines, C.A., Lawson, T. [et al.], 2013. The Trade-off between the Light-Harvesting and Photoprotective Functions of Fucoxanthin-Chlorophyll Proteins Dominates Light Acclimation in *Emiliana Huxleyi* (Clone CCMP 1516). *New Phytologist*, 200(1), pp. 74-85. <https://doi.org/10.1111/nph.12373>
44. Paasche, E., 2002. A Review of the Coccolithophorid *Emiliana Huxleyi* (Prymnesiophyceae) with Particular Reference to Growth, Coccolith Formation, and Calcification-Photosynthesis Interactions. *Phycologia*, 40(6), pp. 503-529. <https://doi.org/10.2216/i0031-8884-40-6-503.1>
45. Gafar, N.A. and Schulz, K.G., 2018. A Three-Dimensional Niche Comparison of *Emiliana Huxleyi* and *Gephyrocapsa Oceanica*: Reconciling Observations with Projections. *Biogeosciences*, 15(11), pp. 3541-3560. <https://doi.org/10.5194/bg-15-3541-2018>
46. Raven, J.A., 2011. The Cost of Photoinhibition. *Physiologia Plantarum*, 142(1), pp. 87-104. <https://doi.org/10.1111/j.1399-3054.2011.01465.x>
47. Neumann, G. and Pierson, W.J., 1966. *Principles of Physical Oceanography*. Englewood Cliffs: Prentice-Hall, pp. 230-233.
48. Suslin, V.V., Korolev, S.N., Kucheryaviy, A.A., Churilova, T.Ya. and Krivenko, O.V., 2015. Photosynthetically Available Radiation on Surface of the Black Sea Based on Ocean Color Data. In: O. A. Romanovskii, ed., 2015. *Proceedings of SPIE. 21st International Symposium Atmospheric and Ocean Optics: Atmospheric Physics*. Tomsk: SPIE. Vol. 9680, 96800T. <https://doi.org/10.1117/12.2203660>
49. Churilova, T.Ya., Skorokhod, E.Yu., Efimova, T.V. and Moiseeva, N.A., 2025. Chlorophyll “a” Concentration and Light Absorption by Coloured Dissolved Organic Matter in the Black Sea in Winter (2018) and Summer (2020). *Fundamental and Applied Hydrophysics*, (1) (being printed) (in Russian).
50. Napp, J.M. and Hunt, G.L.J., 2001. Anomalous Conditions in the South-Eastern Bering Sea 1997: Linkages among Climate, Weather, Ocean and Biology. *Fish Oceanography*, 10(1), pp. 61-68. <https://doi.org/10.1046/j.1365-2419.2001.00155.x>
51. Mohan, R., Mergulhao, L.P., Guptha, M.V.S., Rajakumar, A., Thaban, M., AnilKumar, N., Sudhakar, M. and Ravindra, R., 2008. Ecology of Coccolithophores in the Indian Sector of the Southern Ocean. *Marine Micropaleontology*, 67(1-2), pp. 30-45. <https://doi.org/10.1016/j.marmicro.2007.08.005>
52. Beaufort, L., Couapel, M., Buchet, N., Claustre, H. and Goyet, G., 2008. Calcite Production by Coccolithophores in the South East Pacific Ocean. *Biogeosciences*, 5(4), pp. 1101-1117. <https://doi.org/10.5194/bg-5-1101-2008>

53. O'Brien, C.J., Vogt, M. and Gruber, N., 2016. Global Coccolithophore Diversity: Drivers and Future Change. *Progress in Oceanography*, 140, pp. 27-42. <https://doi.org/10.1016/j.pocean.2015.10.003>
54. Oguz, T. and Merico, A., 2006. Factors Controlling the Summer *Emiliania Huxleyi* Bloom in the Black Sea: A Modeling Study. *Journal of Marine Systems*, 59(3-4), pp. 173-188. <https://doi.org/10.1016/j.jmarsys.2005.08.002>
55. Nanninga, H. and Tyrrell, T., 1996. Importance of Light for the Formation of Algal Blooms by *Emiliania Huxleyi*. *Marine Ecology Progress Series*, 136, pp. 195-203. <https://doi.org/10.3354/meps136195>
56. Karabashev, G.S., Sheberstov, S.V. and Yakubenko, V.G., 2006. The June Maximum of Normalized Radiance and Its Relation to the Hydrological Conditions and Coccolithophorid Bloom in the Black Sea. *Oceanology*, 46(3), pp. 305-317. <https://doi.org/10.1134/S0001437006030027>
57. Mikaelyan, A.S., Pautova, L.A., Pogosyan, S.I. and Sukhanova, I.N., 2005. Summer Blooming of Coccolithophorids in the Northeastern Black Sea. *Oceanology*, 45(suppl. 1), pp. S127-S138.
58. Geider, R.J., Macintyre, H.L. and Kana, T., 1997. Dynamic Model of Phytoplankton Growth and Acclimation: Responses of the Balanced Growth Rate and the Chlorophyll *a*: Carbon Ratio to Light, Nutrient-Limitation and Temperature. *Marine Ecology Progress Series*, 148(1-3), pp. 187-200. <https://doi.org/10.3354/meps148187>
59. Moore, C.M., Mills, M.M., Milne, A., Langlois, R., Achterberg, E.P., Lochte, K., Geider, R.J. and La Roche, J., 2006. Iron Limits Primary Productivity during Spring Bloom Development in the Central North Atlantic. *Global Change Biology*, 12(4), pp. 626-634. <https://doi.org/10.1111/j.1365-2486.2006.01122.x>
60. Cullen, J.J., Yang, X. and MacIntyre, H.L., 1992. Nutrient Limitation of Marine Photosynthesis. In: P. G. Falkowski and A. V. Woodhead, eds., 1992. *Primary Productivity and Biogeochemical Cycles in the Sea*. New York: Plenum Press, pp. 69-88. https://doi.org/10.1007/978-1-4899-0762-2_5
61. Reigman, R., Noordeloos, A.A.M. and Cadee, G.C., 1992. Phaeocystis Blooms and Eutrophication of the Continental Coastal Zones of the North Sea. *Marine Biology*, 112(3), pp. 479-484. <https://doi.org/10.1007/BF00356293>
62. Egge, J.K. and Heimdal, B.R., 1994. Blooms of Phytoplankton Including *Emiliania Huxleyi* (Haptophyta). Effects of Nutrient Supply in Different N:P Ratios. *Sarsia*, 79(4), pp. 333-348. <https://doi.org/10.1080/00364827.1994.10413565>
63. Tyrrell, T. and Taylor, A.H., 1996. A Modelling Study of *Emiliania Huxleyi* in the NE Atlantic. *Journal of Marine Systems*, 9(1-2), pp. 83-112. [https://doi.org/10.1016/0924-7963\(96\)00019-x](https://doi.org/10.1016/0924-7963(96)00019-x)
64. Krivenko, O.V., 2008. Contents and Uptake of Inorganic Nitrogen in the Black Sea. *Marine Ecological Journal*, 7(4), pp. 13-26 (in Russian).
65. Krivenko, O.V., 2006. Basic Regularities of the Formation of "New" and Regeneration Production in the Black Sea. *Physical Oceanography*, 16, pp. 337-349. <https://doi.org/10.1007/s11110-006-0037-6>
66. Krivenko, O.V. and Parkhomenko, A.V., 2015. Upward and Regeneration Fluxes of Inorganic Nitrogen and Phosphorus of the Deep-Water Areas of the Black Sea. *Biology Bulletin Reviews*, 5(3), pp. 268-281.
67. Poulton, A.J., Holligan, P.M., Charalampopoulou, A. and Adey, T.R., 2017. Coccolithophore Ecology in the Tropical and Subtropical Atlantic Ocean: New Perspectives from the Atlantic Meridional Transect (AMT) Programme. *Progress in Oceanography*, 158, pp. 150-170. <https://doi.org/10.1016/j.pocean.2017.01.003>
68. Godrijan, J., Drapeau, D.T. and Balch, W.M., 2022. Osmotrophy of Dissolved Organic Carbon by Coccolithophores in Darkness. *New Phytologist*, 233(2), pp. 781-794. <https://doi.org/10.1111/nph.17819>
69. Mayers, K.M.J., Poulton, A.J., Bidle, K., Thamatrakoln, K., Schieler, B., Giering, S.L.C., Wells, S.R., Tarran, G.A., Mayor, D. [et al.], 2020. The Possession of Coccoliths Fails to Deter

- Microzooplankton Grazers. *Frontiers in Marine Science*, 7, 569896. <https://doi.org/10.3389/fmars.2020.569896>
70. Amelina, A.B., Sergeeva, V.M., Arashkevich, E.G., Drits, A.V., Solovyev, K.A. and Louppova, N.E., 2017. Feeding of the Dominant Herbivorous Plankton Species in the Black Sea and Their Role in Coccolithophorid Consumption. *Oceanology*, 57(6), pp. 806-816. <https://doi.org/10.1134/S000143701706011X>
 71. Grese, V.N. and Fedorina, A.I., 1979. Abundance and Biomass of the Zooplankton. In: V.N. Grese, ed., 1979. *Fundamentals of Biological Productivity of the Black Sea*. Kiev: Naukova Dumka, pp. 143-168 (in Russian).
 72. Gubanova, A.D., Polikarpov, I.G., Saburova, M.A. and Prusova, I., 2002. Long-Term Dynamics of Mesozooplankton by the Example of the Copepoda Community in Sevastopol Bay. *Oceanology*, 42(4), pp. 512-520.
 73. Rost, B. and Riebesell, U., 2004. Coccolithophores and the Biological Pump: Responses to Environmental Changes. In: H. R. Thierstein and J. R. Young, eds., 2004. *Coccolithophores: From Molecular Processes to Global Impact*. Heidelberg; Berlin: Springer, pp. 99-125. https://doi.org/10.1007/978-3-662-06278-4_5
 74. Müller, M.N., 2019. On the Genesis and Function of Coccolithophore Calcification. *Frontiers in Marine Science*, 6, 49. <https://doi.org/10.3389/fmars.2019.00049>
 75. Haunost, M., Riebesell, U., D'Amore, F., Kelting, O. and Bach, L.T., 2021. Influence of the Calcium Carbonate Shell of Coccolithophores on Ingestion and Growth of a Dinoflagellate Predator. *Frontiers in Marine Science*, 8, 664269. <https://doi.org/10.3389/fmars.2021.664269>
 76. Monteiro, F.M., Bach, L.T., Brownlee, C., Bown, P., Rickaby, R.E.M., Poulton, A.J., Tyrrell, T., Beaufort, L., Dutkiewicz, S. [et al.], 2016. Why Marine Phytoplankton Calcify. *Science Advances*, 2(7), e1501822. <https://doi.org/10.1126/sciadv.1501822>
 77. Nelson, N.B. and Siegel, D.A., 2013. The Global Distribution and Dynamics of Chromophoric Dissolved Organic Matter. *Annual Review of Marine Science*, 5(1), pp. 447-476. <https://doi.org/10.1146/annurev-marine-120710-100751>
 78. Oguz, T., ed., 2008. *State of the Environment of the Black Sea (2001–2006/7)*. Istanbul: Commission on the Protection of the Black Sea Against Pollution, 488 p.
 79. Tozzi, S., Schofield, O. and Falkowski, P., 2004. Historical Climate Change and Ocean Turbulence as Selective Agents for Two Key Phytoplankton Functional Groups. *Marine Ecology Progress Series*, 274, pp. 123-132. <https://doi.org/10.3354/meps274123>
 80. Estrada, M., Alcaraz, M. and Marrase, C., 1987. Effects of Turbulence on the Composition of Phytoplankton Assemblages in Marine Microcosms. *Marine Ecology Progress Series*, 38(3), pp. 267-281. <https://doi.org/10.3354/meps038267>
 81. Falkowski, P., Schofield, O., Katz, M.E., de Schootbrugge, B.V. and Knoll, A.H., 2004. Why is the Land Green and the Ocean Red? In: H. R. Thierstein and J. R. Young, eds., 2004. *Coccolithophores: From Molecular Processes to Global Impact*. Heidelberg; Berlin: Springer, pp. 429-453. https://doi.org/10.1007/978-3-662-06278-4_16
 82. Hagino, K., Bendif, E.M., Young, J.R., Kogame, K., Probert, I., Takano, Y., Horiguchi, T., de Vargas, C. and Okada, H., 2011. New Evidence for Morphological and Genetic Variation in the Cosmopolitan Coccolithophore *Emiliana Huxleyi* (Prymnesiophyceae) from the *Cox1b-Atp4* Genes. *Journal of Phycology*, 47(5), pp. 1164-1176. <https://doi.org/10.1111/j.1529-8817.2011.01053.x>
 83. Bendif, E.M., Probert, I., Archontikis, O.A., Young, J.R., Beaufort, L., Rickaby, R.E. and Filatov, D., 2023. Rapid Diversification Underlying the Global Dominance of a Cosmopolitan Phytoplankton. *ISME Journal*, 17(4), pp. 630-640. <https://doi.org/10.1038/s41396-023-01365-5>
 84. Wheeler, G.L., Sturm, D. and Langer, G., 2023. *Gephyrocapsa Huxleyi* (*Emiliana Huxleyi*) as a Model System for Coccolithophore Biology. *Journal of Phycology*, 59(6), pp. 1123-1129. <https://doi.org/10.1111/jpy.13404>

Submitted 22.07.2024; approved after review 31.07.2024;
accepted for publication 12.09.2024

About the authors:

Tatiana Ya. Churilova, Senior Scientist, Head of the Laboratory of Photosynthesis and Marine Biooptics, A. O. Kovalevsky Institute of Biology of the Southern Seas of RAS (2 Nakhimov Ave., Sevastopol, 299011, Russian Federation), CSc (Biol.), **ORCID ID: 0000-0002-0045-7284**, **Scopus Author ID: 6603622802**, **ResearcherID: O-8437-2016**, tanya.churilova@ibss-ras.ru

Vyacheslav V. Suslin, Senior Scientist, Head of the Department of the Dynamics of the Ocean Processes, Marine Hydrophysical Institute of RAS (2 Kapitanskaya Str., Sevastopol, 299011, Russian Federation), CSc (Math.-Phys.), **ORCID ID: 0000-0002-8627-7603**, **Scopus Author ID: 6603566261**, **ResearcherID: B-4994-2017**, slava.suslin@mhi-ras.ru

Olga V. Krivenko, Leading Scientist, Head of the Laboratory of Functional Genomics, Marine Hydrophysical Institute of RAS (2 Kapitanskaya Str., Sevastopol, 299011, Russian Federation), CSc (Biol.), **ORCID ID: 0000-0001-6292-5293**, **Scopus Author ID: 6602415951**, **ResearcherID: O-8541-2016**, krivenko@ibss-ras.ru

Contribution of the co-authors:

Tatiana Ya. Churilova – scientific idea, data analysis and writing of the article

Vyacheslav V. Suslin – data processing and preparation of graphic materials

Olga V. Krivenko – writing of the article

The authors have read and approved the final manuscript.

The authors declare that they have no conflict of interest.

Original article

Biogeochemical Characteristics of the Surface Layer and CO₂ Fluxes in the Ocean – Atmosphere System in the Fjords of Western Spitsbergen

N. K. Alekseeva , A. L. Nikulina, E. V. Bloshkina, Ya. V. Shved,
I. V. Ryzhov, A. E. Novikhin, M. S. Makhotin

Arctic and Antarctic Research Institute, Saint-Petersburg, Russian Federation

 nkalekseeva@aari.ru

Abstract

Purpose. The study is purposed at assessing and analyzing spatial variability and seasonal dynamics of the carbonate system parameters in the fjords of Western Spitsbergen based on the results of field research in the spring (April) and summer (August) seasons, 2023.

Methods and Results. The physical and chemical parameters of water, such as total alkalinity, pH and nutrient contents were studied. The samples were analyzed in the chemical analytical laboratory of the Russian Scientific Center at Spitsbergen (RSCS). The pH was measured using a Mettler Toledo Seven Compact S220 laboratory pH-meter, and total alkalinity – by direct titration of a seawater sample with a 0.02 hydrochloric acid (the equivalence point was determined visually). The concentrations of phosphates and silicates, as well as chlorophyll *a* were measured by standard spectrometric methods. The carbonate system parameters and CO₂ flux direction and speed were calculated using the *Program Developed for CO₂ System Calculations*. The revealed seasonal dynamics and variability of the carbonate system parameters are closely related to the atmospheric conditions, water mass seasonal variability and intensity of bioproductivity. The estimates of carbon dioxide flux obtained using the data for August 2023 allow to conclude that during this period CO₂ is absorbed in Grønfjorden (–1.52 ... –4.76 mmol m^{–2}·day^{–1}) and Isfjorden (–0.12 ... –1.0 mmol m^{–2}·day^{–1}), whereas in Billefjorden a local area with positively directed CO₂ flux (1.2–2.6 mmol m^{–2}·day^{–1}) was discovered.

Conclusions. The studies carried out in the fjords have resulted in revealing seasonal fluctuations in the carbonate system parameters and the carbon dioxide fluxes similar to other inner fjords of Spitsbergen. The obtained results highlight the importance of the carbonate system parameters in understanding the biogeochemical balance and the state of marine ecosystems in the context of climate change.

Keywords: Western Spitsbergen fjords, marine carbonate system, CO₂ flux, chlorophyll *a*, aragonite, Arctic

Acknowledgments: The material was collected by the Arctic and Antarctic Research Institute (AARI) at Spitsbergen within the framework of the Russian Scientific Arctic Expedition to Spitsbergen (RAE-S) in 2023. The authors are grateful to the RAE-S Research Coordination and Planning Department for their constant attention to the work and high-quality organization of field studies, as well as to the RAE-S wintering team in Barentsburg for their assistance in field and laboratory research. The study was carried out within the framework of the Federal Scientific and Technical Program in the field of ecological development of the Russian Federation and climate change for 2021–2030. Agreement No. 169-03-2024-072.

For citation: Alekseeva, N.K., Nikulina, A.L., Bloshkina, E.V., Shved, Ya.V., Ryzhov, I.V., Novikhin, A.E. and Makhotin, M.S., 2024. Biogeochemical Characteristics of the Surface Layer and CO₂ Fluxes in the Ocean – Atmosphere System in the Fjords of Western Spitsbergen. *Physical Oceanography*, 31(6), pp. 826-837.

© 2024, N. K. Alekseeva, A. L. Nikulina, E. V. Bloshkina, Ya. V. Shved, I. V. Ryzhov, A. E. Novikhin, M. S. Makhotin

© 2024, Physical Oceanography

826

ISSN 1573-160X PHYSICAL OCEANOGRAPHY VOL. 31 ISS. 6 (2024)



The content is available under Creative Commons Attribution-NonCommercial 4.0 International (CC BY-NC 4.0) License

Introduction

Global change in the climate system of our planet is one of the key problems that has a significant impact on almost all areas of human activity. The polar regions of the Earth and, in particular, the Arctic Ocean are the most important indicators and factors of these changes. In recent decades, the Arctic region has seen a reduction in the ice cover area, an increase in the influence of Atlantic waters, and an intensification of cyclonic activity, which lead to a restructuring of the water column and a change in the intensity of hydrochemical and hydrobiological processes.

The largest changes in the climate system occur in the western Arctic, including the Spitsbergen region. Studies [1] showed that the mean annual surface air temperature in Western Spitsbergen increased by 4 °C in the period 1970–2012, which significantly exceeds the increase in global air temperature (0.7 °C) over the same period. At the same time, the greatest increase in air temperature of 7 °C in winter was recorded in the north of Spitsbergen since 1979 according to the results of the ERA-Interim reanalysis of the European Centre for Medium-Range Weather Forecasts [2].

At the same time, the temperature of the Atlantic water masses in the Western Spitsbergen fjords increased (e.g. by 0.2 °C in the Isfjorden [3]), and more frequent intrusions of Atlantic water into the western fjord systems were recorded [4, p. 5]. A negative trend in glacier mass balance on the archipelago [5] also occurs, contributing to increased glacier meltwater discharge into coastal seas. All these climate changes affect the ongoing biogeochemical processes in the fjords of Western Spitsbergen, especially the marine carbonate system.

The carbonate system regulates the seawater pH and controls the dioxide (CO₂) circulation between the biosphere, lithosphere, atmosphere and oceans [6]. Its main parameters are total alkalinity (*TA*), dissolved inorganic carbon (*DIC*), pH and partial pressure of CO₂ (*pCO₂*)¹. Knowing these parameters and taking into account wind speed and *pCO₂* in the atmosphere, we can quantify and determine whether the ocean absorbs carbon dioxide or releases it into the atmosphere.

The Western Spitsbergen fjords are located in the zone of active interaction of warm, salty Atlantic and cold, fresher Arctic waters. The study area included Isfjorden, one of the largest fjords in the Arctic and the second longest in Spitsbergen; Grønfjorden, a relatively small fjord on the south side of Isfjorden, not far from its mouth; and Billefjorden, located in the inner part of Isfjorden. For all fjords, 7 types of water masses are distinguished: surface, intermediate, transformed, Atlantic, Arctic, local and winter [7, p. 129].

In contrast to the well-studied hydrological regime, the studies of features of biogeochemical processes and parameters of carbonate system in the Western Spitsbergen fjords are more fragmentary. Moreover, the small amount of data related to this topic is often limited to individual sections of the fjords, which hinders their

¹ Dickson, A.G., 2010. The Carbon Dioxide System in Seawater: Equilibrium Chemistry and Measurements. In: U. Riebesell, V. J. Fabry, L. Hanson and J.-P. Gattuso., eds., 2010. *Guide to Best Practices for Ocean Acidification Research and Data Reporting*. Luxembourg: Publications Office of the European Union, pp. 17-40.

broader interpretation [1, 8–10]. Thus, in the Isfjorden system, most of the studies that described seasonal dynamics of such water parameters as pH, *TA*, dissolved oxygen, *DIC*, the degree of water saturation with aragonite (Ω_{Ar}), etc. [1, 10, 11] were carried out in the small Tempelfjorden and Adventfjorden in 2011–2017. The observations revealed that the glacial impact is reflected in the biogeochemical structure of Tempelfjorden waters both in summer and winter [11]. The results demonstrated a significant influence of coastal runoff and glacial meltwater on the carbonate system and CO₂ absorption capacity. An analysis of the data obtained in Adventfjorden showed that the main driver of *TA* and *DIC* variability was salinity variations associated with river runoff, mixing processes and advection of water masses: 77 and 45%, respectively. Biological activity provided 60% of the monthly Ω_{Ar} variations and salinity changes had virtually no effect (5%) [1]. An analysis of measurements in Tempelfjorden [8] confirmed that an increase in freshwater (terrestrial and glacial) transforms the ocean from a source to a sink of CO₂ and provides positive feedback on ocean acidification.

At the same time, there are very few measurements of biogeochemical structure parameters of waters and the carbonate system carried out directly in Isfjorden itself, and all of them relate to the summer period [12, 13]; such measurements for Grønfjorden and Billefjorden are absent.

The aim of this work is to assess the spatial variability and seasonal dynamics of carbonate system parameters in the fjords of Western Spitsbergen, based on the results of expeditions in the spring (April) and summer (August) of 2023. This work will also make an important contribution to the dataset on the marine carbonate system of fjords.

Materials and methods

The studies of biogeochemical processes in the bays of Western Spitsbergen, carried out in April and August 2023, included oceanographic and hydrochemical analysis. Seawater samples were taken at specific horizons. As a result of laboratory analysis of these samples, the characteristics of *TA*, pH, phosphates, silicate silicon and chlorophyll *a* concentrations were obtained.

Surface water samples were collected at 15 and 28 oceanographic stations in the bays of Isfjorden and Grønfjorden in spring and summer respectively (Fig. 1). The total number of seawater samples processed was 790.

In April 2023, thermohaline profiling was carried out from the small ship *Farm* using the SBE-19plusV2 SeaCat CTD probe. The accuracy of conductivity and temperature sensors was 0.0005 Cm·m⁻¹ and 0.005 °C, respectively. In August 2023, thermohaline profiling in the Isfjorden waters was carried out from the boat *Barentsburg*, and in the Grønfjorden waters – from the boat *PolarCirkel 660 Work* using the RBRconcerto C.T.Dfast CTD probe. The accuracy of the conductivity and temperature sensors was 0.003 Cm·m⁻¹ and 0.002 °C, respectively.

Seawater sampling was carried out at 0, 5, 10, 25, 50 m horizons using the Ruttner bathometer. Sample analysis was carried out in the analytical laboratory of the RSCS.

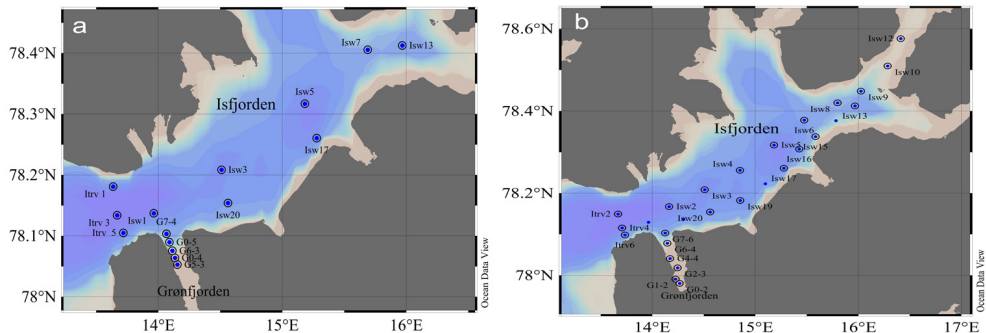


Fig. 1. Sampling stations in the fjords of Western Spitsbergen in April (a) and August (b), 2023

The pH was measured on the NBS scale using the Mettler Toledo Seven Compact S220 laboratory pH meter in accordance with the procedure set out in RD 52.10.735-2010, with a measurement accuracy of $\pm\Delta 0.05$. Calibration was performed at three points (4.01, 7.0, 9.21) using Mettler Toledo buffer solutions.

To determine the total alkalinity, a sample was titrated with a hydrochloric acid solution while simultaneously passing a flux of CO_2 -free air through the titrated sample to the equivalence point. The measurement accuracy was $\pm\Delta 0.014 \text{ mmol}\cdot\text{l}^{-1}$ in accordance with the RD 52.10.743-2010 technique.

The content of nutrient compounds (silicate silicons, phosphates) was determined by the standard spectrometric method (RD 52.10.744-2020 and RD 52.10.738-2010), with a measurement accuracy of $\pm\Delta 0.06$.

The chlorophyll *a* concentrations were obtained by spectrophotometry in accordance with GOST 17.1.4.02-90 standard, with an error of $\pm\Delta 20\%$.

The carbonate system components and the degree of water saturation with aragonite were calculated using the *Program Developed for CO_2 System Calculations*². The dissociation constants for carbonic acid, as outlined in [14], were applied in the calculation of carbonate system parameters.

The direction of carbon dioxide flux in the water – atmosphere system was obtained by Wanninkhof quadratic parameterization from [15] on the basis of the data on $p\text{CO}_2$ in water and in the atmosphere, as well as on wind speed. The calculations were based on the data on carbon dioxide content in atmospheric air, measured by a CO12M Environnement S.A. carbon monoxide and dioxide analyzer, and wind speed in the atmosphere surface layer (up to 2 m) measured by a Campbell Scientific meteorological tower.

² Robbins, L.L., Hansen, M.E., Kleypas, J.A. and Meylan, S.C., 2010. *CO₂calc – A User-Friendly Seawater Carbon Calculator for Windows, Max OS X, and iOS (iPhone)*. Reston, U.S.: Geological Survey Open-File Report 2010-1280, 17 p. <https://doi.org/10.3133/ofr20101280>

Results and discussions

In April 2023, a transformed Atlantic water mass with positive temperature values and a salinity of 34.7–34.8 was recorded in the surface layer of the Isfjorden and Grøn fjorden waters westward of 14.9°E (Fig. 2). The surface layer of the eastern part of Isfjorden was not affected by Atlantic waters. Instead, a local water mass (temperature below 0 °C, salinity less than 34.7) formed in the autumn – winter period as a result of cooling of the surface and intermediate water masses. Furthermore, the entire area under study was characterized by a homogeneous vertical distribution of temperature and salinity, which is typical for this season.

In August 2023, the surface temperature and salinity values of the fjord waters varied from 6.9–9 °C to 24.7–32.3, respectively. The minimum salinity values were observed in Billefjorden at stations *Is*w12 (24.7) and *Is*w10 (25.3). Salinity values at all other stations exceeded 28.8. The lowest temperature value was recorded at station *I*trv6. At all other locations, the temperature values exceeded 8 °C. The lower boundary of the surface water mass ($T > 1$ °C, $S < 34.3$) in the study area was identified at depths of 30–45 m.

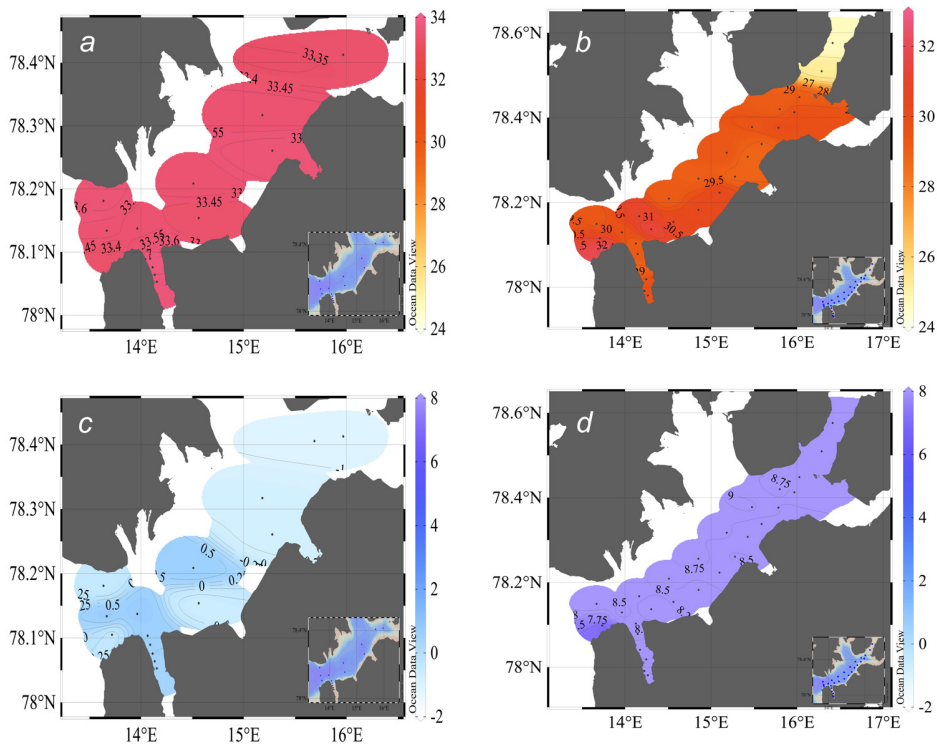


Fig. 2. Distribution of hydrophysical parameters in the surface layer of the Western Spitsbergen fjords, 2023: salinity in April (a) and August (b); temperature in April (c) and August (d)

In April, TA concentrations in Isfjorden varied within the range of 1641–1761 $\mu\text{mol}\cdot\text{kg}^{-1}$, and in Grøn fjorden – within 1686–1743 $\mu\text{mol}\cdot\text{kg}^{-1}$ (Fig. 3). In August, TA concentrations in Isfjorden varied within 1610–1820 $\mu\text{mol}\cdot\text{kg}^{-1}$, in Grøn fjorden – within 1710–1830 $\mu\text{mol}\cdot\text{kg}^{-1}$ and in Billefjorden within 1520–1570 $\mu\text{mol}\cdot\text{kg}^{-1}$.

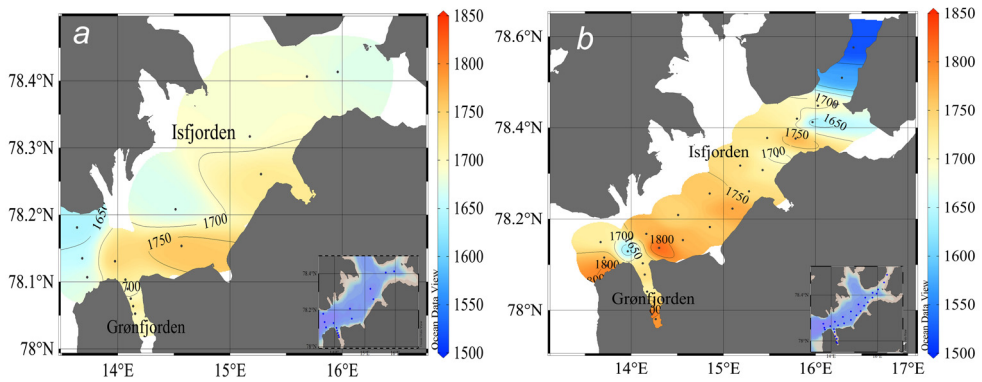


Fig. 3. Distribution of total alkalinity ($\mu\text{mol}\cdot\text{kg}^{-1}$) in the surface layer of the Western Spitsbergen fjords in April (a) and August (b), 2023

In April 2023, slight spatial variability in $p\text{CO}_2$ in Isfjorden and Grøn fjorden surface layers, ranging from 400 to 500 μatm , was recorded. Decreased pH values (7.89–8.00) and increased $p\text{CO}_2$ values (Fig. 4) in both fjords in spring 2023 suggest organic matter mineralization in the surface layer.

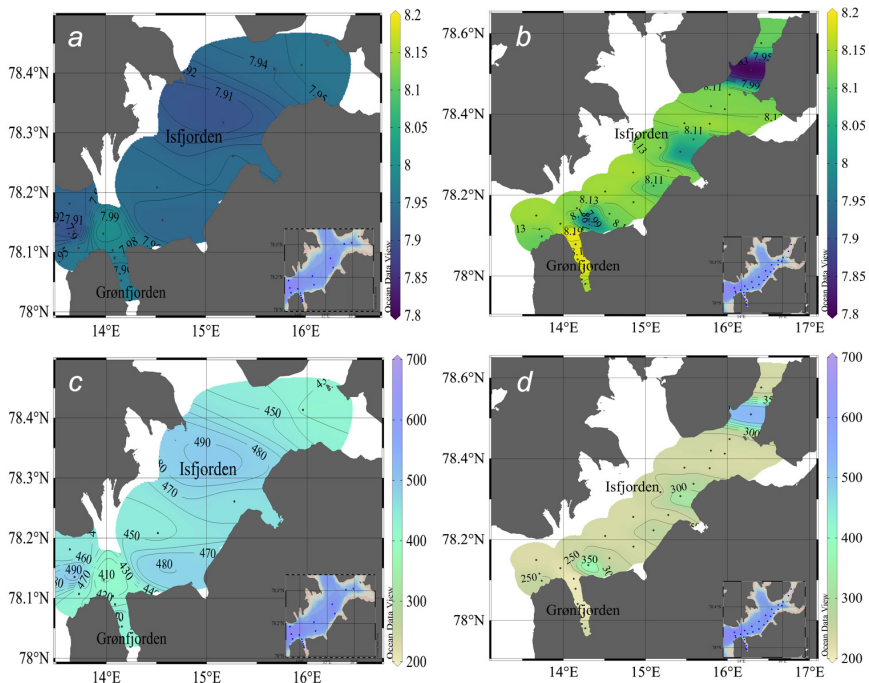


Fig. 4. Surface distribution of pH in April (a) and August (b), and $p\text{CO}_2$ (μatm) in April (c) and August (d) in the Western Spitsbergen fjords, 2023

In August, pH values in the Isfjorden area were within 7.97–8.15. At the same time, $p\text{CO}_2$ values in most of the fjord area were ~ 350 μatm , except for the local

zones with elevated values of 400–450 μatm . In Grøn fjorden, $p\text{CO}_2$ varied within 276–330 μatm , and pH within the range of 8.14–8.20.

The highest values of $p\text{CO}_2$ (730 μatm) and reduced (to 7.8) pH values were observed in Billefjorden (Fig. 5). This distribution pattern of carbon dioxide and pH partial pressure can be explained by two processes occurring simultaneously – organic matter mineralization and photosynthesis. At high concentrations of nutrients and illumination, the photosynthesis process predominates; this leads to carbon dioxide removal from the water for organic matter synthesis. This increases the pH of the environment and makes the water undersaturated with reference to CO_2 and oversaturated with reference to oxygen [16, p. 245].

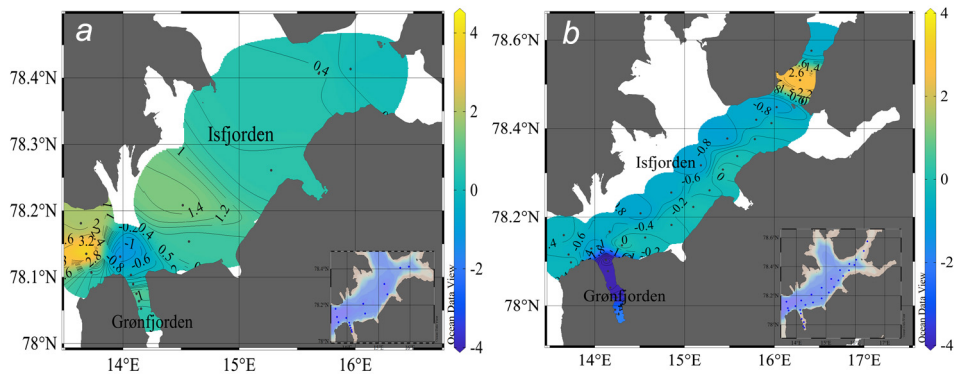


Fig. 5. Distribution of CO_2 flux ($\text{mmol}\cdot\text{m}^{-2}\cdot\text{day}^{-1}$) at the water – atmosphere boundary in the surface layer of the Western Spitsbergen fjords, 2023, in April (a) and August (b)

In general, higher pH and Ω_{Ar} values were recorded in the fjords under study in August compared to April. We observed undersaturation of waters with aragonite ($\Omega_{\text{Ar}} < 1$) in April. The Ω_{Ar} values in August varied within 1.2–1.75. In Billefjorden, a local area with reduced Ω_{Ar} values (0.75) was observed.

In Isfjorden, there was a notable variation in chlorophyll *a* concentrations between April and August. In April, concentrations ranged from 0.04 to 0.11 $\mu\text{g}\cdot\text{L}^{-1}$, while in August, they ranged from 0.26 $\mu\text{g}\cdot\text{L}^{-1}$ (in the inner part of the fjord) to 0.85–0.9 $\mu\text{g}\cdot\text{L}^{-1}$ (in the offshore area). In April, Grøn fjorden was characterized by a uniform distribution of chlorophyll *a* concentrations (0.21 $\mu\text{g}\cdot\text{L}^{-1}$) in the surface layer. In August, the concentrations were significantly higher, increasing from the innermost part (0.64 $\mu\text{g}\cdot\text{L}^{-1}$) to the fjord's mouth (2.04 $\mu\text{g}\cdot\text{L}^{-1}$). Such high chlorophyll *a* concentrations suggest a phytoplankton bloom in Grøn fjorden in August.

The higher chlorophyll *a* concentrations in Grøn fjord compared to Isfjord are probably due to the coastal runoff effect, which increases the amount of nutrients required for microalgae vegetation. In turn, the high pH values in Grøn fjorden contributed to the phytoplankton productivity, increasing the availability of nutrients [17, p. 58].

The distribution of silicon concentrations in the surface layer of the fjords in April was uniform, varying insignificantly within 9–10 $\mu\text{mol}\cdot\text{L}^{-1}$, with minimum values recorded in the mouth of Isfjorden. In August, higher silicon concentrations (4.5–6 $\mu\text{mol}\cdot\text{L}^{-1}$) were typical for Grøn fjorden and Billefjorden compared to Isfjorden (2–4.5 $\mu\text{mol}\cdot\text{L}^{-1}$), which is due to the influence of freshwater runoff. Minimum silicon concentrations were observed along the southern shore of Isfjorden.

In April, phosphate concentrations in the surface layer of the fjords varied within 0.6–0.8 $\mu\text{mol}\cdot\text{L}^{-1}$ at most stations. Higher values (1.4 and 1 $\mu\text{mol}\cdot\text{L}^{-1}$) were recorded at stations *Isw3* and *Isw7*, respectively. In August, phosphate concentrations were 0.09–0.73 $\mu\text{mol}\cdot\text{L}^{-1}$ in Isfjorden, 0.1–0.30 $\mu\text{mol}\cdot\text{L}^{-1}$ in Grøn fjorden and 0.26 $\mu\text{mol}\cdot\text{L}^{-1}$ in Billefjorden.

The exchange of CO_2 between the ocean and the atmosphere takes place in the presence of a vertical partial pressure gradient ($\Delta p\text{CO}_2$) between the surface layer of seawater and the surface layer of the atmosphere. If $\Delta p\text{CO}_2 > 0$, CO_2 is released from the ocean into the atmosphere and vice versa; if $\Delta p\text{CO}_2 < 0$, the flux is considered negative and CO_2 is absorbed by the ocean [18, p. 220].

The studies presented in this paper were carried out at low wind speeds ($< 5 \text{ m}\cdot\text{s}^{-1}$) in both seasons. In April, the calculated water – atmosphere carbon dioxide fluxes (FCO_2) for Isfjorden and Grøn fjorden varied between 0.37–4.18 and 0.2–1.43 $\text{mmol}\cdot\text{m}^{-2}\cdot\text{day}^{-1}$, respectively, indicating the release of carbon dioxide into the atmosphere. The obtained FCO_2 estimates based on the data for August 2023 allow to conclude that during this period CO_2 was absorbed in Grøn fjorden (–1.52 ... –4.76 $\text{mmol}\cdot\text{m}^{-2}\cdot\text{day}^{-1}$) and Isfjorden (–0.12 ... –1.0 $\text{mmol}\cdot\text{m}^{-2}\cdot\text{day}^{-1}$); in Billefjorden, a local area with a positive FCO_2 (1.2–2.6 $\text{mmol}\cdot\text{m}^{-2}\cdot\text{day}^{-1}$) is observed (Fig. 5).

The data from the field observations in April and August 2023 and the results of their analysis are in good agreement with the results of other researchers. For Isfjorden, as well as for other large fjords of Western Spitsbergen – Krossfjorden, Kongsfjorden, Hornsund Bay – a significant spatial variability of TA was typical, which is related to the complexity of the fjord system with numerous freshwater sources (rivers, melting glaciers), which can have different TA concentrations depending on the biogeochemical processes and the geological structure of the catchment. In addition, water column processes such as calcification, CaCO_3 dissolution or brine formation, play an important role in the distribution of TA in coastal areas [12]. For example, in 2012 very low total alkalinity values were observed in Tempelfjorden in April – May (1142 $\mu\text{mol}\cdot\text{kg}^{-1}$) and in September (526 $\mu\text{mol}\cdot\text{kg}^{-1}$), which is associated with the effects of intense glacial runoff [11, p. 16]. Our data show that the minimum total alkalinity values were recorded in Billefjorden in August 2023, where (although the Nordenskiöldbreen marine-terminating glacier has already completely retreated onto land) freshening is still significant enough to reduce the total seawater alkalinity during the maximum ablation period in August.

Our studies indicated that for Isfjorden, as well as for Tempelfjorden [8, 10] and Adventfjorden [1], characteristic processes are a decrease in $p\text{CO}_2$ and an increase in Ω_{Ar} from winter to summer months. At the same time, the $p\text{CO}_2$ values (400–500 μatm) in Isfjorden, according to data for April 2023, were higher than those recorded in Tempelfjorden in mid-March 2012 (370 μatm), according to [8, p. 2423], and in March 2016 (330 μatm), according to [10, p. 8]. The Ω_{Ar} values (1.2–1.75) for Isfjorden in August 2023 were lower than in August 2018 (2–2.5), according to [12, p. 4] but coincided with the values obtained in Tempelfjord in August 2016 (1.45) and 2017 (1.48), according to work [10, p. 9].

The rates of carbon dioxide fluxes in the water – atmosphere system, calculated for Isfjorden and Grønfjorden based on the data for August 2023, turned out to be lower compared to the estimates obtained for Tempelfjorden ($-11 \dots -17 \text{ mmol}\cdot\text{m}^{-2}\cdot\text{day}^{-1}$) for June – early August 2017 [11, p. 5], but close to those obtained in the bays under study in September 2022 ($-0.2 \dots -1.9 \text{ mmol}\cdot\text{m}^{-2}\cdot\text{day}^{-1}$) [19, p. 236].

The narrow ranges of concentrations of the main biogeochemical parameters obtained by us in 2023, and earlier by other researchers, allow us to conclude that such values are typical for the area under study, which is characterized by pronounced seasonal fluctuations.

Conclusion

During the study, we compared the data from two expeditions that took place in Isfjorden, Billefjorden and Grønfjorden (Western Spitsbergen) in April and August 2023. Analysis of the results confirmed the well-studied seasonal variability not only of thermohaline properties but also of several biogeochemical processes in this region. Their seasonal variability was manifested in pronounced fluctuations in the parameters of the carbonate system and carbon dioxide fluxes, indicating the dynamic nature of marine ecosystem response to climate change.

The results of the measurements of silicon and phosphate concentrations showed that April was characterized by an almost uniform spatial distribution of their values. In summer, the ranges in which the concentrations of these nutrient compounds varied increased significantly. High silicon concentrations in Grønfjorden and Billefjorden compared to Isfjorden were due to the influence of freshwater runoff. No patterns were found in the spatial distribution of phosphate concentrations in August.

In spring, an increase in $p\text{CO}_2$ levels in the surface water layer and a decrease in pH, indicating the process of mineralization of organic matter, were observed. Such $p\text{CO}_2$ levels were due to the prevalence of cold water masses and lower solar activity, which affected the intensity of biogeochemical processes. In summer, the opposite trend was observed: a decrease in $p\text{CO}_2$ levels and an increase in pH due to the photosynthetic activity of phytoplankton. The increased bioproductivity for this period of the year is caused by active heating of the surface layer and the influx of freshwater runoff, which contributes to more intensive CO_2 consumption, an increase in the oxygen content and alkalinity of the water. The surface water layer was characterized by different degrees of aragonite saturation in different seasons: undersaturation ($\Omega_{\text{Ar}} < 1$) was observed in April, and

a decrease in corrosivity was observed in August. It should be noted that the bays were ice-free in April, which made it possible to estimate the direction and rate of CO₂ flux in the water – atmosphere system. According to our calculations, small amounts of FCO₂ were released into the surface water layer in April, and CO₂ was absorbed from the atmosphere into the water in Isfjorden and Grønfjorden in August. A local area with a positive FCO₂ flux was recorded in Billefjorden. According to the data for September 2022, FCO₂ was also directed from the atmosphere into the water in Isfjorden and Grønfjorden.

Continued and expanded research in this area will contribute to a better understanding of the seasonal dynamics of processes under ongoing climate change, which will allow us to assess the impact of these global changes on the unique and fragile Arctic ecosystems.

REFERENCES

1. Ericson, Y., Chierici, M., Falck, E., Fransson, A.I., Jones, E.M. and Kristiansen, S., 2019. Seasonal Dynamics of the Marine CO₂ System in Adventfjorden, a West Spitsbergen Fjord. *Polar Research*, 38, 3345. <https://doi.org/10.33265/polar.v38.3345>
2. Onarheim, I.H., Smedsrud, L.H., Ingvaldsen, R.B. and Nilsen, F., 2014. Loss of Sea Ice during Winter North of Svalbard. *Tellus A: Dynamic Meteorology and Oceanography*, 66(1), 23933. <https://doi.org/10.3402/tellusa.v66.23933>
3. Pavlov, A.K., Tverberg, V., Ivanov, B.V., Nilsen, F., Falk-Petersen, S. and Granskog, M.A., 2013. Warming of Atlantic Water in Two West Spitsbergen Fjords over the Last Century (1912–2009). *Polar Research*, 32, 11206. <https://doi.org/10.3402/polar.v32i0.11206>
4. Bloshkina, E.V., Pavlov, A.K. and Filchuk, K., 2021. Warming of Atlantic Water in Three West Spitsbergen Fjords: Recent Patterns and Century-Long Trends. *Polar Research*, 40, 5392. <https://doi.org/10.33265/polar.v40.5392>
5. Van Pelt, W., Pohjola, V., Pettersson, R., Marchenko, S., Kohler, J., Luks, B., Hagen, J.O., Schuler, T.V., Dunse, T. [et al.], 2019. A Long-Term Dataset of Climatic Mass Balance, Snow Conditions, and Runoff in Svalbard (1957–2018). *The Cryosphere*, 13(9), pp. 2259–2280. <https://doi.org/10.5194/tc-13-2259-2019>
6. Millero, F.J., 2000. The Carbonate System in Marine Environments. In: A. Gianguzza, E. Pelizzetti and S. Sammartano, eds., 2000. *Chemical Processes in Marine Environments*. Berlin: Springer, pp. 9–41. https://doi.org/10.1007/978-3-662-04207-6_2
7. Bloshkina, E.V. and Filchuk, K.V., 2018. The Present Water Masses Conditions of West Spitsbergen Fjords. *Arctic and Antarctic Research*, 64(2), pp. 125–140. <https://doi.org/10.30758/0555-2648-2018-64-2-125-140>
8. Fransson, A., Chierici, M., Nomura, D., Granskog, M.A., Kristiansen, S., Martma, T. and Nehrke, G., 2015. Effect of Glacial Drainage Water on the CO₂ System and Ocean Acidification State in an Arctic Tidewater-Glacier Fjord during Two Contrasting Years. *Journal of Geophysical Research: Oceans*, 120(4), pp. 2413–2429. <https://doi.org/10.1002/2014jc010320>
9. Fransson, A., Chierici, M., Hop, H., Findlay, H.S., Kristiansen, S. and Wold, A., 2016. Late Winter-to-Summer Change in Ocean Acidification State in Kongsfjorden, with Implications for Calcifying Organisms. *Polar Biology*, 39, pp. 1841–1857. <https://doi.org/10.1007/s00300-016-1955-5>
10. Ericson, Y., Falck, E., Chierici, M., Fransson, A. and Kristiansen, S., 2019. Marine CO₂ System Variability in a High Arctic Tidewater-Glacier Fjord System, Tempelfjorden, Svalbard. *Continental Shelf Research*, 181, pp. 1–13. <https://doi.org/10.1016/j.csr.2019.04.013>
11. Pogojeva, M., Polukhin, A., Makkaveev, P., Staalstrøm, A., Berezina, A. and Yakushev, E., 2022. Arctic Inshore Biogeochemical Regime Influenced by Coastal Runoff and Glacial Melting (Case Study for the Tempelfjord, Spitsbergen). *Geosciences*, 12(1), 44. <https://doi.org/10.3390/geosciences12010044>

12. Koziarowska-Makuch, K., Szymczycha, B., Thomas, H. and Kuliński, K., 2023. The Marine Carbonate System Variability in High Meltwater Season (Spitsbergen Fjords, Svalbard). *Progress in Oceanography*, 211, 102977. <https://doi.org/10.1016/j.pocean.2023.102977>
13. Saghravani, S.R., Böttcher, M.E., Hong, W.-L., Kuliński, K., Lepland, A., Sen, A. and Szymczycha, B., 2024. Distributions of In-Situ Parameters, Dissolved (In)Organic Carbon, and Nutrients in the Water Column and Pore Waters of Arctic Fjords (Western Spitsbergen) during a Melting Season. *Earth System Science Data*, 16, pp. 3419-3431. <https://doi.org/10.5194/essd-16-3419-2024>
14. Mehrbach, C., Culberson, C.H., Hawley, J.E. and Pytkowicz, R.M., 1973. Measurement of the Apparent Dissociation Constants of Carbonic Acid in Seawater at Atmospheric Pressure. *Limnology and Oceanography*, 18(6), pp. 897-907. <https://doi.org/10.4319/lo.1973.18.6.0897>
15. Wanninkhof, R., 2014. Relationship between Wind Speed and Gas Exchange over the Ocean Revisited. *Limnology and Oceanography: Methods*, 12(6), pp. 351-362. <https://doi.org/10.4319/lom.2014.12.351>
16. Tishchenko, P.Ya., Tishchenko, P.P., Zvalinsky, V.I., Shkirknikova, E.M., Chichkin, R.V. and Lobanov, V.B., 2006. Carbonate System of the Amur Bay (Japan Sea) in Summer 2005. *Izvestiya TINRO*, 146, pp. 235-255 (in Russian).
17. Berezovskaya, V.A. and Lyandsberg, R.A., 2004. [Factors Affecting the pH Value in Coastal Waters of Kamchatka]. *Bulletin of Kamchatka State Technical University*, 3, pp. 58-61 (in Russian).
18. Malinin, V.N. and Obraztsova, A.A., 2011. [Variability of the Exchange of Carbon Dioxide in the System Ocean-Atmosphere]. *Society. Environment. Development = Terra Humana*, (4), pp. 220-226 (in Russian).
19. Alekseeva, N.K., Nikulina, A.L., Ryzhov, I.V., Novikhin, A.E., Kornilova, R.V., Smirnov, N.A. and Fedorova, A.A., 2023. Marine Carbonate System Parameters of the West Spitsbergen Fjords in Late Summer 2022. In: T. Chaplina, ed., 2023. *Complex Investigation of the World Ocean (CIWO-2023)*. CIWO-2023. Springer Proceedings in Earth and Environmental Sciences. Cham: Springer, pp. 233-238. https://doi.org/10.1007/978-3-031-47851-2_27

Submitted 26.06.2024; approved after review 21.08.2024;
accepted for publication 12.09.2024.

About the authors:

Natalia K. Alekseeva, Research Associate, Arctic and Antarctic Research Institute (38 Beringa Str., Saint-Petersburg, 199397, Russian Federation), **ORCID ID: 0000-0002-0705-6408**, **ResearcherID: J-5432-2016**, **Scopus Author ID: 57208470667**, nkalekseeva@aari.ru

Anna L. Nikulina, Deputy Head, Russian Arctic Scientific Expedition on Spitsbergen (RAE-SP), Arctic and Antarctic Research Institute (38 Beringa Str., Saint-Petersburg, 199397, Russian Federation), Dr. rer. nat., **ORCID ID: 0000-0002-7001-338X**, **Scopus Author ID: 26039425600**, anikulina@aari.ru

Ekaterina V. Bloshkina, Junior Research Associate, Arctic and Antarctic Research Institute (38 Beringa Str., Saint-Petersburg, 199397, Russian Federation), **ORCID ID: 0000-0002-2078-7459**, **ResearcherID: I-6901-2015**, **Scopus Author ID: 36166378400**, bloshkinaev@mail.ru

Yana V. Shved, Engineer, Arctic and Antarctic Research Institute (38 Beringa Str., Saint-Petersburg, 199397, Russian Federation), **ORCID ID: 0009-0009-2985-7570**, **ResearcherID: HPE-4386-2023**, yvswede@aari.ru

Ivan V. Ryzhov, Junior Research Associate, Arctic and Antarctic Research Institute (38 Beringa Str., Saint-Petersburg, 199397, Russian Federation), **ORCID ID: 0009-0008-8300-6550**, ryzhov@aari.ru

Andrey E. Novikhin, Research Associate, Arctic and Antarctic Research Institute (38 Beringa Str., Saint-Petersburg, 199397, Russian Federation), **ORCID ID: 0000-0001-5141-8624**, **ResearcherID: J-6005-2016**, **Scopus Author ID: 36669102600**, andrey_n@aari.ru

Mikhail S. Makhotin, Senior Research Associate, Head of Laboratory, Arctic and Antarctic Research Institute (38 Beringa Str., Saint-Petersburg, 199397, Russian Federation), **ORCID ID: 0000-0002-2801-1030**, **ResearcherID: K-8861-2016**, **Scopus Author ID: 23995647100**, makhotin@aari.ru

Contribution of the co-authors:

Natalia K. Alekseeva – chemical data collection; conceptualization and data curation; formal analysis, methodology, visualization, validation, writing of original draft

Anna L. Nikulina – chemical data collection; conceptualization and data curation; formal analysis, methodology, writing of original draft

Ekaterina V. Bloskhina – conceptualization and data curation, formal analysis; investigation; software; evaluative writing – review and editing

Yana V. Shved – formal analysis; investigation; writing of original draft

Ivan V. Ryzhov – formal analysis; investigation; validation

Andrey E. Novikhin – methodology; software; validation

Mikhail S. Makhotin – writing – review and editing

The authors have read and approved the final manuscript.

The authors declare that they have no conflict of interest.

Original article

Suspended Matter of the Deep-Water Part of the Black Sea

I. N. Mukoseev ✉, N. A. Orekhova

Marine Hydrophysical Institute of RAS, Sevastopol, Russian Federation✉ igor.mukos@gmail.com

Abstract

Purpose. The purpose of the work is to analyze the suspended matter (SM) flux in the deep part of the Black Sea, assess its variability and investigate the transformation of its composition under anaerobic conditions based on the data collected in 2021–2022.

Methods and Results. The data were obtained by means of sediment traps installed at five horizons along the transect between Cape Chersonesus and Bosphorus Strait in the Black Sea. The automatic deep-sea sedimentation observatory (AGOS) was installed during the 119th cruise of the R/V *Professor Vodyanitsky* and retrieved during the 124th cruise in 2022. The research covered all the seasons in 2021–2022. To collect the material, two types of traps were incorporated into AGOS: to determine the SM vertical distribution and to study its seasonal variation. The processing of the data was conducted using a uniform methodology, which included filtration, drying, gravimetric analysis for the calculation of suspended particulate matter fluxes, as well as determination of the organic and inorganic carbon contents by the coulometric titration method in the laboratory of Marine Hydrophysical Institute of RAS. The study yielded data on the vertical distribution of SM flux and its seasonal variation. The distribution patterns of SM, as well as the organic and inorganic carbon involved in its composition, were revealed.

Conclusions. The dynamics of SM and carbon fluxes are determined by different physical and biogeochemical processes. The SM fluxes are distributed unevenly across depth and change seasonally throughout the year. An analysis of the integral trap data shows that the SM fluxes exhibit variability across different depths, with a range of 62–99 mg·m⁻²·day⁻¹. At depths of 218 and 1568 m, the intensity is at its maximum. Its decrease depends on various biogeochemical processes, including dissolution, oxidation and mineralization. The increase in SM fluxes can be attributed to both deep-sea currents and physical and chemical sorption processes. The seasonal changes in SM flow are represented by two peaks: the maximum occurs during the period July – September, while the minimum occurs in March. Carbon concentration in SM exhibits fluctuations with depth and across seasonal cycles, which are mainly shaped by biological processes. The discrepancy between the peaks of the coccolithophore bloom at the surface and the maximum values of the inorganic carbon flux recorded by the trap can be explained by the sedimentation rates.

Keywords: suspended matter, organic carbon, inorganic carbon, carbonates, sediment traps, coccolithophores, Black Sea

Acknowledgments: The study was carried out within the framework of the state assignment of FSBSI FRC MHI on the themes “Monitoring of the carbonate system, CO₂ content and fluxes in the marine environment of the Black Sea and the Sea of Azov” FNNN-2022-0002 and “Ensuring climatic and biogeochemical monitoring of carbon fluxes in the Black Sea using long-term *in situ* data and numerical modeling results” FNNN-2023-0001. The authors are grateful to A. A. Klyuvitkin, Ph.D. (Geolog. and Mineralog.), Head Scientist Researcher in the Laboratory of Physical and Geological Research n. a. A. P. Lisitsyn (Institute of Oceanology, RAS) for his assistance in organizing the work and installing the trap.

For citation: Mukoseev, I.N. and Orekhova, N.A., 2024. Suspended Matter of the Deep-Water Part of the Black Sea. *Physical Oceanography*, 31(6), pp. 838-850.

© 2024, I. N. Mukoseev, N. A. Orekhova

© 2024, Physical Oceanography



Introduction

Suspended matter (SM) is an important component of the marine ecosystem. Its composition is mainly formed in the upper water column as a result of the complex interaction of substances from various geospheres, including the lithosphere, atmosphere, hydrosphere, and biosphere [1]. The suspended matter can be divided into two main categories: lithogenic and biogenic. The lithogenic components are of terrigenous and abiogenic origin and enter the system through various means, including river runoff, mechanical destruction of riverbanks, aeolian transport, and melting ice. The biogenic components are the remains of once-living and dead organisms, formed from organic matter (C_{org}), amorphous silica (SiO_{2bio}), and suspended calcium carbonate ($CaCO_3$), which are part of plankton and its detritus [2–4].

A change in oxidation-reduction conditions typically results in the change of ratio and content of lithogenic and biogenic SM components. The qualitative and quantitative SM composition in a water column reflects the transformation processes occurring therein. Given that carbon is a key component of SM, the study of its organic and inorganic forms, as well as their ratio, enables the investigation of the predominant mechanisms governing the carbon cycle in the hydrosphere. The content of organic carbon (C_{org}) in SM reflects the ecosystem productivity, intensity of biochemical processes in it and resistance to the effects of various natural and anthropogenic factors [5, 6]. Carbonates also play a substantial role in the SM, comprising both terrigenous carbonates transported from land and autochthonous carbonates formed in the water column [7]. Inorganic carbon (C_{carb}) is a structural component of carbonate minerals, which are represented in suspension by biogenic and chemogenic formations.

According to long-term studies of phytoplankton, the main carbonate-concentrating biogenic particles in the SM composition in the Black Sea are *Emiliana huxleyi*, species of coccolithophore [8, 9]. These algae act as an intermediary in the transfer of C_{carb} from the atmosphere and the euphotic zone to bottom sediments. This is due to the fact that at the conclusion of the "bloom", coccolithophores partially settle to the bottom, where they constitute the main component of calcareous silts [8].

In the water column, finely dispersed SM micro- and nanoparticles aggregate under the influence of biological (water filtration by zooplankton organisms with the transformation of sedimentary matter into pellets and amorphous lumps (marine snow)), as well as physicochemical (coagulation, flocculation of colloids) processes. As a result, vertical fluxes of sedimentary matter are formed. They are transformed when passing through the water column and are ultimately subject to the burial process in the form of bottom sediments [7]. Accordingly, the study of the vertical distribution of SM is the basis for understanding the modern sedimentation processes [1].

In this way, the study of SM flux and its formation and transformation mechanisms is a pressing oceanographic task.

Until recently, studies of SM in the Russian sector of the Black Sea were episodic in nature [6, 10] and were carried out primarily in shelf areas [11]. The most comprehensive review of SM study and its flux in the Black Sea is presented in [1]. Modern studies of SM are based primarily on satellite data [3–5, 12], but this approach has a number of shortcomings, in particular the inability to study the vertical SM profile and its transformation processes.

In 2015, the researchers of the Institute of Oceanology of RAS began studying the vertical profile and intra-annual variability of SM in the open part of the Black Sea [1]. In the deep part, sediment traps were installed as part of the automatic deep-sea sedimentation observatory (AGOS), the concept of which was developed by the Academician A.P. Lisitsyn and put into practice in sedimentological research [13, 14].

The AGOS concept implies the possibility of using an integrated approach to the study of SM fluxes in order to determine the associated parameters, namely: determination of the main parameters of the upper water layer by remote sensing methods using satellite imagery; use of sediment traps with different time resolutions installed at different depths; connection of additional probes to determine the hydrological parameters of the environment at the trap site (currents, temperature, salinity, content, transparency, fluorescence, etc.).

The purpose of the work is to quantify the suspended matter (SM) flux in the deep part of the Black Sea, its variability and compositional change under anaerobic conditions based on the data of 2021–2022.

Materials and methods

The data were obtained through the installation of sediment traps at five horizons in the deep part of the Black Sea (station installation depth 1968 m) along the transect of Cape Chersonesus – Bosphorus Strait (distance from Cape Chersonesus is 180 km).

Two types of sediment traps were used for sampling: the first is capable of obtaining continuous material collection with a specified exposure time (*Lotus-3* differential 12-cup sediment traps), while the second is an integral small cylindrical sediment trap, *MSL-110*, which collects material throughout the station's operational duration [1]. Fig. 1 shows the location of the sediment traps. The AGOS observatory was installed during the 119th cruise of the R/V *Professor Vodyanitsky* on 24 September 2021. The station was retrieved on 4 October 2022, during the vessel's 124th cruise. For integral collection of material over the course of the year, *MSLs* were installed at depths of 218, 568, 1068, 1568 and 1918 m. At depths of 218 m (*Lotus-3*) and 1918 m (the *Lotus-1* trap was not operational, the data are not discussed in the paper), differential sediment traps with an exposure time of 30 days were installed. Thus, the period of AGOS operation at different depths and with a given discreteness of SM collection was 12 months (375 days), it covered all seasons from September 2021 to October 2022. To preserve the collected material in conditions as close to natural as possible, the receiving containers were filled with

a 4% sodium chloride solution, which is twice the average salinity of the Black Sea waters.

At a depth of 218 m, the traps were installed to estimate the flux from the upper quasi-homogeneous layer, at a depth of 1918 m – to estimate the flux reaching the bottom and participating in the formation of sediments. Three intermediate depths were selected to estimate the SM flux variability with depth.

Following retrieval, the containers containing the SM samples were stored in a refrigerated chamber until laboratory processing, which was carried out using a single method described in [1].

The samples were vacuum filtered through parallel pre-weighed nuclear filters with a 0.45 μm pore size to determine the total SM flux, as well as through *Whatman GF/F* glass fiber filters calcined at 450°C to determine the total, organic and carbonate carbon content.

After drying at 60°C until a constant mass was achieved, the filters were weighed with the filtered substance present. This enabled the total amount of material to be obtained (dry SM mass, mg). The material was weighed using the *Adventurer AR2140* analytical laboratory scale with a measurement accuracy of up to 0.0001 g.

The SM flux was calculated as the ratio of the dry SM mass to the product of the trap collection area and the exposure time:

$$F = \frac{m}{ST}, \quad (1)$$

where F is the SM flux, $\text{mg}\cdot\text{m}^{-2}\cdot\text{day}^{-1}$; m is the dry SM mass, mg; S is the collection area, m^2 ; T is the exposure time, day.

The total, organic and carbonate carbon contents were determined by coulometric titration on an AN-7529 carbon analyzer [15].

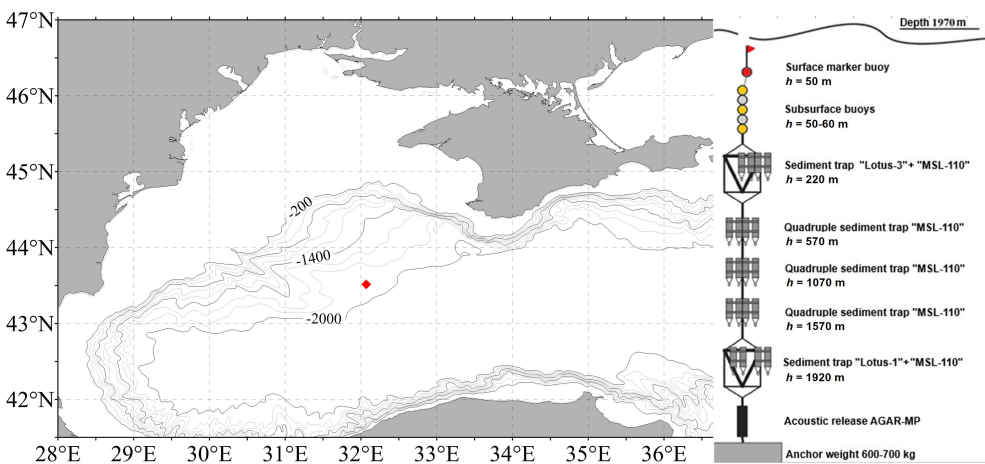


Fig. 1. Scheme of the AGOS (a) and the area of its installation (b)

Results and discussion

The vertical flux of SM, the C_{org} and C_{carb} content in samples were determined using the data obtained from sediment traps, and the fluxes of organic and inorganic carbon with SM were calculated. The seasonal variability of the SM fluxes was studied at a depth of 218 m. The fluxes were characterized by distribution heterogeneity with regard to depth and temporal variation (Fig. 2).

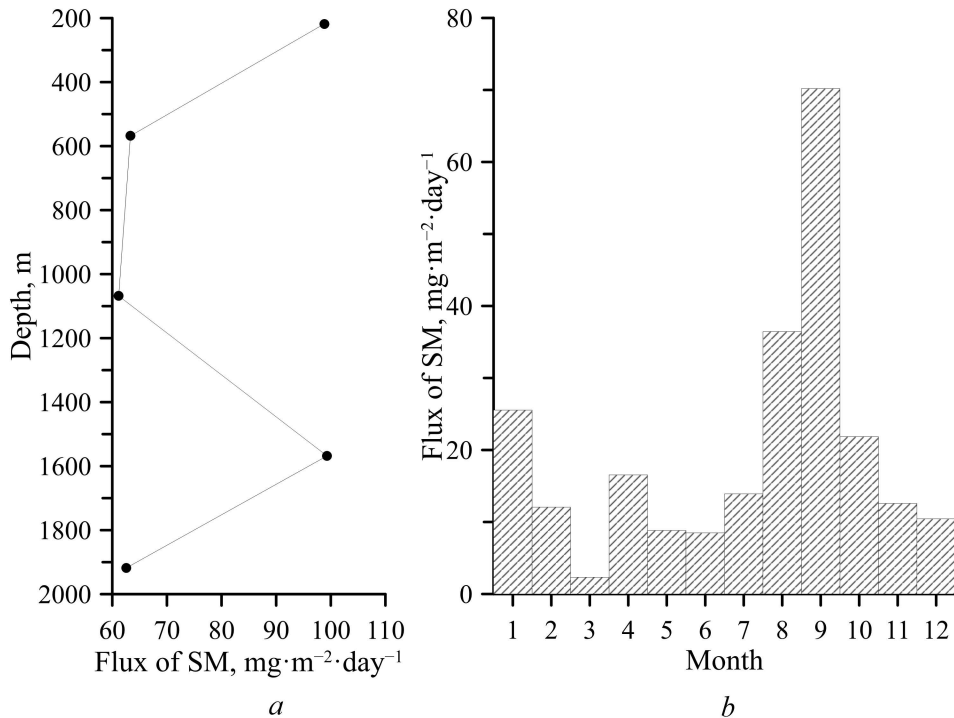


Fig. 2. Vertical (a) and seasonal (b) variability of the SM flux based on the 2021–2022 data

The data obtained from the integral traps indicates that the SM flux exhibited a range of 62–99 mg·m⁻²·day⁻¹ (Fig. 2, a). Two peaks of the same intensity (99 mg·m⁻²·day⁻¹) were noted at depths of 218 and 1568 m. At depths of 568, 1068 and 1918 m, the value decreased and was 61–63 mg·m⁻²·day⁻¹. The order of these values is comparable with both modern data for 2015–2016 for the central part of the sea at the foot of the northwestern slope of the deep-sea basin [1], and with the data from the 1980s for the Anatolian coast [16–18].

The seasonal variability of the SM flux at a depth of 218 m was characterized by a maximum in September (70.2 mg·m⁻²·day⁻¹ over a 30-day period) and a minimum in March (2 mg·m⁻²·day⁻¹) (Fig. 2, b). In general, the SM flux values exhibited a range of 9–36 mg·m⁻²·day⁻¹, which corresponds to the data presented in [1, 16–18].

The distribution of carbon, a principal SM component, correlated with the vertical profile of its flux. Maximum concentrations were observed at depths of 218 and 1568 m (19.25 and 19.52%, respectively), while at depths of 568, 1068 and 1918 m, concentrations remained within narrow limits of 17.29–17.68%. The ratio of organic and inorganic forms of carbon changed slightly with depth (Fig. 3, *b*), with the contribution of organic carbon averaging 83%.

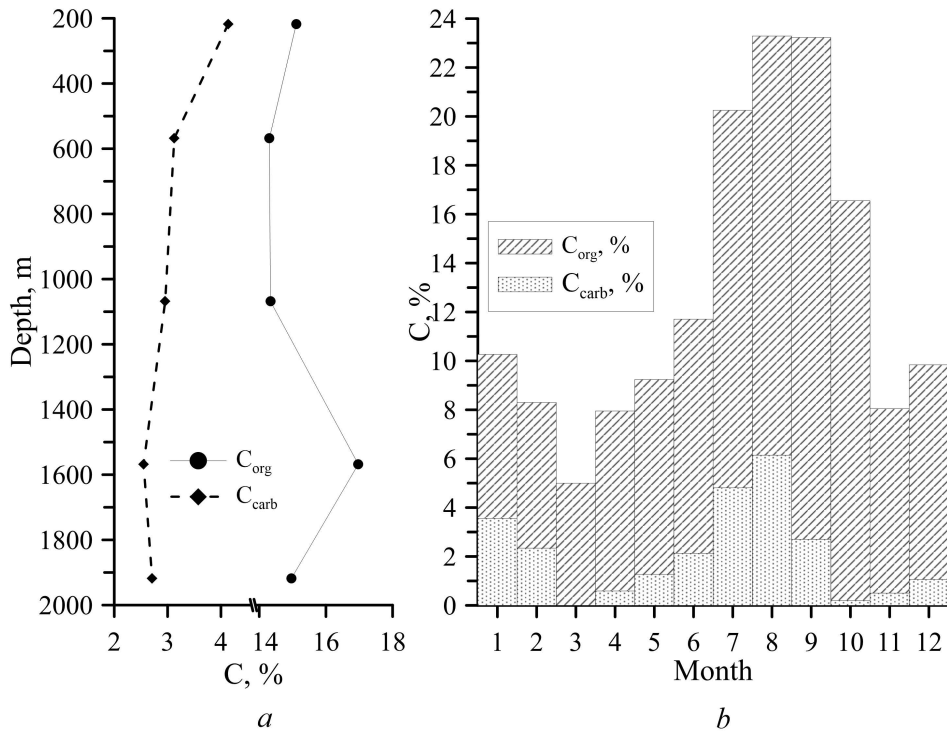


Fig. 3. Distribution of organic (C_{org}) and inorganic (C_{carb}) forms of carbon with depth (*a*) and during a year (*b*)

During the year, the carbon content in SM exhibited a range of 5–23.29%, with a maximum observed in August and September and a minimum in March, when the minimum SM flux was also recorded (Fig. 2, *b*). The seasonal variability of the C_{org} concentration qualitatively coincided with that of the SM flux, with minima observed in March and November (5.0 and 7.54%, respectively) and maxima in July – September (16.3–20.53%) (Fig. 3, *b*). The distribution of C_{carb} in SM was somewhat different: concentration minima were observed in the spring and autumn periods (in March, April and October, November, respectively).

A comparable distribution of organic and inorganic forms of carbon revealed that the organic component is also characterized by pronounced seasonality, with maxima in March and October (Fig. 4). During the first period, a gradual decline in

the C_{org} share was observed, reaching a reduction of 25% from March to August. In contrast, during the second period, a sharper decline in the C_{org} share was noted from October to January.

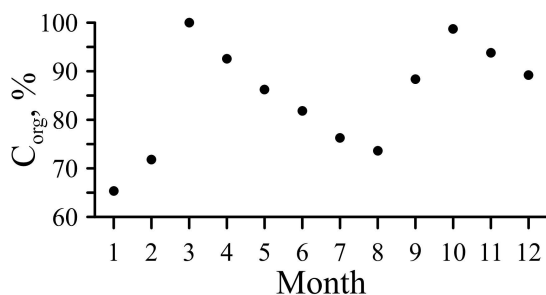
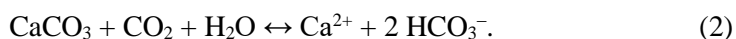


Fig. 4. Share of organic component in total carbon in SM

Discussion of the results

Vertical profile. The variation in SM flux intensity with depth is the result of the influence of physical and biogeochemical processes. The data obtained using sediment traps enabled the determination of vertical fluxes with regard to the C_{org} and C_{carb} content in samples, as well as the calculation of organic and inorganic carbon fluxes with SM. The seasonal variability of these fluxes was studied at a depth of 218 m.

The C_{carb} flux for the Black Sea is primarily influenced by processes involving coccolithophores, given their prevalence as the dominant algae with a carbonate skeleton within this ecosystem [8, 9]. Due to insufficient saturation of deep-water masses with carbonates [19], as well as a pH decrease and an increase in the CO_2 concentration, carbonates should dissolve, which is manifested in a decrease in the C_{carb} flux with depth (Fig. 3, a):



The SM flux increase at a depth of 1568 m and below is possibly due to the influence of deep currents [10]. According to [20], the advective transport of water occurs in the lower nepheloid layers, which are formed as a result of bottom erosion under the action of internal tides and waves. Fine-grained, resuspended sediments, including clay particles, silt and coccolith, are often involved in this form of bottom horizontal transport [16, 17].

The SM concentration increase can also be determined by the influence of anaerobic conditions of the Black Sea waters and a number of features of the biochemical reactions under these conditions. Thus, some researchers associate this with reactions involving manganese, iron and other trace elements that form insoluble sulfides in the hydrogen sulfide zone, which subsequently precipitate, sorbing some of the dissolved compounds, and contribute to the formation of

a complex suspension [10]. The presence of pyrites in the suspension of the deep Black Sea is shown in [1]. In addition, the carbon flux share is 20% of the SM flux, which indicates a complex component composition of the SM and confirms the theory of the formation of metal sulfides in the anaerobic layer, in particular iron and manganese, and their sorption of other dissolved components with the formation of complex compounds:



The results of our studies indicate a reduction in the SM flux with depth, and a qualitative alignment between the organic matter flux profile and the vertical SM flux profile (Fig. 2, *a*; 3, *a*). Consequently, it can be assumed that in the deep Black Sea, the organic component plays a dominant role in the SM formation. Additionally, the data [1] indicate that as depth increases, the concentration of carbonates decreases significantly and is not determined at a depth of 1775 m. At the same time, the observed increase in the SM flux intensity at a depth of 1568 m and the C_{org} concentration is likely attributed to physical transfer processes.

Seasonal variability of SM flux and carbon. Installation of long-term sediment traps with a specified exposure time, followed by collection and analysis of material, enables the investigation of the role of various physical, chemical and biological processes in the formation and transformation of SM under changing conditions.

The seasonal variability of SM characteristics and its flux is primarily determined by biological processes involving plankton and bacteria, which, in turn, are also dependent on hydrological conditions and seasonal phenomena [10], including seasonal cycles of primary producers, the “bloom” of coccolithophores and diatom microalgae, in the euphotic zone of the deep Black Sea [18, 21, 22].

The peaks in the SM flux values at a depth of 218 m occur during the summer (August) and autumn (September) periods (36.4 and 70.2 $\text{mg}\cdot\text{m}^{-2}\cdot\text{day}^{-1}$, respectively). Their total contribution represents 45% of the total annual flux value (Fig. 2).

In consideration of the satellite data (Fig. 5, *a*), which indicates that the coccolithophore “bloom” occurred in June [9], and the trap data, which shows the maximum contribution of carbonates to the SM flux occurred in July, August and September (40.1, 51.1 and 22.5%, respectively (Fig. 5, *c*)), it can be assumed that the SM flux is derived from the carbonate component and the sedimentation of coccolithophores during this period. The SM sedimentation rate in this case should be approximately $7\text{--}9\text{ m}\cdot\text{day}^{-1}$, which is consistent with the data presented by [23].

The observed lag of one to two months between the peak of phytoplankton productivity in the euphotic zone and the maximum values of inorganic carbon flux (represented mainly by coccolithophores) can also be attributed to sedimentation rates (within the $1\text{--}36\text{ m}\cdot\text{day}^{-1}$ range) [24].

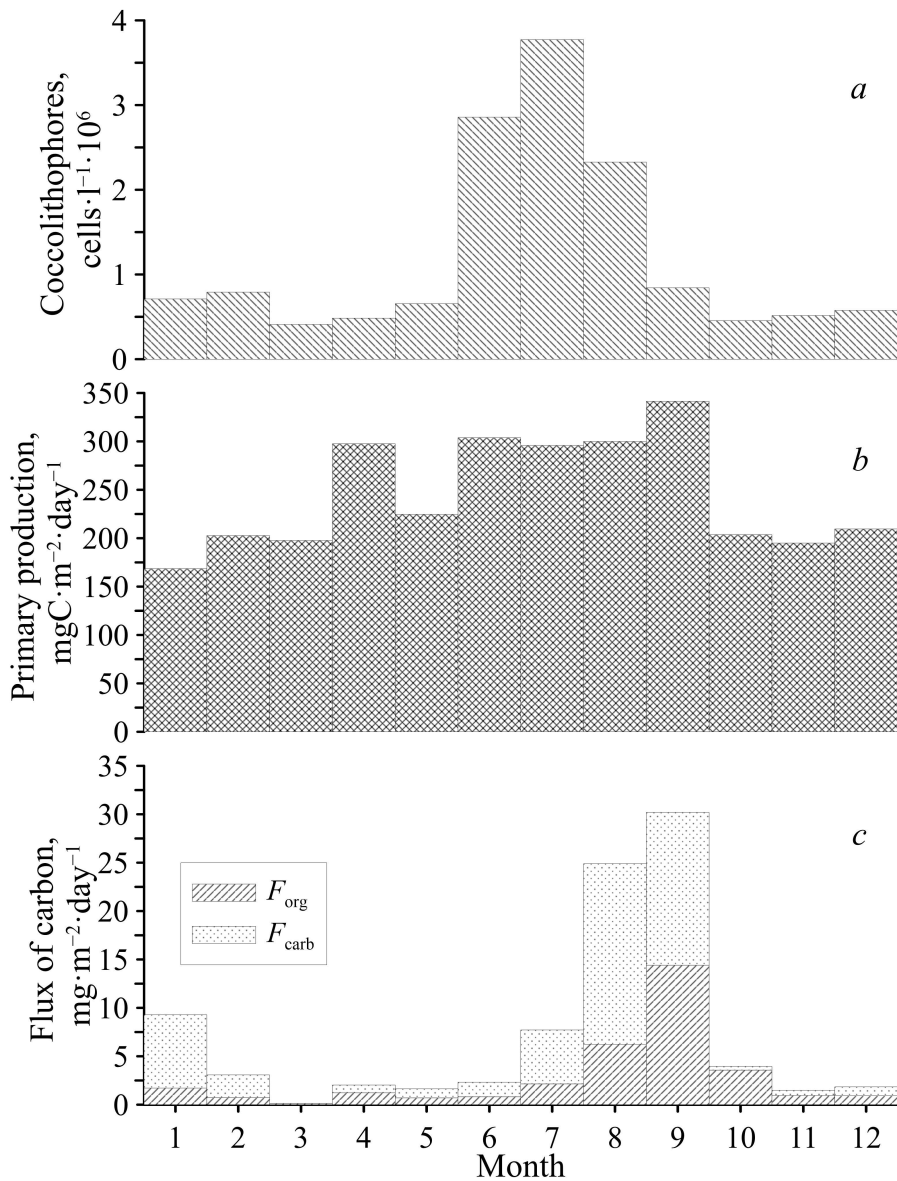


Fig. 5. Concentrations of coccolithophores (a) and primary production (b) in the area of the installed trap, based on satellite data for 2022; seasonal variations of organic carbon flux (F_{org}) and inorganic carbon, as component of carbonates flux (F_{carb}), in SM at a depth of 218 m, based on the *Lotus* trap data (c)

The remainder of the time, the SM flux varied within the range of 2.3–25.5 $\text{mg} \cdot \text{m}^{-2} \cdot \text{day}^{-1}$ with an average value of 13 $\text{mg} \cdot \text{m}^{-2} \cdot \text{day}^{-1}$. It was characterized by alternating maxima and minima (Fig. 2). The minimum SM flux occurred in March; during this period, it was determined only by the organic component with no inorganic component present (Fig. 3, b; 4, 5). The Black Sea waters are characterized

by two peaks of phytoplankton “bloom” – autumn-winter (more intense, the maximum occurs in November – December) and winter-spring [25], this is also reflected in the seasonal distribution of SM and its flux (Fig. 2, b).

Thus, the seasonal dynamics of the SM flux mainly coincides with the dynamics of primary production and the number of coccolithophores (Fig. 5) [9, 26].

Conclusion

The seasonal dynamics of the SM and carbon flux are determined by the influence of both physical and biogeochemical processes. The distribution of SM fluxes was found to exhibit heterogeneity with depth and over the course of the year.

The presence of two SM flux peaks of the same intensity at depths of 218 and 1568 m was observed. The reduction in the SM flux intensity is due to the occurrence of biogeochemical processes leading to the dissolution, oxidation and mineralization of substances that constitute SM. The increase in the concentration of SM and its flux is the result of the influence of currents or the occurrence of physicochemical processes of sorption on metal sulfides.

The seasonal variability of the SM flux was primarily determined by biological processes involving plankton, with the organic component contributing 83%. The peaks in the SM flux values occurred in the summer period, with their total contribution representing 45% of the annual flux values.

The lowest SM flux was recorded in March, during this period it was determined only by the organic component with no contribution from the inorganic component.

The seasonal dynamics of SM flux correspond to satellite data on primary production and coccolithophore abundance. Furthermore, the ratio of the peak times of their “bloom” in the photosynthesis zone and inorganic carbon fluxes at a depth of 218 m correlates with the calculated sedimentation rates, which range from 1 to 36 m·day⁻¹.

The measurements were conducted at the Center for Collective Use of the R/V *Professor Vodyanitsky* of A.O. Kovalevsky Institute of Biology of the Southern Seas of RAS.

REFERENCES

1. Klyuvitkin, A.A., Kravchishina, M.D., Lisitsyn, A.P., Demina, L.L., Dara, O.M., Novigatsky, A.N., Rusanov, I.I. and Solomatina, A.S., 2018. Vertical Fluxes of Dispersed Sedimentary Matter in the Deep-Water Part of the Black Sea. In: A. P. Lisitsyn, ed., 2018. *The Black Sea System*. Moscow: Scientific World, pp. 350-397. <https://doi.org/10.29006/978-5-91522-473-4.2018> (in Russian).
2. Lisitsyn, A.P., 1977. [Terrigenous Sedimentation, Climatic Zonation and Interaction of Terrigenous and Biogenic Material in the Oceans]. *Litologiya i Poleznye Iskopaemye*, (6), pp. 3-22 (in Russian).
3. Kukushkin, A.S. and Parkhomenko, A.V., 2021. Spatiotemporal Variability of Suspended Particulate Matter in the Surface Layer of the Open Part of the Black Sea. *Oceanology*, 61(2), pp. 272-282. <https://doi.org/10.1134/S0001437021010124>

4. Kukushkin, A.S. and Suslin, V.V., 2020. Assessment of Applicability of Satellite-Derived Ocean Color Data for Studying Variability of Total Suspended Matter in the Surface Layer of the Deep Part of the Black Sea. *Physical Oceanography*, 27(5), pp. 547-556. <https://doi.org/10.22449/1573-160X-2020-5-547-556>
5. Kukushkin, A.S. and Parkhomenko, A.V., 2019. Variability of the Content of Suspended Organic Matter along the Southwestern Crimean Coast According to Ship and Satellite Observations. *Sovremennye Problemy Distantionnogo Zondirovaniya Zemli iz Kosmosa*, 16(1) pp. 137-146. <https://doi.org/10.21046/2070-7401-2019-16-1-137-146> (in Russian).
6. Burlakova, Z.P., Eremeeva, L.V. and Kononov, S.K., 2000. Seasonal and Spatial Variability of the Content of Suspended Organic Substances in the Active Layer of the Black Sea. *Physical Oceanography*, 10(5), pp. 419-454. <https://doi.org/10.1007/BF02515365>
7. Lukashin, V.N. and Lisitzin, A.P., 2016. Geochemistry of Dispersed Sedimentary Matter and Its Fluxes in the Water Column of the Caspian Sea. *Oceanology*, 56(5), pp. 675-689. <https://doi.org/10.1134/S000143701605009X>
8. Shoman, N.Yu., Solomonova, E.S. and Akimov, A.I., 2022. Influence of Light on Change in Morphophysiological Characteristics of Coccolithophorids *Emiliania Huxleyi*. *Russian Journal of Plant Physiology*, 69(2), 40. <https://doi.org/10.1134/S1021443722020170>
9. Mikaelyan, A.S., Silkin, V.A. and Pautova, L.A., 2011. Coccolithophorids in the Black Sea: Their Interannual and Long-Term Changes. *Oceanology*, 51(1), pp. 39-48. <https://doi.org/10.1134/S0001437011010127>
10. Vityuk, D.M., 1975. Suspended Matter and Its Components in the Black Sea. *Hydrobiological Journal*, 11(1), pp. 12-18 (in Russian).
11. Denisov, V.I. and Latun, V.V., 2018. Flows of Chemical Elements in Suspended Matter Fluxes in the Shallow Area of the Black Sea Shelf (According to the Sediment Traps Data). *Izvestiya Vuzov. Severo-Kavkazskii Region. Natural Science*, (4), pp. 77-85. <https://doi.org/10.23683/0321-3005-2018-4-77-85> (in Russian).
12. Kukushkin, A.S., 2020. Estimation of the Variability of Suspended Matter Content in the Deep-Water Part of the Black Sea Using Satellite Data. *Sovremennye Problemy Distantionnogo Zondirovaniya Zemli iz Kosmosa*, 17(2), pp. 184-191. <https://doi.org/10.21046/2070-7401-2020-17-2-184-191> (in Russian).
13. Lisitsyn, A.P., Lukashin, V.N., Novigatskii, A.N., Ambrosimov, A.K., Klyuvitkin, A.A. and Filippov, A.S., 2014. Deep-Water Observatories in the Trans-Caspian Cross Section: Continuous Studies of Scattered Sedimentary Matter. *Doklady Earth Sciences*, 456(2), pp. 709-713. <https://doi.org/10.1134/S1028334X14060166>
14. Lisitsyn, A.P., Novigatskii, A.N., Shevchenko, V.P., Klyuvitkin, A.A., Kravchishina, M.D., Filippov, A.S. and Politova, N.V., 2014. Dispersed Organic Matter and Its Fluxes in Oceans and Seas from the Example of the White Sea: Results of a 12-Year Study. *Doklady Earth Sciences*, 456(1), pp. 635-639. <https://doi.org/10.1134/S1028334X14050353>
15. Zabegaev, I.A., Shul'gin, V.F. and Orekhova, N.A., 2021. Application of Instrumental Methods for Analysis of Bottom Sediments for Ecological Monitoring of Marine Ecosystems. *Scientific Notes of V.I. Vernadsky Crimean Federal University. Biology. Chemistry*, 7(4), pp. 242-254 (in Russian).
16. Honjo, S., Hay, B.J., Manganini, S.J., Asper, V.L., Degens, E.T., Kempe, S., Ittekkot, V., Izdar, E., Konuk, Y.T. [et al.], 1987. Seasonal Cyclicity of Lithogenic Particle Fluxes at a Southern

- Black Sea Sediment Trap Station. In: E. T. Degens, E. Izdar and S. Honjo, eds., 1987. *Mitteilungen des Geologisch-Paläontologischen Instituts der Universität Hamburg: SCOPE/UNEP Sonderband*, 62, pp. 19-39.
17. Izdar, E., Konuk, T., Ittekkot, V., Kempe, S. and Degens, E.T., 1987. Particle Flux in the Black Sea: Nature of the Organic Matter. In: E. T. Degens, E. Izdar and S. Honjo, eds., 1987. *Mitteilungen des Geologisch-Paläontologischen Instituts der Universität Hamburg: SCOPE/UNEP Sonderband*, 62, pp.1-18.
 18. Izdar, E., Konuk, T., Honjo, S., Asper, V., Manganini, S., Degens, E.T., Ittekkot, V. and Kempe, S., 1984. First Data on Sediment Trap Experiment in Black Sea Deep Water. *Naturwissenschaften*, 71, pp. 478-479. <https://doi.org/10.1007/BF00455904>
 19. Zeebe, R.E. and Wolf-Gladrow, D., 2001. *CO2 in Seawater: Equilibrium, Kinetics, Isotopes*. Amsterdam: Elsevier, 360 p.
 20. Dickson, R.R. and McCave, I.N., 1986. Nepheloid Layers on the Continental Slope West of Porcupine Bank. *Deep Sea Research Part A. Oceanographic Research Papers*, 33(6), pp. 791-818. [https://doi.org/10.1016/0198-0149\(86\)90089-0](https://doi.org/10.1016/0198-0149(86)90089-0)
 21. Samyshev, E.Z. and Minkina, N.I., 2017. The Seasonal Variability and Sedimentation Rate of Suspended Matter in Photic Layer of the Black Sea. *Environment and Ecology Research*, 5(3), pp. 227-234. <https://doi.org/10.13189/eer.2017.050308>
 22. Smetacek, V., von Bröckel, K., Zeitzschel, B. and Zenk, W., 1978. Sedimentation of Particulate Matter during a Phytoplankton Spring Bloom in Relation to the Hydrographical Regime. *Marine Biology*, 47, pp. 211-226. <https://doi.org/10.1007/BF00541000>
 23. Parkhomenko, A.V. and Kukushkin, A.S., 2018. Sediment Flux of Particulate Organic Phosphorus in the Open Black Sea. *Oceanology*, 58, pp. 240-249. <https://doi.org/10.1134/S0001437018020145>
 24. Asper, V.L., 1987. Measuring the Flux and Sinking Speed of Marine Snow Aggregates. *Deep Sea Research Part A. Oceanographic Research Papers*, 34(1), pp. 1-17. [https://doi.org/10.1016/0198-0149\(87\)90117-8](https://doi.org/10.1016/0198-0149(87)90117-8)
 25. Vostokov, S.V., Lobkovskiy, L.I., Vostokova, A.S. and Solov'ev, D.M., 2019. Seasonal and Interannual Variability of Phytoplankton in the Black Sea on the Basis of Remote Sensing Data and In Situ Measurements of Chlorophyll-a. *Doklady Earth Sciences*, 485(1), pp. 293-297. <https://doi.org/10.1134/S1028334X19030097>
 26. Vostokov, S.V., Vostokova, A.S. and Vazyulya, S.V., 2022. Seasonal and Long-Term Variability of Coccolithophores in the Black Sea According to Remote Sensing Data and the Results of Field Investigations. *Journal of Marine Science and Engineering*, 10(1), 97. <https://doi.org/10.3390/jmse10010097>

Submitted 01.07.2024; approved after review 07.08.2024;
accepted for publication 12.09.2024.

About the authors:

Igor N. Mukoseev, Senior Engineer, Marine Hydrophysical Institute of RAS (2 Kapitanskaya, Str., Sevastopol, 299011, Russian Federation), **ORCID ID: 0009-0000-3485-1004**, igor.mukos@gmail.com

Natalya A. Orekhova, Leading Researcher, Head of the Sea Biogeochemistry Department, Marine Hydrophysical Institute of RAS (2 Kapitanskaya, Str., Sevastopol, 299011, Russian Federation), CSc (Geogr.), **ORCID ID: 0000-0002-1387-970X**, **ResearcherID: I-1755-2017**, **Scopus Author ID: 35784884700**, natalia.orekhova@mhi-ras.ru

Contribution of the co-authors:

Igor N. Mukoseev – obtaining field data, processing measurement data, processing, analysis and description of the research results, correction of the text, preparation of graphic material, discussion of the results

Natalya A. Orekhova – problem statement, processing, analysis and description of the research results, correction of the text, preparation of graphic material, discussion of the results

The authors have read and approved the final manuscript.

The authors declare that they have no conflict of interest.

Original article

Distribution and Vertical Fluxes of Particulate Organic Matter in the Black Sea Based on the Results of Numerical Modeling

V. L. Dorofeev, L. I. Sukhikh ✉

Marine Hydrophysical Institute of RAS, Sevastopol, Russian Federation

✉ l.sukhikh@gmail.com

Abstract

Purpose. The work is purposed at studying the spatial distribution, temporal variability and fluxes of particulate organic matter in the Black Sea based on numerical modeling.

Methods and Results. A model of the lower trophic level of the Black Sea ecosystem is applied to estimate the spatial distribution and vertical fluxes of particulate organic matter in the upper 200-meter layer. To extend the study to the whole thickness of the Black Sea, a model consisting of an equation for the evolution of particulate organic matter concentration in the layer from 200 m to the bottom was developed. The hydrodynamic and thermodynamic fields obtained from the previous reanalysis are used as coefficients in this equation and in the equations of the ecosystem model. The modeling was carried out for the period 2016–2020. The concentrations and vertical fluxes of particulate organic matter are obtained on a regular grid and with a time resolution of 1 day. The particulate organic carbon fluxes derived from numerical modeling are compared with the results of processing the samples collected by the sediment traps at two points in the Black Sea. The simulation results are in a fairly good qualitative and quantitative agreement with the measurement results.

Conclusions. A model for calculating the particulate organic matter content in the deep layers of the Black Sea was developed. The modeling results have shown that due to the biological processes, the particulate organic matter concentration in the surface layer of the Black Sea significantly exceeds that in the deep-sea layer. The magnitude of vertical particulate organic matter fluxes in the surface layer is conditioned mainly by the suspended matter concentration, whereas in the deep-sea layer – by the value of vertical velocity. Based on the modeling results, the carbon flux directed from the water column to the bottom was evaluated as a result of suspended matter settling. The main part of this flux falls on the shelf zone of the sea.

Keywords: carbonate system, particulate organic matter, marine ecosystems, Black Sea, numerical modeling, sediment traps

Acknowledgments: The fields of particulate organic matter concentration and its vertical fluxes were calculated within the framework of the state assignment of FSBSI FRC MHI FNNN-2023-0001, the hydrodynamic fields were prepared within the framework of the state assignment of FSBSI FRC MHI FNNN-2024-0012.

For citation: Dorofeev, V.L. and Sukhikh, L.I., 2024. Distribution and Vertical Fluxes of Particulate Organic Matter in the Black Sea Based on the Results of Numerical Modeling. *Physical Oceanography*, 31(6), pp. 851-862.

© 2024, V. L. Dorofeev, L. I. Sukhikh

© 2024, Physical Oceanography

Introduction

The spatial distribution, temporal variability and fluxes of particulate organic matter (POM) are of great importance in the study of the Black Sea carbonate system. The study of POM vertical distribution and its temporal variability was



carried out in a number of works (e.g., ^{1, 2} [1–3]). One of the main lines of such research is the study of particulate matter samples taken with stationary sediment traps. Currently, the work on the study of vertical particulate matter fluxes, including organic and inorganic carbon, is being carried out jointly by scientists from FSBSI FRC MHI and IO RAS [4, 5] on an ongoing basis. The measurement of particulate matter fluxes is conducted using stationary sediment traps at specific locations in the Black Sea, thereby limiting our understanding of the processes occurring in the sea. In order to obtain spatial distributions and temporal variations of carbonate system components, it is useful to apply numerical 3D models of the marine environment, which can be used for determining the temporal evolution and spatial distribution of the parameter of interest on a regular grid. This paper presents the numerical modeling results of the five-year evolution of particulate organic matter in the Black Sea in order to study the spatio-temporal variability of its concentration and vertical fluxes.

Materials and research method

Biological processes related to the functioning of the plankton community, based on the formation of primary production through the processes of photosynthesis and nutrient assimilation by phytoplankton, play an important role in the formation of POM, especially in the upper oxygenated layer of the sea. Therefore, in order to assess the spatial distribution and vertical fluxes of POM in the upper layer, we used a lower-level model of the food chain of the Black Sea ecosystem [6]. The biogeochemical part of the model is a system of 15 (depending on the number of state variables) transfer-diffusion equations, the right-hand sides of which contain terms describing biogeochemical interactions between the state variables.

The equation system of the biogeochemical part of the model includes current velocity fields as coefficients and turbulent exchange coefficients, which are output parameters of the Black Sea circulation model. In addition, the terms describing the interaction of the ecosystem components of the model use temperature and salinity fields, which are also output parameters of the hydrodynamic model. The unit of measurement for the state variables in the model is nitrogen. The fluxes of inorganic nitrogen compounds (nitrates and ammonium), proportional to their concentration and the intensity of river runoff, are specified at the mouths of large rivers. In order to convert the units of organic matter measurement from nitrogen to carbon, we have used the C:N mass ratios for various parameters of the Black Sea ecosystem taken from [7]. In the following, particulate organic matter is considered in units of carbon.

In this paper, the results of the reanalysis performed for the period 1993–2020 [8], based on a numerical model of the Black Sea circulation with assimilation

¹ Filippov, V.S., 1980. [Suspended Organic Carbon in the Black Sea Aerobic Waters]. In: M.E. Vinogradov, ed., 1980. [*Pelagic Ecosystem of the Black Sea*]. Moscow: Nauka, pp. 62-64 (in Russian).

² Vostokov, S.V., 1987. [Particulate Organic Matter in the Central Part of the Black Sea in Spring of 1984]. In: M.E. Vinogradov and M.V. Flint, eds., 1987. [*Present State of the Black Sea Ecosystem*]. Moscow: Nauka, pp. 59-67 (in Russian).

of satellite measurements of sea surface temperature and sea level topography anomalies, were used as hydrodynamic and thermodynamic fields. The horizontal step of the model is 4.8 km, in the vertical direction the model grid has 35 z -levels, thickening towards the surface.

In the biogeochemical part of the model, the computational domain coincides horizontally with the domain of the circulation model (the grid steps also coincide) and vertically occupies the upper 200 m of the Black Sea (18 computational levels corresponding to the circulation model).

The described biogeochemical model provides POM distribution only in the upper 200 m layer of the sea. In order to extend the study to the entire water column of the Black Sea, an equation for the evolution of the POM concentration in the layer from 200 m down to the bottom was added:

$$\frac{\partial C}{\partial t} + \frac{\partial(UC)}{\partial x} + \frac{\partial(VC)}{\partial y} + \frac{\partial((W + W_s)C)}{\partial z} = K_h \nabla^2 C + \frac{\partial}{\partial z} \left(K_v \frac{\partial C}{\partial z} \right) + R, \quad (1)$$

where C is POM concentration; U, V, W are components of current velocities; K_h, K_v are coefficients of horizontal and vertical turbulent diffusion, respectively, derived from the circulation model; W_s is sedimentation velocity as a function of depth; R is a rate of change of POM concentration due to chemical processes. The sedimentation velocity varies between 0.4–2.5 m/day. The last term on the right-hand side of equation (1) describes the anaerobic degradation of POM. The horizontal grid and calculated levels correspond to the Black Sea circulation model. The source of POM for equation (1) is the upper 200-meter layer, where the ecosystem model operates. The POM concentration obtained there at the lower level (200 m) serves as a boundary condition for equation (1).

The main calculation of the POM concentration evolution was carried out for 5 years from 2016 to 2020. The following procedure was employed to prepare the initial fields for equation (1). The calculation was carried out according to equation (1) with zero initial conditions. In this case, the boundary conditions at the upper boundary and the equation coefficients (flow velocities) were set in the cycle for 2015. When the POM concentration fields at all horizons reached a stable state, the calculation was completed and the resulting fields were used as initials for the main calculation. This operation required about one hundred years of model time.

Results

After obtaining the initial conditions, a three-dimensional POM distribution was calculated over the entire Black Sea area. This resulted in a data array with a discretization of one day being obtained on a regular grid. Fig. 1 shows the temporal variability of the total POM in three layers: 0–56, 56–95 and 95–350 m. The first layer corresponds approximately to the depth of the photosynthetic layer in the Black Sea, the second layer corresponds to the subanaerobic zone, and the third layer corresponds to the hydrogen sulfide zone (see reference [1]). This study examined the distribution of particulate organic carbon (POC) based on the sample data from 11 stations of the 26th cruise of the R/V *Vityaz* in 1992. The main maximum in the 0–56 m layer occurs around March during the diatom “bloom”.

In the lower layers this maximum becomes smaller and shifts to the right in time according to the sedimentation of particulate matter.

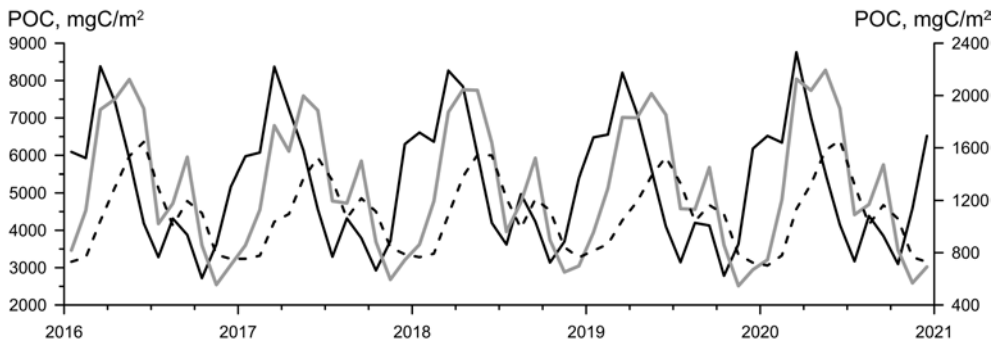


Fig. 1. Temporal variability of total particulate organic carbon in three layers: 0–56 m (black line), 56–95 m (gray line), and 95–350 m (dashed line). The left ordinate axis refers to the 0–56 m layer, and the right one – to the other two layers. The graphs are constructed based on the results of numerical modeling

The study [1] provides the average POC content in these layers – 4.7, 1.0 and 7.9 g. The study [9], which examines the results of measurements in the Black Sea southwestern part, provides similar values. The corresponding values derived from the data in Fig. 1 are 5.2, 1.3 and 1.1 g. While the first two layers demonstrate a reasonable degree of similarity with the measurement results, it should be noted that the measurements were taken for a different time period. For the hydrogen sulfide zone, however, it was found that the modeling results were underestimated.

Fig. 2, a demonstrates vertical profiles of POC averaged over the area and for a period of 5 years for the entire basin and shelf. The profile averaged over the entire Black Sea water area has a maximum value of $\sim 120 \text{ mg/m}^3$ in the upper 20-meter layer. The maximum value recorded at the shelf exceeds 200 mg/m^3 . A POC profile obtained through averaging all measurements is presented in [1]. In the upper 20-meter layer, the POC values have a maximum of 142 mg/m^3 , which is between the maximum values for the entire water area of the sea and the shelf derived from numerical modeling results.

The POC distributions that had been calculated were then used to construct fields of monthly average fluxes (F) of inorganic carbon directed downwards for all model horizons. The calculation of these fluxes is outlined below. The F value was summed up over the month at each point of the model grid and calculated horizon: $F = POC(W + W_s)$ for $W + W_s > 0$ and $F = 0$ for $W + W_s < 0$, where POC is POC concentration; W is liquid velocity, and W_s is sedimentation velocity of organic carbon particles. It is important to note that the velocity is positive if it is directed from the surface towards the bottom. The obtained value was then divided by the number of days in the month. This method for determining the POC flux was selected to ensure the comparison of modeling results with measurement results obtained during the cruises of the R/V *Professor Vodyanitsky*, using sedimentation traps, where sampling was conducted with a one-month exposure. These samples were then applied to study the characteristics of the vertical flux of organic and inorganic carbon [10].

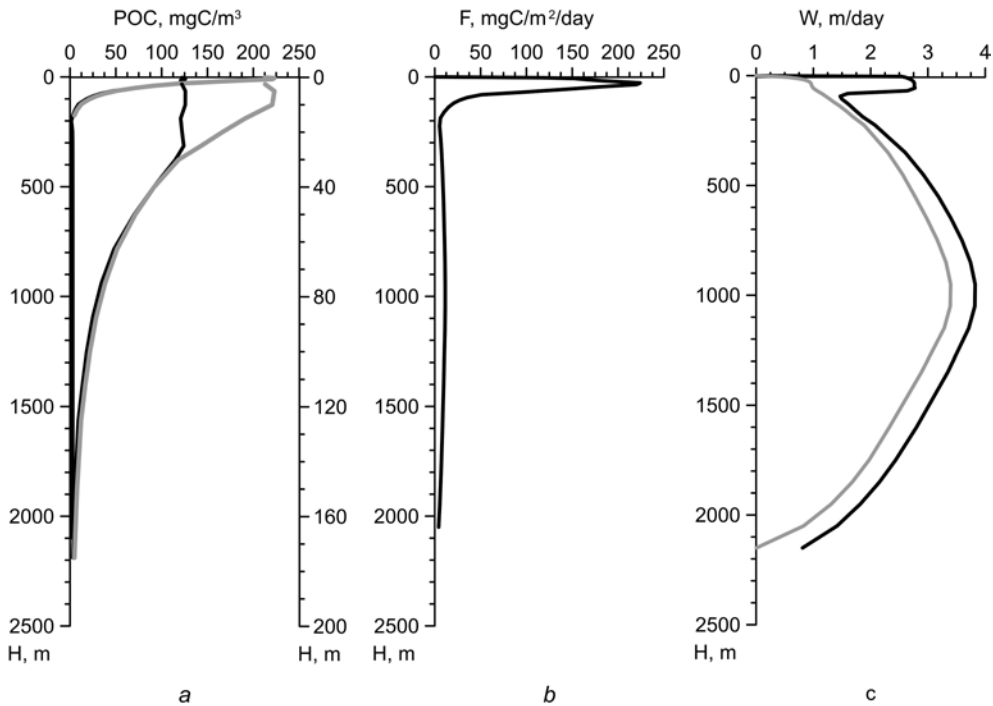


Fig. 2. Vertical profiles of POC for the whole water column (left ordinate axis) and the upper 200-meter layer (right ordinate axis) averaged over the whole basin (black line) and shelf (gray line) (*a*); profile of the POC vertical flux (*b*); profiles of the liquid average vertical velocity directed towards the bottom (gray line), and the liquid velocity plus the sedimentation velocity (black line) (*c*). All the profiles are constructed based on the results of numerical modeling

The vertical flux profile of POC, averaged over the entire Black Sea area and for a 5-year time interval, is shown in Fig. 2, *b*. Similar profiles of the liquid vertical velocity and the sum $W + W_s$ are presented in Fig. 2, *c*. The vertical flux profile of POC in the upper 100-meter layer exhibits a maximum that is at least an order of magnitude greater than the values of the average fluxes below 200 m. The average vertical velocity within the entire layer varies by a maximum of 3 times (excluding the horizons near the surface and at the bottom), and the sum $W + W_s$ varies by a maximum of 4 times. The local maximum of the latter in the upper 100-meter layer is explained by the high sedimentation velocity in this layer. The POC concentration in the near-surface sea layer is also significantly higher than in the layer below 200 m where the average concentration varies insignificantly. Consequently, it can be deduced that the average vertical flux of POM in the surface layer is predominantly determined by the POC concentration, while in the layer below 200 m, it is primarily influenced by the vertical velocity.

The monthly average maps of POC flux distribution, its concentration and vertical velocity at the 30 m horizon given in Fig. 3 were obtained by averaging over

a 5-year period, with data from three months (March, August and December) being used to create the maps. In March, the POC concentration is elevated throughout the Black Sea ($\sim 150 \text{ mg/m}^3$), and accordingly, the vertical POC fluxes also exhibit elevated values ($\sim 300 \text{ mg/m}^2/\text{day}$) across the entire water area. In contrast, the POC concentration in August is notably lower than in March, and the vertical fluxes are also lower, particularly in the western part of the sea. The lowest values of POC concentration and vertical fluxes are observed in December. Therefore, at the 30-m horizon, the values of POC vertical fluxes correlate well with its concentration. This confirms the preceding conclusion that, within the near-surface layer of the Black Sea, vertical POC fluxes are predominantly determined by its concentration. In addition, the vertical velocity (Fig. 3, *c*) exhibits its lowest values in August, while the lowest fluxes are observed in December (Fig. 3, *a*). At the same time, the spatial variability of vertical velocity significantly affects the spatial distribution of fluxes. For instance, in March, elevated values of vertical velocity are observed along the basin periphery, which coincide with the increased POC flux values in these locations. Furthermore, in December, elevated vertical velocities and increased values of POC fluxes are observed along the deep-water section of the western coast and the southern coast of the Black Sea.

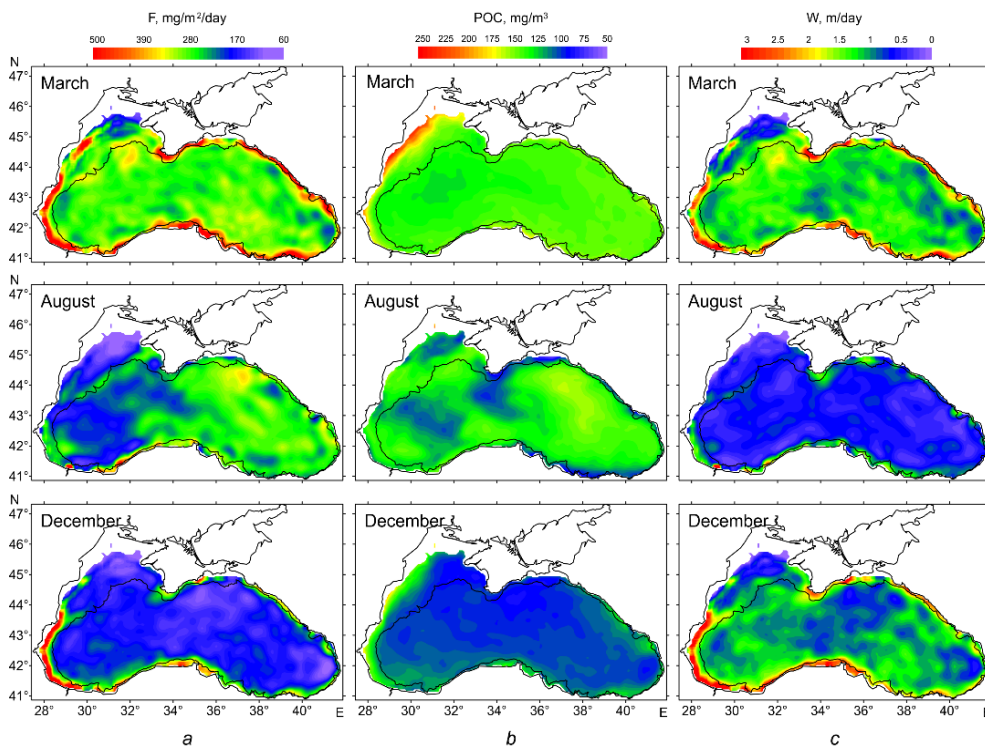


Fig. 3. Maps of distribution of POC fluxes (*a*) and concentration (*b*), and liquid vertical velocity directed downwards (*c*) for the 30 m horizon based on the results of numerical modeling

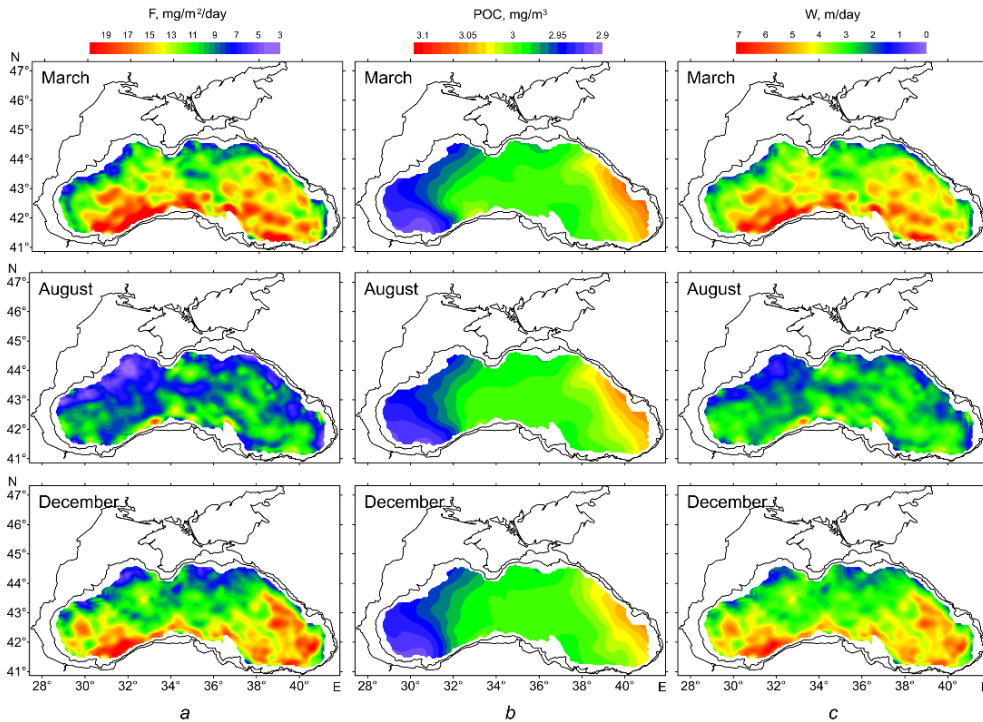


Fig. 4. The same as in Fig. 3 for the 1200 m horizon

At the 1200 m horizon, the POC concentration is practically independent of the month (Fig. 4). Spatial variability is minimal; thus, the vertical velocity of the liquid contributes most significantly to the vertical fluxes. In August, the lowest of vertical velocities shown in Fig. 4, c is observed, and the weakest vertical POC fluxes are also observed in the same month. The spatial distribution of vertical fluxes is found to coincide with that of vertical velocity.

The study [11] presents the analysis results of the material collected during the sediment trap experiment carried out near the town of Amasra, Turkey, in the deep-water part of the Black Sea. The experiment, which lasted three years from October 1982, involved the use of two sediment traps installed at depths of 250 and 1200 m. The study revealed that the total suspended matter flux in the deep-water trap was higher than that in the shallower one. The POC flux in the former reached a maximum of $\sim 40 \text{ mg/m}^2/\text{day}$ and $\sim 20 \text{ mg/m}^2/\text{day}$ in the shallower one, respectively.

As illustrated in Fig. 5, the temporal variability of the POC fluxes obtained from the modeling results is presented for the specified horizons at a grid node with coordinates 42.063°N and 32.362°E . Despite the modeling results relating to a different time period, the main features noted in [11] are also preserved for them. These include the vertical POC flux at the 1200 m horizon being greater than at the 250 m horizon for almost the entire modeling period. Its maximum values reached $\sim 40 \text{ mg/m}^2/\text{day}$, while at the 250 m horizon they reached $\sim 20 \text{ mg/m}^2/\text{day}$.

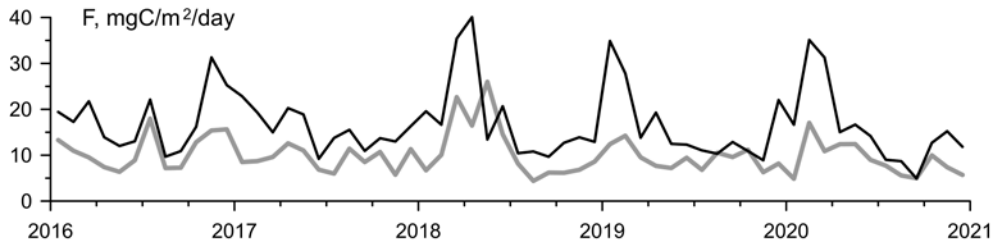


Fig. 5. Graphs of time variability of POC fluxes in the model computational grid node (coordinates are 42.063° N and 32.362° E) at the 250 m (gray line) and 1200 m (black line) horizons

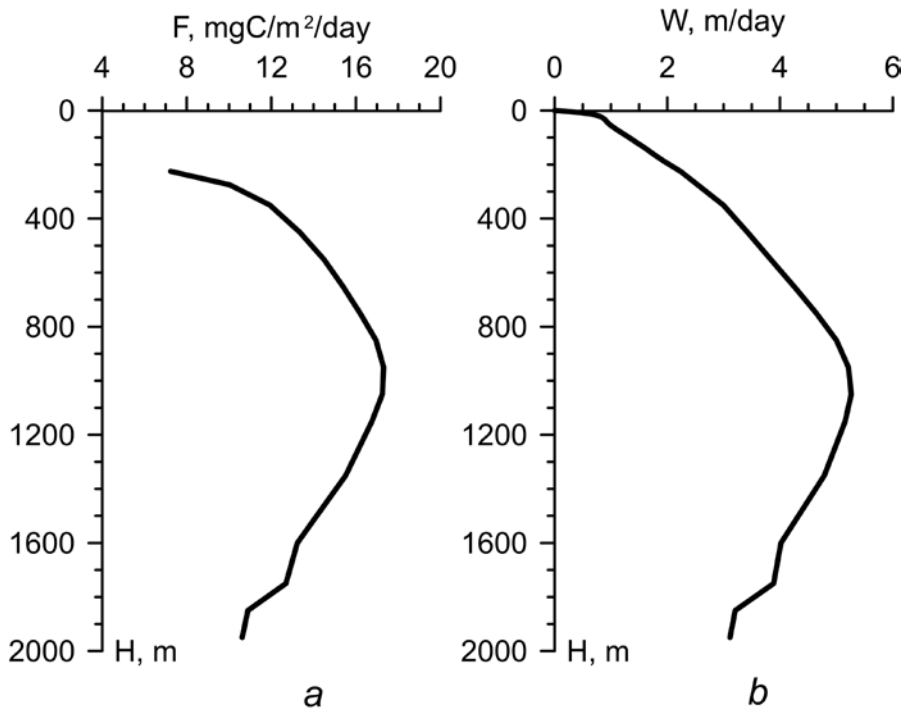


Fig. 6. Profiles of POC flux (*a*) and vertical velocity (*b*) for the model computational grid node (coordinates are 42.063° N and 32.362° E)

The maps in Fig. 4 demonstrate that in the area of coordinates indicated in Fig. 5, elevated values of vertical velocity and, consequently, of the POC fluxes are observed for all months. Fig. 6 presents a comparison of vertical velocity and POC flux profiles derived from the averaging of the entire integration period. The average vertical velocity directed downwards reaches its maximum value at a depth of ~ 1000 m, and the vertical POC flux also exhibits a maximum at a similar depth. This indicates that the nature of currents in this area of the Black Sea is such that at a depth of 1200 m, the vertical flux is noticeably greater than at a depth of 250 m.

In recent years, sampling with sediment traps has been carried out on a continuous basis. The study [10] presents some results of processing the samples obtained using traps installed in the deep-water part of the Black Sea in the section between Cape Chersonesos and the Bosphorus Strait at a point with 43.8° N and

32.1°E coordinates at depths of 150 and 1700 m in November 2018. Sampling was conducted on a year-round basis, with a specified exposure duration of 1 month. The mean vertical POC flux for the entire measurement period, based on the results of sample processing, was 1.9 mg/m²/day for the 150 m horizon and 6.57 mg/m²/day for the 1700 m horizon. This finding indicates that the POC flux values are higher in the deep horizon than in the shallow one.

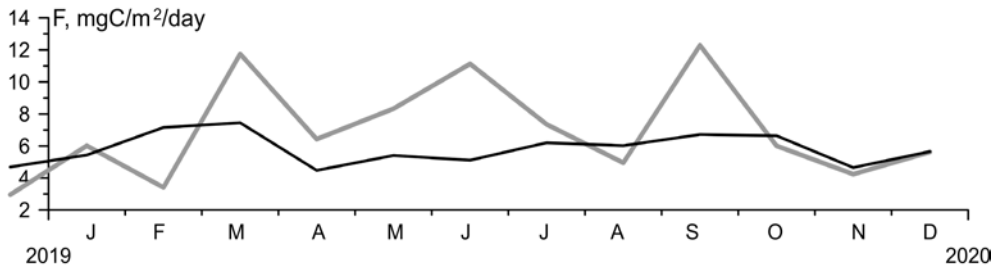


Fig. 7. Temporal variability of POC fluxes in the model computational grid node (coordinates are 43.8°N and 32.1°E) at the 150 m (gray line) and 1700 m (black line) horizons

The vertical fluxes for 2019, as illustrated in Fig. 7, were obtained from the modeling results. It is evident from the figure that the fluxes are generally higher at the 150 m horizon (with the exception of a few months) in comparison to the 1700 m horizon. The mean flux values were found to be 6.95 mg/m²/day at 150 m depth and 5.8 mg/m²/day at 1700 m depth. Thus, the mean value of vertical POC flux at the deep horizon, as determined by the modeling results, is close to the measured value. However, at the 150 m horizon, the modeling results exceed the measured values.

Based on the obtained fields it is possible to estimate an amount of particulate carbon that settles to the bottom and is thereby removed from the Black Sea carbonate system. Given that the liquid vertical velocity at the seabed is zero due to the impermeability condition, the vertical flux of particulate carbon at each point on the seabed will be equal to $F_b = POC_b \cdot W_s$, where POC_b is concentration of particulate carbon in the bottom cell. Fig. 8 illustrates the total flux of particulate carbon towards the Black Sea bottom for the entire water area and the shelf zone. The flux values for the shelf and the entire sea are almost identical. This observation indicates that the sedimentation of particulate carbon to the bottom mainly occurs on the shelf due to the fact that in a significant part of the NWS the depth is less than 50 m. At these depths, the concentration of POC exceeds the corresponding values in the deeper layers of the sea by two orders of magnitude. The maximum settling to the bottom occurs approximately in March, which corresponds to the maximum total POC content in the photosynthetic layer (Fig. 1).

The distribution of POC settling fluxes to the Black Sea bottom for March (maximums on the graphs in Fig. 8) and for July (minimums) is illustrated in Fig. 9. It is evident that settling to the bottom in the shelf area significantly exceeds the amount observed in the deep-water part of the sea. The mean value of carbon loss due to settling is (according to the graph in Fig. 8) $3.1 \cdot 10^6$ t/year ($2.83 \cdot 10^6$ t/year at the shelf). In [11], the influx of POC into the Black Sea via river runoff was

estimated at $2.6 \cdot 10^6$ t/year, which turned out to be close to the value of settling to the bottom derived from the modeling results.

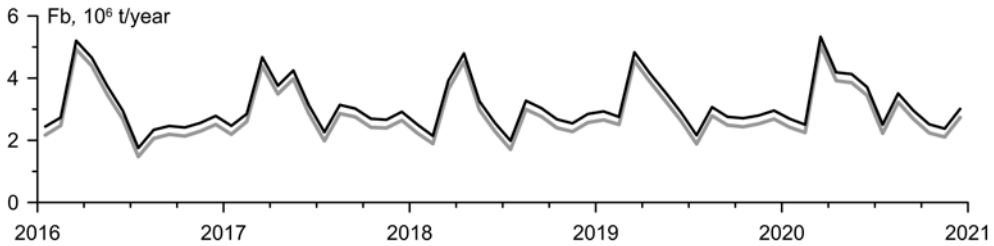


Fig. 8. Total flux of POC settling to the Black Sea bottom (black line) and shelf (gray line) based on the results of numerical modeling

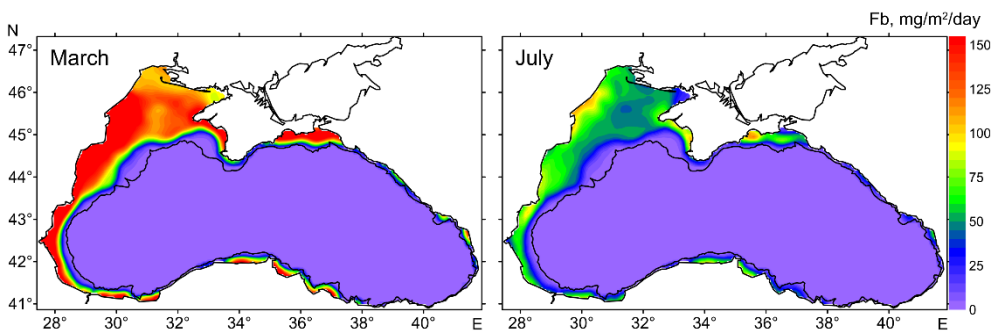


Fig. 9. Maps of distribution of POC settling fluxes to the Black Sea bottom for two months based on the results of numerical modeling

Conclusion

The work considers the developed model for calculation of the POM content in the deep layers of the Black Sea. For calculating the POM in the upper 200-meter layer, the existing model of the food chain lower level of the Black Sea ecosystem is applied. The results of this model are then used at the lower horizon as boundary conditions for computation the organic carbon concentration in the underlying layers.

A model computation was performed over a 5-year period, resulting in the acquisition of POC concentrations on a regular grid with a temporal resolution of 1 day. The modeling results indicate that the concentration of particulate organic matter in the surface layer of the Black Sea is significantly higher than in the deep-water layer, owing to the impact of biological processes.

The vertical POC fluxes were computed using the model fields of POC concentration and hydrodynamic fields from the Black Sea circulation model. As with the concentrations, the flux values are significantly higher in the Black Sea surface layer. The vertical POC flux in the surface layer is determined primarily by particulate matter concentration, while in the deep-water layer, it is determined by the vertical velocity directed downwards. This conclusion is confirmed by the distribution maps of average concentrations, POC fluxes and vertical velocity at the 30 and 1200 m horizons. However, it is notable that the spatial distribution of

POC flux, even at the 30 m horizon, can exhibit a significant correlation with the vertical velocity distribution.

The results of numerical modeling of POC fluxes were compared with the results of processing the samples collected with sediment traps at two points in the Black Sea. The modeling results have demonstrated a relatively strong qualitative and, in certain cases, quantitative agreement with the measurement results.

Based on the modelling results, the carbon flux from the water column to the bottom was estimated as a result of suspended matter settling. The predominant part of this flux is concentrated within the shelf zone of the sea.

REFERENCES

1. Lyutsarev, S.V. and Shanin, S.S., 1996. Peculiarities of Particulate Organic Carbon in the Black Sea Water Column. *Oceanology*, 36(4), pp. 538-542 (in Russian).
2. Burlakova, Z.P., Ereemeeva, L.V and Konovalov, S.K., 2000. Seasonal and Spatial Variability of the Content of Suspended Organic Substances in the Active Layer of the Black Sea. *Physical Oceanography*, 10(5), pp. 419-454. <https://doi.org/10.1007/BF02515365>
3. Burlakova, Z.P., Ereemeeva, L.V and Konovalov, S.K., 2003. Budget and Fluxes of Particulate Organic Carbon and Nitrogen According to the Data on Vertical Distribution in the Deep Part of the Black Sea. *Physical Oceanography*, 13(3), pp. 157-170. <https://doi.org/10.1023/A:1025094902673>
4. Klyuvitkin, A.A., Kozina, N.V., Redzhepova, Z.Yu., Rusanov, I.I., Torgunova, N.I. and Bud'ko, D.F., 2017. Geological Study of the Black Sea (Cruise 81 of the R/V Professor Vodyanitskiy). *Oceanology*, 57(5), pp. 759-761. <https://doi.org/10.1134/S0001437017050095>
5. Klyuvitkin, A.A., Garmashov, A.V., Latushkin, A.A., Orekhova, N.A., Kochenkova, A.I. and Malafeev, G.V., 2019. Comprehensive Studies of the Black Sea during the Cruise 101 of the R/V Professor Vodyanitskiy. *Oceanology*, 59(2), pp. 287-289. <https://doi.org/10.1134/S0001437019020097>
6. Dorofeev, V.L. and Sukhikh, L.I., 2019. Studying Long-Term Variations in Black-Sea Ecosystem Based on the Assimilation of Remote Sensing Data in a Numerical Model. *Water Resources*, 46(1), pp. 65-75. <https://doi.org/10.1134/S0097807819010032>
7. Gregoire, M., Raick, C. and Soetaert, K., 2008. Numerical Modeling of the Central Black Sea Ecosystem Functioning during the Eutrophication Phase. *Progress in Oceanography*, 76(3), pp. 286-333. <https://doi.org/10.1016/j.pocean.2008.01.002>
8. Dorofeev, V.L. and Sukhikh, L.I., 2023. Analysis of Long-Term Variability of Hydrodynamic Fields in the Upper 200-Meter Layer of the Black Sea Based on the Reanalysis Results. *Physical Oceanography*, 30(5), pp. 581-593.
9. Karl, D.M. and Knauer, G.A., 1991. Microbial Production and Particle Flux in the Upper 350 m of the Black Sea. *Deep Sea Research Part A. Oceanographic Research Papers*, 38(Suppl. 2), pp. S921-S942. [https://doi.org/10.1016/S0198-0149\(10\)80017-2](https://doi.org/10.1016/S0198-0149(10)80017-2)
10. Mukoseev, I.N., Gurova, Yu.S. and Orekhova, N.A., 2023. Flows of Carbon with Suspended Matter in the Black Sea. In: MHI, 2023. *Seas of Russia: From Theory to Practice of Oceanological Research: Proceedings of All-Russian Scientific Conference (Sevastopol, 25–29 September 2023)*. Sevastopol, pp. 276-277 (in Russian).
11. Izdar, E., Konuk, T., Ittekkot, V., Kempe, S. and Degen, E.T., 1987. Particle Flux in the Black Sea: Nature of the Organic Matter. *Mitteilungen aus dem Geologisch-Paläontologischen Institut der Universität Hamburg*, (62), pp. 1-18.

Submitted 11.06.2024; approved after review 22.08.2024;
accepted for publication 12.09.2024.

About the authors:

Viktor L. Dorofeev, Leading Research Associate, Department of the Oceanic Processes Dynamics, Marine Hydrophysical Institute of RAS (2 Kapitanskaya Str., Sevastopol, 299011, Russian Federation), CSc (Phys.-Math.), **ResearcherID: G-1050-2014**, dorofeyev_viktor@mail.ru

Larisa I. Sukhikh, Research Associate, Department of the Oceanic Processes Dynamics, Marine Hydrophysical Institute of RAS (2 Kapitanskaya Str., Sevastopol, 299011, Russian Federation), **ResearcherID: M-4381-2018**, l.sukhikh@gmail.com

Contribution of the co-authors:

Viktor L. Dorofeev – general scientific supervision of the study, formulation of the goals and objectives of the study, carrying out numerical simulations, analysis of the obtained results and their interpretation

Larisa I. Sukhikh – literature review, numerical simulations, analysis of the results

The authors have read and approved the final manuscript.

The authors declare that they have no conflict of interest.

Original article

Results of Monitoring of Greenhouse Gas Concentrations and Variations in the Earth's Crust Deformations at Cape Schultz in Winter Period, 2023–2024

M. A. Bovsun, G. I. Dolgikh, S. G. Dolgikh, V. V. Ovcharenko,
I. E. Stepochkin, V. A. Chupin , A. V. Yatsuk

V. I. Il'ichev Pacific Oceanological Institute, Far Eastern Branch of RAS, Vladivostok,
Russian Federation
 chupin@poi.dvo.ru

Abstract

Purpose. The purpose of the study is to monitor climatic changes in the southern part of Primorsky Krai related to the variations in meteorological parameters, greenhouse gas flows, and the effect of catastrophic deformation processes of the Earth's crust.

Methods and Results. At the *Cape Shultz* Marine Experimental Station, complex measurements are continuously performed by a stationary hardware and software measuring complex for gas-deformation monitoring. The measuring complex consisting of several laser interference measuring devices (laser strainmeters, laser nanobarograph and laser meter of hydrosphere pressure variations) and a stationary closed-type gas analyzer for measuring the carbon dioxide and water vapor concentrations in the atmosphere, is briefly described. All the field measurement data obtained using the complex are assembled in a common database for subsequent research. During the measurements performed in winter 2023–2024 and spring 2024, new data on the manifestations and interactions of different geospheric processes were obtained. In winter, an excess of carbon dioxide content in the atmosphere and its decrease in early spring were recorded, that was due to a seasonal change of the prevailing wind direction. The monitoring has resulted in revealing a daily frequency of the carbon dioxide concentration. At the same time, the effect of daily variations in the atmospheric air temperature upon the daily variations in carbon dioxide concentration was recorded. The deformation monitoring made it possible to record a catastrophic earthquake which caused a tsunami in the Sea of Japan. Calculation of the magnitude of the revealed deformation anomaly of the earthquake permitted to determine the magnitude of the Earth's crust displacement that led to the occurrence of a tsunami wave. Complex processing of data shows the data correlation induced by micro-deformations the Earth's crust and the variations in atmospheric pressure, carbon dioxide and water vapor in the atmosphere at tidal harmonics.

Conclusions. Comprehensive monitoring of the greenhouse gas concentrations and the variations in crustal deformations made it possible to identify the dependencies of short-period oscillations during the gas-deformation inter-geospheric interactions. The latest data on the changes in greenhouse gas concentrations in winter in the southern part of Primorsky Krai have been obtained.

Keywords: hardware and software complex, deformation of the Earth's crust, carbon dioxide, water vapor, gas-geochemical monitoring, meteorological monitoring, deformation monitoring, tsunami

Acknowledgments: The study was carried out with the financial support of FSTP “Grounds for the climate monitoring system of the Far Eastern seas and development of methods for monitoring the extreme weather and climate phenomena related to the ocean, based on stationary and mobile measuring complexes as well as multi-sensor satellite sensing” (taking measurements and interpreting the obtained results) and within the framework of theme (No. 124022100074-9) “Study of the origin of linear and nonlinear interaction between the geospheric fields of transition zones of the World Ocean and their consequences” (development of the experimental complex).

For citation: Bovsun, M.A., Dolgikh, G.I., Dolgikh, S.G., Ovcharenko, V.V., Stepochkin, I.E., Chupin, V.A. and Yatsuk, A.V., 2024. Results of Monitoring of Greenhouse Gas Concentrations and Variations in the Earth's Crust Deformations at Cape Schultz in Winter Period, 2023–2024. *Physical Oceanography*, 31(6), pp. 863-879.



Introduction

In recent years, humanity has been monitoring global climate change with growing unease, which is particularly evident in observable meteorological parameters such as greenhouse gases, surface air temperature, precipitation, general atmospheric circulation, state of the land and the World Ocean cryospheres, and climate extremes.

Atmospheric concentrations of three greenhouse gases, from both natural and anthropogenic sources, have increased significantly since the pre-industrial times: CO₂ by 46%, CH₄ by 157%, N₂O by 22%.

As temperatures rise and the number of catastrophic processes increases, so do the volumes of natural emissions. Temperature increases due to deformation and sea wave processes can occur not only in the Earth's crust, but also in the atmosphere, as noted in [1]. The occurrence of microbaroms (gravitational sea waves) correlates with the occurrence of microseisms. Moreover, the same waves excite microseisms and microbaroms. The energy of microseisms depends on the energy of sea waves. In [2], the relationship between microseisms and specific storms was studied. Large storms significantly increase microseismic energy [3–5]. In this regard, the variation of seismic noise on a ten-year scale was studied to determine its relationship with climate variability [6]. The seismic profiling of the Peter the Great Gulf reveals extensive gas emissions associated with their accumulation in the bottom sediments of the shelf area, formed as a result of the transformation of organic matter in sedimentary deposits [7]. At the same time, a high concentration of CO₂ is recorded in the bottom sediments of this water area [8]. A significant effect of the tides on the intensity and frequency of gas emissions is also noted [9].

In formulating our estimates, it is essential to consider the role of deformation processes in the Earth's crust, causing increased emissions of natural gases from the mantle and the Earth's crust into the atmosphere. As a result of complex measurements, new data on regional deformation processes and the correlation of greenhouse gas concentrations was obtained.

The objective of this study is to examine the relationship between deformation processes in the Earth's crust and the emission of natural greenhouse gases at Cape Shultz in Primorsky Krai, Russia, and on the shelf of the Sea of Japan using the developed hardware and software complex for the monitoring of gas deformation in the atmosphere – hydrosphere – lithosphere transition zone [10].

Hardware and software complex for gas deformation monitoring

The complex comprises laser interference installations for the measurement of crustal deformation and atmospheric pressure variations, stationary gas analysis equipment and a weather station. During the experiment to study the relationship between the dynamics of greenhouse gases in the shelf area of the Sea of Japan and variations in crustal deformations over a distinct period of time, the R/V *Professor Gagarinsky* was anchored on the shelf of the Sea of Japan at a distance of 1.8 km from the laser strainmeter location (Fig. 1).

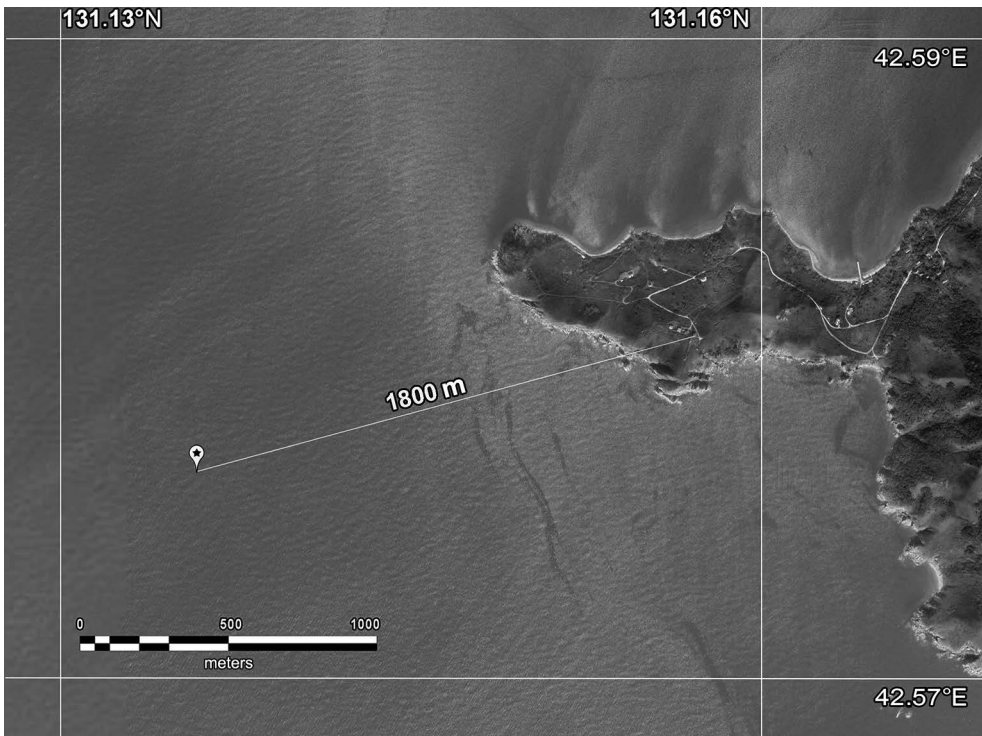


Fig. 1. The R/V *Professor Gagarinsky* anchoring location on the map



Fig. 2. Layout of laser interferometer locations: 1 – laser strainmeter with a measuring arm length 52.5 m; 2 – laser strainmeter with a measuring arm length 17.5 m; 3 – laser nanobarograph; 4 – laser meter of variations of hydrosphere pressure; 5 – laboratory

Laser interference complex. The laser interference measuring complex is situated on the Gamov Peninsula of Primorsky Krai, with its central point located at 42.58°N and 131.15°E on the territory of the *Cape Shultz* Marine Experimental Station (MES). The complex comprises a laser nanobarograph, laser strainmeters with measuring arm lengths of 52.5 and 17.5 m, and a laser meter to measure hydrosphere pressure variations (Fig. 2).

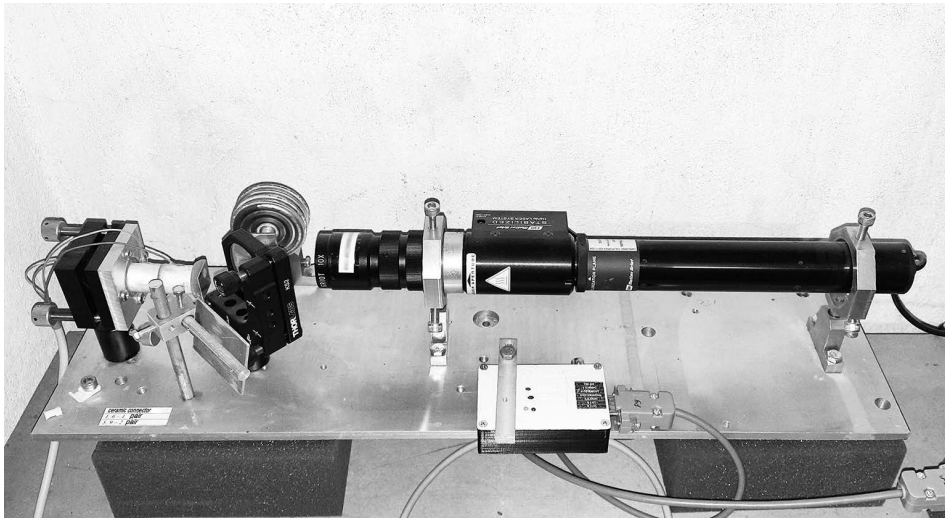


Fig. 3. General view of laser nanobarograph

The laser nanobarograph [11] was developed to study the relationships between processes occurring within the atmosphere, lithosphere and hydrosphere. It uses a block of aneroid boxes, similar to that used in traditional pointer barometric instruments, as a sensor for measuring atmospheric pressure. To increase the sensitivity when registering the movement of the unfixed end of the aneroid block, laser interference techniques are used. They are based on an equal-arm Michelson interferometer with a measuring (and “reference”) arm length of 20 cm. A frequency-stabilized helium-neon laser, manufactured by *Melles Griot*, is used as the radiation source, thereby ensuring frequency stability in the ninth decimal place. Figure 3 illustrates the general appearance of the laser nanobarograph. Its basic technical specifications include an operational frequency range of 0 (conditionally) to 1000 Hz and an accuracy of 1 mPa in measuring atmospheric pressure variations.

The dynamic range of all interferometers is significantly expanded by using a level reset system and a feedback system that regulate the operation of the interferometers. The two-coordinate laser strainmeter described in [12] is based on a 52.5 m and 17.5 m laser strainmeter. The optical elements of each apparatus are affixed to two granite abutments fixed to the Earth's geological formations. One of the abutments of the 52.5 m laser strainmeter is fixed to a natural granite rock formation, while the other stands on a layer of high-density loam. The height of the first abutment is ~ 1 m, while the second is ~ 3 m. All abutments are conical in shape and widen downwards. The abutments of the 17.5-meter laser strainmeter, with a height of about 1.5 m, are mounted on loam. Figure 4 shows a photo of the interference node of a 52.5 m laser strainmeter.

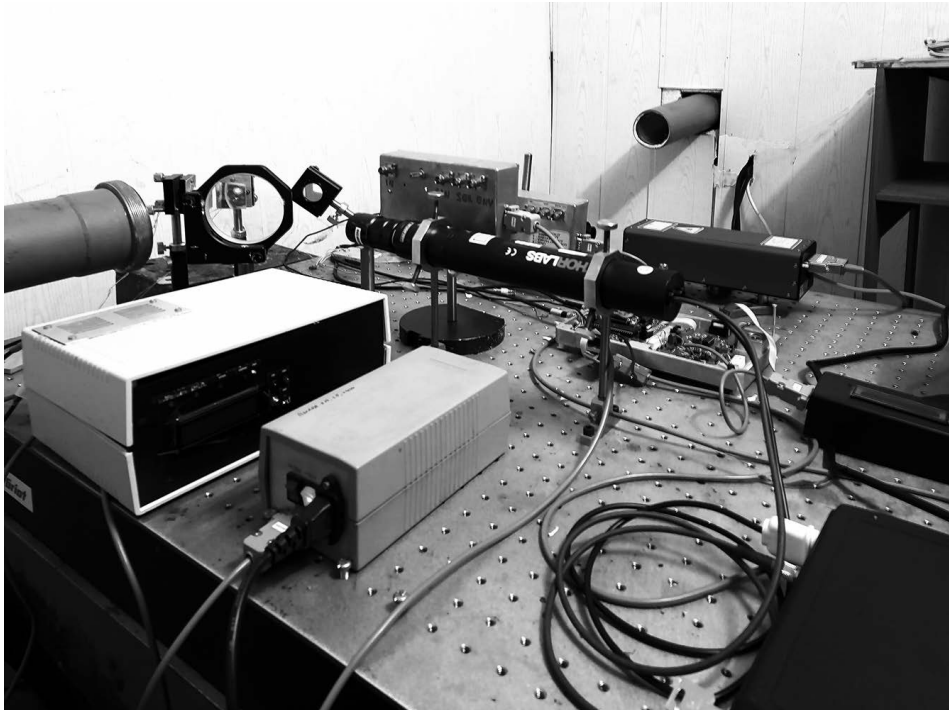


Fig. 4. Central interference node of the 52.5 m laser strainmeter

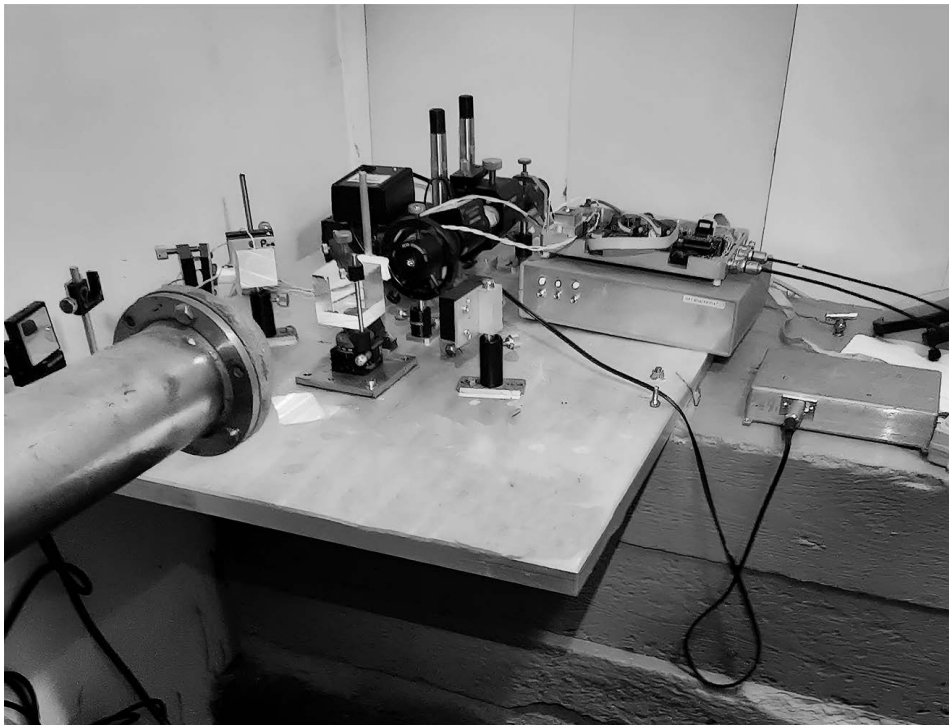


Fig. 5. Central interference node of the 17.5 m laser strainmeter

Figure 5 shows the interference node of a 17.5 m laser strainmeter. The basic technical characteristics of laser strainmeters include an operational frequency range of 0 (conditionally) to 100 Hz and an accuracy in measuring crustal displacements of 0.01 nm.

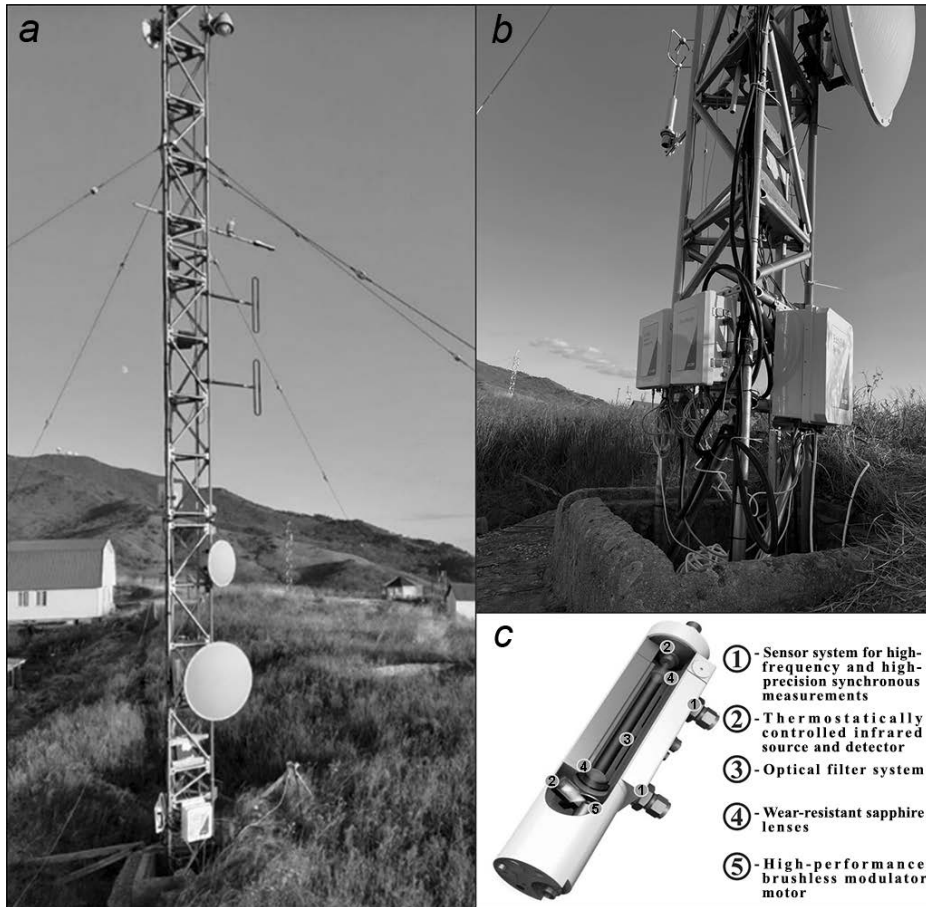


Fig. 6. Eddy Covariance station in combination with weather sensors at the *Cape Shultz* MES (a), closed-type CO₂/H₂O gas analyzer LI-7200 RS (b) and its structure diagram (c)

Stationary closed-type CO₂/H₂O gas analyzer LI-7200 RS. In 2023, an Eddy Covariance station based on the closed-type CO₂/H₂O gas analyzer LI-7200 RS, model LI-7200RSF, LI-COR, air flow module 7200-102 (Fig. 6, a), was installed at the *Cape Shultz* MES. The station is equipped with the SmartFlux 2 data processing system for Eddy Covariance systems in real time. The gas analyzer measurement frequency is 5–20 Hz. The CO₂ measurement range is 0–3000 ppm. The sensitivity of CO₂ measurements (mol H₂O/mol CO₂) ±0.02. The station is equipped with a high-precision digital 3-axis (3D) ultrasonic anemometer Gill Windmaster 3D for measuring turbulent flows. Its basic characteristics: sampling frequency – 20 Hz, range of measured wind speeds – 0–45 m/s, resolution – 0.01 m/s, 1.5% error (RMS) at 12 m/s, working range of wind directions – 0–359°, resolution – 0.1°, 2° error at

12 m/s, housing material – aluminum/carbon fiber. Equipment by LI-COR, closed-type CO₂/H₂O gas analyzer LI-7200RS is specially designed for high-speed and high-precision measurements of CO₂ and water vapor concentrations in the atmosphere (Fig. 6, *b*). It combines the advantages of closed-type gas analyzers (high measurement accuracy, productivity, compactness and resistance to the most adverse conditions) with the low energy consumption of open-type gas analyzers.

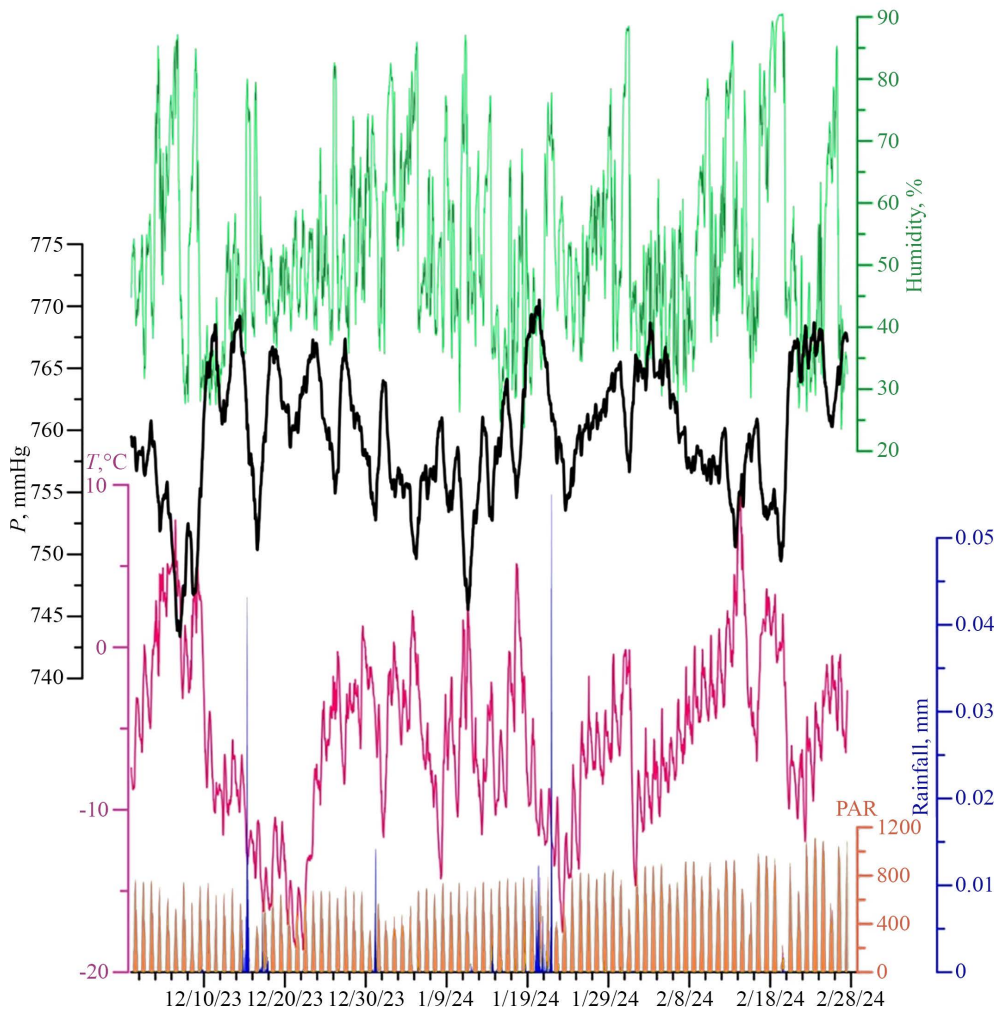


Fig. 7. Results of meteorological monitoring at *Cape Schultz* MES for December 2023 – February 2024. Yellow color shows photosynthetically active radiation, blue – precipitation amount, red – temperature, black – atmospheric pressure, and green – humidity

The LI-7200RS gas analyzer uses the advantages of non-dispersive infrared spectroscopy for quick and reliable CO₂ density and water vapor measurement in the surrounding atmosphere. A solid-state laser diode at the base of the sensor generates infrared radiation, which passes through a system of thermally adjustable optical filters and a limited volume of the air sample and is fed to a thermally

adjustable lead selenide detector (Fig. 6, *c*). Some of the infrared rays are absorbed by the CO₂ and water vapor present in the sample space. Gas concentrations are calculated by the ratio of the absorbed IR radiation to the control value.

The obtained experimental data of the stationary gas analyzer after preliminary processing, filtration and decimation are recorded in the created experimental data base with 2 Hz sampling frequency.

Results of greenhouse gas concentration monitoring

The results of the winter monitoring of CO₂ and water vapor content, conducted between 01 December 2023 and 29 February 2024, are presented in Figs. 7 and 8, along with the main meteorological parameters of the surface atmosphere. Fig. 7 presents synchronous graphs of variations in atmospheric pressure, air temperature, air humidity, precipitation and solar radiation. The monitoring data were integrated with atmospheric transport parameters to estimate the prevailing direction of atmospheric air movement in the vicinity of the monitoring station.

Upon analysis of Fig. 8, it can be concluded that during the winter season in the southern part of Primorsky Krai, the main direction of wind transfer coincides with the general circulation of the atmosphere in this period of the year. North-western and north-eastern winds prevailed (black graph in Fig. 8). These sectors generally coincide with the continental part of the Khasansky District, the internal waters of Posyet Bay and Vityaz Bay. The wind speed varied in the range of 0.5–15.1 m/s, with a mean value of 5 m/s (red graph in Fig. 8). The prevailing wind values were in the range of 5–10 m/s. The maximum values were recorded in December and January, while in February the wind patterns shifted significantly, with an increasing role of south-eastern winds and more moderate wind speed values. This is illustrated in the wind rose on the right side of Fig. 8.

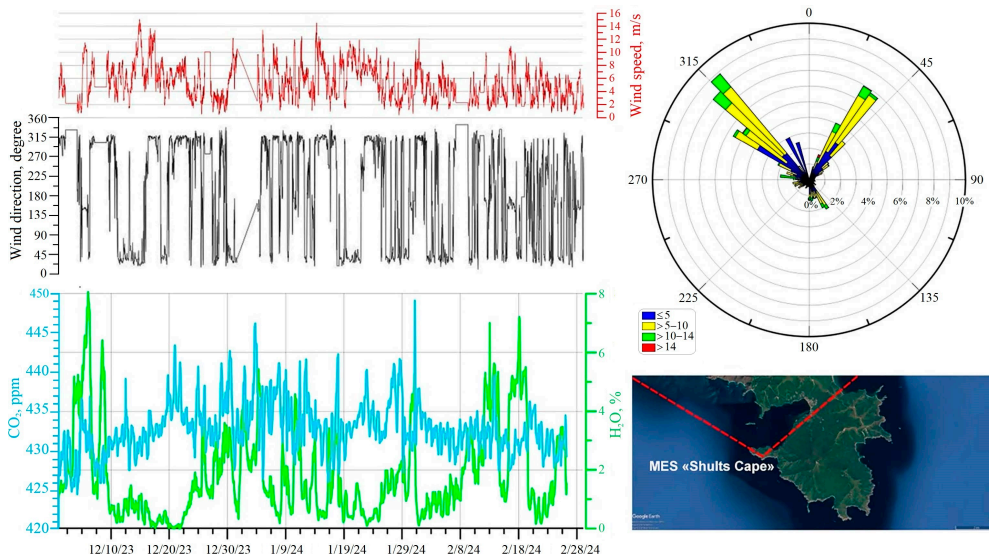


Fig. 8. Results of gas-geochemical monitoring at *Cape Schultz* MES for December 2023 – February 2024. Red color shows wind speed, black – wind direction, blue – concentration of carbon dioxide, and green – concentration of water vapor

The CO₂ content in winter varied in the range of 424.3–449.1 ppm, with an average of 430.8 ppm (as illustrated by the blue graph in Fig. 8). The maximum average concentration of carbon dioxide was recorded in January (434.3 ppm), while the minimum was observed in February (429.2 ppm). The maximum values of water vapor concentration in the atmosphere were recorded in early December and in the second half of February (green graph in Fig. 8). According to the sea research carried out within the framework of an innovative project of national importance on the R/V *Professor Gagarinsky* in October – December 2022, lower values of carbon dioxide concentrations in the atmospheric surface layer were obtained for the water area of the Peter the Great Gulf^{1, 2}:

- on average 424 ppm (83th cruise, the Peter the Great Gulf);
- on average 425 ppm (multi-day anchorage near *Cape Schultz* MES, November 2022);
- on average 427 ppm (84th–85th cruises, December 2022).

The water vapor content in winter varied within 0.1–8.1%, with an average of 2.2% and a median of 2.8%. The maximum monthly mean values were recorded in February and the minimum values in December and January. It is worth noting that the peaks of both gas components often coincide, but the opposite dependence is also found.

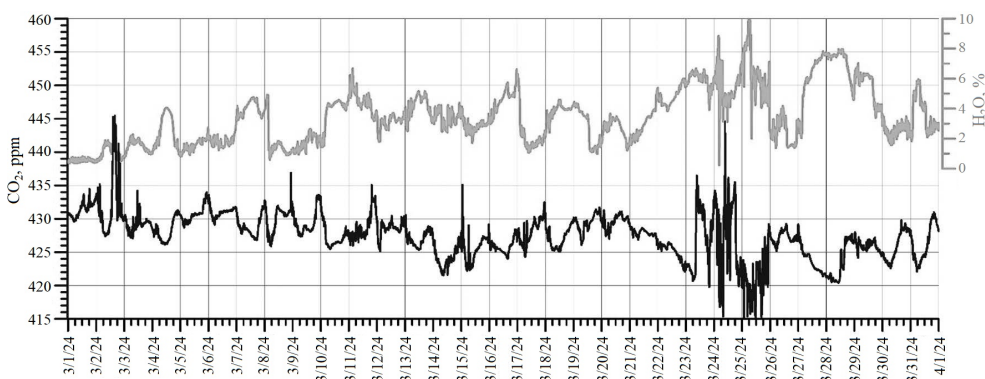


Fig. 9. Results of gas-geochemical monitoring at *Cape Schultz* MES for March 2024

In general, such a level of CO₂ concentration vividly illustrates the increased level of its content in the atmosphere in winter. This is due both to the peculiarities of the atmospheric transfer (mainly from the continental part) and to the almost complete slowing down of photosynthesis and vegetation processes (carbon dioxide

¹ Yatsuk, A.V. and Bovsun, M.A., 2023. *Climatically Active Gases in the Atmospheric Surface Layer of Peter the Great Bay (Sea of Japan), Measured for October 21 – November 30, 2022: Database*. RU Patent 2023620699, Federal Service for Intellectual Property.

² Yatsuk, A.V. and Bovsun, M.A., 2023. *Atmochemical and Meteorological Parameters of the Atmospheric Surface Layer of the Water Areas of Amur and Ussuri Bays (Sea of Japan), Measured on R/V Professor Gagarinsky Board during Cruises No. 84 and No. 85 (01–31.12.2022): Database*. RU Patent 2023623106, Federal Service for Intellectual Property.

drainage is difficult) due to the low temperatures. Furthermore, from December 2023, a characteristic diurnal variability of carbon dioxide concentrations has been detected, with an increase during the day and a smooth decrease at night (with a minimum in the morning), with an average amplitude of 1.3 ppm. This appears to be related to local features of the atmospheric circulation and a change in the direction of the prevailing wind in the land-sea system.

In March 2024, the first regional data on CO₂ concentrations for the spring period were obtained (Fig. 9). The carbon dioxide content in March varied in the range of 388.9–445.5 ppm, with an average of 427.5 ppm and a median of 427.8 ppm. The water vapor content varied in the range of 0.2–10.6%, with an average of 3.5% and a median of 3.3%. In general, similar diurnal dependencies are observed for this season of the year.

The spring period is characterized by the transition to the warm season with positive daytime temperatures and often negative nighttime temperatures. In addition, an important factor influencing the level of concentrations is a relatively dry winter with little snow, which, together with a constant flow of solar radiation and warming of the soil layer, causes frequent occurrence of fire-hazardous periods with the development of forest fires and grass fires in Primorsky Krai. March 2024 was extremely fire hazardous, especially for the southern part of the Khasansky District (Fig. 10).



Fig. 10. Areas of distribution of temperature anomalies (fire sources) in March 2024 based on the NASA FIRMS (Fire Information for Resource Management System) data (site <https://firms.modaps.eosdis.nasa.gov>). Red zones are the short-term fires, light yellow ones – hotbeds of burning for more than 5 days

The main (peak) periods of the fires occurred on 1–4 March and 23–26 March 2024, which is well reflected in the peak-shaped anomalies of carbon dioxide in the surface atmosphere (see Fig. 8).

General characteristics of the distribution of greenhouse gases over four months are shown in Figs. 11 and 12.

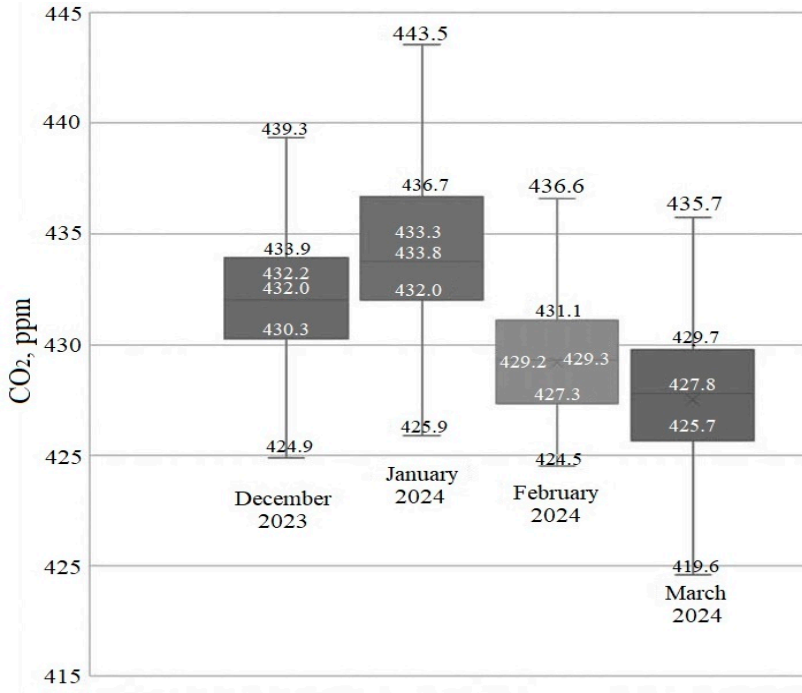


Fig. 11. Statistical estimation parameters for carbon dioxide concentrations. The boundaries of the box plot are the first and the third quartiles (25th and 75th percentiles, respectively), line in the middle of the box is the median (50th percentile). The ends of “whiskers” are the minimum and maximum observed data values; the ones exceeding these values belong to the emission category

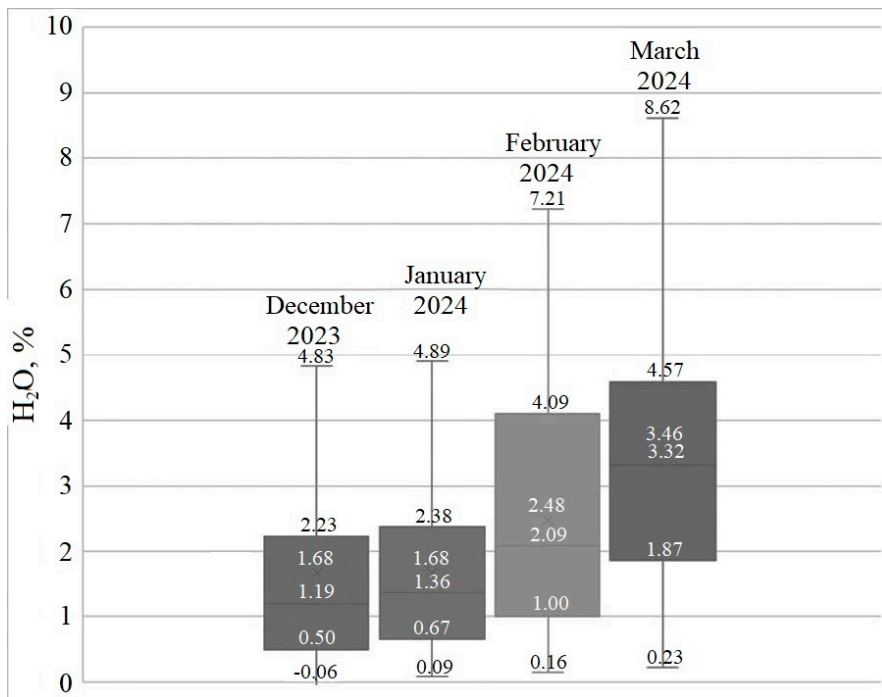


Fig. 12. Statistical estimation parameters for water vapor concentrations

In general, the statistical estimation allows for the discussion of a trend of decreasing carbon dioxide concentrations by March 2024, with a maximum occurring in the middle of the winter season (January 2024). A close relationship has been identified between the temperature regime and the manifestation of daily variability in solar activity. This may also be associated with a change in wind direction during the day/night period. This pattern may be disrupted due to adverse weather events, cyclonic activity and additional emission sources, such as forest fires and grass fires. Further modeling of atmospheric transport will help to identify potential areas – sources of carbon dioxide emissions into the atmosphere.

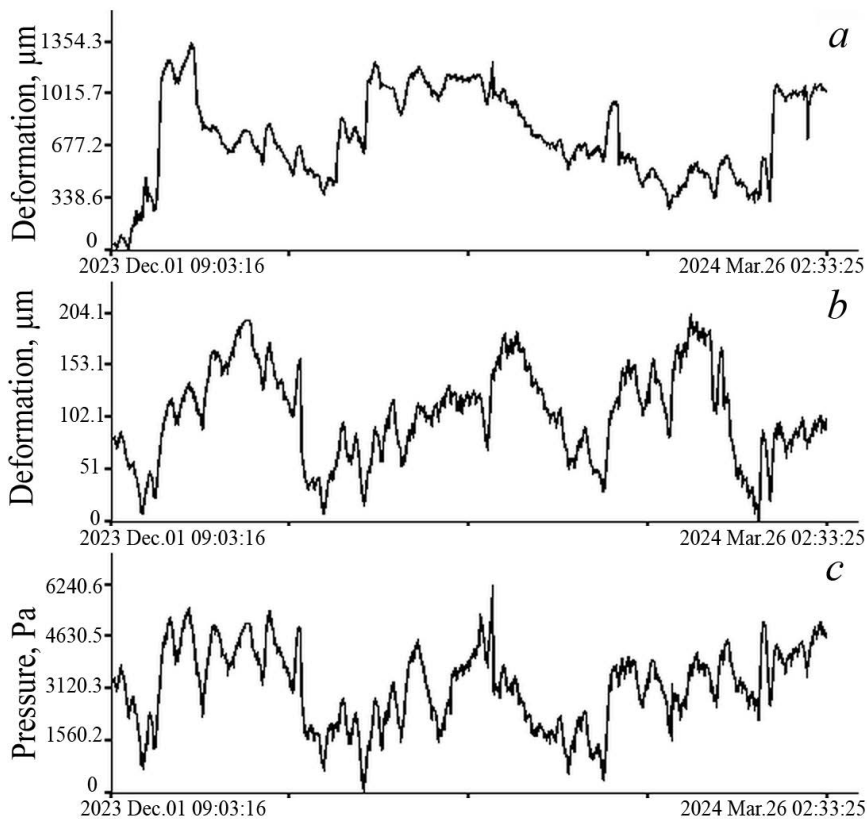


Fig. 13. Results of deformation monitoring from December 1, 2023 to March 26, 2024: records of 52.5 m (a) and 17.5 m laser (b) strainmeters, and laser nanobarograph (c)

The conducted studies have revealed the gas-geochemical background of carbon dioxide in the atmospheric air during the winter period (430.8 ppm) and at the beginning of the spring season of 2024 (427.8 ppm) in the *Cape Schultz* MES

area. The prevailing climatic parameters of the atmosphere were recorded and the fundamental trends of change were identified.

Results of deformation monitoring

Figure 13 shows the results of deformation monitoring for the specified period of time.

The deformation and gas monitoring data for the period of 1–25 December 2023 were subjected to spectral processing using the periodogram method, with a number of averaging of 3. The data processing results given in Figs. 8 and 13 are shown in Fig. 14.

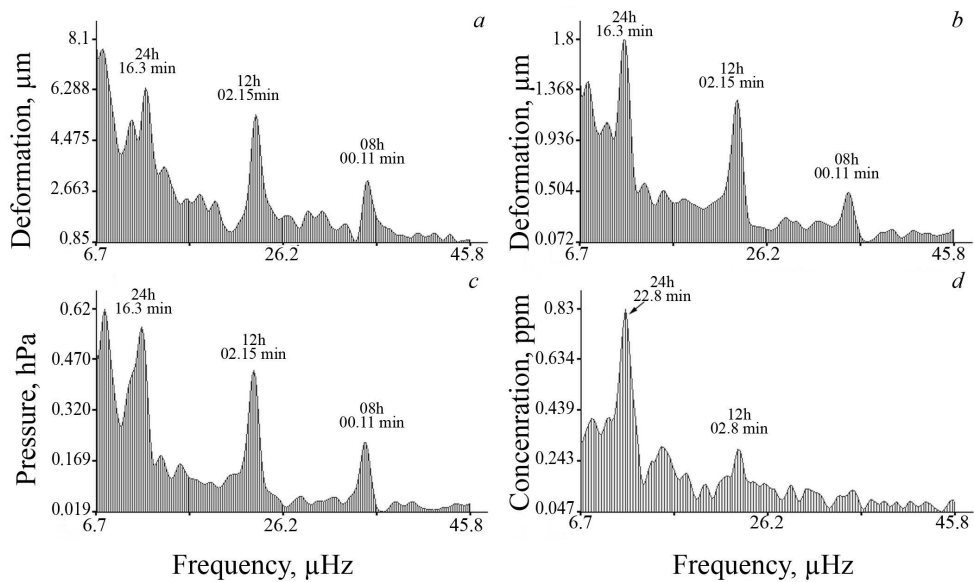


Fig. 14. Spectra obtained by processing the data from 52.5 m (*a*) and 17.5 m (*b*) laser strainmeters, laser nanobarograph (*c*), and CO₂ gas analyzer (*d*) for December 2023

As can be observed, all the spectra show maxima that correspond to both diurnal and semidiurnal tides. A prominent peak with a period of ~ 8 h stands out in the spectra of the laser strainmeter and laser nanobarograph records.

A detailed examination of the synchronous records of the laser interference setups and the gas analyzer revealed the presence of tidal harmonics in the spectra (crustal deformations, variations in atmospheric pressure and carbon dioxide concentration). The correlation at these frequencies is possibly caused by the effect of tides on the sedimentary bottom rocks, which have an increased gas content.

The most remarkable (so far) outcome of the acquired data is the documentation of a tsunamigenic earthquake in the Sea of Japan by laser strainmeters, which resulted in the generation of a tsunami wave reaching up to 0.3 m in height along the Primorsky Krai coastline. Figure 15 shows records of a 52.5 m and 17.5 m laser strainmeters, which registered the earthquake and deformation anomalies (strain

jumps) caused by seafloor movements at the epicenter. The earthquake occurred at the northeastern tip of the Noto Peninsula (Japan) on 1 January 2024 at 07:10:09 UTC with a magnitude of 7.6. The level of this deformation anomaly allows for the calculation of the bottom displacement that resulted in the tsunami generation. According to [13], the calculated bottom displacement based on the 52.5 m laser strainmeter recording was 5.4 m at the earthquake epicenter.

The gas analyzer records showed no similar signals associated with catastrophic earthquakes in the region.

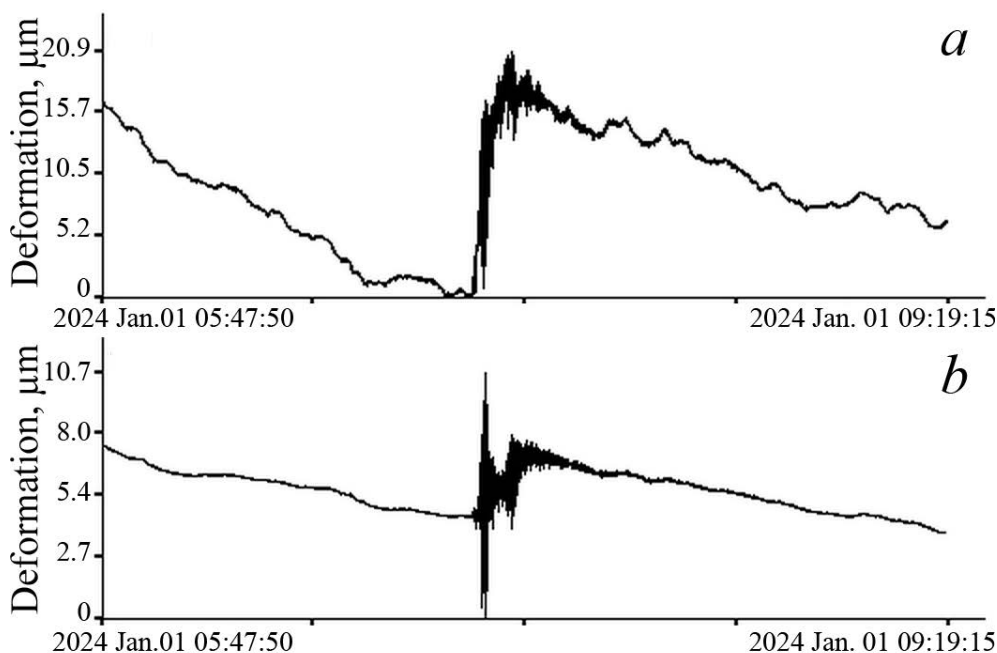


Fig. 15. Tsunamigenic earthquake and deformation anomaly on the records of 52.5 m and 17.5 m laser strainmeters

Conclusion

The measurements of carbon dioxide variations in the winter of 2023–2024 showed that the increase in CO₂ levels was linked to the direction of the wind blowing from the continent. This is due both to the peculiarities of atmospheric transfer and to the almost complete slowing down of photosynthesis and vegetation processes due to low temperatures. In summer, the wind direction is almost reversed. Daily variations in CO₂ concentration are exclusively associated with diurnal temperature variations.

As a result of the deformation monitoring, a tsunamigenic earthquake was registered, which generated a tsunami in the Sea of Japan. Based on the magnitude of the deformation anomaly registered by the laser strainmeter, it was possible to

determine the bottom displacement in the earthquake source, which led to the tsunami generation. According to the measurements, it was ~ 5.4 m. These anomalous deformation processes did not, as expected, manifest themselves in water vapor and carbon dioxide variations at Cape Schultz.

Spectral processing of data from laser strainmeters, a laser nanobarograph and a gas analyzer revealed strong spectral components at tidal harmonics.

REFERENCES

1. Bowman, D.C. and Lees, J.M., 2018. Upper Atmosphere Heating from Ocean-Generated Acoustic Wave Energy. *Geophysical Research Letters*, 45(10), pp. 5144-5150. <https://doi.org/10.1029/2018GL077737>
2. Gerstoft, P., Fehler, M.C. and Sabra, K.G., 2006. When Katrina hit California. *Geophysical Research Letters*, 33(17), L17308. <https://doi.org/10.1029/2006GL027270>
3. Astiz, L. and Creager, K., 1994. Geographic and Seasonal Variations of Microseismic Noise. *EOS: Transactions, American Geophysical Union*, 75, 419.
4. Bromirski, P., Flick, R.E. and Graham, N., 1999. Ocean Wave Height Determined from Inland Seismometer Data: Implications for Investigating Wave Climate Changes in the NE Pacific. *Journal of Geophysical Research: Oceans*, 104(C9), pp. 20753-20766. <https://doi.org/10.1029/1999JC900156>
5. Grevemeyer, I., Herber, R. and Essen, H.-H., 2000. Microseismological Evidence for a Changing Wave Climate in the Northeast Atlantic Ocean. *Nature*, 408(6810), pp. 349-352. <https://doi.org/10.1038/35042558>
6. Aster, R.C., McNamara, D.E. and Bromirski, P.D., 2008. Multidecadal Climate-Induced Variability in Microseisms. *Seismological Research Letters*, 79(2), pp. 194-202. <https://doi.org/10.1785/gssrl.79.2.194>
7. Rybalko, A.E., Scherbakov, V.A., Ivanova, V.V., Slinchenkov, V.N., Belyaev, P.Yu., Andreev, A.Yu., Tokarev, M.Yu., Maev, P.A. and Belov, M.V., 2018. [Assessment of Hazardous Geological Processes in Peter the Great Bay (Sea of Japan) According to the Geological Environment Monitoring Data]. In: N. A. Zhuravleva and K. S. Viskhadzhieva, eds., 2018. *Prospects of Development of Engineering Surveys in Construction in the Russian Federation: Materials of Reports Presented on the XIV All-Russian Scientific and Practical Conference and Exhibition of Surveying Organizations*. Moscow: Geomarketing LLC, pp. 592-597 (in Russian).
8. Okulov, A.K., Obzhairov, A.I., Mishukova, G.I. and Okulov, A.I., 2017. Methane Distribution of the Water Peter Great Gulf. *Underwater Investigations and Robotics*, (1), pp. 68-73 (in Russian).
9. Sultan, N., Plaza-Faverola, A., Vadakkepuliambatta, S., Buenz, S. and Knies, J., 2020. Impact of Tides and Sea-Level on Deep-Sea Arctic Methane Emissions. *Nature Communications*, 11(1), 5087. <https://doi.org/10.1038/s41467-020-18899-3>
10. Dolgikh, G., Bovsun, M., Dolgikh, S., Stepochkin, I., Chupin, V. and Yatsuk, A., 2024. Hard- and Software Controlled Complex for Gas-Strain Monitoring of Transition Zones. *Sensors*, 24(8), 2602. <https://doi.org/10.3390/s24082602>
11. Dolgikh, G.I., Dolgikh, S.G., Kovalev, S.N., Koren, I.A., Novikova, O.V., Ovcharenko, V.V., Okuntseva, O.P., Shvets, V.A., Chupin, V.A. [et al.], 2004. A Laser Nanobarograph and Its

- Application to the Study of Pressure-Strain Coupling. *Izvestiya, Physics of the Solid Earth*, 40(8), pp. 683-691.
12. Dolgikh, G.I., Kovalev, S.N., Koren, I.A. and Ovcharenko, V.V., 1998. A Two-Coordinate Laser Strainmeter. *Izvestiya, Physics of the Solid Earth*, 34(11), pp. 946-950.
 13. Dolgikh, G. and Dolgikh, S., 2021. Deformation Anomalies Accompanying Tsunami Origination. *Journal of Marine Science and Engineering*, 9(10), 1144. <https://doi.org/10.3390/jmse9101144>

Submitted 25.06.2024; approved after review 05.09.2024;
accepted for publication 12.09.2024.

About the authors:

Maria A. Bovsun, Junior Researcher, Gas-Geochemistry Laboratory, V.I. Il'ichev Pacific Oceanological Institute, Far Eastern Branch of RAS (43 Baltiyskaya Str., Vladivostok, 690041, Russian Federation), **Scopus Author ID: 57218099245**, bovsun.ma@poi.dvo.ru

Grigoriy I. Dolgikh, Director, V.I. Il'ichev Pacific Oceanological Institute, Far Eastern Branch of RAS (43 Baltiyskaya Str., Vladivostok, 690041, Russian Federation), DSc (Phys.-Math.), Academician of RAS, **ORCID ID: 000-0002-2806-3834**, **Scopus Author ID: 7003888822**, dolgikh@poi.dvo.ru

Stanislav G. Dolgikh, Head of the Laboratory of Nonlinear Hydrophysics and Natural Disasters, V.I. Il'ichev Pacific Oceanological Institute, Far Eastern Branch of RAS (43 Baltiyskaya Str., Vladivostok, 690041, Russian Federation), DSc (Tech.), **ORCID ID: 0000-0001-9828-5929**, **Scopus Author ID: 6604069353**, sdolgikh@poi.dvo.ru

Vladimir V. Ovcharenko, Senior Researcher, Geosphere Physics Laboratory, V.I. Il'ichev Pacific Oceanological Institute, Far Eastern Branch of RAS (43 Baltiyskaya Str., Vladivostok, 690041, Russian Federation), CSc (Phys.-Math.), **ORCID ID: 0000-0001-7784-2140**, **Scopus Author ID: 7101867413**, ovcharenko@poi.dvo.ru

Igor E. Steepochkin, Researcher, Laboratory for Integrated Research of the Environment and Mineral Resources, V.I. Il'ichev Pacific Oceanological Institute, Far Eastern Branch of RAS (43 Baltiyskaya Str., Vladivostok, 690041, Russian Federation), **ORCID ID: 0000-0001-7784-2140**, **Scopus Author ID: 36816707300**, stepochkin.ie@poi.dvo.ru

Vladimir A. Chupin, Head of the Geosphere Physics Laboratory, V.I. Il'ichev Pacific Oceanological Institute, Far Eastern Branch of RAS (43 Baltiyskaya Str., Vladivostok, 690041, Russian Federation), CSc (Phys.-Math.), **ORCID ID: 0000-0001-5103-8138**, **Scopus Author ID: 7004931608**, chupin@poi.dvo.ru

Andrey V. Yatsuk, Leading Researcher, Gas-Geochemistry Laboratory, V.I. Il'ichev Pacific Oceanological Institute, Far Eastern Branch of RAS (43 Baltiyskaya Str., Vladivostok, 690041, Russian Federation), CSc (Phys.-Math.), CSc (Geol.-Miner.), **ORCID ID: 0000-0003-3975-5438**, **Scopus Author ID: 55189937800**, yatsuk@poi.dvo.ru

Contribution of the co-authors:

Maria A. Bovsun – methodology, data processing, description of the research results

Grigoriy I. Dolgikh – scientific supervision of the research, writing an article text, analysis of results and their interpretation, participation in the discussion of article materials and editing the article text, formulation of conclusions

Stanislav G. Dolgikh – data visualization and presentation, participation in the discussion of article materials

Vladimir V. Ovcharenko – collection of available materials on the research topic

Igor E. Steepochkin – data provision and processing

Vladimir A. Chupin – data systematization, analysis of results and their interpretation, data visualization, text editing, participation in the discussion of article materials

Andrey V. Yatsuk – analysis of results and their interpretation, participation in the discussion of article materials, methodology, data visualization and presentation

The authors have read and approved the final manuscript.

The authors declare that they have no conflict of interest.